Predictive Wireless Antenna Selection for High Mobility Conditions

by

Hassan Abou Saleh

A thesis submitted to the
Department of Electrical and Computer Engineering
in conformity with the requirements for
the degree of Doctor of Philosophy

Queen's University
Kingston, Ontario, Canada
January 2013

Abstract

Accurate channel knowledge is indispensable to the practical success of channel-aware wireless communication technologies. However, channel estimates obtained from pilot symbols rapidly become outdated due to fast time variations of multipath fading channels. To reduce system cost, antenna subset selection reduces radio frequency (RF) chain components. For systems selecting a subset of a plurality of antennas for reception, this outdated channel information is a significant impediment to selection and data decoding reliability. In this thesis, training-based schemes for antenna selection (AS) for time-varying channels which account for practical constraints such as training, packetization and antenna switching time are proposed based on discrete prolate spheroidal sequences. They only operate with knowledge or estimates of the Doppler frequency and the channel signal-to-noise ratio (SNR), but do not require detailed statistical correlation knowledge.

A pilot-based AS scheme for time-varying frequency-flat channels for single input–multiple output (SIMO) systems selecting one of a plurality of antennas using packet or symbol-rate antenna switching is first proposed. It is demonstrated that the presented scheme provides significant performance gain over AS methods using Fourier-based orthogonal training as well as over single antenna systems with perfect channel knowledge. Analytical expressions for the symbol error probability (SEP) of `M`-ary

phase-shift keying (MPSK) for systems employing the suggested techniques are provided.

The second part of this thesis investigates the more general case of selecting a subset of a plurality of receive antennas. A new pilot-based receive antenna subset selection algorithm for time-varying frequency-flat channels is presented. The proposed AS algorithm is shown to outperform AS methods based on Fourier prediction/estimation as well as SIMO systems with perfect channel knowledge. Analysis of MPSK and quadrature amplitude modulation (MQAM) SEP for systems with receive AS is provided.

The combination of AS and orthogonal frequency division multiplexing (OFDM) over the more realistic time-varying and frequency-selective fading scenario is examined in the final part. Training schemes for receive AS using packet-rate antenna switching for SIMO and multiple input–multiple output (MIMO) OFDM systems are developed. The suggested schemes exhibit a superior performance over AS methods using either linear interpolation/extrapolation or Fourier prediction/estimation techniques.

Acknowledgments

I want to thank my advisor Professor Steven D. Blostein for his invaluable guidance, endless support, patience, and for being a true inspiration. This research could not have been performed without his cooperation. My most sincere thanks also go to Prof. Steve Blostein for providing a friendly and supportive environment which facilitated my PhD research.

I also want to thank the other members of my dissertation committee: Profs. Benoit Champagne, Shahram Yousefi, Serdar Yuksel, and Yan-Fei Liu.

My sincere thanks also go to Prof. Andy Molisch, Dr. Thomas Zemen, and Prof. Neelesh Mehta.

The financial support of the Natural Sciences and Engineering Research Council of Canada is gratefully acknowledged.

Finally, my eternal thanks and love go to my parents, Pappa and Mamma, and my two brothers.

Statement of co-authors:

A large part of Chapter 3 has appeared in the following papers:

H. A. Saleh, A. F. Molisch, T. Zemen, S. D. Blostein, and N. B. Mehta, "Receive antenna selection for time-varying channels using discrete prolate spheroidal sequences," *IEEE Trans. Wireless Commun.*, vol. 11, pp. 2616-2627, Jul. 2012.

H. A. Saleh, A. F. Molisch, T. Zemen, S. D. Blostein, and N. B. Mehta, "Antenna selection for time-varying channels based on Slepian subspace projections," in *Proc. IEEE ICC*, Ottawa, Canada, Jun. 2012.

Part of Chapter 4 has appeared in the following paper:

H. A. Saleh and S. D. Blostein, "Receive antenna subset selection for time-varying channels using Slepian subspace projections," in *Proc. IEEE Globecom*, Anaheim, USA, Dec. 2012.

Contents

List of Tables

List of Figures

Acronyms

AS	Antenna Selection
DPS	Discrete Prolate Spheroidal
SP	Slepian Prediction
SE	Slepian Estimation
LTE	Long Term Evolution
SISO	Single Input–Single Output
SIMO	Single Input–Multiple Output
MIMO	Multiple Input–Multiple Output
OFDM	Orthogonal Frequency Division Multiplexing
OFDMA	Orthogonal Frequency Division Multiple Access
IFFT	Inverse Fast Fourier Transform
FFT	Fast Fourier Transform
CSI	Channel State Information
MEMS	Microelectromechanical System
SEP	Symbol Error Probability
`M`PSK	`M`-ary Phase-Shift Keying
`M`QAM	`M`-ary Quadrature Amplitude Modulation
PER	Packet Error Rate

BER	Bit Error Rate
SNR	Signal-to-Noise Ratio
MSE	Mean Square Error
AWGN	Additive White Gaussian Noise
MRC	Maximal-Ratio Combining
WSSUS	Wide Sense Stationary Uncorrelated Scattering
WSS	Wide Sense Stationary
RV	Random Variable
VBC	Virtual Branch Combining
PDP	Power Delay Profile
PSD	Power Spectral Density
FIR	Finite Impulse Response
PDF	Probability Density Function
CDF	Cumulative Distribution Function
ICI	Inter-Carrier Interference
ISI	Inter-Symbol Interference
LNA	Low-Noise Amplifier
ML	Maximum Likelihood
PSD	Power Spectral Density
MGF	Moment Generating Function
FIR	Finite Impulse Response
TTI	Transmission Time Interval

List of Important Symbols

m	Discrete time
D	Subspace dimension
u	Slepian basis function
$\boldsymbol{u}$	Slepian basis vector
$\hat{\boldsymbol{c}}$	Basis expansion coefficients vector
$(\cdot)^{\mathrm{SP}}$	Slepian prediction
$(\cdot)^{\mathrm{SE}}$	Slepian estimation
$\hat{h}^{\mathrm{SP}}$	Predicted channel gain
$\hat{h}^{\mathrm{SE}}$	Estimated channel gain
K_{t}	Number of transmit antennas
K_{r}	Number of receive antennas
K'_{r}	Number of selected receive antennas
f_{D}	Doppler frequency
$\nu_{\max}$	Maximum normalized Doppler frequency
$\triangleq$	Defined as
$\lceil x \rceil$	Smallest integer greater than or equal x
$\lfloor x \rfloor$	Largest integer not greater than x
$d[m]$	Data symbol at time index m

$p[m]$	Pilot symbol at time index m
T_{s}	Symbol duration
T_{os}	OFDM symbol duration
N_{ps}	Number of training pilots for each receive antenna
N	Number of symbols in a packet
N_{pf}	Number of post-selection pilot symbols in a packet
N_{tp}	Number of total pilot symbols at each selected antenna
N_{df}	Number of data symbols in a packet
T_{p}	Duration between consecutive training symbols in each round
T_{r}	Duration between two consecutive rounds of pilot transmission
$\mathcal{I}_{\mathrm{ast}}$	Time span of antenna selection training phase
$\mathcal{I}_{\mathrm{padt}}$	Time span of pilot-assisted data transmission phase
$T_{\mathrm{ps}}^{k_{\mathrm{r}}}$	Set of time indices when the N_{ps} AS training pilots are received by AE k_{r}
$T_{\mathrm{pf}}^{k_{\mathrm{r}}}$	Set of time indices when the N_{pf} post-selection pilots are received by AE k_{r}
$\hat{\imath}$	Index of selected receive antenna
η	Average signal-to-noise ratio
E_{s}	Average symbol energy
N_{o}	Noise power
$\delta(\cdot)$	Dirac delta function
T_{sw}	Antenna switching time
$\mathbb{E}\{\cdot\}$	Statistical expectation
$\mathrm{var}\{\cdot\}$	Statistical variance

N_{sc}	Number of subcarriers
L	Number of channel taps
$\boldsymbol{I}_{\mathrm{n}}$	Identity matrix of size $n \times n$

Chapter 1

Introduction

Wireless communications systems are widely deployed to provide various types of services including wireless mobile data services. In general, a mobile wireless link may be established via single and/or multiple antennas. However, multiple antenna systems have been adopted in several wireless standards [1, 2] ever since recent studies have demonstrated their ability to improve system reliability and capacity/throughput [30, 36, 96]. In long term evolution (LTE) of the third generation partnership project (3GPP), the basestation uses two antenna elements for both transmission and reception, while the mobile station uses two antennas for reception and single antenna for transmission [2]. These promised benefits occur in rich-scattering propagation environments and where channel knowledge can be inferred. Orthogonal frequency division multiplexing (OFDM) and/or orthogonal frequency division multiple access (OFDMA) signaling techniques have also been adapted from wireline DSL/ADSL systems to deal with multipath delay-spread wireless channels. Initially, multiple antenna schemes were developed that do not require channel knowledge, i.e., open-loop systems including space-time coding [4] and spatial multiplexing [29]. Multiple antenna signaling schemes that exploit knowledge of the channel include

antenna selection [65, 80] and beamforming/precoding [36, 76]. While demonstrating performance gains, complexity and cost of multiple antenna systems are often higher than those of conventional single antenna systems.

Antenna selection (AS) judiciously exploits the diversity benefits of multiple antennas while potentially reducing hardware complexity and costs at the transmitter and/or receiver of a wireless system. In AS, only a subset of a plurality of antennas is selected and connected to a limited number of radio-frequency (RF) chains based on the current fading states. This conceivably retains the advantages of multiple antennas, while using fewer of the expensive RF chains. Antenna selection may also be applied to multiple antenna systems employing other existing signaling schemes such as transmit diversity and spatial multiplexing schemes. Through this, additional gains may be realized.

Thus, antenna selection is a promising approach for lowering MIMO system complexity while leveraging most of the advantages of multiple antennas.

1.1 Motivation

There are a number of existing studies on both optimal and suboptimal reduced complexity AS algorithms [11, 12, 15, 22, 32, 38–41, 46, 47, 53, 64, 68]. The capacity, diversity and diversity-muliplexing performance of AS systems are studied in [9, 16, 33, 51, 66, 93, 95, 98, 102, 106]. Antenna selection for OFDM systems is considered in [10, 20, 61, 83, 85, 90, 103]. Bulk versus per-tone AS for MIMO-OFDM systems is examined in [21, 81, 104]. However, to date, far fewer studies exist that deal with the practical issues of pilot-based training methods for antenna selection.

Most of the above references assume slowly time-varying fading and/or perfect

knowledge of the channel at the basestation wherein the selection of antennas is made. In practice, knowledge or estimation of the channel is often obtained through the insertion of training or *pilot* symbols. Unfortunately, the mobile communication environment exhibits a randomly time-varying frequency-selective channel due to the mobility of users and reflections from multiple scatterers. Thus, wireless transmission is impaired by both delay-spread and Doppler induced temporal variations. This implies that preliminary channel estimates obtained from pilot symbols get rapidly outdated. This inaccurate and/or outdated knowledge impacts both the selection and decoding processes. Thus, a need exists for the development of more reliable antenna selection schemes for time-varying frequency-selective, i.e., doubly selective channels which maintain most of the diversity benefits of multiple antennas. At the same time, it is of interest to design schemes which explicitly take into account practical constraints such as training, packetization and antenna switching time. This motivates this investigation into low complexity training-based antenna selection schemes which exploit prediction and estimation of the channel over the data transmission phase in the selection and decoding mechanisms. This study aims to provide accurate knowledge and insight into the realistic achievable gain and benefits of antenna selection over doubly dispersive channels. Therefore, it is beneficial to derive results that give additional analytical insight into such schemes. The objectives of this thesis are to address these issues.

The impact of imperfect channel knowledge on the performance of a space-time coded AS system in Rayleigh fading is presented in [97]. The effects of channel estimation errors on the performance of optimum and suboptimum selection diversity receivers in Rayleigh fading channels is presented in [7]. The performance of a

space-time coded AS system employing transmit AS system along with maximal ratio transmission with feedback delay and channel estimation error is analyzed in [44]. The symbol error probability (SEP) performance for antenna subset selection systems over flat Rayleigh fading with imperfect channel knowledge is studied in [35]. Receive antenna selection for OFDM-based multiple antenna systems with channel estimation error is studied in [67]. The effects of feedback delay on the performance of systems employing transmit AS and maximal ratio combining at the receiver is studied in [71, 73]. It is shown that with perfect demodulation using ideal Wiener filtering at the receiver full diversity order is preserved [71]. In [35, 43, 67, 73, 99], it is shown that channel estimation errors result in a fixed signal-to-noise ratio (SNR) loss and do not affect the diversity gain while feedback delay alters the diversity order. Weighted AS rules for time-varying channels which use temporal correlation knowledge are proposed in [54, 55]. However, it is worth mentioning that only channel gain estimates obtained during the AS training phase are used in the selection and decoding mechanisms in [54] and [55] since channel gain estimates over the data transmission phase are not yet available. This causes a loss in SNR. We also note that the weighted selection criterion used in [54] and [55] requires a priori temporal correlation knowledge.

The above observations motivate investigation into low-complexity training-based AS algorithms for time-varying channels which use channel knowledge or estimates in the data transmission phase in the selection and decoding processes. In addition, reliability and low complexity estimation and prediction is needed to realize these systems in practice. The optimal Wiener predictor/estimator requires detailed accurate channel covariance knowledge, which varies over different environments. This

assumed wide-sense stationary statistics with channel knowledge that is difficult to obtain due to bursty transmission, as for example in vehicular scenarios [70, 100, 101]. Therefore, the optimum Wiener predictor/estimator does not lend itself to a practical low complexity design. This motivates the use of adaptive prediction methods, including that which employs the recently-proposed low-complexity Slepian basis expansion channel estimator and channel predictor to obtain reliable CSI at the receiver. In this thesis, we investigate antenna selection over more realistic doubly selective channels. By explicitly accounting for practical constraints such as training, packetization and antenna switching time, we propose low complexity training-based antenna selection schemes for time-varying and frequency-selective channels which exploit bandlimited Slepian sequences for channel estimation and prediction. Techniques are proposed in this thesis for both per-packet and symbol-by-symbol switching. While they do require knowledge or estimation of the Doppler frequency which is directly proportional to the relative speed between transmitter and receiver, they do not require detailed correlation knowledge. Many techniques have been proposed for estimation of the maximum Doppler frequency [8, 48, 69, 84]. As this topic is well investigated, note that Doppler estimation is beyond the scope of the thesis.

1.2 Thesis Overview

Chapter 2 describes the time-varying multipath wireless channel model used in this thesis. Background information concerning OFDM, basis expansion channel estimation/prediction models including Slepian and Fourier expansion models, as well as linear interpolation/extrapolation techniques are also presented there.

Chapter 3 presents a low complexity training-based single receive antenna selection

scheme for time-varying and frequency-flat channels for per-packet and symbol-by-symbol switching. An approach to determine the subspace dimension, i.e., number of basis functions that reduces the mean square error (MSE) of the Slepian basis expansion channel estimator/predictor is also presented. The proposed antenna selection scheme is then analyzed to evaluate the symbol error probability (SEP) of M-ary phase shift keying (MPSK) in time-varying and frequency-flat channels. The derived results provide insight for the MPSK SEP of subcarriers for OFDM systems selecting the same antenna for all subcarriers. Performance of OFDM in doubly selective fading is postponed to Chapter 5.

Chapter 4 studies the more general case of selecting a subset of a plurality of receive antennas under the same time-varying and frequency-flat channel conditions as in Chapter 3. A new training-based receive antenna subset selection algorithm for time-varying and frequency-flat channels is presented. The proposed method employs both per-packet and symbol-by-symbol switching. Performance analysis to evaluate the SEP of MPSK and M-ary quadrature amplitude modulation (MQAM) in time-varying and frequency-flat fading with receive AS is then provided. The presented expressions provide insight into the MPSK and MQAM SEP of subcarriers for OFDM systems selecting the same subset of receive antennas for all the subcarriers.

The fifth chapter examines antenna selection combined with OFDM over the more realistic double selective fading scenario, i.e., time-varying and frequency-selective channels. The single-carrier training-based receive AS methods for time-varying frequency-flat channels based on Slepian subspace projections from Chapters 3 and 4 are extended to accommodate single input–multiple output (SIMO) and multiple

input–multiple output (MIMO) OFDM-based systems over time-varying frequency-selective fading. The reported results provide insights into the performance/complexity tradeoffs and achievable gain of the presented methods and also of antenna selection in general over realistic fading scenarios.

The sixth and final chapter contains a compendium of the principal results presented in the thesis as well as suggestions for further research.

1.3 Summary of Contributions

The main contributions of the thesis are briefly summarized as follows:

- Predictive pilot-based training receive AS algorithms that explicitly account for fast time variations of channels by using knowledge of preamble pilots and distributed post-selection pilots for selection and data decoding are proposed.
- Performance evaluation of the above receive AS methods for single carrier time-varying Doppler fading channels using packet or symbol-rate antenna switching is reported.
- Symbol error probability (SEP) analysis of the proposed single carrier AS schemes is provided.
- The performance of the above AS techniques are then evaluated for OFDM systems over more realistic time-varying and frequency-selective channels. Training schemes for per-packet receive AS for MIMO OFDM systems are developed. Simulation results that quantify the performance of the presented schemes and existing methods are reported.

- A technique for choosing appropriate subspace dimension for DPS sequences that explicitly accounts for mean squared error estimation/prediction and SNR is developed.

Chapter 2

Background

In this chapter, we discuss the theoretical background related to the thesis. The wireless channel model is first described. Background information concerning orthogonal frequency division multiplexing (OFDM) is summarized in Sec. 2.2. Discrete prolate spheroidal (DPS) sequences are presented in Sec. 2.4. Slepian basis expansion channel estimator and predictor are described in Sec. 2.5. By employing DPS sequences, Slepian estimator/predictor explicitly takes into account temporal variations of the channel. As described in subsequent chapters, the proposed training-based antenna selection schemes uses Slepian subspace projection techniques. Orthogonal Fourier based channel estimation/prediction and linear interpolation/extrapolation techniques are presented in Secs. 2.6 and 2.7, respectively.

2.1 Wireless Channel Model

The mobile communication environment exhibits a randomly time-varying multipath channel due to the relative radial motion between the transmitter and receiver including moving scatterers, and multipath propagation delays. The channel link is modeled as a length-L finite impulse response (FIR) filter, for which the continuous

time impulse response is given by [36, 59, 74, 87]

$$h(t,\tau) = \sum_{\ell=0}^{L-1} \sqrt{P(\tau_\ell)} w_\ell(t)\, \delta(\tau - \tau_\ell) \tag{2.1}$$

where $\delta(t)$ denotes the Dirac delta function, τ_ℓ is the propagation delay of the ℓth complex channel tap $w_\ell(t)$ of average power $P(\tau_\ell)$. $\{P(\tau_\ell)\}_{\ell=0}^{L-1}$ represent the channel power delay profile (PDP), normalized as $\sum_{\ell=0}^{L-1} P(\tau_\ell) = 1$. The wide sense stationary uncorrelated scattering (WSSUS) model is commonly used for multipath wireless channels [36, 72, 74, 87]. The complex channel taps are wide sense stationary (WSS) narrowband complex Gaussian random processes. They are independent for each tap since the scatterers at different delays are uncorrelated. In (2.1), the time dimension t relates to the temporal selectivity of the channel. The delay dimension τ captures the frequency-selectivity of the channel. The multipath delay spread of the frequency-selective (time-dispersive) channel is much longer than the transmitted symbol duration. As described in the next section, OFDM mitigates the effects of delay spread by increasing the symbol duration of each subcarrier. This enables simple per-subcarrier frequency-domain equalization and channel estimation.

Let m index the discrete time with symbol rate $R_\mathrm{s} \triangleq \frac{1}{T_\mathrm{s}}$, where T_s denotes the symbol duration. The discrete-time channel impulse response can thus be expressed as [58, 92]

$$\begin{aligned} h[m,\ell'] &\triangleq h(mT_\mathrm{s}, \ell' T_\mathrm{s}) \\ &= \sum_{\ell=0}^{L-1} \sqrt{P[\ell]} w_\ell[m]\, \delta[\ell' - \ell] \end{aligned} \tag{2.2}$$

where standard sampling notation is used in (2.2), i.e., discrete-time signal $x[n]$ is

obtained from continuous signal $x(t)$ by sampling at period T_s according to $x[n] \triangleq x(nT_s)$ with $n \in \mathbb{Z}$.

Clarke's spectrum which models the Doppler power spectrum in two-dimensional isotropic scattering, i.e., uniform distribution for the azimuth angle of arrival of multipath components, is given by [18, 36, 72]

$$S_h[\nu] = \begin{cases} \frac{1}{\pi\nu_{max}\sqrt{1-\left(\frac{\nu}{\nu_{max}}\right)^2}} & |\nu| < \nu_{max}, \\ 0 & \text{otherwise} \end{cases} \tag{2.3}$$

where the maximum normalized Doppler frequency ν_{max} is given by [74, 87]

$$\nu_{max} \triangleq f_D T_s = \frac{v_{max} f_c}{c_o} T_s. \tag{2.4}$$

In (2.4), the Doppler frequency $f_D \triangleq \frac{v_{max} f_c}{c_o}$ measures the change in frequency with v_{max} the radial component of the user velocity, f_c the carrier frequency, and c_o the speed of light. The larger the Doppler frequency, the more rapidly the channel changes in time (time-selective). The coherence time, within which the channel remains strongly correlated, is inversely proportional to the Doppler frequency f_D. As is apparent from (2.3), the frequency dispersion caused by the Doppler shift is captured by the power spectrum. Specifically, the bandwidth of the spectrum $S_h[\nu]$ is $2\nu_{max}$, i.e., $S_h[\nu]$ is bandlimited to the frequency range $[-\nu_{max}, \nu_{max}]$. As described in more detail in Sec. 2.5, the basis expansion functions of the Slepian estimator/predictor (i.e., Slepian sequences) are also bandlimited to the frequency range $[-\nu_{max}, \nu_{max}]$. Therefore, the rate of channel time variation is captured by the Slepian sequences.

For the aforementioned two dimensional isotropic scattering, the autocorrelation

function of the channel $h[m, \ell']$, which corresponds to the bandlimited power spectral density in (2.3), is given by [18, 36]

$$\begin{aligned} R_h[\Delta m] &\triangleq \mathbb{E}\{h[m, \ell'] h^*[m + \Delta m, \ell']\} \\ &= J_0(2\pi\nu_{\max}\Delta m) \end{aligned} \tag{2.5}$$

where $(\cdot)^*$ denotes complex conjugate and $J_0(\cdot)$ is the zeroth order Bessel function of the first kind. Eq. (2.5) measures how fast the channel decorrelates with time. For time-invariant channels, $\nu_{\max} = 0$ and $R_h[\Delta m] = 1$.

In narrowband channel, i.e., frequency-flat channel the multipath components are superimposed since the delay spread of the channel is much shorter than the signal duration. The discrete-time channel impulse response is given by

$$h[m] \triangleq h(mT_s, 0) = w[m]\delta[m]. \tag{2.6}$$

As discussed in the next sections, each OFDM subcarrier carries a narrowband signal that sees time-varying frequency-flat fading. This enables the use of Slepian estimator/predictor for channel estimation/prediction.

In summary, the wireless channel exhibits delay and Doppler spread, resulting in doubly selective fading (time and frequency selective). Therefore, signalling in wireless environments is impaired by delay and Doppler spread.

2.2 Orthogonal Frequency Division Multiplexing

Orthogonal frequency division multiplexing is a convenient signaling technique for dealing with multipath fading channels [17, 36]. In OFDM, the transmission bandwidth is divided into multiple narrowband subcarriers. The input information symbols are transmitted simultaneously at different frequencies to the receiver. At the transmitter, an N_{sc}-point inverse fast Fourier transform (IFFT) block modulates the N_{sc} frequency domain input information symbols to obtain N_{sc} time-domain samples of the OFDM signal. OFDM subcarriers have $\text{sinc}(x) \triangleq \frac{\sin(\pi x)}{\pi x}$ shaped spectra. Therefore, the OFDM signal spectrum consists of overlapping sinc frequency bands. However, this overlap does not cause any inter-carrier interference (ICI) since OFDM subcarriers are orthogonal. After IFFT modulation, a time-domain guard interval (redundant cyclic prefix) of length-N_{g} larger than the delay spread of the channel is inserted to prevent inter-symbol interference (ISI). The resulting length-$(N_{\text{sc}} + N_{\text{g}})$ OFDM signal is then transmitted over the channel. At the receiver the cyclic prefix is removed, and the N_{sc} time-domain samples of the received OFDM signal are fast Fourier transform (FFT) demodulated to obtain the frequency-domain received data symbols. This enables simple per-subcarrier equalization and channel estimation.

In summary, by using orthogonal subcarriers and cyclic prefix OFDM increases the actual symbol duration. This mitigates the effect of delay spread, i.e., ensures time-varying frequency-flat fading on each subchannel, but this also leads to higher temporal channel variations because Doppler spread increases as well. This causes performance degradation and ICI resulting from Doppler spread since orthogonality of the subcarriers is not preserved [36, 57, 88]. In Chapter 5, it is demonstrated that OFDM can be combined with antenna selection and, a gain can be observed over

OFDM systems with no AS at low and high Doppler rates.

2.3 Switching Technologies

Radio frequency (RF) switches are used in many wireless communications systems. To choose an appropriate RF switch it is essential to first consider the required performance specifications, such as insertion loss and switching speed. RF microelectromechanical system (MEMS) switches operate at RF to mm-wave frequencies (0.1 to 100 GHz) [75]. The switching speed of most RF MEMS switches is 2 to 40 μs with an insertion loss of only 0.1 dB. Current solid-state RF technologies (PIN diode- and FET- based) offer a faster switching time of 1 to 100 ns with an insertion loss of 1 to 3 dB.

2.4 Discrete Prolate Spheroidal Sequences

In [86], Slepian first introduced discrete prolate spheroidal (DPS) sequences. This work has had tremendous impacts in the fields of mathematics and engineering. For instance, DPS sequences have been used for spectrum estimation [91]. In signal processing, they have been used in particular for estimation [100] and approximation and prediction of bandlimited signals [101]. They constantly find applications to new areas. In this thesis, we apply DPS to communications specifically to MIMO systems employing antenna selection. We now introduce the DPS sequences which are used as basis functions to predict and estimate time-varying frequency-flat channels as described in the next section.

The orthogonal DPS sequences are simultaneously bandlimited to the frequency range $[-\nu_{\max}, +\nu_{\max}]$ and energy-concentrated in the time interval $\mathcal{I}_{\text{bl}} = \{0, 1, \ldots,$

$M'-1\}$. The energy concentration of a DPS sequence $\{u_d[m]\}$ in the time interval $\mathcal{I}_{\text{bl}}$ is defined as [86, 100]

$$\lambda_d = \frac{\sum_{m=0}^{M'-1} |u_d[m]|^2}{\sum_{m=-\infty}^{+\infty} |u_d[m]|^2}, \quad d \in \{0, 1, \ldots, M'-1\}. \tag{2.7}$$

The M' DPS sequences $\{u_d[m] \mid m \in \mathbb{Z}\}_{d=0}^{M'-1}$ are defined as the real solutions to the following system of linear equations [86]

$$\sum_{l=0}^{M'-1} A[l-m]\, u_d[l] = \lambda_d u_d[m], \qquad m \in \mathbb{Z},\ d \in \mathcal{I}_{\text{bl}} \tag{2.8}$$

where

$$A[l-m] = \frac{\sin(2\pi\nu_{\max}(l-m))}{\pi(l-m)}. \tag{2.9}$$

The eigenvalues $\{\lambda_d\}_{d=0}^{M'-1}$ decay exponentially for $d \geq D'$, where the essential subspace dimension D' is given by [86]

$$D' = \lceil 2\nu_{\max} M' \rceil + 1 \tag{2.10}$$

and $\lceil x \rceil$ denotes the smallest integer greater than or equal to x.

As mentioned earlier, the DPS sequences $\{u_d[m] \mid m \in \mathbb{Z}\}_{d=0}^{M'-1}$ are orthogonal. Further, even the restrictions of the DPS sequences on $\mathcal{I}_{\text{bl}}$, i.e., $\{u_d[m] \mid m \in \mathcal{I}_{\text{bl}}\}_{d=0}^{M'-1}$, are orthonormal [86], i.e.,

$$\sum_{m=0}^{M'-1} u_d[m] u_{d'}[m] = \lambda_d \sum_{m=-\infty}^{+\infty} u_d[m] u_{d'}[m] = \delta_{dd'} \tag{2.11}$$

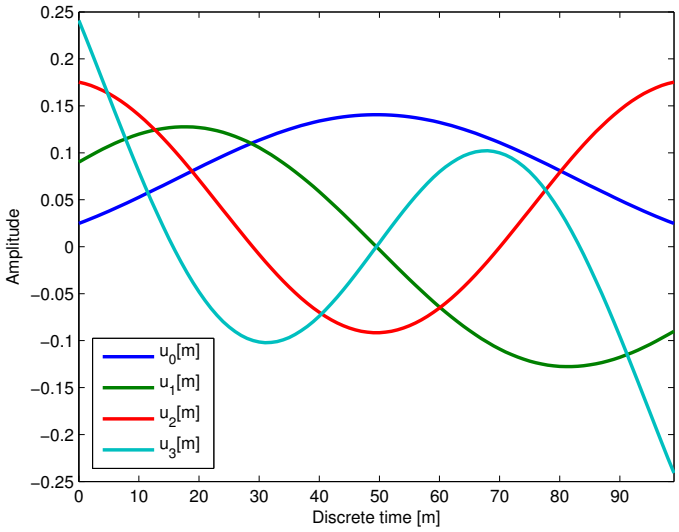

Figure 2.1: Slepian sequences in the discrete time interval $\mathcal{I}_{\mathrm{bl}} = \{0, 1, \ldots, 99\}$ with maximum normalized Doppler bandwidth $\nu_{\max} = 0.0114$.

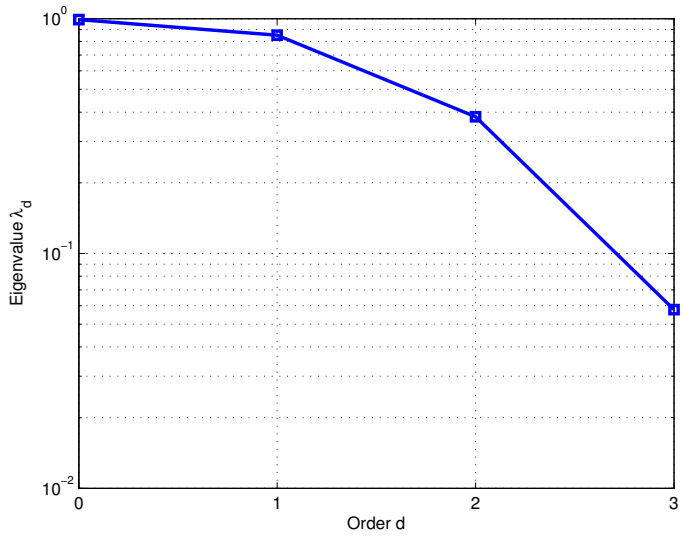

Figure 2.2: The corresponding eigenvalues for the Slepian sequences in the discrete time interval $\mathcal{I}_{\mathrm{bl}} = \{0, 1, \ldots, 99\}$ with $\nu_{\max} = 0.0114$.

where $d, d' \in \{0, \ldots, M'-1\}$. Thus, $\{u_d[m] \mid m \in \mathcal{I}_{\rm bl}\}_{d=0}^{M'-1}$ form a set of M'-length basis vectors $\{\boldsymbol{u}_d\}_{d=0}^{M'-1}$. Based on (2.8), the length-M' basis vectors $\{\boldsymbol{u}_d\}_{d=0}^{M'-1}$ are, thus, the eigenvectors of the $M' \times M'$ matrix $\boldsymbol{A}$ [86]

$$\boldsymbol{A}\boldsymbol{u}_d = \lambda_d \boldsymbol{u}_d \tag{2.12}$$

where $M' \times 1$ basis vector $\boldsymbol{u}_d \triangleq [u_d[0], u_d[1], \ldots, u_d[M'-1]]^T$ with $(\cdot)^T$ denoting the transpose. The entries of $\boldsymbol{A}$ are formed from (2.9) as $[\boldsymbol{A}]_{l,m} = A[l-m]$ for $l,\ m \in \mathcal{I}_{\rm bl}$. As shown in Sec. 2.5.1, the DPS sequences time-limited to $\mathcal{I}_{\rm bl}$, which form an orthonormal set of basis functions $\{\boldsymbol{u}_d\}_{d=0}^{M'-1}$, can be used to estimate the time-varying channel over $\mathcal{I}_{\rm bl}$.

Figs. 2.1 and 2.2 depict the Slepian sequences and their corresponding eigenvalues in the discrete time interval $\mathcal{I}_{\rm bl} = \{0, 1, \ldots, 99\}$ with $\nu_{\max} = 0.0114$. A different example can be found in [100].

2.5 Slepian Basis Expansion Model

Next-generation wireless systems are envisioned to provide high data rate and reliable services in high mobility environments [1, 2]. As mentioned above, the mobile communication environment is characterized by a randomly time-varying multipath channel due to the mobility of users and reflections from multiple scatterers. To achieve reliable communication, accurate channel knowledge is necessary at the receiver. In high mobility environments, the Doppler frequency is high and the channel changes rapidly over time. This implies that channel state information (CSI) gets rapidly outdated, limiting the accuracy of the channel knowledge at the receiver. In time-varying fading, pilot-aided channel prediction/estimation methods are essential

due to the short coherence time of the channel.

The optimal Wiener predictor/estimator utilizes detailed covariance knowledge to estimate time-varying frequency-flat fading [13, 25, 52]. This knowledge is difficult to obtain due to bursty transmission, or over the short time interval in which the channel WSS in vehicular scenarios [70, 100, 101]. This motivates the use of the recently-proposed low-complexity Slepian basis expansion channel estimator [86, 100] and channel predictor [86, 101] to obtain reliable CSI at the receiver. Unlike many linear estimation/prediction techniques that require detailed covariance knowledge, this Slepian basis expansion estimator/predictor requires only knowledge or estimate of the Doppler frequency.

In short, in basis expansion estimation/prediction techniques, preliminary channel gain estimates are first obtained from the observations over the pilot symbols. Then, (time-invariant) basis expansion coefficients are obtained from the estimates. The channel gains over a length-M' time interval are approximated as linear combinations, i.e., weighted linear sum of a specific set of (time-varying) basis functions [14, 34, 56, 62, 82, 100]. The weights are the estimated expansion coefficients. In general, the accuracy of any basis expansion model depends on the set of basis functions. The basis functions of the Slepian channel estimator/predictor are the DPS sequences [86]. They capture the fading temporal variations because they are bandlimited the maximum Doppler frequency of the channel. The Fourier basis expansion estimator uses complex exponential basis functions [34, 56, 62, 82, 100].

In summary, the Slepian estimator/predictor takes into account the Doppler rates of the channel. Only knowledge or estimate of the Doppler bandwidth is needed.

2.5.1 Slepian Basis Expansion Channel Estimator

To enable estimation of a time-varying frequency-flat channel for a length-M' block of data transmission, $M'-J$ data symbols and J interleaved pilot symbols are transmitted in a pattern specified by index set $\mathcal{J}$.

The aforementioned DPS sequences time-limited to $\mathcal{I}_{\rm bl} = \{0, 1, \ldots, M'-1\}$ are used to estimate the time-varying channel over time interval $\mathcal{I}_{\rm bl}$. Denote the channel gain estimates by $\left\{\hat{h}^{\rm SE}[m] \mid m \in \mathcal{I}_{\rm bl}\right\}$, where the superscript $(\cdot)^{\rm SE}$ indicates Slepian esitmation [100]. The basis expansion estimator approximates the $M'\times 1$ true channel vector $\boldsymbol{h} \triangleq [h[0], h[1], \ldots, h[M'-1]]^T$ in terms of a linear combination $\hat{\boldsymbol{h}}^{\rm SE}$ of D length-M' basis vectors $\{\boldsymbol{u}_d\}_{d=0}^{D-1}$ as [100, 101]

$$\boldsymbol{h} \approx \hat{\boldsymbol{h}}^{\rm SE} = \boldsymbol{U}\hat{\boldsymbol{c}} = \sum_{d=0}^{D-1} \hat{c}_d \boldsymbol{u}_d \tag{2.13}$$

where $\boldsymbol{U} \triangleq [\boldsymbol{u}_0, \ldots, \boldsymbol{u}_{D-1}]$ is an $M'\times D$ matrix, $\boldsymbol{u}_d \triangleq [u_d[0], u_d[1], \ldots, u_d[M'-1]]^T$, and D is the subspace dimension, i.e., number of basis functions. It is given by [101]

$$D = \underset{d\,\in\,\{1,\ldots,J\}}{\operatorname{argmin}} \left(\frac{1}{2\nu_{\max} J} \sum_{i=d}^{J-1} \lambda_i + \frac{d}{J} N_{\rm o} \right) \tag{2.14}$$

where the signal-to-noise ratio (SNR) is defined as $\eta \triangleq \frac{1}{N_{\rm o}}$ with $N_{\rm o}$ the noise power and data symbols are drawn with equal probability from a constant modulus constellation, i.e., the average symbol energy $E_{\rm s} = 1$. We note that the dimension D in (2.14) depends on the maximum normalized Doppler frequency $\nu_{\max}$, the channel SNR, and the number of pilot symbols.

In general, estimates of the Doppler rate and SNR are required. Therefore mismatched or imperfect estimates of the Doppler rate and SNR affect the generation of DPS sequences in (2.8) and dimension D in (2.14). This further reduces accuracy of the DPS representation since perfect knowledge of the Doppler frequency and SNR cannot be obtained in practice. It should also be noted that the mean-squared error in the DPS representation is not guaranteed to decrease monotonically as SNR increases. In the subsequent chapters, based on (2.14) an approach to determine the subspace dimension that reduces the mean square error (MSE) of the Slepian estimator/predictor is presented. In (2.14), the eigenvalues are assumed to be ranked as $\lambda_0 \geq \lambda_1 \geq \ldots \geq \lambda_{J-1}$. The $D \times 1$ vector $\hat{\boldsymbol{c}} \triangleq [\hat{c}_0, \hat{c}_1, \ldots, \hat{c}_{D-1}]^T$ contains the basis expansion coefficients. It is estimated using the J interleaved pilot symbols $\{p[l] \mid l \in \mathcal{J}\}$, received at times $l \in \mathcal{J}$, via [100]

$$\hat{\boldsymbol{c}} = \boldsymbol{G}^{-1} \sum_{l \in \mathcal{J}} y[l]\, p^*[l]\, \boldsymbol{f}^*[l] \tag{2.15}$$

where $(\cdot)^*$ denotes complex conjugate, $y[l]$ is the received signal, and the $D \times 1$ vector $\boldsymbol{f}[l]$ is defined as $[u_0[l], \ldots, u_{D-1}[l]]^T$, and $\boldsymbol{G}$ is a $D \times D$ matrix given by

$$\boldsymbol{G} = \sum_{l \in \mathcal{J}} \boldsymbol{f}[l]\, \boldsymbol{f}^\dagger[l]\, |p[l]|^2 \tag{2.16}$$

where $(\cdot)^\dagger$ denotes Hermitian transpose.

2.5.2 Slepian Basis Expansion Channel Predictor

The Slepian predictor uses the extension of the DPS sequences that are time-limited to $\mathcal{I}_{\text{bl}}$ as the basis vectors. They are calculated by [86, 101]

$$u_d[m] = \frac{1}{\lambda_d} \sum_{l=0}^{M'-1} A[l-m]\, u_d[l], \qquad m \in \mathbb{Z} \setminus \mathcal{I}_{\text{bl}} \tag{2.17}$$

where $A \setminus B$ denotes the set that contains all those elements of A that are not in B. Denote the predicted channel gains by $\left\{\hat{h}^{\text{SP}}[m] \mid m \in \mathbb{Z} \setminus \mathcal{I}_{\text{bl}}\right\}$, where the superscript $(\cdot)^{\text{SP}}$ indicates Slepian prediction [86, 101]. The Slepian prediction of a time-varying frequency-flat channel can be expressed as [101]

$$\hat{h}^{\text{SP}}[m] = \boldsymbol{f}^T[m]\, \hat{\boldsymbol{c}} = \sum_{d=0}^{D-1} \hat{c}_d u_d[m], \qquad m \in \mathbb{Z} \setminus \mathcal{I}_{\text{bl}} \tag{2.18}$$

where $\boldsymbol{f}[m] = [u_0[m], \ldots, u_{D-1}[m]]^T$.

We note that to generate the DPS basis functions for channel estimation and prediction $\mathcal{O}((M')^3)$ complex multiplications are required [37]. The matrix inversion of the $D \times D$ matrix $\boldsymbol{G}$ in (2.15) requires $\mathcal{O}(D^3)$ complex multiplications [37].

2.6 Fourier Basis Expansion Model

The Fourier expansion estimator/predictor uses orthogonal Fourier sequences as basis functions. They are given by [34, 100]

$$u_d[m] = \frac{1}{\sqrt{M'}} \exp\left(j2\pi \frac{\left(d - \frac{(D'-1)}{2}\right) m}{M'}\right), \qquad m \in \mathcal{I}_{\text{bl}} \tag{2.19}$$

for $d = 0, 1, \ldots, D' - 1$, where the essential subspace dimension $D' = \lceil 2\nu_{\max} M' \rceil + 1$. The Fourier basis expansion approximates the channel gain estimates over $\mathcal{I}_{\text{bl}}$ using (2.13) and (2.19). We note that the Fourier basis expansion model uses orthogonal Fourier sequences which do not capture the temporal variations of the channel.

Therefore, the Fourier-based estimator uses a fading-independent set of functions for channel estimation. These coefficients were included since they are often used for the quasi-static model where the channel gain variation is negligible.

2.7 Linear Interpolation/Extrapolation

From the observations $\{y[m] \mid m \in \mathcal{J}\}$ over the J received pilot symbols, linear interpolation/extrapolation is carried out to obtain channel gain estimates $\left\{\hat{h}^{\text{LIE}}[m] \mid m \in \mathcal{I}_{\text{bl}}\right\}$ over the discrete time interval $\mathcal{I}_{\text{bl}} = \{0, 1, \ldots, M' - 1\}$ as [23, 31]

$$\hat{h}^{\text{LIE}}[m] = \beta_1 m + \beta_2, \qquad m \in \mathcal{I}_{\text{bl}} \tag{2.20}$$

where the 2×1 vector $\boldsymbol{\beta} \triangleq [\beta_1, \beta_2]^T$ comprises the coefficients of the linear model. It is given by [23, 31]

$$\boldsymbol{\beta} = \left(\boldsymbol{V}^T \boldsymbol{V}\right)^{-1} \boldsymbol{V}^T \tilde{\boldsymbol{h}}, \qquad m \in \mathcal{J} \tag{2.21}$$

where the $J \times 2$ matrix $\boldsymbol{V}$ is given by [23, 31]

$$\boldsymbol{V} = \begin{bmatrix} \mathcal{J}[1] & 1 \\ \vdots & \vdots \\ \mathcal{J}[J] & 1 \end{bmatrix}. \tag{2.22}$$

In (2.22), $\mathcal{J}[l]$ for $l = 1, 2, \ldots, J$ is defined as the ith element of the pilot pattern index set $\mathcal{J}$. In (2.20), the $J \times 1$ vector $\tilde{\boldsymbol{h}}$ contains the preliminary channel gain estimates $\left\{\tilde{h}[m] \mid m \in \mathcal{J}\right\}$ obtained from the observations over the J received pilot symbols $\left\{y[m] \mid m \in \mathcal{J}\right\}$. The lth element of the $J \times 1$ vector $\tilde{\boldsymbol{h}}$ is defined as $\tilde{h}[l] = y[l]\, p^*[l]$, where $y[l]$ and $p[l]$ denote the received signal and pilot symbol at times $l \in \mathcal{J}$, respectively.

Notice that vector $\boldsymbol{V}$ is of size $J \times 2$, i.e., depends on number of pilot symbols. The computational complexity of linear interpolation/extrapolation in (2.20) is $\mathcal{O}(J)$.

Other interpolation methods include quadratic and spline interpolation [23, 31]. For more other techniques for channel prediction, we refer to [13, 19, 23, 26, 31, 60].

Chapter 3

Training Approaches for Selection of Single Antenna Subsystems in Doppler Fading

3.1 Introduction

To accommodate the rate and reliability requirements set by forthcoming applications such as mobile television, next-generation wireless standards such as IEEE 802.11n [1] and long term evolution (LTE) of the third generation partnership project (3GPP) [2] have adopted multiple input–multiple output (MIMO) technology, orthogonal frequency division multiplexing (OFDM) and/or orthogonal frequency division multiple access (OFDMA) as signalling formats over the physical channel. Further, antenna selection (AS) at the transmitter and/or receiver has been standardized in IEEE 802.11n [1].

Antenna selection may be used to reduce hardware complexity at the transmitter and/or receiver of a wireless system. In AS, only a subset of the antenna elements (AEs) is connected to a limited number of radio frequency (RF) chains based on the current channel fades. This potentially retains the advantages of multiple antennas,

despite using fewer of the expensive RF chains that are comprised of low-noise amplifiers (LNAs), mixers, and oscillators [65, 80]. We focus here on the single receive AS scenario because it retains most of the diversity benefits of multiple antennas while minimizing hardware complexity.

There are a number of existing studies on both optimal and suboptimal AS algorithms as well as on the capacity, diversity, and diversity-multiplexing performance of AS [9, 11, 12, 16, 22, 32, 33, 38–41, 46, 47, 51, 64, 66, 68, 95, 98, 102, 106]. However, to date, far fewer studies exist that deal with the practical issues of pilot-based training and AS implementation.

In most of the above references, perfect channel knowledge is assumed. However, the mobile communication environment exhibits a randomly time-varying channel due to the mobility of users and reflections from multiple scatterers. This implies that channel state information (CSI) gets rapidly outdated, limiting the accuracy of the channel knowledge at the receiver. The impact of erroneous CSI on the performance of a space-time coded AS system in Rayleigh fading is studied in [97]. The performance of maximal ratio transmission (MRT) and transmit antenna selection with space-time block coding (TAS/STBC) in MIMO systems with both CSI feedback delay and channel estimation error is analyzed in [44]. An analytical framework to evaluate the symbol error probability (SEP) performance for diversity systems in which a subset of the available diversity branches are selected and combined over flat Rayleigh fading with imperfect channel knowledge is developed in [35]. Receive AS for space-time-frequency (STF) coded MIMO-OFDM systems with imperfect channel estimation is studied in [67]. The effects of feedback delay and channel estimation errors on the performance of a MIMO system employing AS at the transmitter and maximal ratio

combining (MRC) at the receiver is studied in [73]. In [73], it is shown that channel estimation errors result in a fixed signal-to-noise ratio (SNR) loss while feedback delay alters the diversity order. Weighted AS rules for time-varying channels which use temporal correlation knowledge are proposed in [54, 55]. However, it is worth mentioning that only channel gain estimates obtained during the AS training phase are used in the selection and decoding mechanisms in [54] and [55] since channel gain estimates over the data transmission phase are not available, which incurs a loss in SNR. We also note that the weighted selection criterion used in [54] and [55] requires temporal correlation knowledge.

Motivated by the above observations, refs. [77–79] recently proposed low complexity training-based receive AS algorithms for time-varying channels. The methods employ both per-packet and symbol-by-symbol switching. They also use channel knowledge of the data transmission phase in the selection and decoding processes by utilizing a low training overhead Slepian predictor [101] and estimator [100]. This Slepian estimator/predictor only requires knowledge or estimate of the Doppler bandwidth. The contributions of this chapter are summarized as follows:

- A single receive antenna selection method for time-varying frequency-flat fading which uses Slepian basis expansion for prediction [101] and estimation [100] is proposed. An approach to determine the subspace dimension that reduces the mean square error (MSE) of the Slepian estimator/predictor is also presented.

- Analytical expressions for the symbol error probability (SEP) of `M`-ary phase-shift keying (`M`PSK) with receive AS are provided, along with corresponding simulations.

- Extensive simulation results are presented to compare the performance of the

proposed method to that of ideal conventional single input–single output (SISO) systems with perfect CSI but no AS at the receiver as well as AS based on conventional orthogonal Fourier based prediction/estimation. Performance comparison with linear prediction-based training with AS is reported in Chapter 5.

This chapter is organized as follows: the detailed system model is described in Section 3.2. The training-based receive AS method for time-varying frequency-flat fading is developed in Sec. 3.3. The SEP is analyzed in Sec. 3.4. Analytical and simulation results are discussed in Sec. 3.5. Our conclusions follow in Sec. 3.6.

3.2 System Model

Consider a system with one transmit, K_{r} receive antennas, but equipped with only one RF chain as depicted in Fig. 3.1. Depending on the AS switching time, either per-packet or symbol-by-symbol AS can be used. For example, microelectromechanical system (MEMS) switches may perform per-packet switching with negligible attenuation [75]. On the other hand, while solid-state switches can enable switching of antennas between symbols, their attenuation is non-negligible [88].

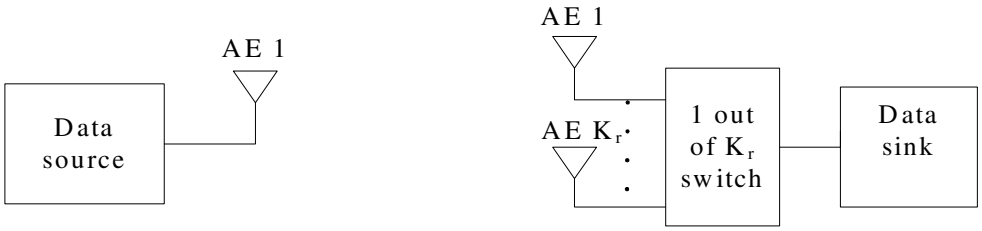

Figure 3.1: Antenna selection system model.

3.2.1 Channel and Signal Model

In wideband signals, the multipath delay spread is much longer than the transmitted signal duration. This implies that a discrete number of multipath components, L, can be resolved in time [36]. The channel is thus frequency-selective and modeled as a length-L finite impulse response (FIR) filter, for which the continuous time impulse response is given by [59, 74, 87]

$$h_{k_\mathrm{r}}(t,\tau) = \sum_{\ell=0}^{L-1} \sqrt{P(\tau_\ell)} w_{k_\mathrm{r},\ell}(t)\, \delta(\tau - \tau_\ell),\ k_\mathrm{r} = 1, 2, \ldots, K_\mathrm{r} \tag{3.1}$$

where $\delta(t)$ denotes the Dirac delta function, τ_ℓ is the propagation delay of the ℓth complex channel tap $w_{k_\mathrm{r},\ell}(t)$ of average power $P(\tau_\ell)$. $\{P(\tau_\ell)\}_{\ell=0}^{L-1}$ represent the channel power delay profile (PDP), normalized as $\sum_{\ell=0}^{L-1} P(\tau_\ell) = 1$. The wide sense stationary uncorrelated scattering (WSSUS) model is commonly used for multipath wireless channels [74,87]. The complex channel taps are wide sense stationary (WSS) narrowband complex Gaussian random processes. They are independent for each tap since the scatterers at different delays are uncorrelated. The Doppler frequency for each channel tap is proportional to the maximum normalized Doppler frequency [74, 87]

$$\nu_{\max} \triangleq f_\mathrm{D} T_\mathrm{s} = \frac{v_{\max} f_\mathrm{c}}{c_\mathrm{o}} T_\mathrm{s} \tag{3.2}$$

where T_s denotes the symbol duration and the Doppler frequency $f_\mathrm{D} \triangleq \frac{v_{\max} f_\mathrm{c}}{c_\mathrm{o}}$ with $v_{\max}$ the radial component of the user velocity, f_c the carrier frequency, and c_o the speed of light.

For narrowband signals the multipath delay spread is much shorter than the signal duration. The received multipath components are thus superimposed [36]. We note

that in multicarrier modulation such as OFDM, each OFDM subcarrier carries a narrowband signal that sees time-varying frequency-flat fading. In this chapter, time-varying frequency-flat fading is considered, i.e., where the symbol duration is much longer than the delay spread of the time-varying impulse response. We note that this assumption is actually relaxed somewhat in Chapter 5. From (3.1), the discrete-time channel impulse response between the single antenna transmitter and receive AE k_{r} is

$$h_{k_{\mathrm{r}}}[m] \triangleq h_{k_{\mathrm{r}}}(mT_{\mathrm{s}}, 0) = w_{k_{\mathrm{r}}}(mT_{\mathrm{s}}) \tag{3.3}$$

where standard sampling notation is used in (3.3), i.e., discrete-time signal $x[n]$ is obtained from continuous signal $x(t)$ by sampling at period T_{s} according to $x[n] \triangleq x(nT_{\mathrm{s}})$ with $n \in \mathbb{Z}$. Therefore, the time-varying frequency-flat channel represents a sequence of complex channel gain scalars at the symbol rate $R_{\mathrm{s}} \triangleq \frac{1}{T_{\mathrm{s}}}$ and bandlimited by $\nu_{\max}$.

Let m index discrete time with symbol rate R_{s}. The received signal at receive AE k_{r} can be expressed as

$$y_{k_{\mathrm{r}}}[m] = h_{k_{\mathrm{r}}}[m]\, s[m] + n_{k_{\mathrm{r}}}[m], \quad k_{\mathrm{r}} = 1, 2, \ldots, K_{\mathrm{r}} \tag{3.4}$$

where $s[m]$ is the transmitted MPSK symbol of unit average energy and $n_{k_{\mathrm{r}}}[m]$ is additive white Gaussian noise (AWGN) with variance N_{o} and is independent of the channel gain $h_{k_{\mathrm{r}}}[m]$.

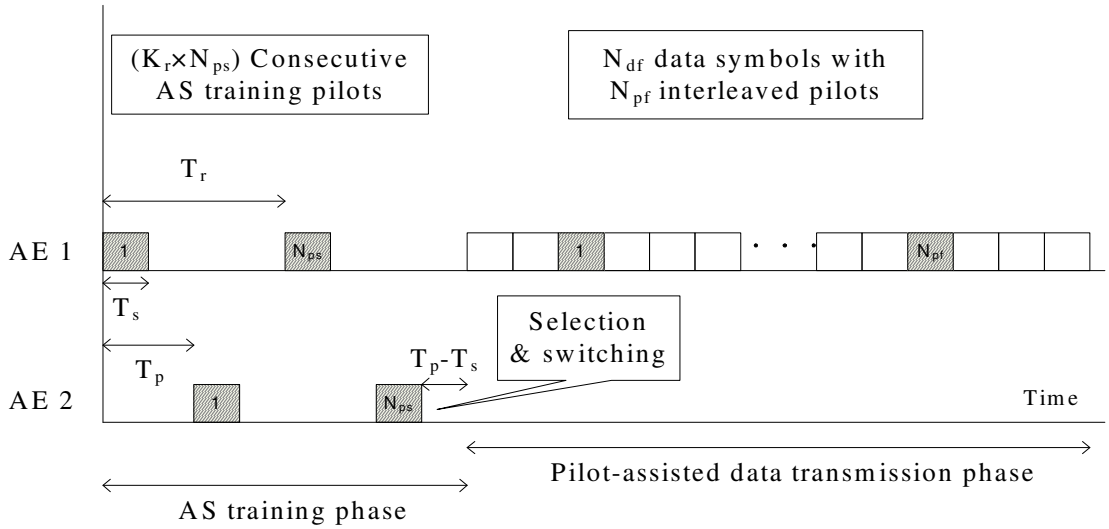

Figure 3.2: Antenna selection cycle for the proposed per-packet AS method. (AE 1 is selected, $K_{\mathrm{r}} = 2$ receive antennas, $N_{\mathrm{pf}} = 2$ post-selection pilots, $N_{\mathrm{ps}} = 2$ AS training pilots, and $T_p = 2\,T_s$).

3.2.2 Antenna Selection Cycle

Each AS cycle consists of an AS training phase followed by a pilot-assisted data transmission phase, as illustrated in Fig. 3.2.

Antenna Selection Training Phase

The AS training phase is formed by N_{ps} rounds of pilot transmission. In each round, one pilot is transmitted to each antenna. Therefore, each antenna receives N_{ps} AS pilot symbols. Thus, in total $K_{\mathrm{r}}N_{\mathrm{ps}}$ pilots are transmitted over N_{ps} rounds of transmission. The duration between consecutive training symbols in each round is $T_{\mathrm{p}} \triangleq \alpha T_{\mathrm{s}}$, where T_{s} is the symbol duration and $\alpha \in \mathbb{Z}^{+}$. Therefore, the duration between two consecutive training symbols transmitted in two consecutive rounds of transmission for each antenna is $T_{\mathrm{r}} \triangleq K_{\mathrm{r}}T_{\mathrm{p}} = \alpha K_{\mathrm{r}}T_{\mathrm{s}}$. In the first round, each transmitted pilot

is received by AE k_{r} at times $m \in (k_{\mathrm{r}}-1)\,T_{\mathrm{p}}$ for $k_{\mathrm{r}} = 1, 2, \ldots, K_{\mathrm{r}}$. In the second round, each transmitted pilot is received by AE k_{r} at times $m \in ((k_{\mathrm{r}}-1)\,T_{\mathrm{p}} + T_{\mathrm{r}})$ for $k_{\mathrm{r}} = 1, 2, \ldots, K_{\mathrm{r}}$, and so on. Thus AE k_{r} receives N_{ps} antenna selection training pilots at times $m \in T_{\mathrm{ps}}^{k_{\mathrm{r}}}$, where

$$\begin{aligned} T_{\mathrm{ps}}^{k_{\mathrm{r}}} &= \{[(k_{\mathrm{r}}-1)\,T_{\mathrm{p}} + (n_{\mathrm{ps}}-1)\,T_{\mathrm{r}}] \mid n_{\mathrm{ps}} = 1, 2, \ldots, N_{\mathrm{ps}}\} \\ &= \{\alpha\,((k_{\mathrm{r}}-1) + (n_{\mathrm{ps}}-1)\,K_{\mathrm{r}})\,T_{\mathrm{s}} \mid n_{\mathrm{ps}} = 1, 2, \ldots, N_{\mathrm{ps}}\} \\ &\triangleq \{\alpha\,[(k_{\mathrm{r}}-1) + (n_{\mathrm{ps}}-1)\,K_{\mathrm{r}}] \mid n_{\mathrm{ps}} = 1, 2, \ldots, N_{\mathrm{ps}}\} \end{aligned} \tag{3.5}$$

for $k_{\mathrm{r}} = 1, 2, \ldots, K_{\mathrm{r}}$, where in the last step, discrete-time notation is adopted.

The channel gain $h_{k_{\mathrm{r}}}[m]$ is estimated from the AS training pilot symbol $p_{k_{\mathrm{r}}}[m]$ that is received by AE k_{r} at time $m \in T_{\mathrm{ps}}^{k_{\mathrm{r}}}$. From (3.4), the received signal is

$$y_{k_{\mathrm{r}}}[m] = h_{k_{\mathrm{r}}}[m]\,p_{k_{\mathrm{r}}}[m] + n_{k_{\mathrm{r}}}[m], \qquad 1 \le k_{\mathrm{r}} \le K_{\mathrm{r}},\ m \in T_{\mathrm{ps}}^{k_{\mathrm{r}}} \tag{3.6}$$

where $T_{\mathrm{ps}}^{k_{\mathrm{r}}}$ is the set of time indices when the N_{ps} AS training pilots are received by AE k_{r}, $h_{k_{\mathrm{r}}}[m]$ is the sampled time-varying channel gain, and $n_{k_{\mathrm{r}}}[m]$ is AWGN with variance N_{o} and is independent of $h_{k_{\mathrm{r}}}[m]$. From the observations over the AS training pilots $\left\{y_{k_{\mathrm{r}}}[m] \mid m \in T_{\mathrm{ps}}^{k_{\mathrm{r}}}\right\}$ in (3.6), channel gain estimates $\left\{\tilde{h}_{k_{\mathrm{r}}}[m] \mid m \in T_{\mathrm{ps}}^{k_{\mathrm{r}}}\right\}$ for AE k_{r} are obtained as

$$\tilde{h}_{k_{\mathrm{r}}}[m] = y_{k_{\mathrm{r}}}[m]\,p_{k_{\mathrm{r}}}^{*}[m] \triangleq h_{k_{\mathrm{r}}}[m] + e_{k_{\mathrm{r}}}^{\mathrm{n}}[m], \quad 1 \le k_{\mathrm{r}} \le K_{\mathrm{r}},\ m \in T_{\mathrm{ps}}^{k_{\mathrm{r}}} \tag{3.7}$$

where $(\cdot)^{*}$ denotes complex conjugate and $e_{k_{\mathrm{r}}}^{\mathrm{n}}[m] \triangleq n_{k_{\mathrm{r}}}[m]\,p_{k_{\mathrm{r}}}^{*}[m]$ is the channel estimation error resulting from the AWGN with $p_{k_{\mathrm{r}}}[m]$ the constant modulus MPSK

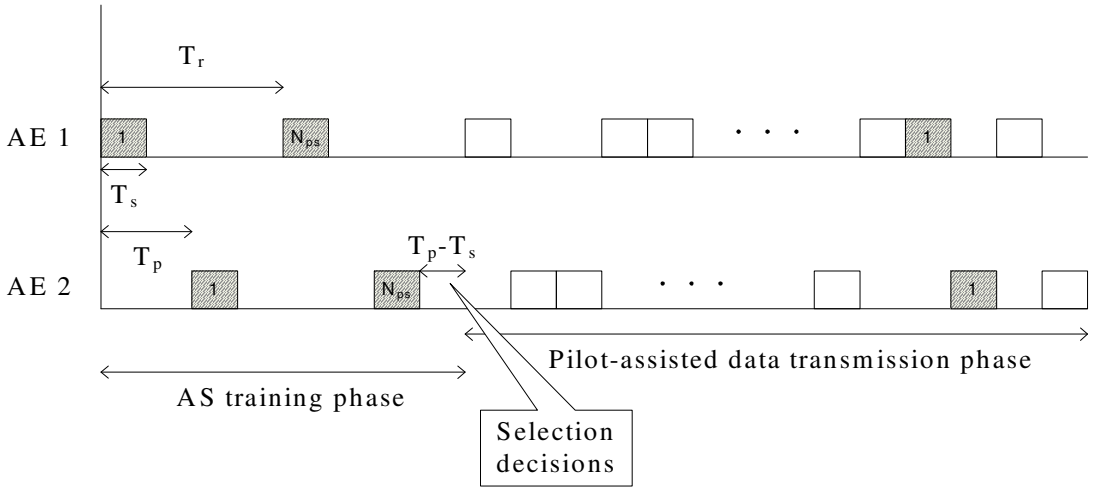

Figure 3.3: Antenna selection cycle for symbol-by-symbol AS method. ($K_{\mathrm{r}} = 2$ receive antennas, $N_{\mathrm{ps}} = 2$ AS training pilots, $N_{\mathrm{pf}} = 1$ post-selection pilot, and $T_p = 2\,T_s$).

pilot symbol of unit average energy. From (3.5) and accounting for the additional selection and switching time of duration $T_{\mathrm{p}} - T_{\mathrm{s}}$, it follows that the AS training phase spans the discrete time interval $\mathcal{I}_{\mathrm{ast}} = \{0, 1, \ldots, M-1\}$, where $M \triangleq \alpha K_{\mathrm{r}} N_{\mathrm{ps}}$.

Using the noisy channel estimates $\left\{\tilde{h}_{k_{\mathrm{r}}}[m] \mid m \in T_{\mathrm{ps}}^{k_{\mathrm{r}}}\right\}$, the receiver performs Slepian channel prediction [101] for each antenna over the pilot-assisted data transmission phase time interval $\mathcal{I}_{\mathrm{padt}}$. Denote the predicted channel gains by $\left\{\hat{h}_{k_{\mathrm{r}}}^{\mathrm{SP}}[m] \mid m \in \mathcal{I}_{\mathrm{padt}}\right\}$, where the superscript $(\cdot)^{\mathrm{SP}}$ indicates Slepian prediction. The receiver selects its receive antenna according to a certain criterion, and then switches its RF chain accordingly. We denote by $\hat{\imath}$ the index of the selected antenna, with $(\hat{\cdot})$ indicating that the selection is based on (imperfect) prediction and/or estimation. As depicted in Fig. 3.3, in symbol-by-symbol AS the most suitable receive AE $\hat{\imath}_m$ is selected for each symbol at time m, where symbol index m has been added to $\hat{\imath}$.

3.2.3 Pilot-Assisted Data Transmission Phase

In this section, the pilot-assisted data transmission phases for per-packet and symbol-by-symbol switching are described.

Per-Packet AS

In each pilot-assisted data transmission phase the transmitter sends out a length-$N \triangleq N_{\rm pf} + N_{\rm df}$ packet, which consists of $N_{\rm df}$ data symbols and $N_{\rm pf}$ interleaved post-selection pilot symbols. The pilot-assisted data transmission phase thus spans $\mathcal{I}_{\rm padt} = \{M, M+1 \ldots, M+N-1\}$. The $N_{\rm pf}$ pilot symbols are uniformly spread in the packet as

$$\begin{aligned} \mathcal{P}_{\rm pf} &\triangleq \left\{ \left\lfloor (n_{\rm pf}-1)\left(\frac{N}{N_{\rm pf}}\right) + \frac{1}{2}\left(\frac{N}{N_{\rm pf}}\right) \right\rfloor \;\middle|\; n_{\rm pf} = 1, \ldots, N_{\rm pf} \right\} \\ &= \left\{ \left\lfloor \frac{(2n_{\rm pf}-1)\,N}{2N_{\rm pf}} \right\rfloor \;\middle|\; n_{\rm pf} = 1, \ldots, N_{\rm pf} \right\} \end{aligned} \tag{3.8}$$

where $\lfloor x \rfloor$ denotes the largest integer not greater than x. From (3.8) and since the AS training phase spans the discrete times $\mathcal{I}_{\rm ast} = \{0, 1, \ldots, M-1\}$, after selection the $N_{\rm pf}$ pilot symbols are received by AE $\hat{\imath}$ at times $m \in T_{\rm pf}$, where

$$T_{\rm pf} \triangleq \left\{ M - 1 + \left\lfloor \frac{(2n_{\rm pf}-1)\,N}{2N_{\rm pf}} \right\rfloor \;\middle|\; n_{\rm pf} = 1, \ldots, N_{\rm pf} \right\}. \tag{3.9}$$

Thus, in total, $N_{\rm tp} \triangleq N_{\rm ps} + N_{\rm pf}$ training symbols are received by AE $\hat{\imath}$ at times

$$T_{\rm tp}^{\hat{\imath}} = T_{\rm ps}^{\hat{\imath}} \cup T_{\rm pf} \tag{3.10}$$

where $T_{\mathrm{ps}}^{\hat{\imath}}$ and T_{pf} are given in (3.5) and (3.9), respectively. From these N_{tp} pilot symbols, refined channel gain estimates $\{\hat{h}_{\hat{\imath}}^{\mathrm{SE}}[m] \mid m \in \mathcal{I}_{\mathrm{padt}}\}$ for the selected AE $\hat{\imath}$ are obtained using the Slepian basis expansion channel estimator and used to decode data.

The received signal at AE $\hat{\imath}$ can be expressed as

$$y_{\hat{\imath}}[m] = h_{\hat{\imath}}[m]\, s[m] + n_{\hat{\imath}}[m], \qquad m \in \mathcal{I}_{\mathrm{padt}} \tag{3.11}$$

where the transmitted symbol $s[m]$ is given by

$$s[m] = \begin{cases} d[m], & m \in \mathcal{I}_{\mathrm{padt}} \backslash T_{\mathrm{pf}} \\ p[m], & m \in T_{\mathrm{pf}} \end{cases} \tag{3.12}$$

where $d[m]$ and $p[m]$ denote the transmitted data and post-selection pilot symbols, respectively. $A \backslash B$ denotes the set that contains all those elements of A that are not in B.

Symbol-By-Symbol AS

The packet based description above can be analogously created for symbol-by-symbol AS. After selection, the transmitter sends out a length-$N' \triangleq N_{\mathrm{df}} + N'_{\mathrm{pf}}$ packet which consists of N_{df} data symbols and $N'_{\mathrm{pf}} \triangleq K_{\mathrm{r}} N_{\mathrm{pf}}$ pilot symbols. The $N'_{\mathrm{pf}} = K_{\mathrm{r}} N_{\mathrm{pf}}$ pilot symbols are needed to obtain refined channel gain estimates $\{\hat{h}_{\hat{\imath}^m}^{\mathrm{SE}}[m] \mid m \in \mathcal{I}_{\mathrm{padt}}\}$. The reason is that in symbol-by-symbol AS, for each symbol an AE is selected. Since different AEs might be selected during the data transmission phase $\mathcal{I}_{\mathrm{padt}}$, N_{pf} pilots should be sent to each AE in the data transmission phase so that refined channel

gain estimates can be obtained for each AE. The symbol locations in the packet that carry the $N_{\rm pf}$ pilots for AE $k_{\rm r}$ are given by

$$\begin{aligned}\mathcal{P}_{\rm pf}^{k_{\rm r}} &= \left\{(k_{\rm r}-1)+\left\lfloor (n_{\rm pf}-1)\left(\frac{N'}{N_{\rm pf}}\right)+\frac{1}{2}\left(\frac{N'}{N_{\rm pf}}\right)\right\rfloor \;\mid\; n_{\rm pf}=1,\ldots,N_{\rm pf}\right\} \\ &\triangleq \left\{(k_{\rm r}-1)+\left\lfloor \frac{(2n_{\rm pf}-1)\,N'}{2N_{\rm pf}}\right\rfloor \;\mid\; n_{\rm pf}=1,\ldots,N_{\rm pf}\right\} \end{aligned} \tag{3.13}$$

for $k_{\rm r}=1,2,\ldots,K_{\rm r}$. From (3.13) and since the AS training phase spans the discrete times $\mathcal{I}_{\rm ast}=\{0,1,\ldots,M-1\}$, the $N_{\rm pf}$ pilot symbols are thus received by AE $k_{\rm r}$ at times $m\in T_{\rm pf}^{k_{\rm r}}$, where

$$T_{\rm pf}^{k_{\rm r}} \triangleq \left\{M-1+(k_{\rm r}-1)+\left\lfloor \frac{(2n_{\rm pf}-1)\,N'}{2N_{\rm pf}}\right\rfloor \;\mid\; n_{\rm pf}=1,\ldots,N_{\rm pf}\right\}. \tag{3.14}$$

Thus $N_{\rm tp}=N_{\rm ps}+N_{\rm pf}$ pilots are received by each AE at times

$$T_{\rm tp}^{k_{\rm r}}=T_{\rm ps}^{k_{\rm r}}\cup T_{\rm pf}^{k_{\rm r}},\qquad k_{\rm r}=1,2,\ldots,K_{\rm r} \tag{3.15}$$

where $T_{\rm ps}^{k_{\rm r}}$ and $T_{\rm pf}^{k_{\rm r}}$ are given in (3.5) and (3.14), respectively. From these $N_{\rm tp}$ pilots, refined channel gain estimates $\{\hat{h}_{\hat{\imath}^m}^{\rm SE}[m]\,|\,m\in\mathcal{I}_{\rm padt}\}$ for the selected AE $\hat{\imath}_m$ are obtained using the Slepian estimator for data decoding.

The data symbols received by AE $\hat{\imath}_m$ are given by

$$y_{\hat{\imath}^m}[m]=h_{\hat{\imath}^m}[m]\,d[m]+n_{\hat{\imath}^m}[m],\quad m\in\mathcal{I}_{\rm padt}\backslash\left(T_{\rm pf}^{1}\cup\ldots\cup T_{\rm pf}^{K_{\rm r}}\right). \tag{3.16}$$

We note that in symbol-by-symbol AS the pilot-assisted data transmission phase spans the discrete times $\mathcal{I}_{\rm padt}=\{M,M+1,\ldots,M+N'-1\}$, where $N'=N_{\rm df}+$

$K_{\mathrm{r}}N_{\mathrm{pf}}$. However, in per-packet switching $\mathcal{I}_{\mathrm{padt}} = \{M, M+1, \ldots, M+N-1\}$ with $N = N_{\mathrm{df}} + N_{\mathrm{pf}}$. Therefore, $N' = N + N_{\mathrm{pf}}(K_{\mathrm{r}} - 1)$. From the above, it is clear that both per-packet and per-symbol AS can be treated in an analogous way.

3.3 Receive Antenna Selection Algorithm

In this section, receive antenna selection algorithms for SIMO systems equipped with K_{r} receive antennas out of which only one antenna is selected for time-varying frequency-flat fading for both per-packet and per-symbol switching are presented.

In summary, the antenna selection training phase is formed by sending N_{ps} training symbols, to each AE. From the observations over the training pilots $\{y_{k_{\mathrm{r}}}[m] \mid m \in T_{\mathrm{ps}}^{k_{\mathrm{r}}}\}$, channel gain estimates $\{\tilde{h}_{k_{\mathrm{r}}}[m] \mid m \in T_{\mathrm{ps}}^{k_{\mathrm{r}}}\}$ for each AE are obtained as in (3.7). We note that the CSI obtained from $\{\tilde{h}_{k_{\mathrm{r}}}[m]\}$ in (3.7) is outdated at the receiver. Slepian channel prediction [101] for each AE over the data transmission phase is therefore needed to perform antenna selection. Denote the number of Slepian basis functions, which are bandlimited by the maximum normalized Doppler frequency $\nu_{\max}$, by D. Note that the temporal variations of the channel are also proportional to $\nu_{\max}$. The D extensions $\{u_d[m] \mid m \in \mathcal{I}_{\mathrm{padt}}\}_{d=0}^{D-1}$ of the orthonormal Slepian sequences of length-M $\{u_d[m] \mid m \in \mathcal{I}_{\mathrm{ast}}\}_{d=0}^{D-1}$ over the data phase $\mathcal{I}_{\mathrm{padt}}$ are used for channel prediction. We note that the Slepian sequences $\{u_d[m] \mid m \in \mathcal{I}_{\mathrm{ast}}\}_{d=0}^{M-1}$ are the restrictions in time of the (infinite) discrete prolate spheroidal (DPS) sequences $\{u_d[m] \mid m \in \mathbb{Z}\}_{d=0}^{M-1}$ over the AS training time interval $\mathcal{I}_{\mathrm{ast}} = \{0, \ldots, M-1\}$. The dth Slepian sequence vector of size $M \times 1$ $\mathbf{u}_d[m] \triangleq [u_d[0], \ldots, u_d[M-1]]^T$ is the dth eigenvector of the $M \times M$ matrix $\mathbf{A}$ with (a, b) entry defined as $[\mathbf{A}]_{a,b} = \frac{\sin[2\pi\nu_{\max}(a-b)]}{\pi(a-b)}$, for $a, b = 0, 1, \ldots, M-1$ corresponding to eigenvalues $\lambda_0 \geq \lambda_1 \geq \ldots \geq \lambda_{M-1}$. The

D extensions $\{u_d[m] \mid m \in \mathcal{I}_{\text{padt}}\}_{d=0}^{D-1}$ of the orthonormal Slepian sequences can be calculated from

$$u_d[m] = \frac{1}{\lambda_d} \sum_{m'=0}^{M-1} \frac{\sin[2\pi\nu_{\max}(m'-m)]}{\pi(m'-m)} u_d[m'], \quad m \in \mathcal{I}_{\text{padt}}. \tag{3.17}$$

Selection is then performed based on the predicted channel gains $\{\hat{h}_{k_\text{r}}^{\text{SP}}[m] \mid m \in \mathcal{I}_{\text{padt}}\}$. In the data transmission phase, a packet containing pilot and data symbols is transmitted. Next, refined channel gain estimates for the selected AE obtained from the Slepian estimator [100] are used for data decoding. The basis functions $\{u_d[m] \mid m \in \mathcal{I}_{\text{padt}}\}_{d=0}^{D-1}$ for the Slepian estimator are a subset over the data phase $\mathcal{I}_{\text{padt}}$ of the complete Slepian sequences $\{u_d[m] \mid m \in \mathcal{I}_{\text{AS}}\}_{d=0}^{D-1}$ over the AS cycle time interval $\mathcal{I}_{\text{AS}} = \mathcal{I}_{\text{ast}} \cup \mathcal{I}_{\text{padt}}$.

3.3.1 Per-Packet AS

We propose the following training-based "one out of K_r" receive AS algorithm for time-varying channels for per-packet switching:

1. Following an AS request, each AE is trained using N_{ps} pilot symbols. The spacing between consecutive AS training pilots transmitted for each AE is $T_\text{r} = \alpha K_\text{r} T_\text{s}$. To keep the AS training phase as short as possible, α is chosen as

$$\alpha = \left\lceil \frac{T_{\text{sw}}}{T_\text{s}} \right\rceil + 1 \tag{3.18}$$

   where T_{sw} is the antenna switching time.

2. On receiving these AS training pilots, the receiver then:

(a) Obtains the preliminary channel gain estimates $\left\{\tilde{h}_{k_\mathrm{r}}[m] \mid m \in T_{\mathrm{ps}}^{k_\mathrm{r}}\right\}_{k_\mathrm{r}=1}^{K_\mathrm{r}}$ using (3.7).

(b) Performs channel prediction for each AE over the data time interval $\mathcal{I}_{\mathrm{padt}} \backslash T_{\mathrm{pf}}$ via (3.19)

$$\hat{h}_{k_\mathrm{r}}^{\mathrm{SP}}[m] = \boldsymbol{f}^T[m]\,\hat{\boldsymbol{c}}_{k_\mathrm{r}} = \sum_{d=0}^{D-1} \hat{c}_{k_\mathrm{r},d}\, u_d[m] \tag{3.19}$$

for $k_\mathrm{r} = 1, 2, \ldots, K_\mathrm{r}$, and D is the subspace dimension, i.e., number of basis functions. In (3.19), $\boldsymbol{f}[m] \triangleq [u_0[m], \ldots, u_{D-1}[m]]^T$ contains the D basis functions which can be calculated from (3.17) for $m \in \mathcal{I}_{\mathrm{padt}} \backslash T_{\mathrm{pf}}$. In (3.19), $\hat{\boldsymbol{c}}_{k_\mathrm{r}} \triangleq [\hat{c}_{k_\mathrm{r},0}, \ldots, \hat{c}_{k_\mathrm{r},D-1}]^T$ comprises the basis expansion coefficients for each AE k_r, is given by

$$\hat{\boldsymbol{c}}_{k_\mathrm{r}} = \Big(\sum_{m \in T_{\mathrm{ps}}^{k_\mathrm{r}}} \boldsymbol{f}[m]\, \boldsymbol{f}^\dagger[m]\, |p_{k_\mathrm{r}}[m]|^2 \Big)^{-1} \sum_{m \in T_{\mathrm{ps}}^{k_\mathrm{r}}} y_{k_\mathrm{r}}[m]\, p_{k_\mathrm{r}}^*[m]\, \boldsymbol{f}^*[m] \tag{3.20}$$

where $(\cdot)^*$ and $(\cdot)^\dagger$ denote complex conjugate and complex conjugate transpose, respectively.

(c) Selects its receive AE $\hat{\imath}$ which maximizes the post-processing SNR over the data time interval $\mathcal{I}_{\mathrm{padt}} \backslash T_{\mathrm{pf}}$, which consists of N_{df} symbol durations, as

$$\hat{\imath} = \underset{1 \le k_\mathrm{r} \le K_\mathrm{r}}{\operatorname{argmax}} \sum_{\substack{m=M \\ (m \neq T_{\mathrm{pf}})}}^{M+N-1} \left| \hat{h}_{k_\mathrm{r}}^{\mathrm{SP}}[m] \right|^2. \tag{3.21}$$

3. The transmitter then sends out a length-N data packet which consists of N_{df} data symbols plus N_{pf} post-selection pilot symbols interleaved according to (3.8). The packet is received by AE $\hat{\imath}$. Using the $N_{\mathrm{tp}} = N_{\mathrm{ps}} + N_{\mathrm{pf}}$ pilots, refined channel

gain estimates $\{\hat{h}_{\hat{\imath}}^{\mathrm{SE}}[m] \mid m \in \mathcal{I}_{\mathrm{padt}} \backslash T_{\mathrm{pf}}\}$ are obtained by

$$\hat{\boldsymbol{h}}_{\hat{\imath}}^{\mathrm{SE}} = \boldsymbol{U}' \, \hat{\boldsymbol{c}}_{\hat{\imath}} = \sum_{d=0}^{D-1} \hat{c}_{\hat{\imath},d} \, \boldsymbol{u}'_d \tag{3.22}$$

where the $N_{\mathrm{df}} \times 1$ vector $\hat{\boldsymbol{h}}_{\hat{\imath}}^{\mathrm{SE}}$ contains the entries $\hat{h}_{\hat{\imath}}^{\mathrm{SE}}[m]$ for $m \in \mathcal{I}_{\mathrm{padt}} \backslash T_{\mathrm{pf}}$, $\boldsymbol{U}' \triangleq \left[\boldsymbol{u}'_0, \ldots, \boldsymbol{u}'_{D-1}\right]$ is the $N_{\mathrm{df}} \times D$ submatrix of the complete $(M+N) \times D$ Slepian sequences matrix $\boldsymbol{U}$, and the $N_{\mathrm{df}} \times 1$ vector $\boldsymbol{u}'_d$ contains the basis functions $\{u_d[m] \mid m \in \mathcal{I}_{\mathrm{padt}} \backslash T_{\mathrm{pf}}\}$. In (3.22), $\hat{\boldsymbol{c}}_{\hat{\imath}} \triangleq [\hat{c}_{\hat{\imath},0}, \ldots, \hat{c}_{\hat{\imath},D-1}]^T$ can be calculated from (3.20) with $T_{\mathrm{tp}}^{\hat{\imath}}$ given in (3.10) replacing $T_{\mathrm{ps}}^{k_{\mathrm{r}}}$.

3.3.2 Symbol-By-Symbol AS

The training-based "one out of K_{r}" symbol-by-symbol receive AS algorithm for time-varying channels comprises the following steps, which are conducted following an AS request:

1. Each antenna is trained using N_{ps} pilot symbols. The spacing between consecutive pilot symbols is $T_{\mathrm{r}} = \alpha K_{\mathrm{r}} T_{\mathrm{s}}$, where $\alpha \geq 1$ since the antenna switching time T_{sw} is less than the symbol duration T_{s}.

2. The receiver then:

   (a) Performs channel prediction for every AE via (3.19) over the data time interval $m \in \mathcal{I}_{\mathrm{padt}} \backslash (T_{\mathrm{pf}}^1 \cup \ldots \cup T_{\mathrm{pf}}^{K_{\mathrm{r}}})$.

   (b) Selects its receive AE $\hat{\imath}_m$ for the data symbol at time $m \in \mathcal{I}_{\mathrm{padt}} \backslash (T_{\mathrm{pf}}^1 \cup \ldots \cup T_{\mathrm{pf}}^{K_{\mathrm{r}}})$ according to

$$\hat{\imath}_m = \underset{1 \leq k_{\mathrm{r}} \leq K_{\mathrm{r}}}{\operatorname{argmax}} \left| \hat{h}_{k_{\mathrm{r}}}^{\mathrm{SP}}[m] \right|^2. \tag{3.23}$$

To denote this alternative AS strategy, symbol index m has been added to $\hat{\imath}$ in (3.23).

3. The transmitter sends out a length-$N' = N_{\rm df}+K_{\rm r}N_{\rm pf}$ data packet, which consists of $N_{\rm df}$ data symbols and $N'_{\rm pf} = K_{\rm r}N_{\rm pf}$ pilots interleaved as (3.13). Each data symbol at time $m \in \mathcal{I}_{\rm padt}\backslash(T^1_{\rm pf} \cup \ldots \cup T^{K_{\rm r}}_{\rm pf})$ is received by a different AE $\hat{\imath}_m$. Using the $N_{\rm tp} = N_{\rm ps} + N_{\rm pf}$ pilots at each AE, refined channel gain estimates $\{\hat{h}^{\rm SE}_{\hat{\imath}_m}[m] \mid m \in \mathcal{I}_{\rm padt}\backslash(T^1_{\rm pf} \cup \ldots \cup T^{K_{\rm r}}_{\rm pf})\}$ are obtained by

$$\hat{h}^{\rm SE}_{\hat{\imath}_m}[m] = \sum_{d=0}^{D-1} \hat{c}_{\hat{\imath}_m,d}\, u_d[m] \tag{3.24}$$

where the basis functions $\left\{u_d[m] \,|\, m \in \mathcal{I}_{\rm padt}\backslash\left(T^1_{\rm pf} \cup \ldots \cup T^{K_{\rm r}}_{\rm pf}\right)\right\}_{d=0}^{D-1}$ are a subset over the data time interval $m \in \mathcal{I}_{\rm padt}\backslash\left(T^1_{\rm pf} \cup \ldots \cup T^{K_{\rm r}}_{\rm pf}\right)$ of the complete length-$(M+N')$ Slepian sequences $\{u_d[m] \,|\, m \in \mathcal{I}_{\rm AS}\}_{d=0}^{D-1}$ over the AS cycle interval $\mathcal{I}_{\rm AS} = \{0, \ldots, M+N'-1\}$ with $N' = N_{\rm df} + K_{\rm r}N_{\rm pf}$.

3.3.3 Choice of Subspace Dimension

In this subsection, an approach for obtaining the subspace dimension D that reduces the MSE of the Slepian estimator/predictor is presented.

The MSE per sample for the Slepian basis expansion estimator of AE $k_{\rm r}$ is [79,101]

$$\mathrm{MSE}^{\rm SE}_{k_{\rm r}}[m] = (\mathrm{bias}^{\rm SE}_{k_{\rm r}}[m])^2 + \mathrm{var}^{\rm SE}_{k_{\rm r}}[m] \tag{3.25}$$

where $\mathrm{bias}^{\rm SE}_{k_{\rm r}}[m]$ and $\mathrm{var}^{\rm SE}_{k_{\rm r}}[m]$ are the bias and variance terms, respectively. In (3.25),

the squared bias term may be calculated in the frequency domain as

$$\begin{aligned}\left(\mathrm{bias}_{k_\mathrm{r}}^{\mathrm{SE}}[m]\right)^2 &= \int_{-\frac{1}{2}}^{+\frac{1}{2}} \left|1-\boldsymbol{f}^T[m]\,\boldsymbol{G}_{k_\mathrm{r}}^{-1}\sum_{m'\in T_{\mathrm{tp}}^{k_\mathrm{r}}}\boldsymbol{f}^*[m']\exp\left(-j2\pi\nu\left(m-m'\right)\right)\right|^2 \\ &\quad \times S_\mathrm{h}(\nu)\,\mathrm{d}\nu \end{aligned} \tag{3.26}$$

where the $D\times 1$ vector $\boldsymbol{f}[m]=[u_0[m],\ldots,u_{D-1}[m]]^T$ and $S_\mathrm{h}(\nu)$ is the power spectral density (PSD) of the time-varying channel. We note that $S_\mathrm{h}(\nu)$ is known as Clarke's spectrum, which is given by [18]

$$S_\mathrm{h}(\nu)=\begin{cases}\frac{1}{\pi\nu_{\max}\sqrt{1-\left(\frac{\nu}{\nu_{\max}}\right)^2}} & |\nu|<\nu_{\max},\\ 0 & \text{otherwise.}\end{cases} \tag{3.27}$$

In (3.26), $\boldsymbol{G}_{k_\mathrm{r}}$ is a $D\times D$ matrix given by

$$\boldsymbol{G}_{k_\mathrm{r}}=\sum_{m'\in T_{\mathrm{tp}}^{k_\mathrm{r}}}\boldsymbol{f}[m']\,\boldsymbol{f}^\dagger[m']\,|p[m']|^2 \tag{3.28}$$

In (3.25), $\mathrm{var}_{k_\mathrm{r}}^{\mathrm{SE}}[m]$ can be well approximated by [79, 100, 101]

$$\mathrm{var}_{k_\mathrm{r}}^{\mathrm{SE}}[m]\approx N_\mathrm{o}\boldsymbol{f}^\dagger[m]\,\boldsymbol{G}_{k_\mathrm{r}}^{-1}\boldsymbol{f}[m]\,. \tag{3.29}$$

The MSE of the Slepian estimator over $\mathcal{I}_{\mathrm{padt}}$ for AE k_r can thus be estimated as

$$\mathrm{MSE}_{k_\mathrm{r},N}^{\mathrm{SE}}=\frac{1}{N}\sum_{m=M}^{M+N-1}\mathrm{MSE}_{k_\mathrm{r}}^{\mathrm{SE}}[m] \tag{3.30}$$

where $\mathrm{MSE}_{k_\mathrm{r}}^{\mathrm{SE}}[m]$ is given in (3.25).

We note that MSE for the Slepian basis expansion predictor can be obtained from (3.25)–(3.30) by replacing superscript $(\cdot)^{\mathrm{SE}}$ by $(\cdot)^{\mathrm{SP}}$ and $T_{\mathrm{tp}}^{k_{\mathrm{r}}}$ by $T_{\mathrm{ps}}^{k_{\mathrm{r}}}$ in (3.26), (3.28), and (3.29).

Note that the MSE in (3.30) depends on the subspace dimension D. This clearly implies that dimension D affects the MSE of Slepian estimator/predictor. The subspace dimension D used in (3.30) can be calculated from [101]

$$D = \underset{d\in\{1,\ldots,N_{\mathrm{tp}}\}}{\operatorname{argmin}} \left(\frac{1}{2\nu_{\max} N_{\mathrm{tp}}} \sum_{i=d}^{N_{\mathrm{tp}}-1} \lambda_i + \frac{d}{N_{\mathrm{tp}}} N_{\mathrm{o}} \right). \tag{3.31}$$

where SNR is defined as $\eta = \frac{1}{N_{\mathrm{o}}}$ with N_{o} the noise power and constant-modulus signal, i.e., average symbol energy $E_{\mathrm{s}} = 1$. The dimension D in (3.31) depends on the maximum normalized Doppler frequency $\nu_{\max}$, SNR, and number of pilot symbols.

In general, estimates of the Doppler frequency and SNR are required. Therefore mismatched or imperfect estimates of the Doppler frequency and SNR affect the generation of DPS sequences and dimension D in (3.31). This further reduces accuracy of the DPS representation since perfect knowledge of the Doppler frequency and SNR cannot be obtained in practice. It should also be noted that the mean-squared error in the DPS representation is not guaranteed to decrease monotonically as SNR increases. We note that the basis expansion coefficients in (3.20) depend on SNR, dimension D, and number of pilot symbols. Thus, an early increase in dimension D at low to moderate SNR values results in inaccurate coefficients estimates. This increases MSE since estimation is performed as a linear sum of basis functions weighted by expansion coefficients. However, at high SNR values expansion coefficients estimates are more reliable since channel gain estimates obtained from pilot symbols are accurate. Notice that the estimator error variance in (3.29) also depends on dimension D, SNR, and

number of pilots. Thus, estimation error variance increases with dimension D at low to moderate SNR which results in an increase in MSE. Therefore, it is always beneficial/desirable to avoid an increase in MSE resulting from an early or bad choice of dimension D.

Using the MSE expression in (3.30) and dimension D in (3.31), we develop an approach for obtaining the subspace dimension that reduces the MSE of the Slepian estimator/predictor. This also reduces the SEP of the proposed system since it affects the selection and decoding mechanisms. The idea is to decrease (and keep fixed) the value of dimension D when an increase in MSE occurs in an SNR interval. The approach comprises the following steps:

1. Calculate the MSE of the Slepian estimator in (3.30), which we denote as MSE$'$, by using D in (3.31) over the SNR interval $[\eta_{\min}, \eta_{\max}]$.

2. If MSE$'$ decreases as SNR increases, i.e., the MSE versus SNR curve shows no upward transition then:

   Solution: The subspace dimension D in (3.31) is used for Slepian estimation over $[\eta_{\min}, \eta_{\max}]$.

3. Otherwise, if there is an upward transition in the MSE curve then:

   (a) Denote the SNR and subspace dimension at which the upward transition occurs by η_{ip} and D_{ip}, respectively. Compute the MSE in (3.30), denoted by MSE$''$, using D_{ip} over $[\eta_{\min}, \eta_{\max}]$.

   (b) Denote the SNR value at which MSE$'$ and MSE$''$ curves intersect over $(\eta_{\text{ip}}, \eta_{\max}]$ by η_{int}.

Solution: The subspace dimension D for Slepian estimation over $[\eta_{\min},\ \eta_{\max}]$ is given by

$$D = \begin{cases} \text{argmin}_{d\in\{1,\ldots,N_{\text{tp}}\}} \left(\frac{1}{2\nu_{\max} N_{\text{tp}}} \sum_{i=d}^{N_{\text{tp}}-1} \lambda_i + \frac{d}{N_{\text{tp}}} N_{\text{o}} \right), & \text{for } [\eta_{\min},\ \eta_{\text{ip}}) \\ D_{\text{ip}}, & \text{for } [\eta_{\text{ip}},\ \eta_{\text{int}}] \\ \text{argmin}_{d\in\{1,\ldots,N_{\text{tp}}\}} \left(\frac{1}{2\nu_{\max} N_{\text{tp}}} \sum_{i=d}^{N_{\text{tp}}-1} \lambda_i + \frac{d}{N_{\text{tp}}} N_{\text{o}} \right), & \text{for } (\eta_{\text{int}},\ \eta_{\max}] \end{cases} . \tag{3.32}$$

We note that (3.32) uses dimension D in (3.31) over SNR intervals $[\eta_{\min},\ \eta_{\text{ip}})$ and $(\eta_{\text{int}},\ \eta_{\max}]$, while in suboptimal SNR interval $[\eta_{\text{ip}},\ \eta_{\text{int}}]$ it uses D_{ip}. Thus, it is constant (equal to D_{ip}) over $[\eta_{\text{ip}},\ \eta_{\text{int}}]$.

3.4 Symbol Error Probability (SEP) Analysis

In this section, we analyze the proposed receive AS algorithm from Section 3.3, to evaluate the SEP of MPSK in time-varying channels. We note that the SEP analysis is extended to include other M-ary modulations in Chapter 4.

3.4.1 Prediction and Estimation CSI Models

To derive analytical expressions for the variances of the predicted/estimated channel gains and prediction/estimation errors, we first define the CSI uncertainty model for Slepian basis expansion estimation as

$$\hat{h}_{k_{\text{r}}}^{\text{SE}}[m] = h_{k_{\text{r}}}[m] + e_{k_{\text{r}}}^{\text{SE}}[m], \qquad 1 \le k_{\text{r}} \le K_{\text{r}},\ m \in \mathcal{I}_{\text{padt}} \tag{3.33}$$

where $\hat{h}_{k_\mathrm{r}}^{\mathrm{SE}}[m]$ is the estimated channel gain, $h_{k_\mathrm{r}}[m]$ is the true channel gain, and $e_{k_\mathrm{r}}^{\mathrm{SE}}[m]$ is the estimation error. We assume the variables $h_{k_\mathrm{r}}[m]$ and $e_{k_\mathrm{r}}^{\mathrm{SE}}[m]$ are uncorrelated. The true channel gain $h_{k_\mathrm{r}}[m]$ is modeled as a zero-mean circularly symmetric complex Gaussian random variable (RV) with unit-variance.

From (3.33), the variance of the channel gain estimate $\hat{h}_{k_\mathrm{r}}^{\mathrm{SE}}[m]$ can be expressed as

$$\sigma^2_{\hat{h}_{k_\mathrm{r}}^{\mathrm{SE}}}[m] = \sigma^2_{h_{k_\mathrm{r}}}[m] + \sigma^2_{e_{k_\mathrm{r}}^{\mathrm{SE}}}[m] = 1 + \mathrm{MSE}_{k_\mathrm{r}}^{\mathrm{SE}}[m] \tag{3.34}$$

where the variance of the Slepian estimation error $\sigma^2_{e_{k_\mathrm{r}}^{\mathrm{SE}}}[m]$ is equal to the MSE for the Slepian basis expansion estimator of AE k_r in (3.25).

The CSI model for the Slepian basis expansion predictor can be obtained from (3.33) and (3.34) by replacing superscript $(\cdot)^{\mathrm{SE}}$ by $(\cdot)^{\mathrm{SP}}$ and $T_{\mathrm{tp}}^{k_\mathrm{r}}$ by $T_{\mathrm{ps}}^{k_\mathrm{r}}$ in (3.25).

3.4.2 SEP Analysis

SEP of Per-Packet Basis Selection

We now analyze the SEP of an MPSK symbol received at time m of a system which employs the per-packet basis receive AS algorithm in Sec. 3.3.1. Note that the predicted channel gains $\left\{\hat{h}_{k_\mathrm{r}}^{\mathrm{SP}}[m] \mid m \in \mathcal{I}_{\mathrm{padt}}\right\}_{k_\mathrm{r}=1}^{K_\mathrm{r}}$ are used to select AE $\hat{\imath}$ to receive the length-N data packet, while the estimated channel gain $\hat{h}_{\hat{\imath}}^{\mathrm{SE}}[m]$ is used to decode the received symbol at time m.

The maximum-likelihood (ML) soft estimate for the symbol received by AE $\hat{\imath}$ at

time m can be expressed as

$$\begin{aligned} r_{\hat{\imath}}[m] &= \left(\hat{h}_{\hat{\imath}}^{\mathrm{SE}}[m]\right)^{*} y_{\hat{\imath}}[m] \\ &= \left|\hat{h}_{\hat{\imath}}^{\mathrm{SE}}[m]\right|^{2} d[m] - \left(\hat{h}_{\hat{\imath}}^{\mathrm{SE}}[m]\right)^{*} d[m]\, e_{\hat{\imath}}^{\mathrm{SE}}[m] + \left(\hat{h}_{\hat{\imath}}^{\mathrm{SE}}[m]\right)^{*} n_{\hat{\imath}}[m] \end{aligned} \quad (3.35)$$

where the last equality follows from substitution of (3.11) and (3.33). Conditioned on $\hat{h}_{\hat{\imath}}^{\mathrm{SE}}[m]$ and $d[m]$, $r_{\hat{\imath}}[m]$ in (3.35) is a complex Gaussian RV whose conditional mean $\mu_{r_{\hat{\imath}}}[m]$ and variance $\sigma_{r_{\hat{\imath}}}^{2}[m]$, as shown in Appendix A, are given by

$$\begin{aligned} \mu_{r_{\hat{\imath}}}[m] &\triangleq \mathbb{E}\left\{ r_{\hat{\imath}}[m] \mid \hat{h}_{\hat{\imath}}^{\mathrm{SE}}[m], d[m] \right\} \\ &= \left|\hat{h}_{\hat{\imath}}^{\mathrm{SE}}[m]\right|^{2} d[m]\, \zeta_{\hat{\imath}}^{\mathrm{SE}}[m] \end{aligned} \quad (3.36)$$

$$\begin{aligned} \sigma_{r_{\hat{\imath}}}^{2}[m] &\triangleq \mathrm{var}\left\{ r_{\hat{\imath}}[m] \mid \hat{h}_{\hat{\imath}}^{\mathrm{SE}}[m], d[m] \right\} \\ &= \left|\hat{h}_{\hat{\imath}}^{\mathrm{SE}}[m]\right|^{2} |d[m]|^{2} \left(1 - \zeta_{\hat{\imath}}^{\mathrm{SE}}[m]\right) + N_{\mathrm{o}} \left|\hat{h}_{\hat{\imath}}^{\mathrm{SE}}[m]\right|^{2} \end{aligned} \quad (3.37)$$

where $\mathbb{E}\{\cdot\}$ and $\mathrm{var}\{\cdot\}$ denote statistical expectation and variance, respectively. $\zeta_{\hat{\imath}}^{\mathrm{SE}}[m] \triangleq \frac{1}{1+\sigma_{e_{\hat{\imath}}^{\mathrm{SE}}}^{2}[m]} = \frac{1}{1+\mathrm{MSE}_{\hat{\imath}}^{\mathrm{SE}}[m]}$, and the other symbols are defined in (3.12) and (3.34).

Conditioned on $\hat{\imath}$ and $\hat{h}_{\hat{\imath}}^{\mathrm{SE}}[m]$, the SEP of an MPSK symbol received at time m $\mathrm{SEP}_m\left(\hat{\imath}, \hat{h}_{\hat{\imath}}^{\mathrm{SE}}[m]\right)$ can be computed via the method found in [5, 54, 79] as

$$\begin{aligned} \mathrm{SEP}_m\left(\hat{\imath}, \hat{h}_{\hat{\imath}}^{\mathrm{SE}}[m]\right) &= \frac{1}{\pi} \int_{0}^{\frac{\mathtt{M}-1}{\mathtt{M}}\pi} \exp\left(\frac{-\left|\mu_{r_{\hat{\imath}}}[m]\right|^{2} \sin^{2}\left(\frac{\pi}{\mathtt{M}}\right)}{\sigma_{r_{\hat{\imath}}}^{2}[m] \sin^{2}(\theta)} \right) \mathrm{d}\theta \\ &= \frac{1}{\pi} \int_{0}^{\frac{\mathtt{M}-1}{\mathtt{M}}\pi} \exp\left(\frac{-\left|\hat{h}_{\hat{\imath}}^{\mathrm{SE}}[m]\right|^{2} b_{\hat{\imath}}^{\mathrm{SE}}[m]}{\sin^{2}(\theta)} \right) \mathrm{d}\theta \end{aligned} \quad (3.38)$$

where $b_{k_\mathrm{r}}^{\mathrm{SE}}[m] \triangleq \frac{\left(\zeta_{k_\mathrm{r}}^{\mathrm{SE}}[m]\right)^2 \sin^2\left(\frac{\pi}{\mathtt{M}}\right)}{\left(1-\zeta_{k_\mathrm{r}}^{\mathrm{SE}}[m]\right)+\frac{1}{\eta}}$ with $\eta = \frac{E_\mathrm{s}}{N_\mathrm{o}}$ the average SNR, and the last equality follows from substitution of (3.36) and (3.37).

Averaging over the index $\hat{\imath}$ to get $\mathrm{SEP}_m\left(\left\{\hat{h}_{k_\mathrm{r}}^{\mathrm{SE}}[m]\right\}_{k_\mathrm{r}=1}^{K_\mathrm{r}}\right)$ yields

$$\begin{aligned}\mathrm{SEP}_m\left(\left\{\hat{h}_{k_\mathrm{r}}^{\mathrm{SE}}[m]\right\}_{k_\mathrm{r}=1}^{K_\mathrm{r}}\right) &= \sum_{k_\mathrm{r}=1}^{K_\mathrm{r}} \Pr\left(\hat{\imath}=k_\mathrm{r}\right) \mathrm{SEP}_m\left(\hat{\imath}=k_\mathrm{r}, \hat{h}_{\hat{\imath}}^{\mathrm{SE}}[m]\right) \\ &= \frac{1}{\pi}\sum_{k_\mathrm{r}=1}^{K_\mathrm{r}}\left(\prod_{\substack{l=1\\ l\neq k_\mathrm{r}}}^{K_\mathrm{r}} \Pr\left(\sum_{\substack{m=M\\ (m\neq T_{\mathrm{pf}})}}^{M+N-1}\left|\hat{h}_l^{\mathrm{SP}}[m]\right|^2 < \sum_{\substack{m=M\\ (m\neq T_{\mathrm{pf}})}}^{M+N-1}\left|\hat{h}_{k_\mathrm{r}}^{\mathrm{SP}}[m]\right|^2\right)\right) \\ &\quad \int_0^{\frac{\mathtt{M}-1}{\mathtt{M}}\pi} \exp\left(\frac{-\left|\hat{h}_{k_\mathrm{r}}^{\mathrm{SE}}[m]\right|^2 b_{k_\mathrm{r}}^{\mathrm{SE}}[m]}{\sin^2(\theta)}\right)\mathrm{d}\theta.\end{aligned} \tag{3.39}$$

After averaging over fading, the SEP as a function of the SNR per branch η is

$$\begin{aligned}\mathrm{SEP}_m(\eta) &= \frac{1}{\pi}\sum_{k_\mathrm{r}=1}^{K_\mathrm{r}} \int_0^{\frac{\mathtt{M}-1}{\mathtt{M}}\pi}\int_0^\infty\int_0^\infty \exp\left(\frac{-x'\, b_{k_\mathrm{r}}^{\mathrm{SE}}[m]}{\sin^2(\theta)}\right) f_{X'_{k_\mathrm{r}},Y'_{k_\mathrm{r}}}(x',y') \\ &\quad \times \prod_{\substack{l=1\\ l\neq k_\mathrm{r}}}^{K_\mathrm{r}} F_{Y'_l}(y')\,\mathrm{d}x'\mathrm{d}y'\mathrm{d}\theta\end{aligned} \tag{3.40}$$

where $f_{X'_{k_\mathrm{r}},Y'_{k_\mathrm{r}}}(x',y')$ is the joint probability distribution of the exponentially distributed RV $X'_{k_\mathrm{r}} \triangleq \left|\hat{h}_{k_\mathrm{r}}^{\mathrm{SE}}[m]\right|^2$ and RV $Y'_{k_\mathrm{r}} \triangleq \sum_{\substack{m=M\\ (m\neq T_{\mathrm{pf}})}}^{M+N-1}\left|\hat{h}_{k_\mathrm{r}}^{\mathrm{SP}}[m]\right|^2$. Thus, Y'_{k_r} is the sum of correlated exponentially distributed RVs, and $F_{Y'_{k_\mathrm{r}}}(y')$ denotes its cumulative distribution function (CDF). Deriving an analytical expression for $\mathrm{SEP}_m(\eta)$ in (3.40) is analytically intractable since analytical expressions for $f_{X'_{k_\mathrm{r}},Y'_{k_\mathrm{r}}}(x',y')$ and $F_{Y'_{k_\mathrm{r}}}(y')$ do not exist. Therefore, Monte Carlo averaging techniques [28] are used to evaluate

the fading-averaged SEP $\mathrm{SEP}_m(\eta)$ from $\mathrm{SEP}_m\left(\left\{\hat{h}_{k_\mathrm{r}}^{\mathrm{SE}}[m]\right\}_{k_\mathrm{r}=1}^{K_\mathrm{r}}\right)$.

We next derive the SEP of MPSK for a system that performs receive AS on a symbol-by-symbol basis as in Sec. 3.3.2. As shown in the next section, symbol-by-symbol AS is analytically tractable and provides insights for per-packet AS.

Symbol-By-Symbol AS SEP

We note that receive AS is on an instantaneous symbol-by-symbol basis according to (3.23) in Sec. 3.3.2.

Theorem 3.1. The SEP of an MPSK symbol received at time m in a time-varying channel for a system with one transmit and K_r receive antennas employing selection criterion (3.23) with channel gain estimate $\hat{h}_{\hat{\iota}_m}^{\mathrm{SE}}[m]$ to decode an MPSK symbol received at time m is given by

$$\begin{aligned}
SEP_m(\eta) \;=\; & \frac{1}{\pi}\sum_{k_r=1}^{K_r}\sum_{z=0}^{K_r-1}\sum_{\substack{l_0,\ldots,l_z=1\\ l_0=1,\, l_1\neq\ldots\neq l_z\neq k_r}}^{K_r}\frac{(-1)^z}{z!\left(4\sigma_{k_r,c_1}^2[m]\right)}\\
&\times\frac{1}{\sigma_{k_r,c_2}^2[m]\left(1-\left[\rho_{k_r,c_1c_2}^2[m]+\rho_{k_r,c_1s_2}^2[m]\right]\right)}\\
&\int_0^{\frac{M-1}{M}\pi}\int_0^\infty\int_0^\infty\exp\left(\frac{-x\,b_{k_r}^{SE}[m]}{\sin^2(\theta)}\right.\\
&-y\sum_{j=1}^{z}\zeta_{l_j}^{SP}[m]-\left[\frac{x}{\sigma_{k_r,c_1}^2[m]}+\frac{y}{\sigma_{k_r,c_2}^2[m]}\right]\\
&\left.\times\frac{1}{2\left(1-\left[\rho_{k_r,c_1c_2}^2[m]+\rho_{k_r,c_1s_2}^2[m]\right]\right)}\right)\\
&\times I_0\left(\frac{\sqrt{\rho_{k_r,c_1c_2}^2[m]+\rho_{k_r,c_1s_2}^2[m]}}{\left(1-\left[\rho_{k_r,c_1c_2}^2[m]+\rho_{k_r,c_1s_2}^2[m]\right]\right)}\right.\\
&\left.\times\frac{\sqrt{xy}}{\sigma_{k_r,c_1}[m]\,\sigma_{k_r,c_2}[m]}\right)\mathrm{d}x\,\mathrm{d}y\,\mathrm{d}\theta
\end{aligned}\tag{3.41}$$

where the notation $\sum_{\substack{l_0,\ldots,l_z=1 \\ l_0=1,\, l_1\neq\ldots\neq l_z\neq k_\mathrm{r}}}^{K_\mathrm{r}}$ denotes $\sum_{l_0=1}^{1}\sum_{\substack{l_1=1 \\ (l_1\neq k_\mathrm{r})}}^{K_\mathrm{r}}\sum_{\substack{l_2=1 \\ (l_2\neq k_\mathrm{r}, l_2\neq l_1)}}^{K_\mathrm{r}}\cdots\sum_{\substack{l_z=1 \\ (l_z\neq k_\mathrm{r},\, l_z\neq l_1,\ldots,\, l_z\neq l_{z-1})}}^{K_\mathrm{r}}$, $\zeta_{l_j}^{\mathrm{SP}}[m] \triangleq \frac{1}{\sigma^2_{\hat{h}_{l_j}^{\mathrm{SP}}}[m]} = \frac{1}{1+\sigma^2_{e_{l_j}^{\mathrm{SP}}}[m]} = \frac{1}{1+\mathrm{MSE}_{l_j}^{\mathrm{SP}}}$, $b_{k_\mathrm{r}}^{\mathrm{SE}}[m] \triangleq \frac{\left(\zeta_{k_\mathrm{r}}^{\mathrm{SE}}[m]\right)^2 \sin^2\left(\frac{\pi}{\mathtt{M}}\right)}{\left(1-\zeta_{k_\mathrm{r}}^{\mathrm{SE}}[m]\right)+\frac{1}{\eta}}$, and $I_0(\cdot)$ is the zeroth-order modified Bessel function of the first kind. In (3.41), $\rho_{k_\mathrm{r},c_1c_2}[m]$ and $\rho_{k_\mathrm{r},c_1s_2}[m]$ denote the correlation coefficients of $(X_{k_\mathrm{r},c_1}[m], X_{k_\mathrm{r},c_2}[m])$ and $(X_{k_\mathrm{r},c_1}[m], X_{k_\mathrm{r},s_2}[m])$, respectively, where $\hat{h}_{k_\mathrm{r}}^{\mathrm{SE}}[m] \triangleq X_{k_\mathrm{r},c_1}[m]+jX_{k_\mathrm{r},s_1}[m]$ and $\hat{h}_{k_\mathrm{r}}^{\mathrm{SP}}[m] \triangleq X_{k_\mathrm{r},c_2}[m] +jX_{k_\mathrm{r},s_2}[m]$, and $(X_{k_\mathrm{r},c_1}[m], X_{k_\mathrm{r},s_1}[m])$ and $(X_{k_\mathrm{r},c_2}[m], X_{k_\mathrm{r},s_2}[m])$ are i.i.d. zero-mean Gaussian RVs with variances $\sigma^2_{k_\mathrm{r},c_1}[m] = \sigma^2_{k_\mathrm{r},s_1}[m]$ and $\sigma^2_{k_\mathrm{r},c_2}[m] = \sigma^2_{k_\mathrm{r},s_2}[m]$, respectively.

Proof. The ML soft estimate for the symbol received by AE $\hat{\imath}_m$ at time m can be expressed as

$$\begin{aligned} r_{\hat{\imath}_m}[m] &= \left(\hat{h}_{\hat{\imath}_m}^{\mathrm{SE}}[m]\right)^* y_{\hat{\imath}_m}[m] \\ &= \left|\hat{h}_{\hat{\imath}_m}^{\mathrm{SE}}[m]\right|^2 d[m] - \left(\hat{h}_{\hat{\imath}_m}^{\mathrm{SE}}[m]\right)^* d[m]\, e_{\hat{\imath}_m}^{\mathrm{SE}}[m] + \left(\hat{h}_{\hat{\imath}_m}^{\mathrm{SE}}[m]\right)^* n_{\hat{\imath}_m}[m] \end{aligned} \tag{3.42}$$

where the last equality follows from substitution of (3.16) and (3.33).

Conditioned on $\hat{h}_{\hat{\imath}_m}^{\mathrm{SE}}[m]$ and $d[m]$, $r_{\hat{\imath}_m}[m]$ in (3.42) is a complex Gaussian RV whose conditional mean $\mu_{r_{\hat{\imath}_m}}[m]$ and variance $\sigma^2_{r_{\hat{\imath}_m}}[m]$ are given by

$$\mu_{r_{\hat{\imath}_m}}[m] = \left|\hat{h}_{\hat{\imath}_m}^{\mathrm{SE}}[m]\right|^2 d[m]\, \zeta_{\hat{\imath}_m}^{\mathrm{SE}}[m] \tag{3.43}$$

$$\sigma^2_{r_{\hat{\imath}_m}}[m] = \left|\hat{h}_{\hat{\imath}_m}^{\mathrm{SE}}[m]\right|^2 |d[m]|^2 \left(1-\zeta_{\hat{\imath}_m}^{\mathrm{SE}}[m]\right) + N_\mathrm{o}\left|\hat{h}_{\hat{\imath}_m}^{\mathrm{SE}}[m]\right|^2 \tag{3.44}$$

where $\zeta_{\hat{\imath}_m}^{\mathrm{SE}}[m] \triangleq \frac{1}{1+\sigma^2_{e_{\hat{\imath}_m}^{\mathrm{SE}}}[m]} = \frac{1}{1+\mathrm{MSE}_{\hat{\imath}_m}^{\mathrm{SE}}}$.

Conditioned on $\hat{\imath}_m$ and $\hat{h}_{\hat{\imath}_m}^{\mathrm{SE}}[m]$, the SEP of an MPSK symbol received at time m can be computed via the method found in [5, 54, 79]

$$\begin{aligned}\mathrm{SEP}_m\left(\hat{\imath}_m, \hat{h}_{\hat{\imath}_m}^{\mathrm{SE}}[m]\right) &= \frac{1}{\pi}\int_0^{\frac{\mathtt{M}-1}{\mathtt{M}}\pi} \exp\left(\frac{-\left|\mu_{r_{\hat{\imath}_m}}[m]\right|^2 \sin^2\left(\frac{\pi}{\mathtt{M}}\right)}{\sigma^2_{r_{\hat{\imath}_m}}[m]\,\sin^2(\theta)}\right) \mathrm{d}\theta \\ &= \frac{1}{\pi}\int_0^{\frac{\mathtt{M}-1}{\mathtt{M}}\pi} \exp\left(\frac{-\left|\hat{h}_{\hat{\imath}_m}^{\mathrm{SE}}[m]\right|^2 b_{\hat{\imath}_m}^{\mathrm{SE}}[m]}{\sin^2(\theta)}\right) \mathrm{d}\theta\end{aligned} \tag{3.45}$$

where $b_{k_{\mathrm{r}}}^{\mathrm{SE}}[m] \triangleq \frac{\left(\zeta_{k_{\mathrm{r}}}^{\mathrm{SE}}[m]\right)^2 \sin^2\left(\frac{\pi}{\mathtt{M}}\right)}{\left(1-\zeta_{k_{\mathrm{r}}}^{\mathrm{SE}}[m]\right)+\frac{1}{\eta}}$, and the last equality follows from substituting (3.43) and (3.44).

Now averaging over the index $\hat{\imath}_m$ to get $\mathrm{SEP}_m\left(\left\{\hat{h}_{k_{\mathrm{r}}}^{\mathrm{SE}}[m]\right\}_{k_{\mathrm{r}}=1}^{K_{\mathrm{r}}}\right)$ yields

$$\begin{aligned}\mathrm{SEP}_m\left(\left\{\hat{h}_{k_{\mathrm{r}}}^{\mathrm{SE}}[m]\right\}_{k_{\mathrm{r}}=1}^{K_{\mathrm{r}}}\right) &= \sum_{k_{\mathrm{r}}=1}^{K_{\mathrm{r}}} \Pr\left(\hat{\imath}_m = k_{\mathrm{r}}\right) \mathrm{SEP}_m\left(\hat{\imath}_m = k_{\mathrm{r}}, \hat{h}_{\hat{\imath}_m}^{\mathrm{SE}}[m]\right) \\ &= \frac{1}{\pi}\sum_{k_{\mathrm{r}}=1}^{K_{\mathrm{r}}} \left(\prod_{\substack{l=1 \\ l\neq k_{\mathrm{r}}}}^{K_{\mathrm{r}}} \Pr\left(\left|\hat{h}_l^{\mathrm{SP}}[m]\right|^2 < \left|\hat{h}_{k_{\mathrm{r}}}^{\mathrm{SP}}[m]\right|^2\right)\right) \\ &\quad \times \int_0^{\frac{\mathtt{M}-1}{\mathtt{M}}\pi} \exp\left(\frac{-\left|\hat{h}_{k_{\mathrm{r}}}^{\mathrm{SE}}[m]\right|^2 b_{k_{\mathrm{r}}}^{\mathrm{SE}}[m]}{\sin^2(\theta)}\right) \mathrm{d}\theta.\end{aligned} \tag{3.46}$$

The expression for the SEP, when averaging over fading, becomes

$$\begin{aligned}\mathrm{SEP}_m(\eta) &= \frac{1}{\pi}\sum_{k_\mathrm{r}=1}^{K_\mathrm{r}}\int_0^{\frac{\mathtt{M}-1}{\mathtt{M}}\pi}\int_0^{\infty}\int_0^{\infty}\exp\left(\frac{-x\, b_{k_\mathrm{r}}^{\mathrm{SE}}[m]}{\sin^2(\theta)}\right) f_{X_{k_\mathrm{r}},Y_{k_\mathrm{r}}}(x,y)\\ &\quad\times\prod_{\substack{l=1\\ l\neq k_\mathrm{r}}}^{K_\mathrm{r}} F_{Y_l}(y)\,\mathrm{d}x\mathrm{d}y\mathrm{d}\theta \qquad (3.47)\end{aligned}$$

where $f_{X_{k_\mathrm{r}},Y_{k_\mathrm{r}}}(x,y)$ is the joint probability density function (PDF) of the two correlated exponentially distributed RVs $X_{k_\mathrm{r}} \triangleq \left|\hat{h}_{k_\mathrm{r}}^{\mathrm{SE}}[m]\right|^2 = |X_{k_\mathrm{r},c_1}[m] + jX_{k_\mathrm{r},s_1}[m]|^2 = (X_{k_\mathrm{r},c_1}[m])^2 + (X_{k_\mathrm{r},s_1}[m])^2$ and $Y_{k_\mathrm{r}} \triangleq \left|\hat{h}_{k_\mathrm{r}}^{\mathrm{SP}}[m]\right|^2 = |X_{k_\mathrm{r},c_2}[m] + jX_{k_\mathrm{r},s_2}[m]\,|^2 = (X_{k_\mathrm{r},c_2}[m])^2 + (X_{k_\mathrm{r},s_2}[m])^2$ given by [63]

$$\begin{aligned}f_{X_{k_\mathrm{r}},Y_{k_\mathrm{r}}}(x,y) &= \frac{1}{4\sigma_{k_\mathrm{r},c_1}^2[m]\,\sigma_{k_\mathrm{r},c_2}^2[m]\left(1-\left[\rho_{k_\mathrm{r},c_1c_2}^2[m]+\rho_{k_\mathrm{r},c_1s_2}^2[m]\right]\right)}\\ &\quad\times\exp\left(\frac{-1}{2\left(1-\left[\rho_{k_\mathrm{r},c_1c_2}^2[m]+\rho_{k_\mathrm{r},c_1s_2}^2[m]\right]\right)}\left[\frac{x}{\sigma_{k_\mathrm{r},c_1}^2[m]}+\frac{y}{\sigma_{k_\mathrm{r},c_2}^2[m]}\right]\right)\\ &\quad\times I_0\left(\frac{\sqrt{\rho_{k_\mathrm{r},c_1c_2}^2[m]+\rho_{k_\mathrm{r},c_1s_2}^2[m]}}{\left(1-\left[\rho_{k_\mathrm{r},c_1c_2}^2[m]+\rho_{k_\mathrm{r},c_1s_2}^2[m]\right]\right)}\times\frac{\sqrt{xy}}{\sigma_{k_\mathrm{r},c_1}[m]\,\sigma_{k_\mathrm{r},c_2}[m]}\right) \qquad (3.48)\end{aligned}$$

where $x, y \geq 0$, $I_0(\cdot)$ is the zeroth-order modified Bessel function of the first kind, $(X_{k_\mathrm{r},c_1}[m], X_{k_\mathrm{r},s_2}[m])$ and $(X_{k_\mathrm{r},c_2}[m], X_{k_\mathrm{r},s_2}[m])$ are i.i.d. zero-mean Gaussian RVs with variances $\sigma_{k_\mathrm{r},c_1}^2[m] = \sigma_{k_\mathrm{r},s_1}^2[m]$ and $\sigma_{k_\mathrm{r},c_2}^2[m] = \sigma_{k_\mathrm{r},s_2}^2[m]$, respectively. $\rho_{k_\mathrm{r},c_1c_2}[m]$ and $\rho_{k_\mathrm{r},c_1s_2}[m]$ are the correlation coefficients of $(X_{k_\mathrm{r},c_1}[m], X_{k_\mathrm{r},c_2}[m])$ and $(X_{k_\mathrm{r},c_1}[m]$, $X_{k_\mathrm{r},s_2}[m])$, respectively, and lie in $(-1,1)$.

In (3.47), $F_{Y_l}(y)$ is the CDF of the exponentially distributed RV $Y_l \triangleq \left|\hat{h}_l^{\mathrm{SP}}[m]\right|^2$,

and is given by

$$F_{Y_l}(y) = \begin{cases} 1 - \exp\left(-\zeta_l^{\mathrm{SP}}[m]\ y\right), & y \geq 0 \\ 0, & y < 0 \end{cases} \tag{3.49}$$

where the rate parameter is $\zeta_l^{\mathrm{SP}}[m] \triangleq \frac{1}{1+\sigma^2_{e_l^{\mathrm{SP}}}[m]} = \frac{1}{1+\mathrm{MSE}_l^{\mathrm{SP}}[m]}$.

Substituting (3.49) and (3.48) into (3.47) yields

$$\begin{aligned} \mathrm{SEP}_m(\eta) &= \frac{1}{\pi}\sum_{k_{\mathrm{r}}=1}^{K_{\mathrm{r}}} \int_0^{\frac{\mathtt{M}-1}{\mathtt{M}}\pi} \int_0^{\infty}\int_0^{\infty} \exp\left(\frac{-x\, b_{k_{\mathrm{r}}}^{\mathrm{SE}}[m]}{\sin^2(\theta)}\right) f_{X_{k_{\mathrm{r}}},Y_{k_{\mathrm{r}}}}(x,y) \\ &\quad \times \prod_{\substack{l=1 \\ l\neq k_{\mathrm{r}}}}^{K_{\mathrm{r}}} \left(1-\exp\left(-\zeta_l^{\mathrm{SP}}[m]\ y\right)\right) \mathrm{d}x\,\mathrm{d}y\,\mathrm{d}\theta \qquad (3.50) \\ &= \frac{1}{\pi}\sum_{k_{\mathrm{r}}=1}^{K_{\mathrm{r}}}\sum_{z=0}^{K_{\mathrm{r}}-1} \sum_{\substack{l_0,\ldots,l_z=1 \\ l_0=1,\, l_1\neq\ldots\neq l_z\neq k_{\mathrm{r}}}}^{K_{\mathrm{r}}} \frac{(-1)^z}{z!\left(4\sigma^2_{k_{\mathrm{r}},c_1}[m]\right)} \\ &\quad \frac{1}{\sigma^2_{k_{\mathrm{r}},c_2}[m]\left(1-\left[\rho^2_{k_{\mathrm{r}},c_1c_2}[m]+\rho^2_{k_{\mathrm{r}},c_1s_2}[m]\right]\right)} \\ &\quad \int_0^{\frac{\mathtt{M}-1}{\mathtt{M}}\pi}\int_0^{\infty}\int_0^{\infty} \exp\left(\frac{-x\, b_{k_{\mathrm{r}}}^{\mathrm{SE}}[m]}{\sin^2(\theta)} - y\sum_{j=1}^{z}\zeta_{l_j}^{\mathrm{SP}}[m]\right. \\ &\quad \left. -\frac{1}{2\left(1-\left[\rho^2_{k_{\mathrm{r}},c_1c_2}[m]+\rho^2_{k_{\mathrm{r}},c_1s_2}[m]\right]\right)}\left[\frac{x}{\sigma^2_{k_{\mathrm{r}},c_1}[m]}+\frac{y}{\sigma^2_{k_{\mathrm{r}},c_2}[m]}\right]\right) \\ &\quad I_0\left(\frac{\sqrt{\rho^2_{k_{\mathrm{r}},c_1c_2}[m]+\rho^2_{k_{\mathrm{r}},c_1s_2}[m]}}{\left(1-\left[\rho^2_{k_{\mathrm{r}},c_1c_2}[m]+\rho^2_{k_{\mathrm{r}},c_1s_2}[m]\right]\right)} \times \frac{\sqrt{xy}}{\sigma_{k_{\mathrm{r}},c_1}[m]\,\sigma_{k_{\mathrm{r}},c_2}[m]}\right)\mathrm{d}x\mathrm{d}y\mathrm{d}\theta \qquad (3.51) \end{aligned}$$

where the identity $\prod_{\substack{l=1 \\ l\neq k_{\mathrm{r}}}}^{K_{\mathrm{r}}}\left(1-\exp\left(-\zeta_l^{\mathrm{SP}}[m]\ y\right)\right) = \sum_{z=0}^{K_{\mathrm{r}}-1}\frac{(-1)^z}{z!}\sum_{\substack{l_0,\ldots,l_z=1 \\ l_0=1,\, l_1\neq\ldots\neq l_z\neq k_{\mathrm{r}}}}^{K_{\mathrm{r}}} \exp\left(-y\sum_{j=1}^{z}\zeta_{l_j}^{\mathrm{SP}}[m]\right)$ is used in the last equality [54].

In Theorem 3.1, Eq. (3.50) may be numerically more efficient to compute than Eq. (3.51). □

3.5 Simulations

We now present numerical results to gain further insight into the previous analysis and study performance over time-varying channels.

3.5.1 Setup

In the sequel, a system with one transmit and one receive antenna is denoted as 1×1, while a system with one transmit and K_{r} receive antennas out of which only one is selected is denoted as $1 \times (1; K_{\mathrm{r}})$. Unless otherwise stated, a $1 \times (1; K_{\mathrm{r}})$ system is simulated with the following parameters: the carrier frequency $f_{\mathrm{c}} = 2\,\mathrm{GHz}$ and a single user moves with radial velocity $v_{\max} = 100\,\mathrm{km/h}$. The symbol duration $T_{\mathrm{s}} = 20.57\ \mu\mathrm{s}$ [3, 79]. Using (3.2), these parameters give a Doppler bandwidth $\nu_{\max} = 3.8 \times 10^{-3}$. A Rayleigh fading channel with Clarke's Doppler spectrum for each tap is used [18]. The complex channel at the k_{r}th receive antenna is given by [18, 27]

$$h_{k_{\mathrm{r}}}[m] = \sum_{n_{\mathrm{path}}=0}^{N_{\mathrm{path}}} a_{k_{\mathrm{r}},n_{\mathrm{path}}} \exp\left(j2\pi\nu_{k_{\mathrm{r}},n_{\mathrm{path}}} m\right) \tag{3.52}$$

where the number of propagation paths is set to $N_{\mathrm{path}} = 20$. In (3.52), $a_{k_{\mathrm{r}},n_{\mathrm{path}}} = \frac{1}{\sqrt{N_{\mathrm{path}}}} \exp\left(j\psi_{k_{\mathrm{r}},n_{\mathrm{path}}}\right)$ with phase angles $\psi_{k_{\mathrm{r}},n_{\mathrm{path}}}$ uniformly distributed over $[-\pi\ \pi)$. The Doppler shifts $\nu_{k_{\mathrm{r}},n_{\mathrm{path}}} = \nu_{\max}\cos\left(\alpha_{k_{\mathrm{r}},n_{\mathrm{path}}}\right)$ with angles of incidence $\alpha_{k_{\mathrm{r}},n_{\mathrm{path}}}$ uniformly distributed in $[-\pi\ \pi)$. The path parameters $\left\{a_{k_{\mathrm{r}},n_{\mathrm{path}}}\right\}$ and $\left\{\nu_{k_{\mathrm{r}},n_{\mathrm{path}}}\right\}$ are modelled as independent and identically distributed [18, 74]. They are assumed

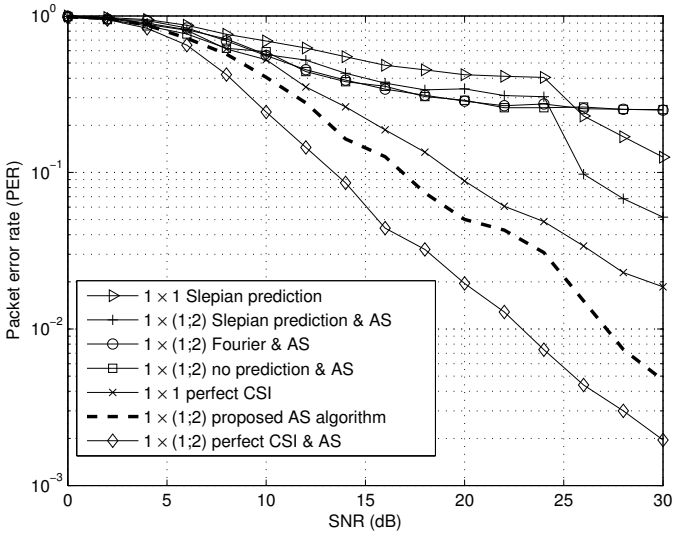

Figure 3.4: PER performance of the proposed AS method for a $1 \times (1;2)$ system when the user velocity $v_{\max} = 100$ km/h corresponding to a maximum normalized Doppler frequency $\nu_{\max} = 0.0038$. (4PSK, packet length $N = 42$, $N_{\mathrm{df}} = 40$ data symbols, $N_{\mathrm{pf}} = 2$ post-selection pilots, $N_{\mathrm{ps}} = 2$ selection training pilots, and $T_p = 3\,T_s$).

constant over an AS cycle but change independently from cycle to cycle.

3.5.2 Packet Error Rate

Figs. 3.4 and 3.5 show the PER of the proposed receive AS algorithm as a function of average SNR for $1 \times (1;2)$ and $1 \times (1;4)$ systems, respectively. For comparison, we also show the PER performance of:

1. a 1×1 system with perfect CSI and no AS.

2. a 1×1 system employing Slepian basis expansion channel prediction and no AS.

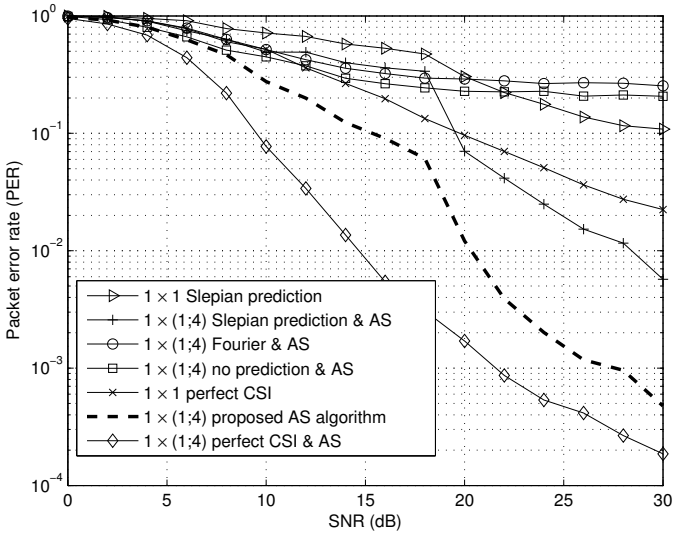

Figure 3.5: PER performance of the proposed AS method for a $1 \times (1;4)$ system when the user velocity $v_{\max} = 100$ km/h corresponding to a maximum normalized Doppler frequency $\nu_{\max} = 0.0038$. (4PSK, packet length $N = 42$, $N_{\rm df} = 40$ data symbols, $N_{\rm pf} = 2$ post-selection pilots, $N_{\rm ps} = 2$ selection training pilots, and $T_p = 3\,T_s$).

3. $1 \times (1;2)$ and $1 \times (1;4)$ systems employing Fourier basis expansion channel prediction and AS according to the maximum total post-processing SNR selection criterion, as in (3.21), with the refined channel gain estimates are used for data decoding.

4. $1 \times (1;2)$ and $1 \times (1;4)$ systems employing AS without channel prediction. We note that the antenna with the highest channel gain estimate $\tilde{h}_{k_{\rm r}}[m]$ in (3.7) is selected since no channel prediction is used.

5. $1 \times (1;2)$ and $1 \times (1;4)$ systems employing Slepian channel prediction and AS according to (3.21), with the predicted channel gains $\{\hat{h}_{k_{\rm r}}^{\rm SP}[m] \mid m \in \mathcal{I}_{\rm padt}\}$ used not only for selection but also for data decoding.

6. $1 \times (1;2)$ and $1 \times (1;4)$ systems employing the AS algorithm proposed in Sec. 3.3.1. Note that the predicted channel gains are used for AE selection, while the refined channel gain estimates $\{\hat{h}_{\hat{\imath}}^{\mathrm{SE}}[m] \mid m \in \mathcal{I}_{\mathrm{padt}}\}$ are used for decoding.

7. $1 \times (1;2)$ and $1 \times (1;4)$ systems with perfect CSI and employing AS according to (3.21) $\big($with $h_{k_{\mathrm{r}}}[m]$ replacing $\hat{h}_{k_{\mathrm{r}}}^{\mathrm{SP}}[m]\big)$.

Inspection of Figs. 3.4 and 3.5 reveal that the $1\times(1;2)$ and $1\times(1;4)$ systems employing the proposed AS algorithm achieve SNR performance gains in excess of 3 dB and 10 dB over the 1×1 system with perfect CSI and no AS, respectively, at a PER equal to 10^{-2}. The performance of the same proposed $1 \times (1;2)$ and $1 \times (1;4)$ systems are about 5 dB and 6 dB worse than $1 \times (1;2)$ and $1 \times (1;4)$ systems employing AS with perfect CSI at the same PER of 10^{-2}, respectively. Also, error floors exist at moderate to high SNR for the $1 \times (1;2)$ and $1 \times (1;4)$ systems employing AS either with Fourier basis expansion or without channel prediction.

Remark: Exact knowledge of the Doppler frequency $\nu_{\max}$ by the proposed algorithms in the thesis is not needed. We note that, as mentioned in Chapter 2 and Sec. 3.3.3, the DPS representation is not exact as well as the fact that perfect knowledge of the Doppler frequency and SNR is unavailable in practice.

3.5.3 Mean Square Error

The effect of the subspace dimension D on the MSE of the Slepian estimator for the selected AE $\hat{\imath}$ of a $1 \times (1;2)$ system employing the proposed per-packet AS method is depicted in Fig. 3.6. We note that the MSE of the Slepian estimator for AE $\hat{\imath}$ is $\mathrm{MSE}_{\hat{\imath},N}^{\mathrm{SE}} = \frac{1}{N}\sum_{m=M}^{M+N-1}\mathbb{E}\{|h_{\hat{\imath}}[m] - \hat{h}_{\hat{\imath}}^{\mathrm{SE}}[m]\,|^2\}$. The simulated and analytically obtained

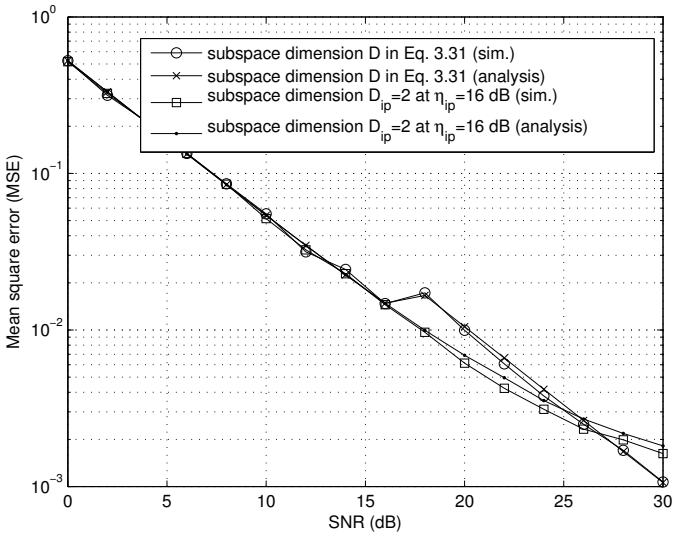

Figure 3.6: MSE of the Slepian estimator for a $1 \times (1; 2)$ system employing the proposed per-packet AS method when the user velocity $v_{\max} = 100$ km/h corresponding to a maximum normalized Doppler frequency $\nu_{\max} = 0.0038$. (estimation horizon $N = 42$, $N_{\rm pf} = 2$ post-selection pilots, $N_{\rm ps} = 2$ selection training pilots, and $T_p = 5\,T_s$).

MSE results from (3.30) are plotted. The curves with circle and cross markers represent, respectively, the simulated and analytical MSE for the subspace dimension in (3.30). It can be observed that there is an upward transition in the MSE curves which occur at $\eta_{\rm ip} = 16$ dB, which is the result of an increase of the subspace dimension. Notice also the upward transitions in Figs. 3.8 and 3.9. Therefore, the method in Sec. 3.3.3 is used to determine the subspace dimension. The curves with square and point markers represent, respectively, the simulated and analytical MSE for the subspace dimension $D_{\rm ip} = 2$ calculated from (3.30) at SNR $\eta_{\rm ip} = 16$ dB as in Step 3(a) in Sec. 3.3.3. From (3.32), the subspace dimension D for the Slepian estimator is $D = 2$ for $[0,\ 16)$ dB range, which is evaluated from (3.30) for $[0,\ 16)$ dB range, $D = D_{\rm ip} = 2$ for $[16,\ 26]$ dB range, which is evaluated from (3.30) at SNR $\eta_{\rm ip} = 16$

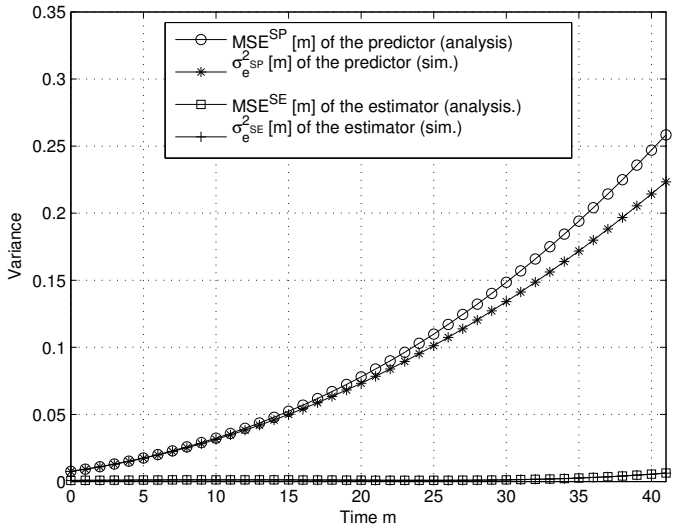

Figure 3.7: Comparison of the simulated and calculated expressions for the basis expansion error variance for a 1×1 system when the user velocity $v_{\max} = 100$ km/h corresponding to a maximum normalized Doppler frequency $\nu_{\max} = 0.0038$ at an average SNR $\eta = 20$ dB. (prediction/estimation horizon $N = 42$, $N_{\rm ps} = 2$ training pilots, $N_{\rm pf} = 2$ pilots, and $T_p = 3\,T_s$).

dB, and $D = 3$, which is evaluated from (3.30) for $(26,\ 30]$ dB SNR range.

Fig. 3.7 compares the simulated and analytically obtained variances of the estimation and prediction errors in Sec. 3.4.1. It can be observed that: (i) these variances are close to each other, and (ii) not surprisingly, the MSE per sample of the predicted $\mathrm{MSE}^{\rm SP}\,[m]$, in contrast to the MSE per sample of the estimated $\mathrm{MSE}^{\rm SE}\,[m]$, increases with the prediction horizon, which is consistent with the behavior of typical prediction algorithms.

3.5.4 Symbol Error Probability

The SEP of the $20th$ and first 4PSK symbols as a function of average SNR for a $1\times(1;2)$ system employing the proposed receive AS algorithm are depicted in Figs. 3.8

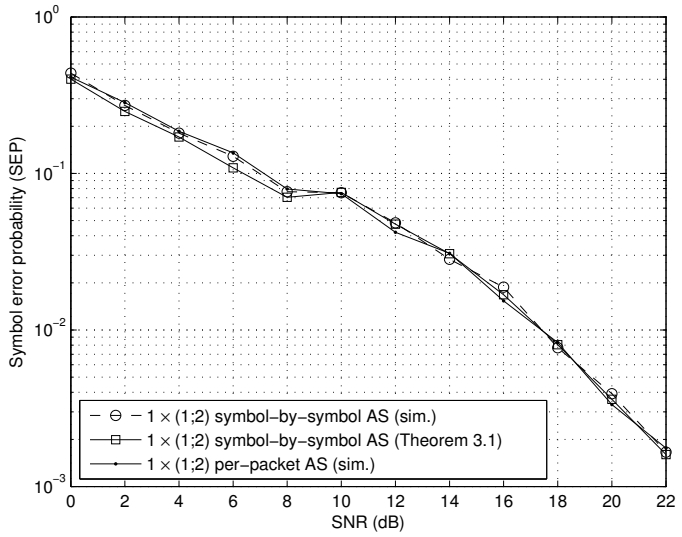

Figure 3.8: SEP for the $20th$ 4PSK data symbol for a $1 \times (1;2)$ system when the user velocity $v_{\max} = 100$ km/h corresponding to a maximum normalized Doppler frequency $\nu_{\max} = 0.0038$. (packet length $N = 42$, $N_{\rm df} = 40$ data symbols, $N_{\rm pf} = 2$ post-selection pilots, $N_{\rm ps} = 2$ selection training pilots, and $T_p = 5\,T_s$).

and 3.9, respectively. The SEP curves analyzed in *Theorem 3.1* are also shown. As is apparent from Fig. 3.9, the SEP for the first 4PSK symbol of a $1 \times (1;2)$ system employing symbol-by-symbol AS is about one order of magnitude less than that of a $1 \times (1;2)$ system employing per-packet AS at an SNR = 22 dB. As the packet size increases, the SEP performance gap between symbol-by-symbol and per-packet AS increases as well. The reason for this is that selection, which is based on predicted channel gains, for per-packet AS is on per-packet basis rather than per-symbol. Note that the packet size influences accuracy of channel prediction, i.e., channel prediction for first symbol of a packet is typically more accurate than that for last symbol. Thus as the packet size greatly increases, the uncertainty of per-packet selection increases as well. The SEP of the $20th$ and first 4PSK symbols as a function of average SNR

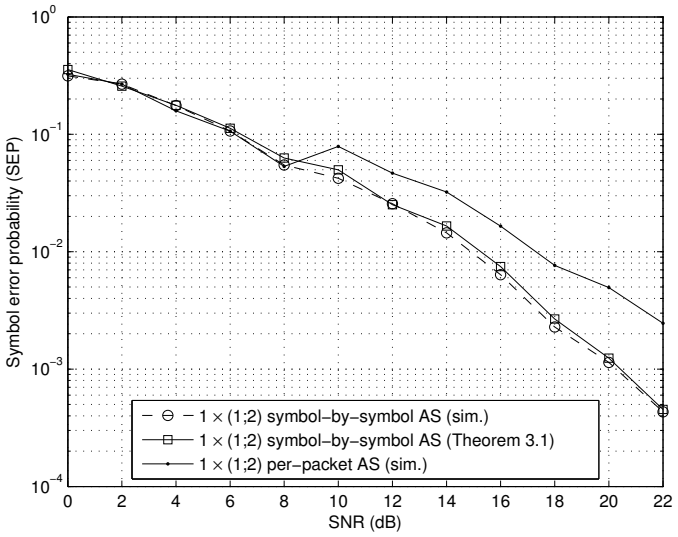

Figure 3.9: SEP for the first 4PSK data symbol for a $1 \times (1;2)$ system when the user velocity $v_{\max} = 100$ km/h corresponding to a maximum normalized Doppler frequency $\nu_{\max} = 0.0038$. (packet length $N = 42$, $N_{\rm df} = 40$ data symbols, $N_{\rm pf} = 2$ post-selection pilots, $N_{\rm ps} = 2$ selection training pilots, and $T_p = 5\,T_s$).

for a $1 \times (1;4)$ system employing the proposed receive AS algorithm are shown in Figs. 3.10 and 3.11, respectively. Also, the SEP of the $20th$ and first 16PSK symbols as a function of average SNR for a $1 \times (1;6)$ system employing the proposed receive AS algorithm are shown in Figs. 3.12 and 3.13.

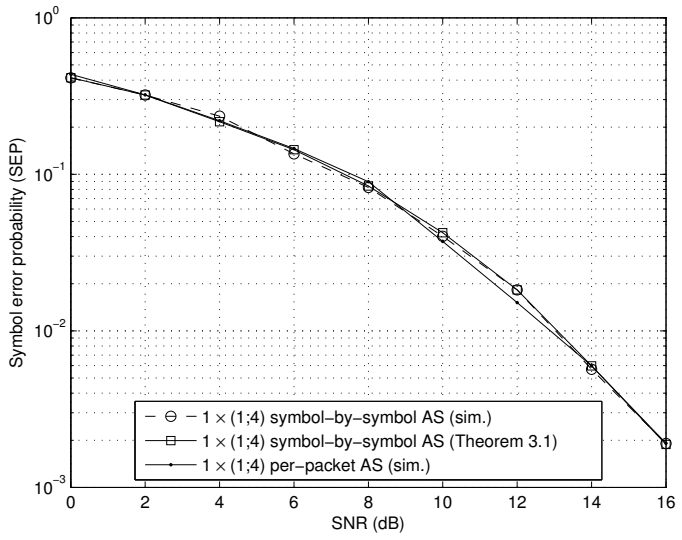

Figure 3.10: SEP for the $20th$ 4PSK data symbol for a $1 \times (1; 4)$ system when the user velocity $v_{\max} = 100$ km/h corresponding to a maximum normalized Doppler frequency $\nu_{\max} = 0.0038$. (packet length $N = 42$, $N_{\rm df} = 40$ data symbols, $N_{\rm pf} = 2$ post-selection pilots, $N_{\rm ps} = 2$ selection training pilots, and $T_p = 5\,T_s$).

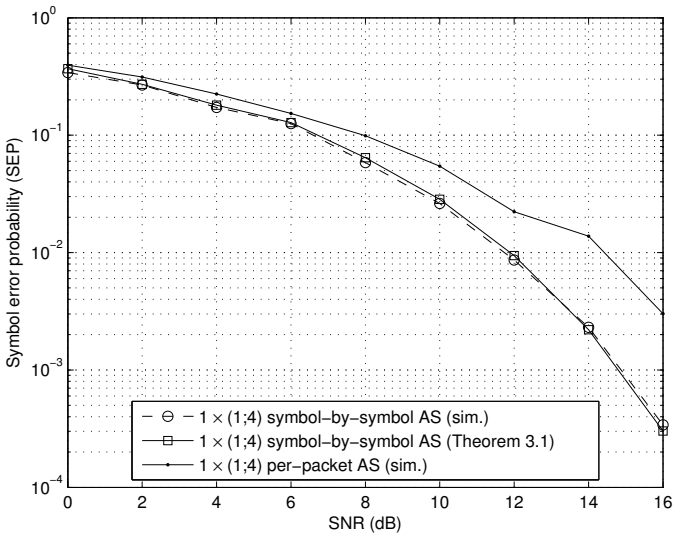

Figure 3.11: SEP for the first 4PSK data symbol for a $1 \times (1;4)$ system when the user velocity $v_{\max} = 100$ km/h corresponding to a maximum normalized Doppler frequency $\nu_{\max} = 0.0038$. (packet length $N = 42$, $N_{\rm df} = 40$ data symbols, $N_{\rm pf} = 2$ post-selection pilots, $N_{\rm ps} = 2$ selection training pilots, and $T_p = 5\,T_s$).

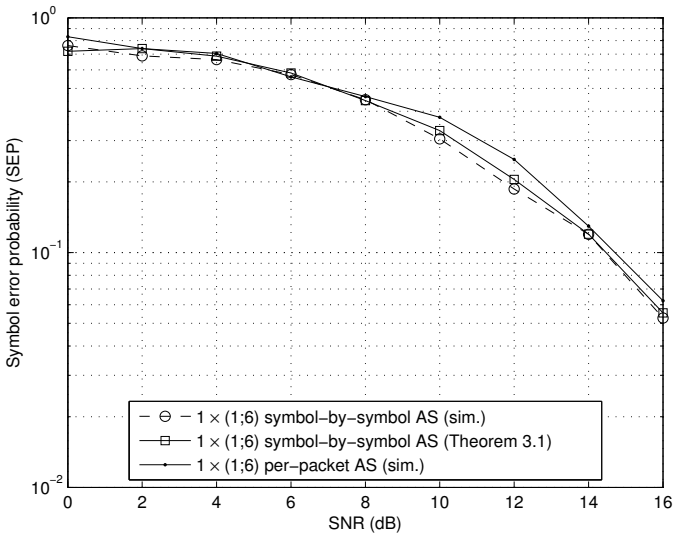

Figure 3.12: SEP for the $20th$ 16PSK data symbol for a $1 \times (1; 6)$ system when the user velocity $v_{\max} = 100$ km/h corresponding to a maximum normalized Doppler frequency $\nu_{\max} = 0.0038$. (packet length $N = 42$, $N_{\rm df} = 40$ data symbols, $N_{\rm pf} = 2$ post-selection pilots, $N_{\rm ps} = 2$ selection training pilots, and $T_p = 5\,T_s$).

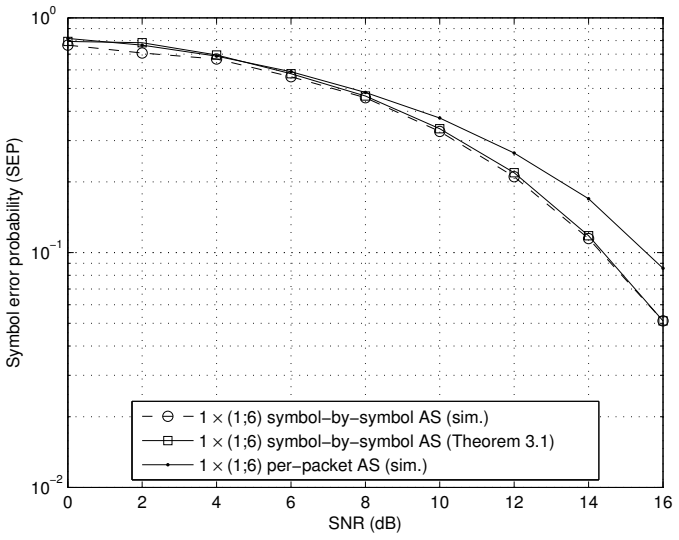

Figure 3.13: SEP for the first 16PSK data symbol for a $1 \times (1;6)$ system when the user velocity $v_{\max} = 100$ km/h corresponding to a maximum normalized Doppler frequency $\nu_{\max} = 0.0038$. (packet length $N = 42$, $N_{\mathrm{df}} = 40$ data symbols, $N_{\mathrm{pf}} = 2$ post-selection pilots, $N_{\mathrm{ps}} = 2$ selection training pilots, and $T_p = 5\,T_s$).

3.6 Summary and Conclusion

A training-based single receive antenna selection scheme for time-varying frequency-flat fading which uses Slepian basis expansion for prediction and estimation is proposed. It takes into account packet and symbol-by-symbol switching for antenna selection (AS). An approach to determine the subspace dimension that reduces the mean square error (MSE) of the Slepian estimator/predictor is also presented. Analytical expressions are derived for the channel prediction and estimation error as well as the SEP of MPSK with receive AS. It is shown that the proposed AS scheme outperforms ideal conventional SISO systems with perfect channel knowledge and no AS at the receiver and Fourier basis expansion channel estimation/prediction.

Chapter 4

Training Methods for Selection of Multiple Receive Antenna Subsystems in High-Mobility

4.1 Introduction

Receive antenna selection (AS) reduces hardware complexity by using a limited number of radio frequency (RF) chains at the receiver of a wireless system. In receive AS, only a subset of the antenna elements (AEs) is selected and connected to the RF chains [65, 80]. We note that AS is included in IEEE 802.11n [1].

Algorithms and performance analysis for AS systems are reported in numerous previous studies [9, 11, 12, 16, 22, 32, 33, 38–41, 46, 47, 51, 64, 66, 68, 95, 98, 102, 106]. However, practical issues such as pilot-based training and implementation of AS have only been considered recently and only in a limited number of studies [103]. In most of the above references, perfect channel knowledge is assumed. However, the channel is time-varying which results in outdated channel state information (CSI) at the receiver. The channel variations over time are mainly caused by the Doppler effect, which results from relative radial motion between the transmitter and receiver including moving reflectors. A user traveling at a maximum speed of $v_{\max}$ m/s causes

a maximum Doppler shift $f_{\mathrm{D}} \triangleq \frac{v_{\max} f_{\mathrm{c}}}{c_{\mathrm{o}}}$ to the carrier frequency f_{c}, where c_{o} is the speed of light. We note that the rate of channel variations is usually much slower than the transmission rate. However, current and future high data rate wireless systems use multicarrier modulation techniques such as orthogonal frequency division multiplexing (OFDM) to combat the effects of dispersive multipath fading [1, 2, 36]. Consequently, the transmitted symbol length is much longer than the input information symbol duration, resulting in higher temporal channel variations. The rate of channel variations is upper bounded by the maximum normalized Doppler bandwidth

$$\nu_{\max} \triangleq f_{\mathrm{D}} T_{\mathrm{s}} = \frac{v_{\max} f_{\mathrm{c}}}{c_{\mathrm{o}}} T_{\mathrm{s}} \tag{4.1}$$

where T_{s} and f_{D} are the symbol duration and Doppler frequency, respectively.

The impact of imperfect channel knowledge on the performance of AS systems is studied in [7, 35, 97, 105]. The performance of AS systems with CSI feedback delay is studied in [44, 73]. Weighted AS rules for time-varying channels which use temporal correlation knowledge are proposed in [54, 55]. In [54] and [55], only channel gain estimates obtained from the AS training phase are used in the selection and decoding mechanisms. This incurs a loss in signal-to-noise ratio (SNR).

Motivated by the above observations, in this chapter we propose a low complexity training-based receive antenna subset selection algorithm for time-varying channels. The method employs both per-packet and symbol-by-symbol switching. It also uses channel knowledge of the data transmission phase in the selection and decoding processes by utilizing the low training overhead Slepian predictor [101] and estimator [100]. This Slepian estimator/predictor only requires knowledge or estimate of the Doppler bandwidth. References [79] and [78] recently proposed a receive AS

method for time varying channels based on Slepian subspace projections. However, only the simpler problem of selecting a single antenna at the receiver is considered in [78, 79]. In [77], a Slepian-based receive AS method which accommodates the selection of multiple receive antennas for time-varying channels is recently proposed. The contributions of this chapter are summarized as follows:

- A receive antenna subset selection method for time-varying frequency-flat fading which uses Slepian basis expansion for prediction [101] and estimation [100] is proposed. An approach to determine the subspace dimension that reduces the mean square error (MSE) of the Slepian estimator/predictor is also presented.

- Analytical expressions for the symbol error probability (SEP) of `M`-ary phase-shift keying (`M`PSK) and quadrature amplitude modulation (`M`QAM) with receive AS are provided, along with corresponding simulations.

- Extensive simulation results are presented to compare the performance of the proposed method to that of ideal conventional single input–multiple output (SIMO) systems with perfect CSI but no AS at the receiver as well as AS based on conventional orthogonal Fourier based prediction/estimation.

This chapter is organized as follows: the detailed system model is described in Section 4.2. The training-based receive AS method for time-varying frequency-flat fading is developed in Sec. 4.3. The SEP is analyzed in Sec. 4.4. Analytical and simulation results are discussed in Sec. 4.5. Our conclusions follow in Sec. 4.6.

4.2 System Model

Consider a system with one transmit, K_{r} receive antennas, but equipped with only $K'_{\mathrm{r}} < K_{\mathrm{r}}$ RF chains. Depending on the AS switching time, either per-packet or symbol-by-symbol AS can be used. For example, microelectromechanical system (MEMS) switches may perform per-packet switching with negligible attenuation [75]. On the other hand, while solid-state switches can enable switching of antennas between symbols, their attenuation is non-negligible [88].

4.2.1 Channel and Signal Model

In wideband signals, the multipath delay spread is much longer than the transmitted signal duration. This implies that a discrete number of multipath components L, can be resolved in time [36]. The channel is thus frequency-selective and modeled as a length-L finite impulse response (FIR) filter, for which the continuous time impulse response is given by [59]

$$h_{k_{\mathrm{r}}}(t,\tau) = \sum_{\ell=0}^{L-1} \sqrt{P(\tau_\ell)} w_{k_{\mathrm{r}},\ell}(t)\, \delta(\tau - \tau_\ell), \;\; k_{\mathrm{r}} = 1, 2, \ldots, K_{\mathrm{r}} \tag{4.2}$$

where $\delta(t)$ denotes the Dirac delta function, τ_ℓ is the propagation delay of the ℓth complex channel tap $w_{k_{\mathrm{r}},\ell}(t)$ of average power $P(\tau_\ell)$. $\{P(\tau_\ell)\}_{\ell=0}^{L-1}$ represent the channel power delay profile (PDP), normalized as $\sum_{\ell=0}^{L-1} P(\tau_\ell) = 1$.

For narrowband signals the multipath delay spread is much shorter than the signal duration. The received multipath components are thus superimposed [36]. For instance, in multicarrier modulation such as OFDM, the symbol duration is much longer than the input information symbol duration T_{s}. Each OFDM subcarrier thus

carries a narrowband signal that sees time-varying frequency-flat fading.

In this chapter, time-varying frequency-flat fading is considered, i.e., where the symbol duration is much longer than the delay spread of the time-varying impulse response. From (4.2), the discrete-time channel impulse response between the single antenna transmitter and receive AE k_{r} is

$$h_{k_{\mathrm{r}}}[m] \triangleq h_{k_{\mathrm{r}}}(mT_{\mathrm{s}}, 0) = w_{k_{\mathrm{r}}}(mT_{\mathrm{s}}) \tag{4.3}$$

where standard sampling notation is used in (4.3), i.e., discrete-time signal $x[n]$ is obtained from continuous signal $x(t)$ by sampling at period T_{s} according to $x[n] \triangleq x(nT_{\mathrm{s}})$ with $n \in \mathbb{Z}$.

As shown in Sec. 4.5, each complex channel tap in (4.2) and (4.3) is modeled as the superposition of N_{path} discrete paths, each with Doppler shift $f_{k_{\mathrm{r}},n_{\mathrm{path}}} \triangleq f_{\mathrm{D}} \cos(\alpha_{k_{\mathrm{r}},n_{\mathrm{path}}}) \leq f_{\mathrm{D}}$, where $\alpha_{k_{\mathrm{r}},n_{\mathrm{path}}}$ is the angle of incidence for the n_{path} path. Therefore, the time-varying frequency-flat channel represents a sequence of complex channel gain scalars at the symbol rate and bandlimited by $\nu_{\max}$.

Let m index discrete time with symbol rate $R_{\mathrm{s}} \triangleq \frac{1}{T_{\mathrm{s}}}$. The received signal at receive AE k_{r} can be expressed as

$$y_{k_{\mathrm{r}}}[m] = h_{k_{\mathrm{r}}}[m]\, s[m] + n_{k_{\mathrm{r}}}[m], \quad k_{\mathrm{r}} = 1, 2, \ldots, K_{\mathrm{r}} \tag{4.4}$$

where $s[m]$ is the transmitted symbol of unit average power and $n_{k_{\mathrm{r}}}[m]$ is additive white Gaussian noise (AWGN) with variance N_{o} and is independent of the channel gain $h_{k_{\mathrm{r}}}[m]$.

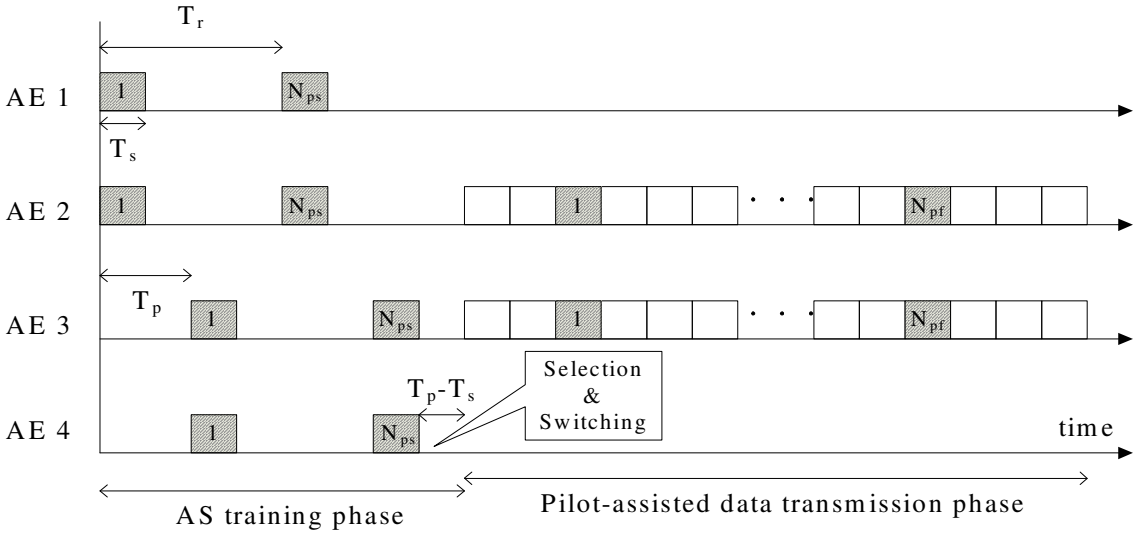

Figure 4.1: Antenna selection cycle for the proposed per-packet AS method. (AEs 2 and 3 are selected, $K_{\mathrm{r}} = 4$ receive antennas, $N_{\mathrm{pf}} = 2$ post-selection pilots, $N_{\mathrm{ps}} = 2$ AS training pilots, and $T_p = 2\,T_s$).

4.2.2 Antenna Selection Cycle

Fig. 4.1 depicts an AS cycle which consists of an AS training phase followed by a pilot-assisted data transmission phase. We now describe the AS training and pilot-assisted data transmission phases.

Antenna Selection Training Phase

The AS training phase is formed by N_{ps} rounds of pilot transmission. In each round, in total $\left\lceil \frac{K_{\mathrm{r}}}{K'_{\mathrm{r}}} \right\rceil$ pilots are transmitted to the $\left\lceil \frac{K_{\mathrm{r}}}{K'_{\mathrm{r}}} \right\rceil$ different subsets of antennas. Therefore, each of the $\left\lceil \frac{K_{\mathrm{r}}}{K'_{\mathrm{r}}} \right\rceil$ subsets of antennas receives N_{ps} antenna selection pilot symbols. Thus, in total $\left\lceil \frac{K_{\mathrm{r}}}{K'_{\mathrm{r}}} \right\rceil N_{\mathrm{ps}}$ pilots are transmitted over N_{ps} rounds of transmission. The duration between consecutive training symbols in each round is $T_{\mathrm{p}} \triangleq \alpha T_{\mathrm{s}}$, where T_{s} is the symbol duration and $\alpha \in \mathbb{Z}^{+}$. Therefore, the duration between two consecutive

training symbols transmitted in two consecutive rounds of transmission for each of the $\left\lceil \frac{K_\mathrm{r}}{K'_\mathrm{r}} \right\rceil$ antenna subsets is $T_\mathrm{r} \triangleq \left\lceil \frac{K_\mathrm{r}}{K'_\mathrm{r}} \right\rceil T_\mathrm{p} = \alpha \left\lceil \frac{K_\mathrm{r}}{K'_\mathrm{r}} \right\rceil T_\mathrm{s}$. In the first round, each transmitted pilot is received by a different subset of antennas at times $m \in \left(\left\lceil \frac{k_\mathrm{r}}{K'_\mathrm{r}} \right\rceil - 1 \right) T_\mathrm{p}$ for $k_\mathrm{r} = 1, 2, \ldots, K_\mathrm{r}$. In the second round, each transmitted pilot is received by a different subset of antennas at times $m \in \left(\left(\left\lceil \frac{k_\mathrm{r}}{K'_\mathrm{r}} \right\rceil - 1 \right) T_\mathrm{p} + T_\mathrm{r} \right)$ for $k_\mathrm{r} = 1, 2, \ldots, K_\mathrm{r}$, and so on. Thus AE k_r receives N_ps antenna selection training pilots at times $m \in T_\mathrm{ps}^{k_\mathrm{r}}$, where

$$\begin{aligned} T_\mathrm{ps}^{k_\mathrm{r}} &= \left\{ \left[\left(\left\lceil \frac{k_\mathrm{r}}{K'_\mathrm{r}} \right\rceil - 1 \right) T_\mathrm{p} + (n_\mathrm{ps} - 1)\, T_\mathrm{r} \right] \;\middle|\; n_\mathrm{ps} = 1, 2, \ldots, N_\mathrm{ps} \right\} \\ &= \left\{ \alpha \left(\left(\left\lceil \frac{k_\mathrm{r}}{K'_\mathrm{r}} \right\rceil - 1 \right) + (n_\mathrm{ps} - 1) \left\lceil \frac{K_\mathrm{r}}{K'_\mathrm{r}} \right\rceil \right) T_\mathrm{s} \;\middle|\; n_\mathrm{ps} = 1, 2, \ldots, N_\mathrm{ps} \right\} \\ &\triangleq \left\{ \alpha \left[\left(\left\lceil \frac{k_\mathrm{r}}{K'_\mathrm{r}} \right\rceil - 1 \right) + (n_\mathrm{ps} - 1) \left\lceil \frac{K_\mathrm{r}}{K'_\mathrm{r}} \right\rceil \right] \;\middle|\; n_\mathrm{ps} = 1, 2, \ldots, N_\mathrm{ps} \right\} \end{aligned} \tag{4.5}$$

for $k_\mathrm{r} = 1, 2, \ldots, K_\mathrm{r}$, where in the last step, discrete-time notation is adopted. From (4.4), the received pilot symbol can be written as

$$y_{k_\mathrm{r}}[m] = h_{k_\mathrm{r}}[m]\, p_{k_\mathrm{r}}[m] + n_{k_\mathrm{r}}[m], \quad k_\mathrm{r} = 1, 2, \ldots, K_\mathrm{r}, \quad m \in T_\mathrm{ps}^{k_\mathrm{r}} \tag{4.6}$$

where $p_{k_\mathrm{r}}[m]$ is the unit energy pilot symbol. The observations $\{y_{k_\mathrm{r}}[m] \,|\, m \in T_\mathrm{ps}^{k_\mathrm{r}}\}$ over the AS training pilots are necessary to perform Slepian channel prediction to obtain a prediction of the channel seen by the data at each receive AE $\{\hat{h}_{k_\mathrm{r}}^{\mathrm{SP}}[m] \,|\, m \in \mathcal{I}_\mathrm{padt}\}$ over the pilot-assisted data transmission phase $\mathcal{I}_\mathrm{padt}$. Based on the predicted channel gains $\{\hat{h}_{k_\mathrm{r}}^{\mathrm{SP}}[m] \,|\, m \in \mathcal{I}_\mathrm{padt}\}_{k_\mathrm{r}=1}^{K_\mathrm{r}}$, the receiver then selects its receive AEs subset $\mathcal{S} \triangleq \{\text{AE } \hat{\imath}_1, \text{AE } \hat{\imath}_2, \ldots, \text{AE } \hat{\imath}_{K'_\mathrm{r}}\}$ and connects them to the RF chains for the time duration of $T_\mathrm{p} - T_\mathrm{s}$. Therefore, the AS training phase spans the discrete time interval

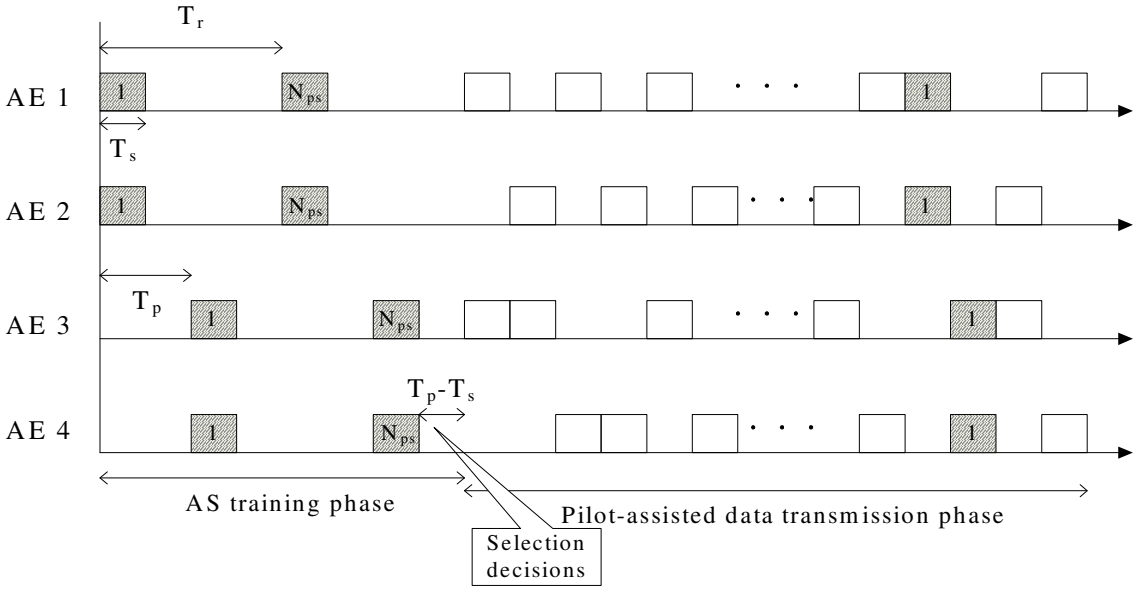

Figure 4.2: Antenna selection cycle for symbol-by-symbol AS method. ($K_{\mathrm{r}} = 4$ receive antennas, $N_{\mathrm{ps}} = 2$ AS training pilots, $N_{\mathrm{pf}} = 1$ post-selection pilots, and $T_p = 2\,T_s$).

$\mathcal{I}_{\mathrm{ast}} = \{0, 1, \ldots, M-1\}$, where $M \triangleq \alpha \left\lceil \frac{K_{\mathrm{r}}}{K'_{\mathrm{r}}} \right\rceil N_{\mathrm{ps}}$. As shown in Fig. 4.2, in symbol-by-symbol AS, the most suitable receive AEs subset $\mathcal{S}_m \triangleq \{\text{AE } \hat{\imath}_1^m, \ldots, \text{AE } \hat{\imath}_{K'_{\mathrm{r}}}^m\}$ is selected for each symbol at time m, where symbol index m has been added to $\mathcal{S}$ and $\{\hat{\imath}_{k_{\mathrm{r}}}\}_{k_{\mathrm{r}}=1}^{K'_{\mathrm{r}}}$.

Pilot-Assisted Data Transmission Phase

In this section, the pilot-assisted data transmission phases for per-packet and symbol-by-symbol switching are described.

Per-Packet AS

The pilot-assisted data transmission phase spans $\mathcal{I}_{\text{padt}} = \{M, M+1, \ldots, M+N-1\}$, where the transmitter sends out a length-$N \triangleq N_{\text{pf}} + N_{\text{df}}$ packet containing N_{pf} pilots time-multiplexed with N_{df} data symbols. The N_{pf} pilot symbols are uniformly spread in the packet as

$$\begin{aligned} \mathcal{P}_{\text{pf}} &\triangleq \left\{ \left\lfloor (n_{\text{pf}}-1)\left(\frac{N}{N_{\text{pf}}}\right) + \frac{1}{2}\left(\frac{N}{N_{\text{pf}}}\right) \right\rfloor \;\middle|\; n_{\text{pf}} = 1, \ldots, N_{\text{pf}} \right\} \\ &= \left\{ \left\lfloor \frac{(2n_{\text{pf}}-1)\,N}{2N_{\text{pf}}} \right\rfloor \;\middle|\; n_{\text{pf}} = 1, \ldots, N_{\text{pf}} \right\}. \end{aligned} \tag{4.7}$$

The received signal at each selected AE $\hat{\imath}_{k_{\text{r}}}$, for $1 \le k_{\text{r}} \le K'_{\text{r}}$, is

$$y_{\hat{\imath}_{k_{\text{r}}}}[m] = \begin{cases} h_{\hat{\imath}_{k_{\text{r}}}}[m]\; d[m] + n_{\hat{\imath}_{k_{\text{r}}}}[m], & m \in \mathcal{I}_{\text{padt}} \backslash T_{\text{pf}} \\ h_{\hat{\imath}_{k_{\text{r}}}}[m]\; p[m] + n_{\hat{\imath}_{k_{\text{r}}}}[m], & m \in T_{\text{pf}} \end{cases} \tag{4.8}$$

where $d[m]$ and $p[m]$ denote the transmitted data and pilot symbols, respectively. $A \backslash B$ denotes the set that contains all those elements of A that are not in B. From (4.7) and since the AS training phase spans the discrete times $\mathcal{I}_{\text{ast}} = \{0, 1, \ldots, M-1\}$, the N_{pf} post-selection pilot symbols are thus received by the selected AEs at times $m \in T_{\text{pf}}$, where

$$T_{\text{pf}} \triangleq \left\{ M - 1 + \left\lfloor \frac{(2n_{\text{pf}}-1)\,N}{2N_{\text{pf}}} \right\rfloor \;\middle|\; n_{\text{pf}} = 1, \ldots, N_{\text{pf}} \right\}. \tag{4.9}$$

Thus, in total, $N_{\text{tp}} \triangleq N_{\text{ps}} + N_{\text{pf}}$ training symbols are received by the selected AEs at times

$$T_{\text{tp}}^{\hat{\imath}_{k_{\text{r}}}} = T_{\text{ps}}^{\hat{\imath}_{k_{\text{r}}}} \cup T_{\text{pf}} \tag{4.10}$$

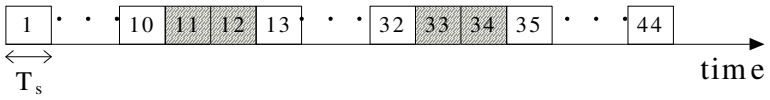

Figure 4.3: A packet of length $N' = 44$ symbols for a system with one transmit antenna and $K_{\rm r} = 4$ receive antennas out of which $K'_{\rm r} = 2$ antennas are instantaneously selected at time m using the proposed symbol-by-symbol AS method. ($N_{\rm df} = 40$ data symbols, $N'_{\rm pf} = 4$ pilot symbols).

where $T_{\rm ps}^{\hat{\iota}_{k_{\rm r}}}$ and $T_{\rm pf}$ are given in (4.5) and (4.9), respectively. From these $N_{\rm tp}$ pilot symbols, refined channel gain estimates $\left\{\hat{h}_{\hat{\iota}_{k_{\rm r}}}^{\rm SE}[m] \,|\, m \in \mathcal{I}_{\rm padt} \backslash T_{\rm pf}\right\}_{k_{\rm r}=1}^{K'_{\rm r}}$ for $\mathcal{S}$ are obtained using the Slepian estimator for data decoding.

Symbol-By-Symbol AS

After selection, the transmitter sends out a length-$N' \triangleq N_{\rm df} + N'_{\rm pf}$ packet which consists of $N_{\rm df}$ data symbols and $N'_{\rm pf} \triangleq \left\lceil \frac{K_{\rm r}}{K'_{\rm r}} \right\rceil N_{\rm pf}$ pilot symbols. The $N'_{\rm pf} = \left\lceil \frac{K_{\rm r}}{K'_{\rm r}} \right\rceil N_{\rm pf}$ pilot symbols are needed to obtain refined channel gain estimates $\{\hat{h}_{\hat{\iota}_{k_{\rm r}}^m}^{\rm SE}[m] \,|\, m \in \mathcal{I}_{\rm padt}\}$. This is because in symbol-by-symbol AS, for each symbol an antenna subset $\mathcal{S}_m$ is selected at time m. Since different antenna subsets might be selected during the data transmission phase, $N_{\rm pf}$ pilots should be sent to each of the $\left\lceil \frac{K_{\rm r}}{K'_{\rm r}} \right\rceil$ antenna subsets. The symbol locations in the packet that carry the $N_{\rm pf}$ pilots for AE $k_{\rm r}$ for $k_{\rm r} = 1, 2, \ldots, K_{\rm r}$ are given by

$$\begin{aligned} \mathcal{P}_{\rm pf}^{k_{\rm r}} &= \left\{ \left(\left\lceil \frac{k_{\rm r}}{K'_{\rm r}} \right\rceil - 1 \right) + \left\lfloor (n_{\rm pf} - 1) \left(\frac{N'}{N_{\rm pf}} \right) + \frac{1}{2} \left(\frac{N'}{N_{\rm pf}} \right) \right\rfloor \;\middle|\; n_{\rm pf} = 1, \ldots, N_{\rm pf} \right\} \\ &\triangleq \left\{ \left(\left\lceil \frac{k_{\rm r}}{K'_{\rm r}} \right\rceil - 1 \right) + \left\lfloor \frac{(2n_{\rm pf} - 1)\, N'}{2N_{\rm pf}} \right\rfloor \;\middle|\; n_{\rm pf} = 1, \ldots, N_{\rm pf} \right\}. \end{aligned} \tag{4.11}$$

Fig. 4.3 shows a transmitted packet during the pilot-assisted data transmission phase for a system with one transmit antenna and $K_{\rm r} = 4$ receive antennas out of which $K'_{\rm r} =$

2 antennas are selected using the symbol-by-symbol AS method. Based on (4.11), the pilot locations in the packet for AEs 1 and 2 are $\mathcal{P}_{\rm pf}^1 = \mathcal{P}_{\rm pf}^2 = \{11, 33\}$, where each pilot is received by two antennas since two RF chains are available at the receiver. Similarly, the pilot locations in the packet for AEs 3 and 4 are $\mathcal{P}_{\rm pf}^3 = \mathcal{P}_{\rm pf}^4 = \{12, 34\}$.

From (4.11) and since the AS training phase spans the discrete times $\mathcal{I}_{\rm ast} = \{0, 1, \ldots, M-1\}$, the $N_{\rm pf}$ pilot symbols are thus received by AE $k_{\rm r}$ at times $m \in T_{\rm pf}^{k_{\rm r}}$, where

$$T_{\rm pf}^{k_{\rm r}} \triangleq \left\{ M - 1 + \left(\left\lceil \frac{k_{\rm r}}{K_{\rm r}'} \right\rceil - 1 \right) + \left\lfloor \frac{(2n_{\rm pf} - 1)\, N'}{2N_{\rm pf}} \right\rfloor \;\middle|\; n_{\rm pf} = 1, \ldots, N_{\rm pf} \right\}. \tag{4.12}$$

Thus $N_{\rm tp} = N_{\rm ps} + N_{\rm pf}$ pilots are received by each AE at times

$$T_{\rm tp}^{k_{\rm r}} = T_{\rm ps}^{k_{\rm r}} \cup T_{\rm pf}^{k_{\rm r}}, \qquad k_{\rm r} = 1, 2, \ldots, K_{\rm r} \tag{4.13}$$

where $T_{\rm ps}^{k_{\rm r}}$ and $T_{\rm pf}^{k_{\rm r}}$ are given in (4.5) and (4.12), respectively. From these $N_{\rm tp}$ pilots, refined channel gain estimates $\{\hat{h}_{i_{k_{\rm r}}^m}^{\rm SE}[m] \mid m \in \mathcal{I}_{\rm padt}\}$ for $\mathcal{S}_m$ are obtained using the Slepian estimator for data decoding.

The data symbols received by $\mathcal{S}_m$ are given by

$$y_{i_{k_{\rm r}}^m}[m] = h_{i_{k_{\rm r}}^m}[m]\, d[m] + n_{i_{k_{\rm r}}^m}[m], \quad m \in \mathcal{I}_{\rm padt} \backslash \left(T_{\rm pf}^1 \cup \ldots \cup T_{\rm pf}^{K_{\rm r}} \right). \tag{4.14}$$

We note that in symbol-by-symbol AS the pilot-assisted data transmission phase spans the discrete times $\mathcal{I}_{\rm padt} = \{M, M+1, \ldots, M+N'-1\}$, where $N' = N_{\rm df} + \left\lceil \frac{K_{\rm r}}{K_{\rm r}'} \right\rceil N_{\rm pf}$. However, in per-packet switching $\mathcal{I}_{\rm padt} = \{M, M+1, \ldots, M+N-1\}$ with $N = N_{\rm df} + N_{\rm pf}$. Therefore, $N' = N + N_{\rm pf}\left(\left\lceil \frac{K_{\rm r}}{K_{\rm r}'} \right\rceil - 1 \right)$.

4.3 Receive Antenna Subset Selection Algorithm

In this section, receive antenna subset selection algorithms for single input–multiple output systems equipped with $K_{\rm r}$ receive antennas out of which only $K'_{\rm r}$ ($K'_{\rm r} < K_{\rm r}$) antennas are selected for time-varying frequency-flat fading for both per-packet and per-symbol switching are presented.

In summary, the antenna selection training phase is formed by sending $N_{\rm ps}$ training symbols, to each of the antenna subsets. From the observations over the training pilots $\{y_{k_{\rm r}}[m] \mid m \in T_{\rm ps}^{k_{\rm r}}\}$, channel gain estimates $\{\tilde{h}_{k_{\rm r}}[m] \mid m \in T_{\rm ps}^{k_{\rm r}}\}$ for each AE are obtained based on (4.4) as

$$\tilde{h}_{k_{\rm r}}[m] = y_{k_{\rm r}}[m]\, p^*_{k_{\rm r}}[m]\,. \tag{4.15}$$

We note that the CSI $\{\tilde{h}_{k_{\rm r}}[m]\}$ in (4.15) is outdated at the receiver. Slepian channel prediction for each AE over the data transmission phase is therefore needed to perform antenna subset selection. Denote the number of Slepian basis functions, which are bandlimited by the maximum normalized Doppler frequency $\nu_{\max}$, by D. Note that the temporal variations of the channel are also proportional to $\nu_{\max}$. The D extensions $\{u_d[m] \mid m \in \mathcal{I}_{\rm padt}\}_{d=0}^{D-1}$ of the orthonormal Slepian sequences of length-M $\{u_d[m] \mid m \in \mathcal{I}_{\rm ast}\}_{d=0}^{D-1}$ over the data phase $\mathcal{I}_{\rm padt}$ are used for channel prediction. We note that the Slepian sequences $\{u_d[m] \mid m \in \mathcal{I}_{\rm ast}\}_{d=0}^{M-1}$ are the restrictions in time of the (infinite) discrete prolate spheroidal (DPS) sequences $\{u_d[m] \mid m \in \mathbb{Z}\}_{d=0}^{M-1}$ over the AS training time interval $\mathcal{I}_{\rm ast} = \{0, \ldots, M-1\}$. The dth Slepian sequence vector of size $M \times 1$ $\mathbf{u}_d[m] \triangleq [u_d[0], \ldots, u_d[M-1]]^T$ is the dth eigenvector of the $M \times M$ matrix $\mathbf{A}$ with (a,b) entry defined as $[\mathbf{A}]_{a,b} = \frac{\sin[2\pi\nu_{\max}(a-b)]}{\pi(a-b)}$, for

$a, b = 0, 1, \ldots, M-1$ corresponding to eigenvalues $\lambda_0 \geq \lambda_1 \geq \ldots \geq \lambda_{M-1}$. The D extensions $\{u_d[m] \,|\, m \in \mathcal{I}_{\text{padt}}\}_{d=0}^{D-1}$ of the orthonormal Slepian sequences can be calculated from

$$u_d[m] = \frac{1}{\lambda_d} \sum_{m'=0}^{M-1} \frac{\sin\left[2\pi\nu_{\max}(m'-m)\right]}{\pi(m'-m)} u_d[m'], \quad m \in \mathcal{I}_{\text{padt}}. \tag{4.16}$$

Selection is then performed based on the predicted channel gains $\{\hat{h}_{k_\text{r}}^{\text{SP}}[m] \,|\, m \in \mathcal{I}_{\text{padt}}\}$. In the data transmission phase, a packet containing pilot and data symbols is transmitted. Next, refined channel gain estimates for the selected AEs obtained from the Slepian estimator are used for data decoding. The basis functions $\{u_d[m] \,|\, m \in \mathcal{I}_{\text{padt}}\}_{d=0}^{D-1}$ for the Slepian estimator are a subset over the data phase $\mathcal{I}_{\text{padt}}$ of the complete Slepian sequences $\{u_d[m] \,|\, m \in \mathcal{I}_{\text{AS}}\}_{d=0}^{D-1}$ over the AS cycle time interval $\mathcal{I}_{\text{AS}} = \mathcal{I}_{\text{ast}} \cup \mathcal{I}_{\text{padt}}$.

4.3.1 Per-Packet AS

The receive AS algorithm for per-packet switching comprises the following steps, which are conducted following an AS request:

1. Each antenna subset out of the $\left\lceil \frac{K_\text{r}}{K_\text{r}'} \right\rceil$ total subsets is trained using N_{ps} pilot symbols. The spacing between consecutive pilot symbols is $T_\text{r} = \alpha \left\lceil \frac{K_\text{r}}{K_\text{r}'} \right\rceil T_\text{s}$, where T_s is the symbol duration. To keep the AS training phase as short as possible, α is chosen as $\alpha = \left\lceil \frac{T_\text{sw}}{T_\text{s}} \right\rceil + 1$, where T_sw is the antenna switching time.

2. The receiver then:

(a) Performs channel prediction over the data $\mathcal{I}_{\text{padt}} \backslash T_{\text{pf}}$ for every AE as

$$\hat{h}_{k_{\text{r}}}^{\text{SP}}[m] = \boldsymbol{f}^T[m]\,\hat{\boldsymbol{c}}_{k_{\text{r}}} = \sum_{d=0}^{D-1} \hat{c}_{k_{\text{r}},d} u_d[m] \qquad m \in \mathcal{I}_{\text{padt}} \backslash T_{\text{pf}} \tag{4.17}$$

for $k_{\text{r}} = 1, 2, \ldots, K_{\text{r}}$, and D is the subspace dimension, i.e., number of basis functions. In (4.17), $\boldsymbol{f}[m] \triangleq [u_0[m], \ldots, u_{D-1}[m]]^T$ contains the D basis functions which can be calculated from (4.16) for $m \in \mathcal{I}_{\text{padt}} \backslash T_{\text{pf}}$. In (4.17), $\hat{\boldsymbol{c}}_{k_{\text{r}}} \triangleq [\hat{c}_{k_{\text{r}},0}, \ldots, \hat{c}_{k_{\text{r}},D-1}]^T$ includes the basis expansion coefficients for each AE k_{r}, is given by

$$\hat{\boldsymbol{c}}_{k_{\text{r}}} = \Big(\sum_{m \in T_{\text{ps}}^{k_{\text{r}}}} \boldsymbol{f}[m]\,\boldsymbol{f}^{\dagger}[m]\,|p_{k_{\text{r}}}[m]|^2 \Big)^{-1} \sum_{m \in T_{\text{ps}}^{k_{\text{r}}}} y_{k_{\text{r}}}[m]\,p_{k_{\text{r}}}^{*}[m]\,\boldsymbol{f}^{*}[m] \tag{4.18}$$

where $(\cdot)^*$ and $(\cdot)^\dagger$ denote complex conjugate and complex conjugate transpose, respectively.

(b) Selects its receive subset of antennas $\mathcal{S}$ which maximizes the post-processing SNR over the data phase $\mathcal{I}_{\text{padt}} \backslash T_{\text{pf}}$, i.e., the first K_{r}' order statistics of $\Big\{ \sum\limits_{\substack{m=M \\ (m \neq T_{\text{pf}})}}^{M+N-1} \Big| \hat{h}_{k_{\text{r}}}^{\text{SP}}[m] \Big|^2 \mid k_{\text{r}} = 1, \ldots, K_{\text{r}} \Big\}$.

3. The transmitter sends out a length-$N = N_{\text{df}} + N_{\text{pf}}$ data packet in which N_{pf} pilots are time multiplexed with N_{df} data symbols as (4.7). The packet is received by the subset of antennas $\mathcal{S} = \{\text{AE } \hat{\imath}_1, \text{AE } \hat{\imath}_2, \ldots, \text{AE } \hat{\imath}_{K_{\text{r}}'}\}$.

4. Refined channel gain estimates $\big\{ \hat{h}_{\hat{\imath}_{k_{\text{r}}}}^{\text{SE}}[m] \mid m \in \mathcal{I}_{\text{padt}} \backslash T_{\text{pf}} \big\}$ for $\mathcal{S}$ are obtained via

$$\hat{\boldsymbol{h}}_{\hat{\imath}_{k_{\text{r}}}}^{\text{SE}} = \boldsymbol{U}'\,\hat{\boldsymbol{c}}_{\hat{\imath}_{k_{\text{r}}}} = \sum_{d=0}^{D-1} \hat{c}_{\hat{\imath}_{k_{\text{r}}},d}\,\boldsymbol{u}_d' \tag{4.19}$$

where the $N_{\rm df}\times 1$ vector $\hat{\boldsymbol{h}}^{\rm SE}_{\hat{\imath}_{k_{\rm r}}}$ contains the entries $\hat{h}^{\rm SE}_{\hat{\imath}_{k_{\rm r}}}[m]$ for $m \in \mathcal{I}_{\rm padt}\backslash T_{\rm pf}$, $\boldsymbol{U}' \triangleq \left[\boldsymbol{u}'_0, \ldots, \boldsymbol{u}'_{D-1}\right]$ is the $N_{\rm df} \times D$ submatrix of the complete $(M+N)\times D$ Slepian sequences matrix $\boldsymbol{U}$, and the $N_{\rm df} \times 1$ vector $\boldsymbol{u}'_d$ contains the basis functions $\{u_d[m] \mid m \in \mathcal{I}_{\rm padt}\backslash T_{\rm pf}\}$. In (4.19), $\hat{\boldsymbol{c}}_{\hat{\imath}_{k_{\rm r}}} \triangleq [\hat{c}_{\hat{\imath}_{k_{\rm r}},0}, \ldots, \hat{c}_{\hat{\imath}_{k_{\rm r}},D-1}]^T$ can be calculated from (4.18) with $T^{\hat{\imath}_{k_{\rm r}}}_{\rm tp}$ given in (4.10) replacing $T^{k_{\rm r}}_{\rm ps}$.

4.3.2 Symbol-By-Symbol AS

The symbol-by-symbol receive AS algorithm comprises the following steps, which are conducted following an AS request:

1. Each antenna subset out of the $\left\lceil \frac{K_{\rm r}}{K'_{\rm r}} \right\rceil$ total subsets is trained using $N_{\rm ps}$ pilot symbols. The spacing between consecutive pilot symbols is $T_{\rm r} = \alpha \left\lceil \frac{K_{\rm r}}{K'_{\rm r}} \right\rceil T_{\rm s}$, where $\alpha \geq 1$ since the antenna switching time $T_{\rm sw}$ is less than the symbol duration $T_{\rm s}$.

2. The receiver then:

   (a) Performs channel prediction for every AE via (4.17) for $m \in \mathcal{I}_{\rm padt}\backslash(T^1_{\rm pf} \cup \ldots \cup T^{K_{\rm r}}_{\rm pf})$.

   (b) Selects its instantaneous subset of antennas $\mathcal{S}_m$ which consists of the first $K'_{\rm r}$ order statistics of $\left\{|\hat{h}^{\rm SP}_{k_{\rm r}}[m]|^2 \,\middle|\, k_{\rm r} = 1, \ldots, K_{\rm r}\right\}$ for $m \in \mathcal{I}_{\rm padt}\backslash(T^1_{\rm pf} \cup \ldots \cup T^{K_{\rm r}}_{\rm pf})$.

3. The transmitter sends out a length-$N' = N_{\rm df} + \left\lceil \frac{K_{\rm r}}{K'_{\rm r}} \right\rceil N_{\rm pf}$ data packet, which consists of $N_{\rm df}$ data symbols and $N'_{\rm pf} = \left\lceil \frac{K_{\rm r}}{K'_{\rm r}} \right\rceil N_{\rm pf}$ pilots interleaved as (4.11). Each data symbol at time m is received by a different subset of antennas $\mathcal{S}_m = \{\text{AE } \hat{\imath}^m_1, \text{AE } \hat{\imath}^m_2, \ldots, \text{AE } \hat{\imath}^m_{K'_{\rm r}}\}$.

4. To decode data the receiver obtains $\left\{\hat{h}^{\mathrm{SE}}_{i^m_{k_\mathrm{r}}}[m] \,|\, m \in \mathcal{I}_{\mathrm{padt}} \backslash \left(T^1_{\mathrm{pf}} \cup \ldots \cup T^{K_\mathrm{r}}_{\mathrm{pf}}\right)\right\}$ for $\mathcal{S}_m$ via

$$\hat{h}^{\mathrm{SE}}_{i^m_{k_\mathrm{r}}}[m] = \sum_{d=0}^{D-1} \hat{c}_{i^m_{k_\mathrm{r}},d}\, u_d[m] \tag{4.20}$$

where the basis functions $\left\{u_d[m] \,|\, m \in \mathcal{I}_{\mathrm{padt}} \backslash \left(T^1_{\mathrm{pf}} \cup \ldots \cup T^{K_\mathrm{r}}_{\mathrm{pf}}\right)\right\}_{d=0}^{D-1}$ are a subset over the data symbols for $m \in \mathcal{I}_{\mathrm{padt}} \backslash \left(T^1_{\mathrm{pf}} \cup \ldots \cup T^{K_\mathrm{r}}_{\mathrm{pf}}\right)$ of the complete length-$(M+N')$ Slepian sequences $\{u_d[m] \,|\, m \in \mathcal{I}_{\mathrm{AS}}\}_{d=0}^{D-1}$ over the AS cycle interval $\mathcal{I}_{\mathrm{AS}} = \{0, \ldots, M+N'-1\}$ with $N' = N_{\mathrm{df}} + \left\lceil \frac{K_\mathrm{r}}{K'_\mathrm{r}} \right\rceil N_{\mathrm{pf}}$.

4.3.3 Choice of Subspace Dimension

To determine the subspace dimension D, the method of Sec. 3.3.3 in Chapter 3 is used, i.e., Eq. (3.32).

4.4 Symbol Error Probability (SEP) Analysis

In this section, we analyze the proposed receive AS algorithm from Section 4.3, to evaluate the SEP of MPSK and MQAM in time-varying channels.

4.4.1 CSI Model

The estimate of the channel gain $h[m]$ can be expressed in terms of the true channel gain $h[m]$ and the error in the estimate of $h[m]$ [45, 89]. The CSI uncertainty model for Slepian basis expansion estimation can be expressed as

$$\hat{h}^{\mathrm{SE}}_{k_\mathrm{r}}[m] = h_{k_\mathrm{r}}[m] + e^{\mathrm{SE}}_{k_\mathrm{r}}[m], \qquad 1 \le k_\mathrm{r} \le K_\mathrm{r} \tag{4.21}$$

where $h_{k_\mathrm{r}}[m]$ is the true channel gain, $e^{\mathrm{SE}}_{k_\mathrm{r}}[m]$ is the estimation error, and $\hat{h}^{\mathrm{SE}}_{k_\mathrm{r}}[m]$ is the estimated channel gain. We assume the variables $h_{k_\mathrm{r}}[m]$ and $e^{\mathrm{SE}}_{k_\mathrm{r}}[m]$ are uncorrelated. The true channel gain $h_{k_\mathrm{r}}[m]$ is modelled as a zero-mean circularly symmetric complex Gaussian RV with unit-variance. We refer to Secs. 3.4.1 and 3.3.3 in Chapter 3 for more details about CSI uncertainty model for Slepian basis expansion method.

From (4.21), the variance of the channel gain estimate $\hat{h}^{\mathrm{SE}}_{k_\mathrm{r}}[m]$ can be expressed as

$$\sigma^2_{\hat{h}^{\mathrm{SE}}_{k_\mathrm{r}}}[m] = \sigma^2_{h_{k_\mathrm{r}}}[m] + \sigma^2_{e^{\mathrm{SE}}_{k_\mathrm{r}}}[m] = 1 + \mathrm{MSE}^{\mathrm{SE}}_{k_\mathrm{r}}[m]\,. \tag{4.22}$$

The CSI model for the Slepian basis expansion predictor can be obtained from (4.21)–(4.22) by replacing superscript $(\cdot)^{\mathrm{SE}}$ by $(\cdot)^{\mathrm{SP}}$ and $T^{k_\mathrm{r}}_{\mathrm{tp}}$ by $T^{k_\mathrm{r}}_{\mathrm{ps}}$.

4.4.2 SEP Analysis

The soft estimate is obtained by maximal-ratio combining (MRC) of the received soft symbols from $\mathcal{S}_m$ as

$$r_{\mathcal{S}_m}[m] = \sum_{k_\mathrm{r}=1}^{K'_\mathrm{r}} \left(\hat{h}^{\mathrm{SE}}_{i^m_{k_\mathrm{r}}}[m]\right)^* y_{i^m_{k_\mathrm{r}}}[m]\,. \tag{4.23}$$

Conditioned on $\left\{\hat{h}^{\mathrm{SP}}_{i^m_{k_\mathrm{r}}}[m]\right\}_{k_\mathrm{r}=1}^{K'_\mathrm{r}}$, $\left\{\hat{h}^{\mathrm{SE}}_{i^m_{k_\mathrm{r}}}[m]\right\}_{k_\mathrm{r}=1}^{K'_\mathrm{r}}$ and $d[m]$, using standard results on moments of conditional Gaussian RVs it is shown in Appendix B that $r_{\mathcal{S}_m}[m]$ in (4.23) is a complex Gaussian RV whose conditional mean $\mu_{r_{\mathcal{S}_m}}[m]$ and variance

$\sigma^2_{r_{\mathcal{S}_m}}[m]$ are given, respectively, by

$$\begin{aligned}
\mu_{r_{\mathcal{S}_m}}[m] &\triangleq \mathbb{E}\left\{ r_{\mathcal{S}_m}[m] \;\middle|\; \left\{\hat{h}^{\mathrm{SP}}_{i^m_{k_\mathrm{r}}}[m]\right\}_{k_\mathrm{r}=1}^{K'_\mathrm{r}}, \left\{\hat{h}^{\mathrm{SE}}_{i^m_{k_\mathrm{r}}}[m]\right\}_{k_\mathrm{r}=1}^{K'_\mathrm{r}}, d[m] \right\} \\
&= \sum_{k_\mathrm{r}=1}^{K'_\mathrm{r}} \left(\hat{h}^{\mathrm{SE}}_{i^m_{k_\mathrm{r}}}[m]\right)^* \mathbb{E}\left\{ y_{i^m_{k_\mathrm{r}}}[m] \;\middle|\; \hat{h}^{\mathrm{SP}}_{i^m_{k_\mathrm{r}}}[m], \hat{h}^{\mathrm{SE}}_{i^m_{k_\mathrm{r}}}[m], d[m] \right\} \\
&= d[m] \sum_{k_\mathrm{r}=1}^{K'_\mathrm{r}} \left(\frac{\sigma^2_{\hat{h}^{\mathrm{SE}}_{i^m_{k_\mathrm{r}}}}[m] - \sigma_{\hat{h}^{\mathrm{SE}}_{i^m_{k_\mathrm{r}}}}[m]\, \sigma_{\hat{h}^{\mathrm{SP}}_{i^m_{k_\mathrm{r}}}}[m]\, \rho_{\hat{h}^{\mathrm{SE}}_{i^m_{k_\mathrm{r}}}[m], \hat{h}^{\mathrm{SP}}_{i^m_{k_\mathrm{r}}}[m]}}{\sigma^2_{\hat{h}^{\mathrm{SP}}_{i^m_{k_\mathrm{r}}}}[m]\, \sigma^2_{\hat{h}^{\mathrm{SE}}_{i^m_{k_\mathrm{r}}}}[m] \left(1 - \left|\rho_{\hat{h}^{\mathrm{SP}}_{i^m_{k_\mathrm{r}}}[m], \hat{h}^{\mathrm{SE}}_{i^m_{k_\mathrm{r}}}[m]}\right|^2\right)} \right) \\
&\quad \times \left(\hat{h}^{\mathrm{SE}}_{i^m_{k_\mathrm{r}}}[m]\right)^* \hat{h}^{\mathrm{SP}}_{i^m_{k_\mathrm{r}}}[m] \\
&\quad + \left(\frac{\sigma^2_{\hat{h}^{\mathrm{SP}}_{i^m_{k_\mathrm{r}}}}[m] - \sigma_{\hat{h}^{\mathrm{SP}}_{i^m_{k_\mathrm{r}}}}[m]\, \sigma_{\hat{h}^{\mathrm{SE}}_{i^m_{k_\mathrm{r}}}}[m]\, \rho_{\hat{h}^{\mathrm{SP}}_{i^m_{k_\mathrm{r}}}[m], \hat{h}^{\mathrm{SE}}_{i^m_{k_\mathrm{r}}}[m]}}{\sigma^2_{\hat{h}^{\mathrm{SP}}_{i^m_{k_\mathrm{r}}}}[m]\, \sigma^2_{\hat{h}^{\mathrm{SE}}_{i^m_{k_\mathrm{r}}}}[m] \left(1 - \left|\rho_{\hat{h}^{\mathrm{SP}}_{i^m_{k_\mathrm{r}}}[m], \hat{h}^{\mathrm{SE}}_{i^m_{k_\mathrm{r}}}[m]}\right|^2\right)} \right) \left|\hat{h}^{\mathrm{SE}}_{i^m_{k_\mathrm{r}}}[m]\right|^2 \qquad (4.24)
\end{aligned}$$

$$\begin{aligned}
\sigma^2_{r_{\mathcal{S}_m}}[m] &\triangleq \mathrm{var}\left\{ r_{\mathcal{S}_m}[m] \;\middle|\; \left\{\hat{h}^{\mathrm{SP}}_{i^m_{k_\mathrm{r}}}[m]\right\}_{k_\mathrm{r}=1}^{K'_\mathrm{r}}, \left\{\hat{h}^{\mathrm{SE}}_{i^m_{k_\mathrm{r}}}[m]\right\}_{k_\mathrm{r}=1}^{K'_\mathrm{r}}, d[m] \right\} \\
&= \sum_{k_\mathrm{r}=1}^{K'_\mathrm{r}} \left|\hat{h}^{\mathrm{SE}}_{i^m_{k_\mathrm{r}}}[m]\right|^2 \mathrm{var}\left\{ y_{i^m_{k_\mathrm{r}}}[m] \;\middle|\; \hat{h}^{\mathrm{SP}}_{i^m_{k_\mathrm{r}}}[m], \hat{h}^{\mathrm{SE}}_{i^m_{k_\mathrm{r}}}[m], d[m] \right\} \\
&= \sum_{k_\mathrm{r}=1}^{K'_\mathrm{r}} \left|\hat{h}^{\mathrm{SE}}_{i^m_{k_\mathrm{r}}}[m]\right|^2 \left[|d[m]|^2 \left(1 - \frac{\sigma^2_{\hat{h}^{\mathrm{SP}}_{i^m_{k_\mathrm{r}}}}[m] + \sigma^2_{\hat{h}^{\mathrm{SE}}_{i^m_{k_\mathrm{r}}}}[m]}{\sigma^2_{\hat{h}^{\mathrm{SP}}_{i^m_{k_\mathrm{r}}}}[m]\, \sigma^2_{\hat{h}^{\mathrm{SE}}_{i^m_{k_\mathrm{r}}}}[m] \left(1 - \left|\rho_{\hat{h}^{\mathrm{SP}}_{i^m_{k_\mathrm{r}}}[m], \hat{h}^{\mathrm{SE}}_{i^m_{k_\mathrm{r}}}[m]}\right|^2\right)} \right.\right. \\
&\quad \left.\left. + \frac{2\Re\left\{ \rho_{\hat{h}^{\mathrm{SP}}_{i^m_{k_\mathrm{r}}}[m], \hat{h}^{\mathrm{SE}}_{i^m_{k_\mathrm{r}}}[m]} \right\}}{\sigma_{\hat{h}^{\mathrm{SP}}_{i^m_{k_\mathrm{r}}}}[m]\, \sigma_{\hat{h}^{\mathrm{SE}}_{i^m_{k_\mathrm{r}}}}[m] \left(1 - \left|\rho_{\hat{h}^{\mathrm{SP}}_{i^m_{k_\mathrm{r}}}[m], \hat{h}^{\mathrm{SE}}_{i^m_{k_\mathrm{r}}}[m]}\right|^2\right)} \right) + N_\mathrm{o} \right] \qquad (4.25)
\end{aligned}$$

where $\rho_{\hat{h}^{\mathrm{SP}}_{i^m_{k_\mathrm{r}}}[m],\hat{h}^{\mathrm{SE}}_{i^m_{k_\mathrm{r}}}[m]} = \frac{\mathbb{E}\left\{\hat{h}^{\mathrm{SP}}_{i^m_{k_\mathrm{r}}}[m]\left(\hat{h}^{\mathrm{SE}}_{i^m_{k_\mathrm{r}}}[m]\right)^*\right\}}{\sqrt{\mathbb{E}\left\{\left|\hat{h}^{\mathrm{SP}}_{i^m_{k_\mathrm{r}}}[m]\right|^2\right\}\mathbb{E}\left\{\left|\hat{h}^{\mathrm{SE}}_{i^m_{k_\mathrm{r}}}[m]\right|^2\right\}}}$ denotes the complex correlation coefficient of $\hat{h}^{\mathrm{SP}}_{i^m_{k_\mathrm{r}}}[m]$ and $\hat{h}^{\mathrm{SE}}_{i^m_{k_\mathrm{r}}}[m]$, and $\Re\{\cdot\}$ denotes taking the real part. We note that (4.24) depends on both $\left(\hat{h}^{\mathrm{SE}}_{i^m_{k_\mathrm{r}}}[m]\right)^* \hat{h}^{\mathrm{SP}}_{i^m_{k_\mathrm{r}}}[m]$ and $\left|\hat{h}^{\mathrm{SE}}_{i^m_{k_\mathrm{r}}}[m]\right|^2$ which themselves are complicated functions of the observed quantities and the a priori CSI uncertainty model.

Denote the random variable (RV) $A' \triangleq \frac{\left|\mu_{r_{\mathcal{S}_m}}[m]\right|^2}{\sigma^2_{r_{\mathcal{S}_m}}[m]}$. From (4.24) and (4.25), notice that the RV A' depends on the selected antennas subset $\mathcal{S}_m$, $\{\hat{h}^{\mathrm{SE}}_{i^m_{k_\mathrm{r}}}[m] \mid k_\mathrm{r} = 1,\ldots,K'_\mathrm{r}\}$, and $\{\hat{h}^{\mathrm{SP}}_{i^m_{k_\mathrm{r}}}[m] \mid k_\mathrm{r} = 1,\ldots,K'_\mathrm{r}\}$. The SEP of MPSK and MQAM symbols received at time m conditioned on $A' = \frac{\left|\mu_{r_{\mathcal{S}_m}}[m]\right|^2}{\sigma^2_{r_{\mathcal{S}_m}}[m]}$, i.e., $\mathcal{S}_m$, $\left\{\hat{h}^{\mathrm{SP}}_{i^m_{k_\mathrm{r}}}[m]\right\}$ and $\left\{\hat{h}^{\mathrm{SE}}_{i^m_{k_\mathrm{r}}}[m]\right\}$ for $k_\mathrm{r} = 1,\ldots,K'_\mathrm{r}$ can be computed via the method found in [5,53,77,79], respectively, as

$$\mathrm{SEP}_m(A') = \frac{1}{\pi}\int_0^{\frac{\mathtt{M}-1}{\mathtt{M}}\pi} \exp\left(\frac{-\sin^2\left(\frac{\pi}{\mathtt{M}}\right)}{\sin^2(\theta)}A'\right)\mathrm{d}\theta \tag{4.26}$$

$$\begin{aligned}\mathrm{SEP}_m(A') &= \frac{4}{\pi}\left(1-\frac{1}{\sqrt{\mathtt{M}}}\right)\int_0^{\frac{\pi}{2}} \exp\left(\frac{-3}{2(\mathtt{M}-1)\sin^2(\theta)}A'\right)\mathrm{d}\theta \\ &\quad -\frac{4}{\pi}\left(1-\frac{1}{\sqrt{\mathtt{M}}}\right)^2\int_0^{\frac{\pi}{4}} \exp\left(\frac{-3}{2(\mathtt{M}-1)\sin^2(\theta)}A'\right)\mathrm{d}\theta.\end{aligned} \tag{4.27}$$

After averaging over A', the SEP of MPSK and MQAM as a function of the SNR per branch $\eta \triangleq \frac{E_s}{N_0}$ are given, respectively, by

$$\mathrm{SEP}_m(\eta) = \frac{1}{\pi}\int_0^{\frac{\mathtt{M}-1}{\mathtt{M}}\pi}\int_0^{\infty} \exp\left(\frac{-\sin^2\left(\frac{\pi}{\mathtt{M}}\right)}{\sin^2(\theta)}a'\right) f_{A'}(a')\,\mathrm{d}a'\,\mathrm{d}\theta \tag{4.28}$$

$$\begin{aligned}\mathrm{SEP}_m(\eta) &= \frac{4}{\pi}\left(1-\frac{1}{\sqrt{\mathtt{M}}}\right)\int_0^{\frac{\pi}{2}}\int_0^{\infty}\exp\left(\frac{-3}{2(\mathtt{M}-1)\sin^2(\theta)}a'\right)f_{A'}(a')\,\mathrm{d}\theta \\ &\quad -\frac{4}{\pi}\left(1-\frac{1}{\sqrt{\mathtt{M}}}\right)^2\int_0^{\frac{\pi}{4}}\int_0^{\infty}\exp\left(\frac{-3}{2(\mathtt{M}-1)\sin^2(\theta)}a'\right)f_{A'}(a')\,\mathrm{d}\theta\end{aligned} \tag{4.29}$$

where $f_{A'}(a')$ is the probability density function (PDF) of the RV $A' = \frac{\left|\mu_{r_{\mathcal{S}_m}}[m]\right|^2}{\sigma^2_{r_{\mathcal{S}_m}}[m]}$. The SEP expressions in (4.28) and (4.29) can be, respectively, integrated numerically from $\mathrm{SEP}_m(A')$ in (4.26) and (4.27) using Monte Carlo averaging techniques [28].

To avoid numerical integration, we next derive SEP expressions of MPSK and MQAM which provide analytical insight for both symbol-by-symbol and per-packet AS described in Sec. 4.3. The first and second order statistics in (4.24) and (4.25) are replaced by (4.35) and (4.36), respectively. In summary, (4.24) and (4.25) are conditioned on $\left\{\hat{h}^{\mathrm{SP}}_{\hat{\iota}^m_{k_\mathrm{r}}}[m]\right\}_{k_\mathrm{r}=1}^{K'_\mathrm{r}}$ and $\left\{\hat{h}^{\mathrm{SE}}_{\hat{\iota}^m_{k_\mathrm{r}}}[m]\right\}_{k_\mathrm{r}=1}^{K'_\mathrm{r}}$, while the statistics in (4.35) and (4.36) are conditioned on the refined channel gain estimates $\left\{\hat{h}^{\mathrm{SE}}_{\hat{\iota}^m_{k_\mathrm{r}}}[m]\right\}_{k_\mathrm{r}=1}^{K'_\mathrm{r}}$.

SEP for MPSK

Theorem 4.1. The first and second order statistics conditioned on $\left\{\hat{h}^{\mathrm{SP}}_{\hat{\iota}^m_{k_\mathrm{r}}}[m]\right\}_{k_\mathrm{r}=1}^{K'_\mathrm{r}}$ and $\left\{\hat{h}^{\mathrm{SE}}_{\hat{\iota}^m_{k_\mathrm{r}}}[m]\right\}_{k_\mathrm{r}=1}^{K'_\mathrm{r}}$ of the MRC decision variable in (4.23) are given, respectively, by (4.24) and (4.25). By replacing the first and second order conditional statistics in (4.24) and (4.25), respectively, by the first and second order statistics in (4.35) and (4.36) conditioned only on the refined channel gain estimates $\left\{\hat{h}^{\mathrm{SE}}_{\hat{\iota}^m_{k_\mathrm{r}}}[m]\right\}_{k_\mathrm{r}=1}^{K'_\mathrm{r}}$, the MPSK SEP for a symbol received at time m for a system with one transmit and K_r receive antennas employing the K'_r out of K_r symbol-by-symbol receive AS in Sec. 4.3

is

$$SEP'_m(\eta) = \frac{1}{\pi}\sum_{P_\pi\in\mathfrak{P}}\left(\prod_{k_r=1}^{K_r}\left[\sum_{r=1}^{k_r}\frac{\Gamma_{P_\pi(k_r)}[m]}{\Gamma_{P_\pi(r)}[m]}\right]^{-1}\right)\int_0^{\frac{M-1}{M}\pi}\left(\prod_{k_r=1}^{K'_r}\frac{\sin^2(\theta)}{\sin^2(\theta)+\sigma^2_{X^{SE}_{i^m_{k_r}}}[m]}\right)$$
$$\times\left(\prod_{k_r=1}^{K_r}\frac{\sin^2(\theta)+\sigma^2_{X^{SE}_{i^m_{k_r}}}[m]}{\sin^2(\theta)+\sigma^2_{X^{SE}_{i^m_{k_r}}}[m]+\digamma_{k_r}}\right)\mathrm{d}\theta \tag{4.30}$$

where $\eta=\frac{E_s}{N_0}$ is SNR, P_π is a permutation of set $\{1,2,\ldots,K_r\}$ and $\mathfrak{P}$ the set of all $K_r!$ permutations. $\sigma^2_{X^{SE}_{i^m_{k_r}}}[m]=\frac{b^{SE}_{i^m_{k_r}}[m]\left(1-\left|\rho_{\hat{h}^{SE}_{i^m_{k_r}}[m],\hat{h}^{SP}_{i^m_{k_r}}[m]}\right|^2\right)}{\zeta^{SE}_{i^m_{k_r}}[m]}$ where $\zeta^{SE}_{i^m_{k_r}}[m]\triangleq\frac{1}{1+\sigma^2_{e^{SE}_{i^m_{k_r}}}[m]}=\frac{1}{1+\mathrm{MSE}^{SE}_{i^m_{k_r}}[m]}$, $b^{SE}_{i^m_{k_r}}[m]\triangleq\frac{\left(\zeta^{SE}_{i^m_{k_r}}[m]\right)^2\sin^2\left(\frac{\pi}{M}\right)}{1-\zeta^{SE}_{i^m_{k_r}}[m]+\eta^{-1}}$, and $\rho_{\hat{h}^{SE}_{i^m_{k_r}}[m],\hat{h}^{SP}_{i^m_{k_r}}[m]}$ denote the correlation coefficient of $\hat{h}^{SE}_{i^m_{k_r}}[m]$ and $\hat{h}^{SP}_{i^m_{k_r}}[m]$. Also $\digamma_{k_r}\triangleq k_r\left[\sum_{r=1}^{k_r}\frac{1}{\Gamma_{P_\pi(r)}[m]}\right]^{-1}$ for $k_r\le K'_r$, and $\digamma_{k_r}\triangleq K'_r\left[\sum_{r=1}^{k_r}\frac{1}{\Gamma_{P_\pi(r)}[m]}\right]^{-1}$ for $k_r>K'_r$ where $\Gamma_{i^m_{k_r}}[m]=\frac{b^{SE}_{i^m_{k_r}}[m]\left|\rho_{\hat{h}^{SE}_{i^m_{k_r}}[m],\hat{h}^{SP}_{i^m_{k_r}}[m]}\right|^2}{\zeta^{SE}_{i^m_{k_r}}[m]}$.

Proof. The received signal in (4.14) can be expressed as

$$y_{i^m_{k_r}}[m]=\hat{h}^{SE}_{i^m_{k_r}}[m]\,d[m]-e^{SE}_{i^m_{k_r}}[m]\,d[m]+n_{i^m_{k_r}}[m] \tag{4.31}$$

where we have used $\hat{h}^{SE}_{i^m_{k_r}}[m]=h_{i^m_{k_r}}[m]+e^{SE}_{i^m_{k_r}}[m]$ with $e^{SE}_{i^m_{k_r}}[m]$ the estimation error and $k_r=1,2,\ldots,K'_r$.

Conditioned on $\hat{h}^{SE}_{i^m_{k_r}}[m]$ and $d[m]$, using standard results on moments of conditional Gaussian RVs it is shown in Appendix C that $y_{i^m_{k_r}}[m]$ in (4.31) is a complex

Gaussian RV whose conditional mean $\mu_{y_{\hat{\imath}^m_{k_\mathrm{r}}}}[m]$ and variance $\sigma^2_{y_{\hat{\imath}^m_{k_\mathrm{r}}}}[m]$ are given by

$$\begin{aligned}
\mu_{y_{\hat{\imath}^m_{k_\mathrm{r}}}}[m] &\triangleq \mathbb{E}\left\{ y_{\hat{\imath}^m_{k_\mathrm{r}}}[m] \mid \hat{h}^{\mathrm{SE}}_{\hat{\imath}^m_{k_\mathrm{r}}}[m], d[m] \right\} \\
&= \hat{h}^{\mathrm{SE}}_{\hat{\imath}^m_{k_\mathrm{r}}}[m]\, d[m] - \mathbb{E}\left\{ e^{\mathrm{SE}}_{\hat{\imath}^m_{k_\mathrm{r}}}[m] \mid \hat{h}^{\mathrm{SE}}_{\hat{\imath}^m_{k_\mathrm{r}}}[m] \right\} d[m] \\
&\quad + \mathbb{E}\left\{ n_{\hat{\imath}^m_{k_\mathrm{r}}}[m] \mid \hat{h}^{\mathrm{SE}}_{\hat{\imath}^m_{k_\mathrm{r}}}[m] \right\} \\
&= \hat{h}^{\mathrm{SE}}_{\hat{\imath}^m_{k_\mathrm{r}}}[m]\, d[m]\, \zeta^{\mathrm{SE}}_{\hat{\imath}^m_{k_\mathrm{r}}}[m] \qquad (4.32) \\
\sigma^2_{y_{\hat{\imath}^m_{k_\mathrm{r}}}}[m] &\triangleq \mathrm{var}\left\{ y_{\hat{\imath}^m_{k_\mathrm{r}}}[m] \mid \hat{h}^{\mathrm{SE}}_{\hat{\imath}^m_{k_\mathrm{r}}}[m], d[m] \right\} \\
&= |d[m]|^2 \,\mathrm{var}\left\{ e^{\mathrm{SE}}_{\hat{\imath}^m_{k_\mathrm{r}}}[m] \mid \hat{h}^{\mathrm{SE}}_{\hat{\imath}^m_{k_\mathrm{r}}}[m] \right\} \\
&\quad + \mathrm{var}\left\{ n_{\hat{\imath}^m_{k_\mathrm{r}}}[m] \mid \hat{h}^{\mathrm{SE}}_{\hat{\imath}^m_{k_\mathrm{r}}}[m] \right\} \\
&= |d[m]|^2 \left(1 - \zeta^{\mathrm{SE}}_{\hat{\imath}^m_{k_\mathrm{r}}}[m] + \eta^{-1} \right) \qquad (4.33)
\end{aligned}$$

where $\zeta^{\mathrm{SE}}_{\hat{\imath}^m_{k_\mathrm{r}}}[m] = \frac{1}{1+\sigma^2_{e^{\mathrm{SE}}_{\hat{\imath}^m_{k_\mathrm{r}}}}[m]} = \frac{1}{1+\mathrm{MSE}^{\mathrm{SE}}_{\hat{\imath}^m_{k_\mathrm{r}}}[m]}$ and $\eta = \frac{E_s}{N_\mathrm{o}}$ is SNR per branch.

The maximum-likelihood (ML) soft estimate is obtained by conducting MRC on the received soft symbols from $\mathcal{S}_m$ as

$$r'_{\mathcal{S}_m}[m] = \sum_{k_\mathrm{r}=1}^{K'_\mathrm{r}} \left(\frac{\zeta^{\mathrm{SE}}_{\hat{\imath}^m_{k_\mathrm{r}}}[m] \left(\hat{h}^{\mathrm{SE}}_{\hat{\imath}^m_{k_\mathrm{r}}}[m] \right)^* y_{\hat{\imath}^m_{k_\mathrm{r}}}[m]}{1 - \zeta^{\mathrm{SE}}_{\hat{\imath}^m_{k_\mathrm{r}}}[m] + \eta^{-1}} \right) \qquad (4.34)$$

where the scaling factor explicitly takes account of the channel estimation uncertainty, i.e., the variances in (4.33).

Conditioned on $\left\{ \hat{h}^{\mathrm{SE}}_{\hat{\imath}^m_{k_\mathrm{r}}}[m] \right\}_{k_\mathrm{r}=1}^{K'_\mathrm{r}}$ and $d[m]$, from (4.32) and (4.33) we get that $r'_{\mathcal{S}_m}[m]$ in (4.34) is a complex Gaussian RV whose conditional mean $\mu_{r'_{\mathcal{S}_m}}[m]$ and

variance $\sigma^2_{r'_{\mathcal{S}_m}}[m]$ are given by

$$\begin{aligned}
\mu_{r'_{\mathcal{S}_m}}[m] &\triangleq \mathbb{E}\left\{r'_{\mathcal{S}_m}[m] \mid \left\{\hat{h}^{\mathrm{SE}}_{i^m_{k_\mathrm{r}}}[m]\right\}_{k_\mathrm{r}=1}^{K'_\mathrm{r}}, d[m]\right\} \\
&= \sum_{k_\mathrm{r}=1}^{K'_\mathrm{r}} \frac{\zeta^{\mathrm{SE}}_{i^m_{k_\mathrm{r}}}[m]\left(\hat{h}^{\mathrm{SE}}_{i^m_{k_\mathrm{r}}}[m]\right)^*}{1-\zeta^{\mathrm{SE}}_{i^m_{k_\mathrm{r}}}[m]+\eta^{-1}}\mathbb{E}\left\{y_{i^m_{k_\mathrm{r}}}[m] \mid \hat{h}^{\mathrm{SE}}_{i^m_{k_\mathrm{r}}}[m], d[m]\right\} \\
&= \sum_{k_\mathrm{r}=1}^{K'_\mathrm{r}} \frac{\left|\hat{h}^{\mathrm{SE}}_{i^m_{k_\mathrm{r}}}[m]\right|^2\left(\zeta^{\mathrm{SE}}_{i^m_{k_\mathrm{r}}}[m]\right)^2 d[m]}{1-\zeta^{\mathrm{SE}}_{i^m_{k_\mathrm{r}}}[m]+\eta^{-1}} \qquad (4.35) \\
\sigma^2_{r'_{\mathcal{S}_m}}[m] &\triangleq \mathrm{var}\left\{r'_{\mathcal{S}_m}[m] \mid \left\{\hat{h}^{\mathrm{SE}}_{i^m_{k_\mathrm{r}}}[m]\right\}_{k_\mathrm{r}=1}^{K'_\mathrm{r}}, d[m]\right\} \\
&= \sum_{k_\mathrm{r}=1}^{K'_\mathrm{r}} \frac{\left|\hat{h}^{\mathrm{SE}}_{i^m_{k_\mathrm{r}}}[m]\right|^2\left(\zeta^{\mathrm{SE}}_{i^m_{k_\mathrm{r}}}[m]\right)^2}{\left(1-\zeta^{\mathrm{SE}}_{i^m_{k_\mathrm{r}}}[m]+\eta^{-1}\right)^2}\mathrm{var}\left\{y_{i^m_{k_\mathrm{r}}}[m] \mid \hat{h}^{\mathrm{SE}}_{i^m_{k_\mathrm{r}}}[m], d[m]\right\} \\
&= \sum_{k_\mathrm{r}=1}^{K'_\mathrm{r}} \frac{\left|\hat{h}^{\mathrm{SE}}_{i^m_{k_\mathrm{r}}}[m]\right|^2\left(\zeta^{\mathrm{SE}}_{i^m_{k_\mathrm{r}}}[m]\right)^2|d[m]|^2}{1-\zeta^{\mathrm{SE}}_{i^m_{k_\mathrm{r}}}[m]+\eta^{-1}}. \qquad (4.36)
\end{aligned}$$

The SEP of an MPSK symbol received at time m conditioned on $\left\{\hat{h}^{\mathrm{SP}}_{i^m_{k_\mathrm{r}}}[m]\right\}_{k_\mathrm{r}=1}^{K'_\mathrm{r}}$ and $\left\{\hat{h}^{\mathrm{SE}}_{i^m_{k_\mathrm{r}}}[m]\right\}_{k_\mathrm{r}=1}^{K'_\mathrm{r}}$ can be computed via the method found in [5, 53, 77, 79] as

$$\begin{aligned}
\mathrm{SEP}'_m\left(\left\{\hat{h}^{\mathrm{SP}}_{i^m_{k_\mathrm{r}}}[m]\right\}_{k_\mathrm{r}=1}^{K'_\mathrm{r}}, \left\{\hat{h}^{\mathrm{SE}}_{i^m_{k_\mathrm{r}}}[m]\right\}_{k_\mathrm{r}=1}^{K'_\mathrm{r}}\right) &= \frac{1}{\pi}\int_0^{\frac{\mathtt{M}-1}{\mathtt{M}}\pi}\exp\left(\frac{-\left|\mu_{r'_{\mathcal{S}_m}}[m]\right|^2\sin^2\left(\frac{\pi}{\mathtt{M}}\right)}{\sigma^2_{r'_{\mathcal{S}_m}}[m]\sin^2(\theta)}\right)\mathrm{d}\theta \\
&= \frac{1}{\pi}\int_0^{\frac{\mathtt{M}-1}{\mathtt{M}}\pi}\exp\left(\frac{-Y^{\mathrm{SE}}_{\mathcal{S}_m}[m]}{\sin^2(\theta)}\right)\mathrm{d}\theta \qquad (4.37)
\end{aligned}$$

where $\frac{\left|\mu_{r'_{\mathcal{S}_m}}[m]\right|^2}{\sigma^2_{r'_{\mathcal{S}_m}}[m]} = \sum_{k_\mathrm{r}=1}^{K'_\mathrm{r}} \frac{\left|\hat{h}^{\mathrm{SE}}_{i^m_{k_\mathrm{r}}}[m]\right|^2\left(\zeta^{\mathrm{SE}}_{i^m_{k_\mathrm{r}}}[m]\right)^2}{1-\zeta^{\mathrm{SE}}_{i^m_{k_\mathrm{r}}}[m]+\eta^{-1}}$ and the last equality follows from $Y^{\mathrm{SE}}_{\mathcal{S}_m}[m] \triangleq \sum_{k_\mathrm{r}=1}^{K'_\mathrm{r}}\left|X^{\mathrm{SE}}_{i^m_{k_\mathrm{r}}}[m]\right|^2$ with $X^{\mathrm{SE}}_{i^m_{k_\mathrm{r}}}[m] \triangleq \sqrt{b^{\mathrm{SE}}_{i^m_{k_\mathrm{r}}}[m]}\hat{h}^{\mathrm{SE}}_{i^m_{k_\mathrm{r}}}[m]$ and $b^{\mathrm{SE}}_{i^m_{k_\mathrm{r}}}[m] = \frac{\left(\zeta^{\mathrm{SE}}_{i^m_{k_\mathrm{r}}}[m]\right)^2\sin^2\left(\frac{\pi}{\mathtt{M}}\right)}{1-\zeta^{\mathrm{SE}}_{i^m_{k_\mathrm{r}}}[m]+\eta^{-1}}$.

The SEP averaged over $\left\{\hat{h}^{\mathrm{SE}}_{i^m_{k_\mathrm{r}}}[m]\right\}_{k_\mathrm{r}=1}^{K'_\mathrm{r}}$ is

$$\mathrm{SEP}'_m\left(\left\{\hat{h}^{\mathrm{SP}}_{i^m_{k_\mathrm{r}}}[m]\right\}_{k_\mathrm{r}=1}^{K'_\mathrm{r}}\right)=\frac{1}{\pi}\int_0^{\frac{\mathtt{M}-1}{\mathtt{M}}\pi}\mathcal{M}_{Y^{\mathrm{SE}}_{\mathcal{S}_m}[m]\ \mid\ \{\hat{h}^{\mathrm{SP}}_{i^m_{k_\mathrm{r}}}[m]\}_{k_\mathrm{r}=1}^{K'_\mathrm{r}}}\left(\frac{-1}{\sin^2(\theta)}\right)\mathrm{d}\theta \tag{4.38}$$

where $\mathcal{M}_{Y^{\mathrm{SE}}_{\mathcal{S}_m}[m]\ \mid\ \{\hat{h}^{\mathrm{SP}}_{i^m_{k_\mathrm{r}}}[m]\}_{k_\mathrm{r}=1}^{K'_\mathrm{r}}}(\cdot)$ is the moment generating function (MGF) of $Y^{\mathrm{SE}}_{\mathcal{S}_m}[m]$ conditioned on $\left\{\hat{h}^{\mathrm{SP}}_{i^m_{k_\mathrm{r}}}[m]\right\}_{k_\mathrm{r}=1}^{K'_\mathrm{r}}$.

Now conditioned on $\left\{\hat{h}^{\mathrm{SP}}_{i^m_{k_\mathrm{r}}}[m]\right\}_{k_\mathrm{r}=1}^{K'_\mathrm{r}}$, using standard results on moments of conditional Gaussian RVs it is shown in Appendix D that $X^{\mathrm{SE}}_{i^m_{k_\mathrm{r}}}[m]$ is a complex Gaussian RV with conditional mean $\mu_{X^{\mathrm{SE}}_{i^m_{k_\mathrm{r}}}}[m]$ and variance $\sigma^2_{X^{\mathrm{SE}}_{i^m_{k_\mathrm{r}}}}[m]$ are given by

$$\begin{aligned}
\mu_{X^{\mathrm{SE}}_{i^m_{k_\mathrm{r}}}}[m] &\triangleq \mathbb{E}\left\{X^{\mathrm{SE}}_{i^m_{k_\mathrm{r}}}[m]\ \mid\ \hat{h}^{\mathrm{SP}}_{i^m_{k_\mathrm{r}}}[m]\right\}\\
&= \sqrt{b^{\mathrm{SE}}_{i^m_{k_\mathrm{r}}}[m]}\,\mathbb{E}\left\{\hat{h}^{\mathrm{SE}}_{i^m_{k_\mathrm{r}}}[m]\ \mid\ \hat{h}^{\mathrm{SP}}_{i^m_{k_\mathrm{r}}}[m]\right\}\\
&= \sqrt{\frac{b^{\mathrm{SE}}_{i^m_{k_\mathrm{r}}}[m]\,\zeta^{\mathrm{SP}}_{i^m_{k_\mathrm{r}}}[m]}{\zeta^{\mathrm{SE}}_{i^m_{k_\mathrm{r}}}[m]}}\rho_{\hat{h}^{\mathrm{SE}}_{i^m_{k_\mathrm{r}}}[m],\hat{h}^{\mathrm{SP}}_{i^m_{k_\mathrm{r}}}[m]}\hat{h}^{\mathrm{SP}}_{i^m_{k_\mathrm{r}}}[m] \qquad (4.39)\\
\sigma^2_{X^{\mathrm{SE}}_{i^m_{k_\mathrm{r}}}}[m] &\triangleq \mathrm{var}\left\{X^{\mathrm{SE}}_{i^m_{k_\mathrm{r}}}[m]\ \mid\ \hat{h}^{\mathrm{SP}}_{i^m_{k_\mathrm{r}}}[m]\right\}\\
&= b^{\mathrm{SE}}_{i^m_{k_\mathrm{r}}}[m]\,\mathrm{var}\left\{\hat{h}^{\mathrm{SE}}_{i^m_{k_\mathrm{r}}}[m]\ \mid\ \hat{h}^{\mathrm{SP}}_{i^m_{k_\mathrm{r}}}[m]\right\}\\
&= \frac{b^{\mathrm{SE}}_{i^m_{k_\mathrm{r}}}[m]\left(1-\left|\rho_{\hat{h}^{\mathrm{SE}}_{i^m_{k_\mathrm{r}}}[m],\hat{h}^{\mathrm{SP}}_{i^m_{k_\mathrm{r}}}[m]}\right|^2\right)}{\zeta^{\mathrm{SE}}_{i^m_{k_\mathrm{r}}}[m]} \qquad (4.40)
\end{aligned}$$

where $\zeta^{\mathrm{SE}}_{i^m_{k_\mathrm{r}}}[m]\triangleq\frac{1}{1+\sigma^2_{e^{\mathrm{SE}}_{i^m_{k_\mathrm{r}}}}[m]}=\frac{1}{1+\mathrm{MSE}^{\mathrm{SE}}_{i^m_{k_\mathrm{r}}}[m]}$ and $\zeta^{\mathrm{SP}}_{i^m_{k_\mathrm{r}}}[m]\triangleq\frac{1}{1+\sigma^2_{e^{\mathrm{SP}}_{i^m_{k_\mathrm{r}}}}[m]}=\frac{1}{1+\mathrm{MSE}^{\mathrm{SP}}_{i^m_{k_\mathrm{r}}}[m]}$.

Therefore $Y^{\mathrm{SE}}_{\mathcal{S}_m}[m]$ follows a non-central Chi-squared distribution with conditional

MGF given by [24]

$$\mathcal{M}_{Y_{\mathcal{S}_m}^{\mathrm{SE}}[m] \mid \{\hat{h}_{i_{k_\mathrm{r}}^m}^{\mathrm{SP}}[m]\}_{k_\mathrm{r}=1}^{K_\mathrm{r}'}}(x) = \left(\prod_{k_\mathrm{r}=1}^{K_\mathrm{r}'} \frac{1}{1-\sigma^2_{X_{i_{k_\mathrm{r}}^m}^{\mathrm{SE}}}[m]\,x}\right) \exp\left(\sum_{k_\mathrm{r}=1}^{K_\mathrm{r}'} \frac{\mu^2_{X_{i_{k_\mathrm{r}}^m}^{\mathrm{SE}}}[m]\,x}{1-\sigma^2_{X_{i_{k_\mathrm{r}}^m}^{\mathrm{SE}}}[m]\,x}\right). \tag{4.41}$$

Substituting (4.41) in (4.38), yields

$$\begin{aligned}\mathrm{SEP}'_m\left(\left\{\hat{h}_{i_{k_\mathrm{r}}^m}^{\mathrm{SP}}[m]\right\}_{k_\mathrm{r}=1}^{K_\mathrm{r}'}\right) &= \frac{1}{\pi}\int_0^{\frac{\mathtt{M}-1}{\mathtt{M}}\pi}\left(\prod_{k_\mathrm{r}=1}^{K_\mathrm{r}'}\frac{\sin^2(\theta)}{\sin^2(\theta)+\sigma^2_{X_{i_{k_\mathrm{r}}^m}^{\mathrm{SE}}}[m]}\right)\times \\ &\quad \exp\left(-\sum_{k_\mathrm{r}=1}^{K_\mathrm{r}'}\frac{\xi_{i_{k_\mathrm{r}}^m}[m]\left|\hat{h}_{i_{k_\mathrm{r}}^m}^{\mathrm{SP}}[m]\right|^2}{\sin^2(\theta)+\sigma^2_{X_{i_{k_\mathrm{r}}^m}^{\mathrm{SE}}}[m]}\right)\mathrm{d}\theta \end{aligned}\tag{4.42}$$

where $\xi_{i_{k_\mathrm{r}}^m}[m] \triangleq \frac{b_{i_{k_\mathrm{r}}^m}^{\mathrm{SE}}[m]\zeta_{i_{k_\mathrm{r}}^m}^{\mathrm{SP}}[m]\left|\rho_{\hat{h}_{i_{k_\mathrm{r}}^m}^{\mathrm{SE}}[m],\hat{h}_{i_{k_\mathrm{r}}^m}^{\mathrm{SP}}[m]}\right|^2}{\zeta_{i_{k_\mathrm{r}}^m}^{\mathrm{SE}}[m]}$. Denoting by $\Upsilon_{i_{k_\mathrm{r}}^m}[m] \triangleq \xi_{i_{k_\mathrm{r}}^m}[m]\left|\hat{h}_{i_{k_\mathrm{r}}^m}^{\mathrm{SP}}[m]\right|^2$ the exponential RV with mean $\Gamma_{i_{k_\mathrm{r}}^m}[m] \triangleq \mathbb{E}\left\{\Upsilon_{i_{k_\mathrm{r}}^m}[m]\right\} = \frac{b_{i_{k_\mathrm{r}}^m}^{\mathrm{SE}}[m]\left|\rho_{\hat{h}_{i_{k_\mathrm{r}}^m}^{\mathrm{SE}}[m],\hat{h}_{i_{k_\mathrm{r}}^m}^{\mathrm{SP}}[m]}\right|^2}{\zeta_{i_{k_\mathrm{r}}^m}^{\mathrm{SE}}[m]}$, averaging over $\left\{\hat{h}_{i_{k_\mathrm{r}}^m}^{\mathrm{SP}}[m]\right\}_{k_\mathrm{r}=1}^{K_\mathrm{r}'}$ and using the virtual branch combining (VBC) technique [94], yields the desired result. □

SEP for MQAM

Theorem 4.2. The first and second order statistics conditioned on $\left\{\hat{h}_{i_{k_\mathrm{r}}^m}^{\mathrm{SP}}[m]\right\}_{k_\mathrm{r}=1}^{K_\mathrm{r}'}$ and $\left\{\hat{h}_{i_{k_\mathrm{r}}^m}^{\mathrm{SE}}[m]\right\}_{k_\mathrm{r}=1}^{K_\mathrm{r}'}$ of the MRC decision variable in (4.23) are given, respectively, by (4.24) and (4.25). By replacing the first and second order conditional statistics in (4.24) and (4.25), respectively, by the first and second order statistics in (4.35)

and (4.36) conditioned only on the refined channel gain estimates $\left\{\hat{h}^{\mathrm{SE}}_{i^m_{k_\mathrm{r}}}[m]\right\}_{k_\mathrm{r}=1}^{K'_\mathrm{r}}$, the MQAM SEP for a symbol received at time m for a system with one transmit and K_r receive antennas employing the K'_r out of K_r symbol-by-symbol receive AS in Sec. 4.3 is

$$\begin{aligned}
SEP'_m(\eta) &= \frac{4}{\pi}\left(1-\frac{1}{\sqrt{M}}\right)\sum_{P_\pi\in\mathfrak{P}}\left(\prod_{k_r=1}^{K_r}\left[\sum_{r=1}^{k_r}\frac{\Gamma_{P_\pi(k_r)}[m]}{\Gamma_{P_\pi(r)}[m]}\right]^{-1}\right)\\
&\quad\times\int_0^{\frac{\pi}{2}}\left(\prod_{k_r=1}^{K'_r}\frac{\sin^2(\theta)}{\sin^2(\theta)+\frac{3}{2(M-1)}\sigma^2_{X^{SE}_{i^m_{k_r}}}[m]}\right)\\
&\quad\times\left(\prod_{k_r=1}^{K_r}\frac{\sin^2(\theta)+\frac{3}{2(M-1)}\sigma^2_{X^{SE}_{i^m_{k_r}}}[m]}{\sin^2(\theta)+\frac{3}{2(M-1)}\sigma^2_{X^{SE}_{i^m_{k_r}}}[m]+\digamma_{k_r}}\right)\mathrm{d}\theta\\
&\quad-\frac{4}{\pi}\left(1-\frac{1}{\sqrt{M}}\right)^2\sum_{P_\pi\in\mathfrak{P}}\left(\prod_{k_r=1}^{K_r}\left[\sum_{r=1}^{k_r}\frac{\Gamma_{P_\pi(k_r)}[m]}{\Gamma_{P_\pi(r)}[m]}\right]^{-1}\right)\\
&\quad\times\int_0^{\frac{\pi}{4}}\left(\prod_{k_r=1}^{K'_r}\frac{\sin^2(\theta)}{\sin^2(\theta)+\frac{3}{2(M-1)}\sigma^2_{X^{SE}_{i^m_{k_r}}}[m]}\right)\\
&\quad\times\left(\prod_{k_r=1}^{K_r}\frac{\sin^2(\theta)+\frac{3}{2(M-1)}\sigma^2_{X^{SE}_{i^m_{k_r}}}[m]}{\sin^2(\theta)+\frac{3}{2(M-1)}\sigma^2_{X^{SE}_{i^m_{k_r}}}[m]+\digamma_{k_r}}\right)\mathrm{d}\theta
\end{aligned}\tag{4.43}$$

where $\eta=\frac{E_s}{N_0}$ is SNR, P_π is a permutation of set $\{1,2,\ldots,K_\mathrm{r}\}$ and $\mathfrak{P}$ the set of all $K_\mathrm{r}!$ permutations. $\sigma^2_{X^{\mathrm{SE}}_{i^m_{k_\mathrm{r}}}}[m]=\frac{b^{\mathrm{SE}}_{i^m_{k_\mathrm{r}}}[m]\left(1-\left|\rho_{\hat{h}^{\mathrm{SE}}_{i^m_{k_\mathrm{r}}}[m],\hat{h}^{\mathrm{SP}}_{i^m_{k_\mathrm{r}}}[m]}\right|^2\right)}{\zeta^{\mathrm{SE}}_{i^m_{k_\mathrm{r}}}[m]}$ where $\zeta^{\mathrm{SE}}_{i^m_{k_\mathrm{r}}}[m]=\frac{1}{1+\sigma^2_{e^{\mathrm{SE}}_{i^m_{k_\mathrm{r}}}}[m]}=\frac{1}{1+\mathrm{MSE}^{\mathrm{SE}}_{i^m_{k_\mathrm{r}}}[m]}$, $b^{\mathrm{SE}}_{i^m_{k_\mathrm{r}}}[m]=\frac{\left(\zeta^{\mathrm{SE}}_{i^m_{k_\mathrm{r}}}[m]\right)^2}{1-\zeta^{\mathrm{SE}}_{i^m_{k_\mathrm{r}}}[m]+\eta^{-1}}$, and $\rho_{\hat{h}^{\mathrm{SE}}_{i^m_{k_\mathrm{r}}}[m],\hat{h}^{\mathrm{SP}}_{i^m_{k_\mathrm{r}}}[m]}$ denote the correlation coefficient of $\hat{h}^{\mathrm{SE}}_{i^m_{k_\mathrm{r}}}[m]$ and $\hat{h}^{\mathrm{SP}}_{i^m_{k_\mathrm{r}}}[m]$. Also $\digamma_{k_\mathrm{r}}\triangleq k_\mathrm{r}\left[\sum_{r=1}^{k_\mathrm{r}}\frac{1}{\Gamma_{P_\pi(r)}[m]}\right]^{-1}$ for $k_\mathrm{r}\leq K'_\mathrm{r}$, and $\digamma_{k_\mathrm{r}}\triangleq$

$K'_{\mathrm{r}}\left[\sum_{r=1}^{k_{\mathrm{r}}}\frac{1}{\Gamma_{P_\pi(r)}[m]}\right]^{-1}$ for $k_{\mathrm{r}} > K'_{\mathrm{r}}$ where $\Gamma_{i^m_{k_{\mathrm{r}}}}[m] = \frac{3}{2(\mathtt{M}-1)}\left(\frac{b^{\mathrm{SE}}_{i^m_{k_{\mathrm{r}}}}[m]\left|\rho_{\hat{h}^{\mathrm{SE}}_{i^m_{k_{\mathrm{r}}}}[m],\hat{h}^{\mathrm{SP}}_{i^m_{k_{\mathrm{r}}}}[m]}\right|^2}{\zeta^{\mathrm{SE}}_{i^m_{k_{\mathrm{r}}}}[m]}\right)$.

Proof. The SEP of an MQAM symbol received at time m conditioned on $\left\{\hat{h}^{\mathrm{SP}}_{i^m_{k_{\mathrm{r}}}}[m]\right\}_{k_{\mathrm{r}}=1}^{K'_{\mathrm{r}}}$ and $\left\{\hat{h}^{\mathrm{SE}}_{i^m_{k_{\mathrm{r}}}}[m]\right\}_{k_{\mathrm{r}}=1}^{K'_{\mathrm{r}}}$ can be computed via the method found in [5, 53, 77, 79]

$$\begin{aligned}
\mathrm{SEP}'_m\left(\left\{\hat{h}^{\mathrm{SP}}_{i^m_{k_{\mathrm{r}}}}[m]\right\}_{k_{\mathrm{r}}=1}^{K'_{\mathrm{r}}},\left\{\hat{h}^{\mathrm{SE}}_{i^m_{k_{\mathrm{r}}}}[m]\right\}_{k_{\mathrm{r}}=1}^{K'_{\mathrm{r}}}\right) &= \frac{4}{\pi}\left(1-\frac{1}{\sqrt{\mathtt{M}}}\right)\int_0^{\frac{\pi}{2}} \\
&\quad \exp\left(\frac{-3}{2\left(\mathtt{M}-1\right)\sin^2\left(\theta\right)}\frac{\left|\mu_{r'_{\mathcal{S}_m}}[m]\right|^2}{\sigma^2_{r'_{\mathcal{S}_m}}[m]}\right)\mathrm{d}\theta \\
&\quad -\frac{4}{\pi}\left(1-\frac{1}{\sqrt{\mathtt{M}}}\right)^2\int_0^{\frac{\pi}{4}} \\
&\quad \exp\left(\frac{-3}{2\left(\mathtt{M}-1\right)\sin^2\left(\theta\right)}\frac{\left|\mu_{r'_{\mathcal{S}_m}}[m]\right|^2}{\sigma^2_{r'_{\mathcal{S}_m}}[m]}\right)\mathrm{d}\theta \\
&= \frac{4}{\pi}\left(1-\frac{1}{\sqrt{\mathtt{M}}}\right)\int_0^{\frac{\pi}{2}} \\
&\quad \exp\left(\frac{-3Y^{\mathrm{SE}}_{\mathcal{S}_m}[m]}{2\left(\mathtt{M}-1\right)\sin^2\left(\theta\right)}\right)\mathrm{d}\theta \\
&\quad -\frac{4}{\pi}\left(1-\frac{1}{\sqrt{\mathtt{M}}}\right)^2\int_0^{\frac{\pi}{4}} \\
&\quad \exp\left(\frac{-3Y^{\mathrm{SE}}_{\mathcal{S}_m}[m]}{2\left(\mathtt{M}-1\right)\sin^2\left(\theta\right)}\right)\mathrm{d}\theta \qquad (4.44)
\end{aligned}$$

where $\frac{\left|\mu_{r'_{\mathcal{S}_m}}[m]\right|^2}{\sigma^2_{r'_{\mathcal{S}_m}}[m]} = \sum_{k_{\mathrm{r}}=1}^{K'_{\mathrm{r}}}\frac{\left|\hat{h}^{\mathrm{SE}}_{i^m_{k_{\mathrm{r}}}}[m]\right|^2\left(\zeta^{\mathrm{SE}}_{i^m_{k_{\mathrm{r}}}}[m]\right)^2}{1-\zeta^{\mathrm{SE}}_{i^m_{k_{\mathrm{r}}}}[m]+\eta^{-1}}$ and the last equality follows from $Y^{\mathrm{SE}}_{\mathcal{S}_m}[m] = \sum_{k_{\mathrm{r}}=1}^{K'_{\mathrm{r}}}\left|X^{\mathrm{SE}}_{i^m_{k_{\mathrm{r}}}}[m]\right|^2$ with $X^{\mathrm{SE}}_{i^m_{k_{\mathrm{r}}}}[m] = \sqrt{b^{\mathrm{SE}}_{i^m_{k_{\mathrm{r}}}}[m]}\hat{h}^{\mathrm{SE}}_{i^m_{k_{\mathrm{r}}}}[m]$ and $b^{\mathrm{SE}}_{i^m_{k_{\mathrm{r}}}}[m] = \frac{\left(\zeta^{\mathrm{SE}}_{i^m_{k_{\mathrm{r}}}}[m]\right)^2}{1-\zeta^{\mathrm{SE}}_{i^m_{k_{\mathrm{r}}}}[m]+\eta^{-1}}$.

The SEP averaged over $\left\{\hat{h}^{\mathrm{SE}}_{i^m_{k_\mathrm{r}}}[m]\right\}_{k_\mathrm{r}=1}^{K'_\mathrm{r}}$ is

$$\begin{aligned}\mathrm{SEP}'_m\left(\left\{\hat{h}^{\mathrm{SP}}_{i^m_{k_\mathrm{r}}}[m]\right\}_{k_\mathrm{r}=1}^{K'_\mathrm{r}}\right) &= \frac{4}{\pi}\left(1-\frac{1}{\sqrt{\mathtt{M}}}\right)\int_0^{\frac{\pi}{2}} \\ &\quad \mathcal{M}_{Y^{\mathrm{SE}}_{\mathcal{S}_m}[m]\ \mid\ \{\hat{h}^{\mathrm{SP}}_{i^m_{k_\mathrm{r}}}[m]\}_{k_\mathrm{r}=1}^{K'_\mathrm{r}}}\left(\frac{-3}{2\left(\mathtt{M}-1\right)\sin^2\left(\theta\right)}\right)\mathrm{d}\theta \\ &\quad -\frac{4}{\pi}\left(1-\frac{1}{\sqrt{\mathtt{M}}}\right)^2\int_0^{\frac{\pi}{4}} \\ &\quad \mathcal{M}_{Y^{\mathrm{SE}}_{\mathcal{S}_m}[m]\ \mid\ \{\hat{h}^{\mathrm{SP}}_{i^m_{k_\mathrm{r}}}[m]\}_{k_\mathrm{r}=1}^{K'_\mathrm{r}}}\left(\frac{-3}{2\left(\mathtt{M}-1\right)\sin^2\left(\theta\right)}\right)\mathrm{d}\theta\end{aligned} \tag{4.45}$$

where $\mathcal{M}_{Y^{\mathrm{SE}}_{\mathcal{S}_m}[m]\ \mid\ \{\hat{h}^{\mathrm{SP}}_{i^m_{k_\mathrm{r}}}[m]\}_{k_\mathrm{r}=1}^{K'_\mathrm{r}}}(\cdot)$ is the MGF of $Y^{\mathrm{SE}}_{\mathcal{S}_m}[m]$ conditioned on $\left\{\hat{h}^{\mathrm{SP}}_{i^m_{k_\mathrm{r}}}[m]\right\}_{k_\mathrm{r}=1}^{K'_\mathrm{r}}$.

Conditioned on $\left\{\hat{h}^{\mathrm{SP}}_{i^m_{k_\mathrm{r}}}[m]\right\}_{k_\mathrm{r}=1}^{K'_\mathrm{r}}$, using standard results on moments of conditional Gaussian RVs it is shown in Appendix D that $X^{\mathrm{SE}}_{i^m_{k_\mathrm{r}}}[m]$ is a complex Gaussian RV with conditional mean $\mu_{X^{\mathrm{SE}}_{i^m_{k_\mathrm{r}}}}[m]$ and variance $\sigma^2_{X^{\mathrm{SE}}_{i^m_{k_\mathrm{r}}}}[m]$ given in (4.39) and (4.40), respectively, but with $b^{\mathrm{SE}}_{i^m_{k_\mathrm{r}}}[m]=\frac{\left(\zeta^{\mathrm{SE}}_{i^m_{k_\mathrm{r}}}[m]\right)^2}{1-\zeta^{\mathrm{SE}}_{i^m_{k_\mathrm{r}}}[m]+\eta^{-1}}$ in this case.

Therefore $Y^{\mathrm{SE}}_{\mathcal{S}_m}[m]$ follows a non-central Chi-squared distribution with conditional MGF given in (4.41) with $b^{\mathrm{SE}}_{i^m_{k_\mathrm{r}}}[m]=\frac{\left(\zeta^{\mathrm{SE}}_{i^m_{k_\mathrm{r}}}[m]\right)^2}{1-\zeta^{\mathrm{SE}}_{i^m_{k_\mathrm{r}}}[m]+\eta^{-1}}$.

Substituting (4.41) in (4.45), yields

$$\begin{aligned}\mathrm{SEP}'_m\left(\left\{\hat{h}^{\mathrm{SP}}_{i^m_{k_\mathrm{r}}}[m]\right\}_{k_\mathrm{r}=1}^{K'_\mathrm{r}}\right) &= \frac{4}{\pi}\left(1-\frac{1}{\sqrt{\mathtt{M}}}\right)\int_0^{\frac{\pi}{2}}\left(\prod_{k_\mathrm{r}=1}^{K'_\mathrm{r}}\frac{\sin^2(\theta)}{\sin^2(\theta)+\frac{3}{2(\mathtt{M}-1)}\sigma^2_{X^{\mathrm{SE}}_{i^m_{k_\mathrm{r}}}}[m]}\right)\\ &\quad\times\exp\left(-\sum_{k_\mathrm{r}=1}^{K'_\mathrm{r}}\frac{\xi_{i^m_{k_\mathrm{r}}}[m]\left|\hat{h}^{\mathrm{SP}}_{i^m_{k_\mathrm{r}}}[m]\right|^2}{\sin^2(\theta)+\frac{3}{2(\mathtt{M}-1)}\sigma^2_{X^{\mathrm{SE}}_{i^m_{k_\mathrm{r}}}}[m]}\right)\mathrm{d}\theta\\ &\quad-\frac{4}{\pi}\left(1-\frac{1}{\sqrt{\mathtt{M}}}\right)^2\int_0^{\frac{\pi}{4}}\left(\prod_{k_\mathrm{r}=1}^{K'_\mathrm{r}}\frac{\sin^2(\theta)}{\sin^2(\theta)+\frac{3}{2(\mathtt{M}-1)}\sigma^2_{X^{\mathrm{SE}}_{i^m_{k_\mathrm{r}}}}[m]}\right)\\ &\quad\times\exp\left(-\sum_{k_\mathrm{r}=1}^{K'_\mathrm{r}}\frac{\xi_{i^m_{k_\mathrm{r}}}[m]\left|\hat{h}^{\mathrm{SP}}_{i^m_{k_\mathrm{r}}}[m]\right|^2}{\sin^2(\theta)+\frac{3}{2(\mathtt{M}-1)}\sigma^2_{X^{\mathrm{SE}}_{i^m_{k_\mathrm{r}}}}[m]}\right)\mathrm{d}\theta\end{aligned} \tag{4.46}$$

where $\xi_{i^m_{k_\mathrm{r}}}[m]=\frac{3}{2(\mathtt{M}-1)}\left(\frac{b^{\mathrm{SE}}_{i^m_{k_\mathrm{r}}}[m]\zeta^{\mathrm{SP}}_{i^m_{k_\mathrm{r}}}[m]\left|\rho_{\hat{h}^{\mathrm{SE}}_{i^m_{k_\mathrm{r}}}[m],\hat{h}^{\mathrm{SP}}_{i^m_{k_\mathrm{r}}}[m]}\right|^2}{\zeta^{\mathrm{SE}}_{i^m_{k_\mathrm{r}}}[m]}\right)$ with $b^{\mathrm{SE}}_{i^m_{k_\mathrm{r}}}[m]=\frac{\left(\zeta^{\mathrm{SE}}_{i^m_{k_\mathrm{r}}}[m]\right)^2}{1-\zeta^{\mathrm{SE}}_{i^m_{k_\mathrm{r}}}[m]+\eta^{-1}}$.

Denoting by $\Upsilon_{i^m_{k_\mathrm{r}}}[m]=\xi_{i^m_{k_\mathrm{r}}}[m]|\hat{h}^{\mathrm{SP}}_{i^m_{k_\mathrm{r}}}[m]|^2$ the exponential RV with mean $\Gamma_{i^m_{k_\mathrm{r}}}[m]=\mathbb{E}\left\{\Upsilon_{i^m_{k_\mathrm{r}}}[m]\right\}=\frac{3}{2(\mathtt{M}-1)}\left(\frac{b^{\mathrm{SE}}_{i^m_{k_\mathrm{r}}}[m]\left|\rho_{\hat{h}^{\mathrm{SE}}_{i^m_{k_\mathrm{r}}}[m],\hat{h}^{\mathrm{SP}}_{i^m_{k_\mathrm{r}}}[m]}\right|^2}{\zeta^{\mathrm{SE}}_{i^m_{k_\mathrm{r}}}[m]}\right)$. Averaging over $\left\{\hat{h}^{\mathrm{SP}}_{i^m_{k_\mathrm{r}}}[m]\right\}_{k_\mathrm{r}=1}^{K'_\mathrm{r}}$ and using the virtual branch combining (VBC) technique [94], yields the desired result. □

4.5 Simulations

We now present numerical results to gain insight into the previous analysis and study performance over time-varying channels.

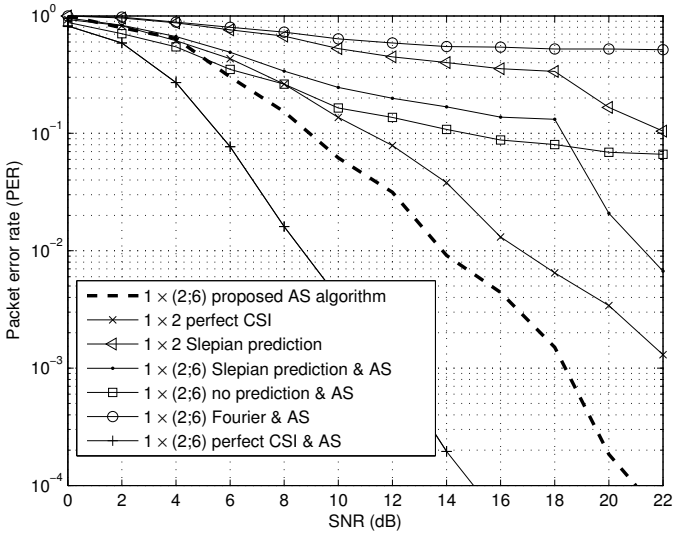

Figure 4.4: PER performance of the proposed AS method for a $1 \times (2; 6)$ system when the user velocity $v_{\max} = 100$ km/h corresponding to a maximum normalized Doppler frequency $\nu_{\max} = 0.0038$. (4PSK, packet length $N = 42$, $N_{\mathrm{df}} = 40$ data symbols, $N_{\mathrm{pf}} = 2$ post-selection pilots, $N_{\mathrm{ps}} = 2$ selection training pilots, and $T_p = 3\,T_s$).

4.5.1 Setup

In the sequel, a system with one transmit and K_{r} receive antenna is denoted as $1 \times K_{\mathrm{r}}$. Unless otherwise stated, the simulation parameters are as follows: a system with one transmit and K_{r} receive antennas out of which K'_{r} is selected, denoted by $1 \times (K'_{\mathrm{r}}; K_{\mathrm{r}})$, is simulated. The carrier frequency $f_{\mathrm{c}} = 2\,\mathrm{GHz}$ and a single user moves with radial velocity $v_{\max} = 100\,\mathrm{km/h}$. The symbol duration $T_{\mathrm{s}} = 20.57\ \mu\mathrm{s}$ [3, 79]. Using Eq. (4.1), these parameters give a Doppler bandwidth $\nu_{\max} = 3.8 \times 10^{-3}$. A Rayleigh fading channel with Clarke's Doppler spectrum for each tap is used [18].

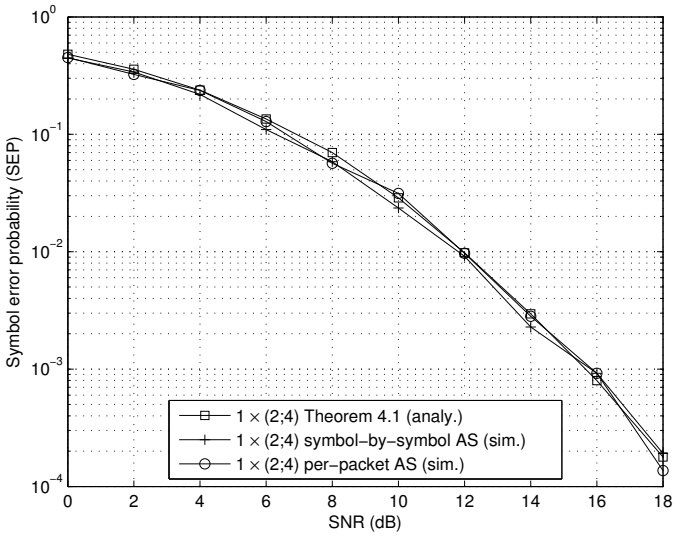

Figure 4.5: SEP for the first 8PSK data symbol for a $1 \times (2;4)$ system when the user velocity $v_{\max} = 100$ km/h corresponding to a maximum normalized Doppler frequency $\nu_{\max} = 0.0038$. (packet length $N = 42$, $N_{\rm df} = 40$ data symbols, $N_{\rm pf} = 2$ post-selection pilots, $N_{\rm ps} = 2$ selection training pilots, and $T_p = 3\,T_s$).

The complex channel at the $k_{\rm r}$th receive antenna is given by [18, 27]

$$h_{k_{\rm r}}[m] = \sum_{n_{\rm path}=0}^{N_{\rm path}} a_{k_{\rm r},n_{\rm path}} \exp\left(j2\pi\nu_{k_{\rm r},n_{\rm path}}\, m\right) \tag{4.47}$$

where the number of propagation paths is set to $N_{\rm path} = 20$. In (4.47), $a_{k_{\rm r},n_{\rm path}} = \frac{1}{\sqrt{N_{\rm path}}} \exp\left(j\psi_{k_{\rm r},n_{\rm path}}\right)$ with phase angles $\psi_{k_{\rm r},n_{\rm path}}$ uniformly distributed over $[-\pi\ \pi)$. The Doppler shifts $\nu_{k_{\rm r},n_{\rm path}} = \nu_{\max}\cos\left(\alpha_{k_{\rm r},n_{\rm path}}\right)$ with angles of incidence $\alpha_{k_{\rm r},n_{\rm path}}$ uniformly distributed in $[-\pi\ \pi)$. The path parameters $\left\{a_{k_{\rm r},n_{\rm path}}\right\}$ and $\left\{\nu_{k_{\rm r},n_{\rm path}}\right\}$ are modelled as independent and identically distributed [18]. They are assumed constant over an AS cycle but change independently from cycle to cycle.

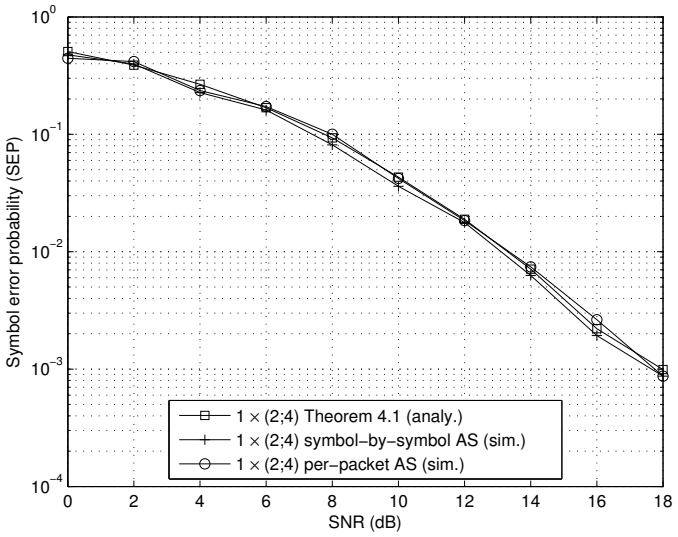

Figure 4.6: SEP for the $20th$ 8PSK data symbol for a $1 \times (2;4)$ system when the user velocity $v_{\max} = 100$ km/h corresponding to a maximum normalized Doppler frequency $\nu_{\max} = 0.0038$. (packet length $N = 42$, $N_{\rm df} = 40$ data symbols, $N_{\rm pf} = 2$ post-selection pilots, $N_{\rm ps} = 2$ selection training pilots, and $T_p = 3\,T_s$).

4.5.2 Packet Error Rate

The packet error rate (PER) of the proposed per-packet AS method in Sec. 4.3 for a $1 \times (2;6)$ system is illustrated in Fig. 4.4. The packet consists of $N = N_{\rm pf} + N_{\rm df} = 42$ symbols, in which $N_{\rm pf} = 2$ pilot symbols are time-multiplexed with $N_{\rm df} = 40$ data symbols. For comparison, we also show the PER performance of (i) a 1×2 system with perfect CSI using MRC and no AS, (ii) $1 \times (2;6)$ system with perfect CSI and AS according to Step 2(b) in Sec. 4.3.1 (with $h_{k_{\rm r}}[m]$ replacing $\hat{h}^{\rm SP}_{k_{\rm r}}[m]$), (iii) a $1 \times (2;6)$ system employing AS without channel prediction. We note that the antenna with the highest channel gain estimate $\tilde{h}_{k_{\rm r}}[m]$ in (4.15) is selected since no channel prediction is used, (iv) a $1 \times (2;6)$ system employing Fourier basis expansion channel

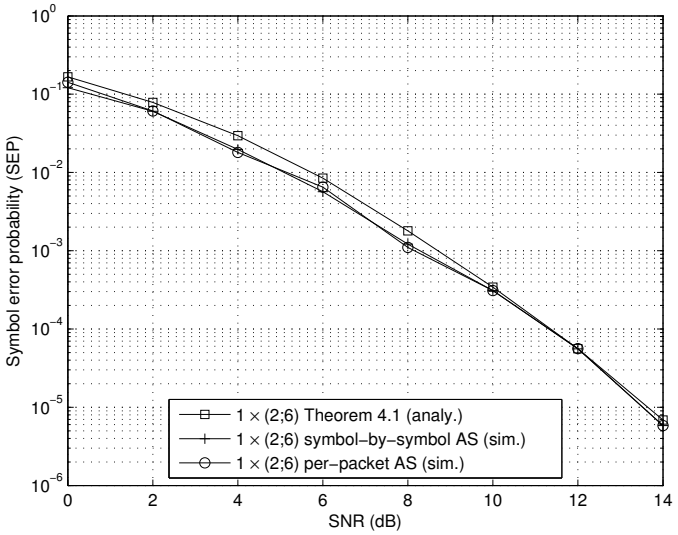

Figure 4.7: SEP for the first 4PSK data symbol for a $1 \times (2;6)$ system when the user velocity $v_{\max} = 100$ km/h corresponding to a maximum normalized Doppler frequency $\nu_{\max} = 0.0038$. (packet length $N = 42$, $N_{\rm df} = 40$ data symbols, $N_{\rm pf} = 2$ post-selection pilots, $N_{\rm ps} = 2$ selection training pilots, and $T_p = 3\,T_s$).

prediction and AS according to Step 2(b) in Sec. 4.3.1, with the refined channel gain estimates are used for data decoding, (v) a $1\times(2;6)$ system employing Slepian channel prediction and AS according to Step 2(b) in Sec. 4.3.1, with the predicted channel gains $\left\{\hat{h}_{k_{\rm r}}^{\rm SP}[m]\,|m \in \mathcal{I}_{\rm padt}\backslash T_{\rm pf}\right\}$ used not only for selection but also for data decoding. Inspection of Fig. 4.4 reveals that the $1 \times (2;6)$ system employing the proposed per-packet AS algorithm achieves an SNR performance gain of about 4 dB over the 1×2 system with perfect CSI and no AS at a PER $= 10^{-3}$. The performance of the same proposed $1 \times (2;6)$ system is about 6 dB worse than $1 \times (2;6)$ system employing AS with perfect CSI at PER of 10^{-3}. Also, error floors exist at moderate to high SNR for the $1 \times (2;6)$ systems employing AS either with Fourier basis expansion or without channel prediction.

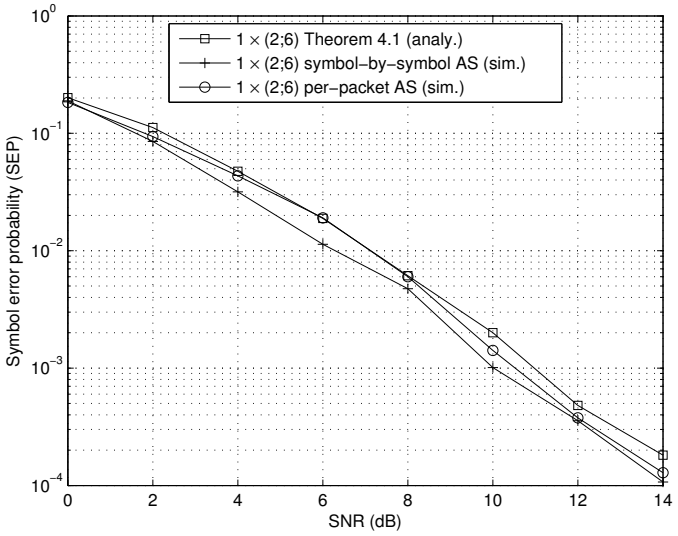

Figure 4.8: SEP for the $20th$ 4PSK data symbol for a $1 \times (2; 6)$ system when the user velocity $v_{\max} = 100$ km/h corresponding to a maximum normalized Doppler frequency $\nu_{\max} = 0.0038$. (packet length $N = 42$, $N_{\rm df} = 40$ data symbols, $N_{\rm pf} = 2$ post-selection pilots, $N_{\rm ps} = 2$ selection training pilots, and $T_p = 3\,T_s$).

We note that the complexity of the proposed AS method is higher than that of a system employing AS with Fourier expansion model. The generation of length-N Slepian sequences requires the use of singular value decomposition (SVD) to calculate the eigenvectors of the $N \times N$ matrix $\mathbf{A}$ with (a, b) entry defined as $[\mathbf{A}]_{a,b} = \frac{\sin[2\pi\nu_{\max}(a-b)]}{\pi(a-b)}$ for $a, b = 0, 1, \ldots, N-1$. This requires $\mathcal{O}\big(N^3\big)$ complex multiplications [37]. However, the Fourier basis functions, which do not require the knowledge of the Doppler spread and SVD, can be stored in memory using pre-calculated look-up tables.

The SEP of the first and $20th$ 8PSK symbols as a function of average SNR for a $1\times(2; 4)$ system employing the proposed receive AS algorithm are depicted in Figs. 4.5 and 4.6, respectively. The SEP curves analyzed in *Theorem 4.1* are also shown. It

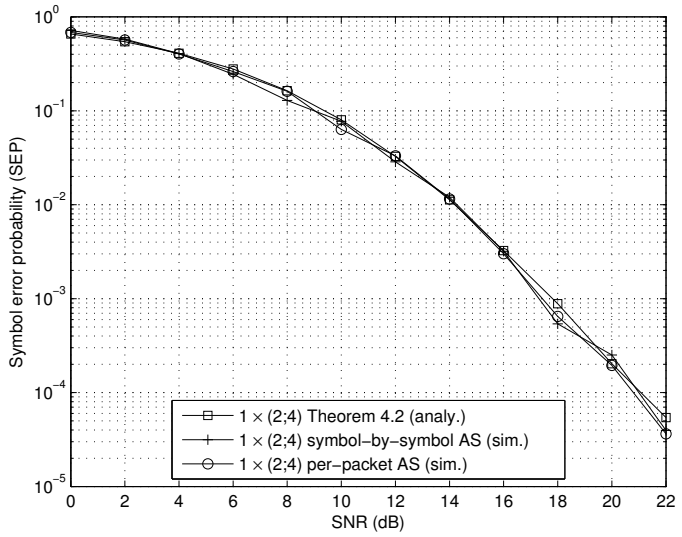

Figure 4.9: SEP for the first 16QAM data symbol for a $1 \times (2;4)$ system when the user velocity $v_{\max} = 100$ km/h corresponding to a maximum normalized Doppler frequency $\nu_{\max} = 0.0038$. (packet length $N = 42$, $N_{\rm df} = 40$ data symbols, $N_{\rm pf} = 2$ post-selection pilots, $N_{\rm ps} = 2$ selection training pilots, and $T_p = 3\,T_s$).

can be observed that the curves are close to each other. More specifically, the gap between the curves is about 0.2 dB. Note that the SEP behaviour might be slightly different for the different symbols of the length-N data packet. This is because the channel prediction for the first symbol is much better than channel prediction for the $20th$ symbol, which clearly affects the selection decision and, thus, the SEP. As is apparent from Figs. 4.5 and 4.6, the SEP for the first 8PSK symbol is about one order of magnitude less than that of the 20th 8PSK symbol at an SNR = 18 dB.

The SEP of the first and $20th$ 4PSK symbols for a $1 \times (2;6)$ system employing the proposed receive AS algorithm are also depicted in Figs. 4.7 and 4.8, respectively. The SEP curves analyzed in *Theorem 4.1* are also shown. A gap of about 1 dB can be observed between the curves. In summary, from Figs. 4.5–4.8 and from other

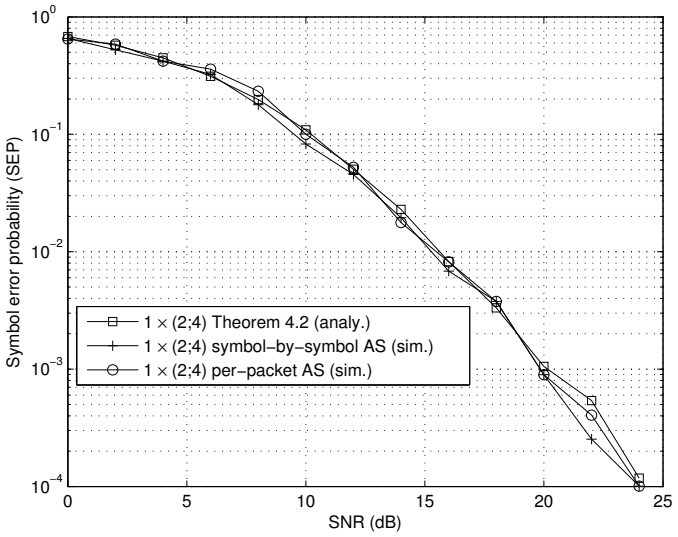

Figure 4.10: SEP for the $20th$ 16QAM data symbol for a $1 \times (2;4)$ system when the user velocity $v_{\max} = 100$ km/h corresponding to a maximum normalized Doppler frequency $\nu_{\max} = 0.0038$. (packet length $N = 42$, $N_{\rm df} = 40$ data symbols, $N_{\rm pf} = 2$ post-selection pilots, $N_{\rm ps} = 2$ selection training pilots, and $T_p = 3\,T_s$).

simulations, we also observe that *Theorem 4.1* reasonably approximates the MPSK SEP performance of systems employing the proposed receive AS algorithm in Sec. 4.3.

The SEP of the first and $20th$ 16QAM symbols for a $1 \times (2;4)$ system employing the proposed receive AS algorithm are also depicted in Figs. 4.9 and 4.10, respectively. The SEP curves analyzed in *Theorem 4.2* are also shown. It can be observed that the curves are close to each other, where a gap of about 0.2 dB exists between the curves. Note also that the SEP behaviour might be slightly different for the different symbols of the packet. For instance, the SEP for the first 16QAM is about one order of magnitude lower than that for the $20th$ 16QAM symbol at SNR = 20 dB.

The SEP for the first and $20th$ 16QAM symbols for a $1 \times (2;6)$ system employing the proposed receive AS algorithm are shown in Figs. 4.11 and 4.12, respectively. The

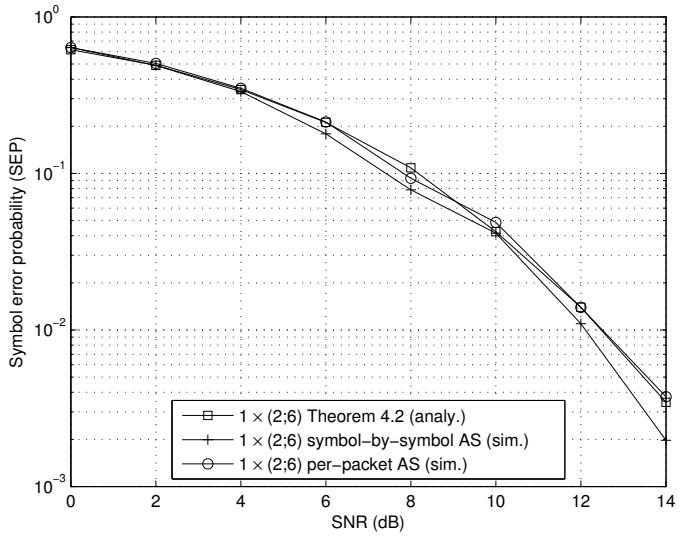

Figure 4.11: SEP for the first 16QAM data symbol for a $1 \times (2; 6)$ system when the user velocity $v_{\max} = 100$ km/h corresponding to a maximum normalized Doppler frequency $\nu_{\max} = 0.0038$. (packet length $N = 42$, $N_{\rm df} = 40$ data symbols, $N_{\rm pf} = 2$ post-selection pilots, $N_{\rm ps} = 2$ selection training pilots, and $T_p = 3\,T_s$).

analytical curves from *Theorem 4.2* are also plotted. Note the curves are close to each other. A gap of about 0.2 to 0.5 dB exists between the curves. From Figs. 4.9–4.12 and from other simulations, we also observe that *Theorem 4.2* reasonably approximates the MQAM SEP performance of systems employing the proposed receive AS algorithm in Sec. 4.3.

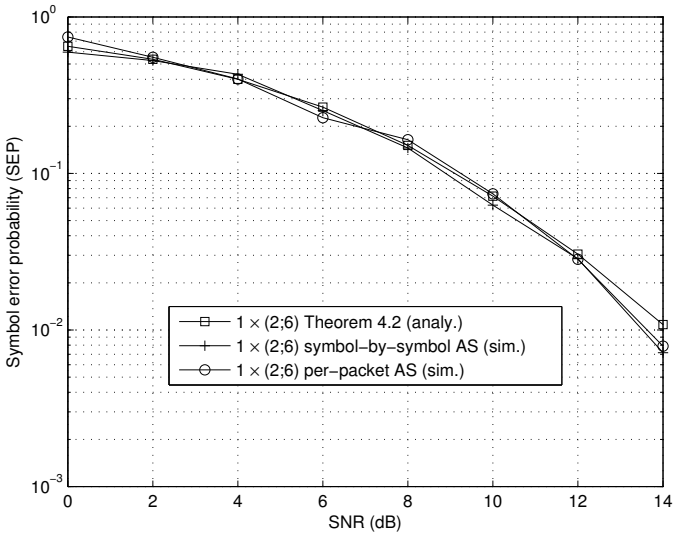

Figure 4.12: SEP for the $20th$ 16QAM data symbol for a $1 \times (2;6)$ system when the user velocity $v_{\max} = 100$ km/h corresponding to a maximum normalized Doppler frequency $\nu_{\max} = 0.0038$. (packet length $N = 42$, $N_{\rm df} = 40$ data symbols, $N_{\rm pf} = 2$ post-selection pilots, $N_{\rm ps} = 2$ selection training pilots, and $T_p = 3\,T_s$).

4.6 Conclusions

A training-based receive antenna subset selection approach for time-varying frequency-flat fading which uses Slepian basis expansion for prediction and estimation is proposed. It takes into account packet and symbol-by-symbol reception/switching for antenna selection (AS). An approach to determine the subspace dimensions that reduces the mean square error (MSE) of the Slepian estimator/predictor is also presented. It is used in the proposed AS method since it affects the antenna selection and decoding processes and, thus, reduces the symbol error probability (SEP) of the system. It is shown that the proposed AS scheme outperforms ideal conventional systems with perfect channel knowledge and no AS at the receiver and conventional

complex basis based estimation. Analytical expressions for the MPSK and MQAM SEP with the receive AS method are also derived, and verified with simulations.

Chapter 5

Training Schemes for Selection of OFDM Subsystems in High-Doppler Fading

5.1 Introduction

Orthogonal frequency division multiplexing (OFDM) and multiple antenna technologies have been adopted by next generation wireless standards, such as long term evolution (LTE) of the third generation partnership project (3GPP) [2]. Due to the mobility of users and multipath propagation with delay spread, the wireless channel is time-varying and frequency-selective. OFDM modulation transforms a time-varying frequency-selective channel into a set of parallel time-varying frequency-flat subchannels [36]. This enables simple frequency-domain equalization and channel estimation. The use of multiple antennas for transmission and reception improves the system performance through diversity and/or multiplexing gains.

However, the use of multiple antennas increases the hardware complexity and costs because each antenna requires an expensive radio frequency (RF) chain that is comprised of low-noise amplifiers (LNAs), mixers, and oscillators. An effective

method of retaining most of the diversity benefits of multiple antennas with considerable reduction of hardware complexity and costs at the receiver is to perform receive antenna subset selection. In receive antenna subset selection, only a subset of the antenna elements (AEs) is connected to a limited number of RF chains based on the current channel fades. We note that antenna selection (AS) has been standardized in IEEE 802.11n [1]. Algorithms and performance analysis for single-carrier AS systems are reported in numerous previous studies [9, 11, 12, 16, 32, 33, 38–41, 46, 47, 51, 64–66, 68, 80, 95, 98, 102, 106]. Antenna selection for OFDM systems is considered in [10, 20, 61, 83, 85, 90, 103]. Bulk versus per-tone AS for MIMO-OFDM systems are examined in [21, 81, 104]. To perform receive antenna subset selection, the channel is estimated by sending training symbols to different subsets of antennas. To date, only few studies exist that deal with the practical issues of pilot-based training and AS implementation. The above references consider the channel to be perfectly known at the receiver and/or slowly-time-varying. However, as mentioned above the wireless channel is frequency-selective and time-varying which results in outdated channel state information (CSI) at the receiver. We note that OFDM systems have a relatively long time symbol duration compared to single carrier systems due to their multicarrier features. This makes OFDM systems more sensitive than single carrier systems to Doppler shifts, which results in higher temporal channel variations. As noted above, each OFDM subcarrier experiences time-varying and frequency-flat fading. Each realization of the time-varying frequency-flat channel impulse response is modeled as the superposition of a discrete number of paths, each with potentially different Doppler shift, delay, and amplitude values. We note that the Doppler frequency depend on the user velocity, the carrier frequency, and the scattering environment (i.e., angles

of incidence). Therefore, the time-varying channel of each subcarrier represents a sequence of complex channel gain scalars at the OFDM symbol rate. The temporal variation of this sequence is also bandlimited by the maximum normalized Doppler frequency

$$\nu_{\max} \triangleq f_{\mathrm{D}} T_{\mathrm{os}} = \frac{v_{\max} f_{\mathrm{c}}}{c_{\mathrm{o}}} T_{\mathrm{os}} \tag{5.1}$$

where T_{os} denotes the OFDM symbol duration and the Doppler frequency $f_{\mathrm{D}} \triangleq \frac{v_{\max} f_{\mathrm{c}}}{c_{\mathrm{o}}}$ with $v_{\max}$ the radial component of the user velocity, f_{c} the carrier frequency, and c_{o} the speed of light. The impact of imperfect channel knowledge on the performance of single carrier AS systems is studied in [7, 35, 42, 97, 105]. Receive antenna selection for OFDM-based multiple antenna systems with channel estimation error is treated in [67]. The performance of single carrier AS systems with CSI feedback delay are studied in [44] and [73]. Weighted AS rules for single carrier systems over time-varying channels which utilize temporal correlation knowledge are proposed in [54] and [55]. Training-based receive AS algorithms for single carrier systems which use CSI knowledge of the data transmission phase in selection and decoding processes by utilizing Slepian prediction [101] and estimation [100] have been recently proposed in [77–79]. However, only the simpler problem of time-varying and frequency-flat fading is considered in [77–79]. We note that the Slepian estimator/predictor only requires knowledge or estimate of the Doppler bandwidth. It uses the orthonormal Slepian sequences, which are bandlimited by $\nu_{\max}$, as basis functions. We note that the fading process is bandlimited to the maximum normalized Doppler frequency $\nu_{\max}$. Linear interpolation/extrapolation techniques which estimate/predict the channel by connecting the channel samples obtained from the observations over the training pilots by straight line segments also do not require any statistical knowledge of the channel.

However, the Slepian predictor estimator explicitly takes into account the fact that the fading process is bandlimited by $\nu_{\max}$.

Motivated by the above observations, our objective in this chapter is to investigate AS for OFDM-based systems over more realistic fading scenarios. Specifically, we investigate the performance of AS for OFDM systems for realistic doubly selective channels (i.e., time and frequency selective). Therefore, we consider the more general problem of frequency-selective and time-varying fading. We note that in a single carrier receive AS system with $K_{\rm r}$ receive AEs, the receiver connects $K'_{\rm r}$ RF chains for $1 \leq K'_{\rm r} < K_{\rm r}$ to the $K'_{\rm r}$-element selected subset of antennas, denoted by $\mathcal{S} \triangleq \left\{\text{AE } \hat{\imath}_1, \ldots, \text{AE } \hat{\imath}_{K'_{\rm r}}\right\}$. In an OFDM system with $N_{\rm sc}$ subcarriers, if receive antenna subset selection is performed separately for each of the $N_{\rm sc}$ subcarriers (per-carrier basis) $K_{\rm r}$ RF chains at the receiver would be required. However, if the selected subset of antennas is the same for all the subcarriers, then only $K'_{\rm r}$ RF chains would be needed at the receiver as in the single-carrier case. The contributions are summarized as follows:

- Single carrier receive AS methods for time-varying channels based on Slepian subspace projections [77–79] are extended to accommodate single input–multiple output (SIMO) and multiple input–multiple output (MIMO) OFDM-based systems over time-varying frequency-selective fading.

- Through simulation, the performance of the proposed method is compared to that of AS methods based on conventional Fourier as well as linear interpolation/extrapolation prediction/estimation methods.

This chapter is organized as follows: the detailed system model is described in

Section 5.2. The training-based receive AS methods for SIMO and MIMO OFDM-based systems for time-varying frequency-selective fading is developed in Sec. 5.3. Simulation results are discussed in Sec. 5.4. Our conclusions follow in Sec. 5.5.

5.2 System Model

Consider an $N_{\rm sc}$ subcarrier frequency SIMO OFDM system with $K_{\rm r}$ receive AEs equipped with only $1 \leq K'_{\rm r} < K_{\rm r}$ RF chains as in Fig. 5.1. The selected subset of AEs must be the same for all the $N_{\rm sc}$ tones. The OFDM symbol duration is $T_{\rm os} \triangleq (N_{\rm sc} + N_g)\, T_{\rm s}$, where $N_{\rm g}$ is the number of guard tones and $T_{\rm s} \triangleq \frac{1}{B}$ is the sampling time with B the entire RF channel bandwidth. A $K_{\rm r}$-select-$K'_{\rm r}$ micro-electromechanical system (MEMS) based antenna switch connects the selected AEs to the RF chains. The switching speed of the RF MEMS switches is 2 to 40 μs with an insertion loss of only 0.1 dB [75]. Since the duration $T_{\rm s}$ of each time-domain data symbols (samples) is usually much less than the switching time $T_{\rm sw}$ ($T_{\rm s} \ll T_{\rm sw}$), this implies that all OFDM symbols, each of duration $T_{\rm os} \geq T_{\rm sw}$, of a transmitted packet are received by the same selected subset of antennas. Selection is thus performed on a per-packet basis rather than on a per OFDM symbol basis. If the switching is performed between OFDM symbols of a transmitted packet (i.e., OFDM symbol-by-symbol basis), this results in loss of time-domain samples of the cyclic prefix and possibly data symbols. The number of lost time-domain samples is equal to $\lceil \frac{T_{\rm sw}}{T_{\rm s}} \rceil$ ($\lceil \frac{T_{\rm sw}}{T_{\rm s}} \rceil \gg 1$). This causes performance degradation and inter-carrier interference (ICI) since orthogonality of the subcarriers is not preserved. We now introduce the channel and signal model. Antenna selection training and pilot-assisted data transmission phases are described next.

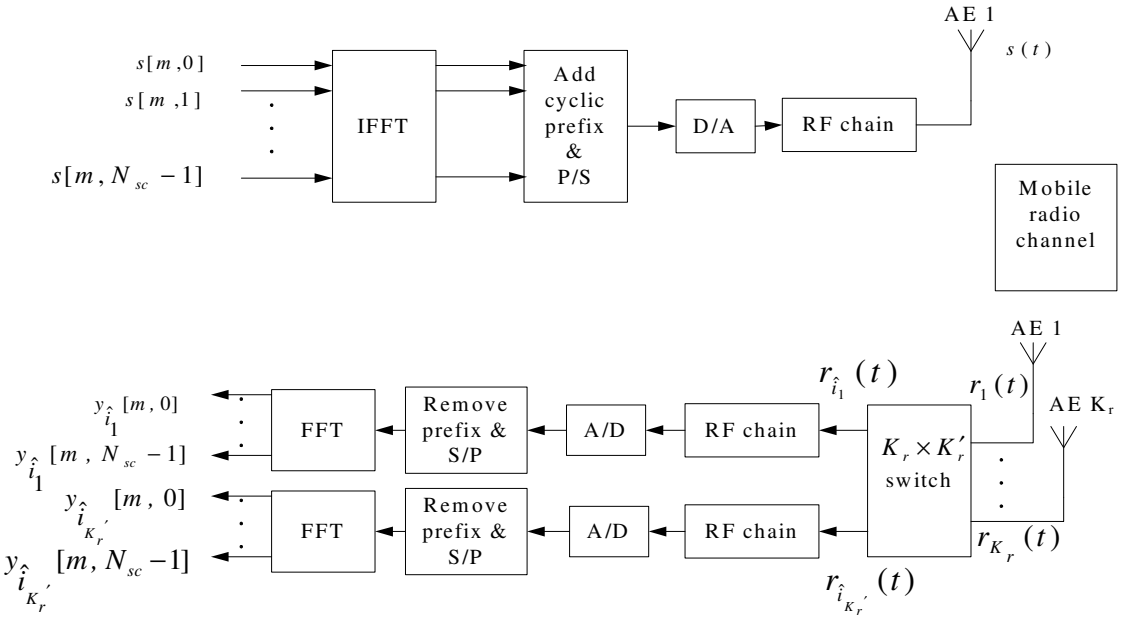

Figure 5.1: System model with receive antenna subset selection, for all the N_{sc} subcarriers, in time-varying frequency-selective fading.

5.2.1 Channel and Signal Model

The channel between the single transmit antenna and each receive AE is modelled as having a multipath structure with L taps. The impulse response for this time-varying frequency-selective channel can be written as [59]

$$h_{k_{\text{r}}}(t,\tau) = \sum_{\ell=0}^{L-1} \sqrt{P(\tau_\ell)}\, w_{k_{\text{r}},\ell}(t)\, \delta(\tau - \tau_\ell), \;\; k_{\text{r}} = 1, 2, \ldots, K_{\text{r}} \tag{5.2}$$

where $\delta(t)$ denotes the Dirac delta function, τ_ℓ is the propagation delay of the ℓth complex channel tap $w_{k_{\text{r}},\ell}(t)$ of average power $P(\tau_\ell)$. The time-varying complex gains $\{w_{k_{\text{r}},\ell}(t)\}$ in (5.2) are wide sense stationary (WSS) narrowband complex Gaussian processes, which are independent for different taps [74, 87]. The average powers

$\{P(\tau_\ell)\}$ depend on the channel delay profiles. The channel impulse response in (5.2) is thus a series of time-delayed impulses weighted by complex channel taps. As explained in more detail in Sec. 5.4, each complex channel tap is modeled as the superposition of N_{path} paths, each with Doppler shift $f_{k_\text{r},\ell}^{n_\text{path}} \triangleq f_\text{D}\cos\left(\alpha_{k_\text{r},\ell}^{n_\text{path}}\right)$ with $\alpha_{k_\text{r},\ell}^{n_\text{path}}$ the angle of incidence for the n_path path of the ℓth complex channel tap. The normalized Doppler frequencies $\nu_{k_\text{r},\ell}^{n_\text{path}} \triangleq f_{k_\text{r},\ell}^{n_\text{path}} T_\text{os}$ are thus upper bounded by the maximum normalized Doppler frequency ν_max $\left(\text{i.e., } \left|\nu_{k_\text{r},\ell}^{n_\text{path}}\right| \leq \nu_\text{max}\right)$. We assume that the channel remains constant over an OFDM symbol duration T_os, since T_os is much less than the channel coherence time [57]. Hence, the discrete-time channel impulse response at AE k_r can thus be expressed as [58, 92]

$$\begin{aligned} h_{k_\text{r}}[m,\ell'] &\triangleq h_{k_\text{r}}(mT_\text{os},\ell' T_\text{s}) \\ &= \sum_{\ell=0}^{L-1} \sqrt{P[\ell]}\, w_{k_\text{r},\ell}[m]\,\delta[\ell'-\ell] \end{aligned} \tag{5.3}$$

where standard sampling notation is used in (5.3), i.e., discrete-time signal $x[n]$ is obtained from continuous signal $x(t)$ by sampling at period T_s according to $x[n] \triangleq x(nT_\text{s})$ with $n \in \mathbb{Z}$.

Provided that the cyclic prefix is made sufficiently long ($\geq L-1$) to avoid inter-symbol interference (ISI) and ICI, the received signal vector of the mth OFDM symbol at AE k_r can be expressed as [92]

$$\mathbf{y}_{k_\text{r}}[m] = \text{diag}(\mathbf{s}[m])\,\mathbf{g}_{k_\text{r}}[m] + \mathbf{z}_{k_\text{r}}[m], \quad 1 \leq k_\text{r} \leq K_\text{r} \tag{5.4}$$

where $\mathbf{y}_{k_\text{r}}[m] \triangleq [y_{k_\text{r}}[m,0],\ldots,y_{k_\text{r}}[m,N_\text{sc}-1]]^T$ is the $N_\text{sc}\times 1$ received signal vector at time index m, with $y_{k_\text{r}}[m,q]$ the symbol received on the qth tone during the

mth OFDM symbol. $\mathbf{z}_{k_\mathrm{r}}[m] \triangleq [z_{k_\mathrm{r}}[m,0],\ldots,z_{k_\mathrm{r}}[m,N_\mathrm{sc}-1]]^T$ is the $N_\mathrm{sc}\times 1$ additive white Gaussian noise (AWGN) with covariance $N_\mathrm{o}\mathbf{I}_{N_\mathrm{sc}}$, with $\mathbf{I}_{N_\mathrm{sc}}$ denoting the identity matrix of size N_sc. In (5.4), $\mathbf{g}_{k_\mathrm{r}}[m] \triangleq [g_{k_\mathrm{r}}[m,0],\ldots,g_{k_\mathrm{r}}[m,N_\mathrm{sc}-1]]^T = \mathbf{F}\mathbf{h}_{k_\mathrm{r}}[m]$ is the $N_\mathrm{sc}\times 1$ channel frequency response vector, where $g_{k_\mathrm{r}}[m,q]$ is the channel gain for the qth tone at time m, $\mathbf{F}$ is the $N_\mathrm{sc}\times L$ discrete Fourier transform (DFT) matrix with (q,ℓ) entry defined as $F[q,\ell] = \exp\left(-j\frac{2\pi q\ell}{N_\mathrm{sc}}\right)$ for $q=0,\ldots,N_\mathrm{sc}-1$ and $\ell=0,\ldots,L-1$, and $\mathbf{h}_{k_\mathrm{r}}[m] \triangleq [h_{k_\mathrm{r}}[m,0],\ldots,h_{k_\mathrm{r}}[m,L-1]]^T$ includes the L taps of the channel from the single transmit AE to receive antenna k_r in the time-domain. In (5.4), $\mathbf{s}[m] \triangleq [s[m,0],\ldots,s[m,N_\mathrm{sc}-1]]^T$ is the $N_\mathrm{sc}\times 1$ transmitted signal vector, where $s[m,q]$ denotes the unit average energy transmitted symbol on the qth tone in the mth OFDM symbol. $\mathrm{diag}(\mathbf{s}[m])$ denotes the $N_\mathrm{sc}\times N_\mathrm{sc}$ diagonal matrix with the $N_\mathrm{sc}\times 1$ vector $\mathbf{s}[m]$ on its diagonal.

5.2.2 Antenna Selection Cycle

Each AS cycle consists of an AS training phase followed by a pilot-assisted data transmission phase, as illustrated in Fig. 5.2. We now describe the AS training and pilot-assisted data transmission phases.

AS Training Phase

In each AS training phase, in total $\left\lceil \frac{K_\mathrm{r}}{K'_\mathrm{r}} \right\rceil N_\mathrm{ps}$ OFDM training symbols, each with N_sc pilot tones, are transmitted in N_ps rounds of transmission. In each round, $\left\lceil \frac{K_\mathrm{r}}{K'_\mathrm{r}} \right\rceil$ OFDM training symbols are transmitted sequentially in time to the receive antenna subsets. Each OFDM training symbol corresponds to a different subset of the $\left\lceil \frac{K_\mathrm{r}}{K'_\mathrm{r}} \right\rceil$ receive antenna subsets. The duration between consecutive training symbols in each

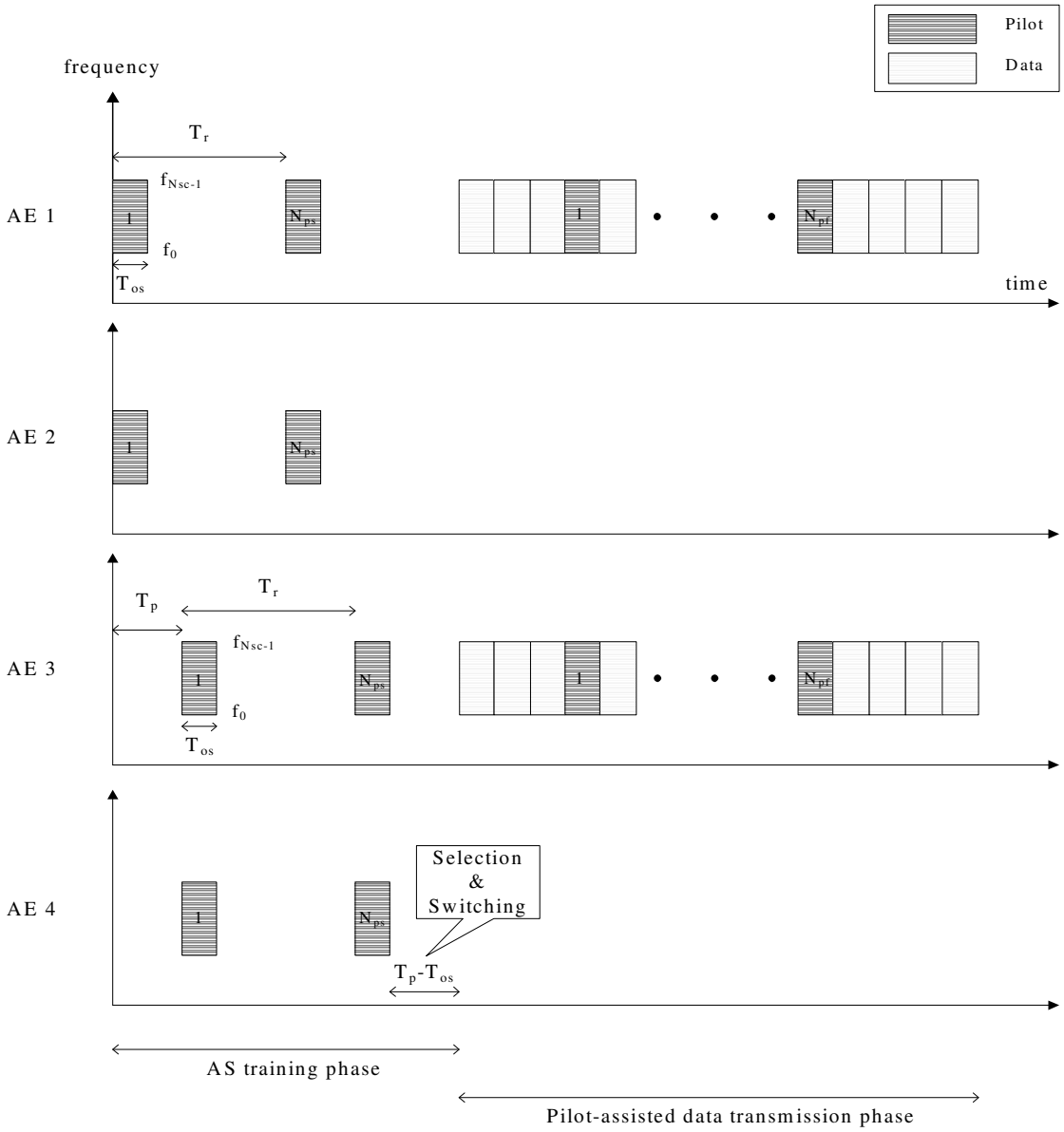

Figure 5.2: Antenna selection cycle consists of AS training and pilot-assisted data transmission phases. ($K_{\mathrm{r}} = 4$, AEs 1 and 3 are selected, $N_{\mathrm{ps}} = 2$ training pilots, length-$N = N_{\mathrm{df}} + N_{\mathrm{pf}}$ packet containing N_{df} data symbols and $N_{\mathrm{pf}} = 2$ post-selection pilots. In the figure, the pilot and data symbols are represented by grey and white cells, respectively).

round is $T_{\rm p} \triangleq \alpha T_{\rm os}$, where $\alpha = \left\lceil \frac{T_{\rm sw}}{T_{\rm os}} \right\rceil + 1$ with $T_{\rm sw}$ and $T_{\rm os}$ denote antenna switching time and OFDM symbol duration, respectively. Therefore, the duration between two consecutive training symbols transmitted in two consecutive rounds of transmission for each of the $\left\lceil \frac{K_{\rm r}}{K'_{\rm r}} \right\rceil$ antenna subsets is $T_{\rm r} \triangleq \left\lceil \frac{K_{\rm r}}{K'_{\rm r}} \right\rceil T_{\rm p} = \alpha \left\lceil \frac{K_{\rm r}}{K'_{\rm r}} \right\rceil T_{\rm os}$. In the first round, each transmitted pilot is received by a different subset of antennas at times $m \in \left(\left\lceil \frac{k_{\rm r}}{K'_{\rm r}} \right\rceil - 1 \right) T_{\rm p}$ for $k_{\rm r} = 1, 2, \ldots, K_{\rm r}$. In the second round, each transmitted pilot is received by a different subset of antennas at times $m \in \left(\left(\left\lceil \frac{k_{\rm r}}{K'_{\rm r}} \right\rceil - 1 \right) T_{\rm p} + T_{\rm r} \right)$ for $k_{\rm r} = 1, 2, \ldots, K_{\rm r}$, and so on. Thus AE $k_{\rm r}$ receives $N_{\rm ps}$ AS OFDM training pilots at times $m \in T_{\rm ps}^{k_{\rm r}}$, where

$$\begin{aligned} T_{\rm ps}^{k_{\rm r}} &= \left\{ \left[\left(\left\lceil \frac{k_{\rm r}}{K'_{\rm r}} \right\rceil - 1 \right) T_{\rm p} + (n_{\rm ps} - 1)\, T_{\rm r} \right] \;\middle|\; n_{\rm ps} = 1, \ldots, N_{\rm ps} \right\} \\ &= \left\{ \alpha \left(\left(\left\lceil \frac{k_{\rm r}}{K'_{\rm r}} \right\rceil - 1 \right) + (n_{\rm ps} - 1) \left\lceil \frac{K_{\rm r}}{K'_{\rm r}} \right\rceil \right) T_{\rm os} \;\middle|\; n_{\rm ps} = 1, \ldots, N_{\rm ps} \right\} \\ &\triangleq \left\{ \alpha \left[\left(\left\lceil \frac{k_{\rm r}}{K'_{\rm r}} \right\rceil - 1 \right) + (n_{\rm ps} - 1) \left\lceil \frac{K_{\rm r}}{K'_{\rm r}} \right\rceil \right] \;\middle|\; n_{\rm ps} = 1, \ldots, N_{\rm ps} \right\} \end{aligned} \tag{5.5}$$

for $k_{\rm r} = 1, 2, \ldots, K_{\rm r}$, where in the last step, discrete-time notation is adopted. From (5.4), the received symbol on the qth pilot subcarrier, for $q = 0, 1, \ldots, N_{\rm sc} - 1$, can be written as

$$y_{k_{\rm r}}[m, q] = g_{k_{\rm r}}[m, q]\, p_{k_{\rm r}}[m, q] + z_{k_{\rm r}}[m, q], \quad m \in T_{\rm ps}^{k_{\rm r}} \tag{5.6}$$

where $p_{k_{\rm r}}[m, q]$ is the pilot modulating the qth tone during the mth OFDM training symbol. From the observations on each subcarrier $\{y_{k_{\rm r}}[m, q] \mid m \in T_{\rm ps}^{k_{\rm r}}\}$, Slepian channel prediction for each subcarrier of every AE is performed over the pilot-assisted data transmission phase $\mathcal{I}_{\rm padt}$ to obtain a prediction of the frequency-domain channel seen

by the data in the qth subcarrier $\{\hat{g}_{k_\mathrm{r}}^{\mathrm{SP}}[m,q] \mid m \in \mathcal{I}_{\mathrm{padt}}\}$. Based on $\{\{\hat{g}_{k_\mathrm{r}}^{\mathrm{SP}}[m,q] \mid m \in \mathcal{I}_{\mathrm{padt}}\}_{q=0}^{N_{\mathrm{sc}}-1}\}_{k_\mathrm{r}=1}^{K_\mathrm{r}}$ the receiver then selects and connects the received subset of antennas $\mathcal{S} = \left\{\mathrm{AE}\ \hat{\imath}_1, \ldots, \mathrm{AE}\ \hat{\imath}_{K_\mathrm{r}'}\right\}$ to the RF chains for a duration of $T_\mathrm{p} - T_\mathrm{os}$. Therefore, the AS training phase spans the discrete times $\mathcal{I}_{\mathrm{ast}} = \{0, 1, \ldots, M-1\}$, where $M \triangleq \alpha \left\lceil \frac{K_\mathrm{r}}{K_\mathrm{r}'} \right\rceil N_{\mathrm{ps}}$.

Pilot-Assisted Data Transmission Phase

The pilot-assisted data transmission phase spans the discrete times $\mathcal{I}_{\mathrm{padt}} = \{M, \ldots, M+N-1\}$ where the transmitter sends out a length-$N \triangleq N_{\mathrm{df}} + N_{\mathrm{pf}}$ OFDM packet containing N_{df} and N_{pf} OFDM data and pilot symbols, respectively. The N_{pf} OFDM pilot symbols are uniformly spread over the packet as

$$\begin{aligned} \mathcal{P}_{\mathrm{pf}} &\triangleq \left\{ \left\lfloor (n_{\mathrm{pf}}-1)\left(\frac{N}{N_{\mathrm{pf}}}\right) + \frac{1}{2}\left(\frac{N}{N_{\mathrm{pf}}}\right) \right\rfloor \mid n_{\mathrm{pf}} = 1, \ldots, N_{\mathrm{pf}} \right\} \\ &= \left\{ \left\lfloor \frac{(2n_{\mathrm{pf}}-1)\,N}{2N_{\mathrm{pf}}} \right\rfloor \mid n_{\mathrm{pf}} = 1, \ldots, N_{\mathrm{pf}} \right\}. \end{aligned} \tag{5.7}$$

The received signal $\mathbf{y}_{\hat{\imath}_{k_\mathrm{r}}}[m] \triangleq \left[y_{\hat{\imath}_{k_\mathrm{r}}}[m,0], \ldots, y_{\hat{\imath}_{k_\mathrm{r}}}[m, N_{\mathrm{sc}}-1]\right]^T$ at each selected AE $\hat{\imath}_{k_\mathrm{r}}$ for $k_\mathrm{r} = 1, 2, \ldots, K_\mathrm{r}'$ has the form

$$\mathbf{y}_{\hat{\imath}_{k_\mathrm{r}}}[m] = \begin{cases} \mathbf{g}_{\hat{\imath}_{k_\mathrm{r}}}[m]\,\mathbf{p}_{\hat{\imath}_{k_\mathrm{r}}}[m] + \mathbf{z}_{\hat{\imath}_{k_\mathrm{r}}}[m], & m \in \mathcal{I}_{\mathrm{padt}} \backslash T_{\mathrm{pf}} \\ \mathbf{g}_{\hat{\imath}_{k_\mathrm{r}}}[m]\,\mathbf{d}_{\hat{\imath}_{k_\mathrm{r}}}[m] + \mathbf{z}_{\hat{\imath}_{k_\mathrm{r}}}[m], & m \in T_{\mathrm{pf}} \end{cases} \tag{5.8}$$

where $\mathbf{p}_{\hat{\imath}_{k_\mathrm{r}}}[m] \triangleq \left[p_{\hat{\imath}_{k_\mathrm{r}}}[m,0], \ldots, p_{\hat{\imath}_{k_\mathrm{r}}}[m, N_{\mathrm{sc}}-1]\right]^T$ denotes the $N_{\mathrm{sc}} \times 1$ pilot vector and $\mathbf{d}_{\hat{\imath}_{k_\mathrm{r}}}[m] \triangleq \left[d_{\hat{\imath}_{k_\mathrm{r}}}[m,0], \ldots, d_{\hat{\imath}_{k_\mathrm{r}}}[m, N_{\mathrm{sc}}-1]\right]^T$ is the $N_{\mathrm{sc}} \times 1$ data symbol vector. In (5.8), $A \backslash B$ denotes the relative complement of A in B, i.e., the set that contains all those elements of A that are not in B. From (5.7) and since the AS training phase

spans the discrete times $\mathcal{I}_{\text{ast}} = \{0, 1, \ldots, M-1\}$, the N_{pf} OFDM post-selection pilot symbols are thus received by the selected AEs at times $m \in T_{\text{pf}}$, where

$$T_{\text{pf}} \triangleq \left\{ M - 1 + \left\lfloor \frac{(2n_{\text{pf}} - 1)\, N}{2N_{\text{pf}}} \right\rfloor \;\middle|\; n_{\text{pf}} = 1, \ldots, N_{\text{pf}} \right\}. \tag{5.9}$$

Thus, in total, $N_{\text{tp}} \triangleq N_{\text{ps}} + N_{\text{pf}}$ OFDM training symbols are received by the selected AEs at times

$$T_{\text{tp}}^{\hat{\iota}_{k_{\text{r}}}} = T_{\text{ps}}^{\hat{\iota}_{k_{\text{r}}}} \cup T_{\text{pf}} \tag{5.10}$$

where $T_{\text{ps}}^{\hat{\iota}_{k_{\text{r}}}}$ and T_{pf} are given in (5.5) and (5.9), respectively. From these N_{tp} OFDM training symbols refined frequency-domain channel gain estimates $\left\{ \left\{ \hat{g}_{\hat{\iota}_{k_{\text{r}}}}^{\text{SE}}[m, q] \mid m \in \mathcal{I}_{\text{padt}} \backslash T_{\text{pf}} \right\}_{q=0}^{N_{\text{sc}}-1} \right\}_{k_{\text{r}}=1}^{K'_{\text{r}}}$ are obtained to decode data.

5.3 Receive Antenna Subset Selection Algorithm

In this section, a receive antenna subset selection algorithm for SIMO OFDM-based systems equipped with K_{r} receive antennas out of which only K'_{r} antennas are selected for time-varying frequency-selective channels for per-packet switching is first presented. The method is then extended to accommodate MIMO OFDM-based systems in Sec. 5.3.1.

In short, the AS training phase is formed by sending N_{ps} OFDM training symbols, each with N_{sc} pilot tones, to each of the $\left\lceil \frac{K_{\text{r}}}{K'_{\text{r}}} \right\rceil$ antenna subsets. To perform antenna subset selection, frequency-domain channel prediction for each OFDM subcarrier over the data transmission phase is needed since the CSI, obtained from the observations over the AS training pilots, becomes outdated at the receiver. However, these same observations can be used to perform Slepian channel prediction on each subcarrier

for every AE. Each subcarrier experiences time-varying frequency-flat fading. As mentioned above, the rate of channel time variation on each subcarrier is upper bounded by the maximum normalized Doppler frequency $\nu_{\max}$. The orthonormal Slepian sequences, which are bandlimited by $\nu_{\max}$, are used as basis functions to predict the time-varying frequency-flat channel for each subcarrier. Selection is then performed based on the predicted frequency-domain channel gains. After selection, a packet consisting of $N = N_{\rm pf} + N_{\rm df}$ OFDM symbols is transmitted with $N_{\rm df}$ data symbols and $N_{\rm pf}$ post-selection pilot symbols to the selected AEs. The $N_{\rm tp} = N_{\rm ps} + N_{\rm pf}$ are used to obtain refined frequency-domain channel gain estimates for every subcarrier of the selected antennas over the data transmission phase for data decoding. The algorithm comprises the following steps, which are conducted following an AS request:

1. Every antenna subset of the $\left\lceil \frac{K_{\rm r}}{K'_{\rm r}} \right\rceil$ is trained using $N_{\rm ps}$ OFDM training symbols, each with $N_{\rm sc}$ pilot tones. The spacing between consecutive OFDM training symbols transmitted for each of the $\left\lceil \frac{K_{\rm r}}{K'_{\rm r}} \right\rceil$ is $T_{\rm r} = \alpha \left\lceil \frac{K_{\rm r}}{K'_{\rm r}} \right\rceil T_{\rm os}$, where $T_{\rm os}$ is the OFDM symbol duration. To keep the AS training phase as short as possible, α is chosen as $\alpha = \left\lceil \frac{T_{\rm sw}}{T_{\rm os}} \right\rceil + 1 = 2$ since the switching time $T_{\rm sw} \ll T_{\rm os}$.

2. The receiver then:

   (a) Performs frequency-domain channel prediction over the data time slots $\mathcal{I}_{\rm padt} \backslash T_{\rm pf}$ for each subcarrier of every AE via

$$\hat{g}_{k_{\rm r}}^{\rm SP}[m,q] = \boldsymbol{f}^T[m]\,\hat{\boldsymbol{c}}_{k_{\rm r}}[q] = \sum_{d=0}^{D-1} \hat{c}_{k_{\rm r},d}[q]\,u_d[m], \quad m \in \mathcal{I}_{\rm padt} \backslash T_{\rm pf} \tag{5.11}$$

for $q = 0, 1, \ldots, N_{\rm sc}-1$ and $k_{\rm r} = 1, 2, \ldots, K_{\rm r}$, and D is the subspace dimension, i.e., number of basis functions. In (5.11), $\boldsymbol{f}\left[m\right] \triangleq \left[u_0\left[m\right], \ldots, u_{D-1}\left[m\right]\right]^T$ contains the D extensions $\left\{u_d\left[m\right] \mid m \in \mathcal{I}_{\rm padt} \backslash T_{\rm pf}\right\}_{d=0}^{D-1}$ of the orthonormal Slepian sequences of length-M $\left\{u_d\left[m\right] \mid m \in \mathcal{I}_{\rm ast}\right\}_{d=0}^{M-1}$ over the data transmission phase $\mathcal{I}_{\rm padt} \backslash T_{\rm pf}$. As described in more detail in Chapter 2, the Slepian sequences $\left\{u_d\left[m\right] \mid m \in \mathcal{I}_{\rm ast}\right\}_{d=0}^{M-1}$ are the restrictions in time of the (infinite) discrete prolate spheroidal (DPS) sequences $\left\{u_d\left[m\right] \mid m \in \mathbb{Z}\right\}_{d=0}^{M-1}$ on the AS training time interval $\mathcal{I}_{\rm ast} = \{0, \ldots, M-1\}$. The dth Slepian sequence vector of size $M \times 1$ $\mathbf{u}_d\left[m\right] \triangleq \left[u_d\left[0\right], \ldots, u_d\left[M-1\right]\right]^T$ is the dth eigenvector of the $M \times M$ matrix $\mathbf{A}$ with (a, b) entry defined as $\left[\mathbf{A}\right]_{a,b} = \frac{\sin[2\pi\nu_{\max}(a-b)]}{\pi(a-b)}$, for $a, b = 0, 1, \ldots, M-1$ corresponding to eigenvalues $\lambda_0 \geq \lambda_1 \geq \ldots \geq \lambda_{M-1}$. The D extensions $\left\{u_d\left[m\right] \mid m \in \mathcal{I}_{\rm padt} \backslash T_{\rm pf}\right\}_{d=0}^{D-1}$ of the orthonormal Slepian sequences can be calculated from

$$u_d\left[m\right] = \frac{1}{\lambda_d} \sum_{m'=0}^{M-1} \frac{\sin\left[2\pi\nu_{\max}\left(m'-m\right)\right]}{\pi\left(m'-m\right)} u_d\left[m'\right], \; m \in \mathcal{I}_{\rm padt} \backslash T_{\rm pf}. \tag{5.12}$$

We refer to Chapter 2 for more details on DPS basis expansion models for channel prediction and estimation. In (5.11), $\hat{\boldsymbol{c}}_{k_{\rm r}}[q] \triangleq \left[\hat{c}_{k_{\rm r},0}[q], \ldots, \hat{c}_{k_{\rm r},D-1}[q]\right]^T$ comprises the basis expansion coefficients for subcarrier q, and is given by

$$\hat{\boldsymbol{c}}_{k_{\rm r}}\left[q\right] = \Big(\sum_{m \in T_{\rm ps}^{k_{\rm r}}} \boldsymbol{f}\left[m\right] \boldsymbol{f}^{\dagger}\left[m\right] \left|p_{k_{\rm r}}\left[m, q\right]\right|^2 \Big)^{-1} \sum_{m \in T_{\rm ps}^{k_{\rm r}}} y_{k_{\rm r}}\left[m, q\right] p_{k_{\rm r}}^{*}\left[m, q\right] \boldsymbol{f}^{*}\left[m\right] \tag{5.13}$$

where $(\cdot)^*$ and $(\cdot)^\dagger$ denote complex conjugate and complex conjugate transpose, respectively.

(b) Selects its receive antenna subset $\mathcal{S} = \left\{\text{AE } \hat{\imath}_1, \ldots, \text{AE } \hat{\imath}_{K_\text{r}'}\right\}$ which contains the first K_r' order statistics of $\left\{ \sum_{\substack{m=M \\ (m \neq T_\text{pf})}}^{M+N-1} \sum_{q=0}^{N_\text{sc}-1} \left|\hat{g}_{k_\text{r}}^{\text{SP}}[m,q]\right|^2 \right\}_{k_\text{r}=1}^{K_\text{r}}$, where the frequency-domain predicted channel gains $\{\hat{g}_{k_\text{r}}^{\text{SP}}[m,q]\}$ are given in (5.11).

3. The transmitter sends out a length-$N \triangleq N_\text{pf} + N_\text{df}$ OFDM packet in which N_pf OFDM pilot symbols, each with N_sc pilot tones, are time multiplexed with N_df OFDM data symbols as (5.7). The packet is received by the subset of antennas $\mathcal{S} = \left\{\text{AE } \hat{\imath}_1, \ldots, \text{AE } \hat{\imath}_{K_\text{r}'}\right\}$.

4. Refined frequency-domain channel gain estimates for all subcarriers of the selected AEs are obtained as

$$\hat{g}_{\hat{\imath}_{k_\text{r}}}^{\text{SE}}[m,q] = \boldsymbol{f}^T[m]\,\hat{\boldsymbol{c}}_{\hat{\imath}_{k_\text{r}}}[q] = \sum_{d=0}^{D-1} \hat{c}_{\hat{\imath}_{k_\text{r}},d}[q]\,u_d[m]\,,\ m \in \mathcal{I}_\text{padt}\backslash T_\text{pf} \tag{5.14}$$

where the basis functions $\{u_d[m] \mid m \in \mathcal{I}_\text{padt}\backslash T_\text{pf}\}_{d=0}^{D-1}$ are a subset over $\mathcal{I}_\text{padt}\backslash T_\text{pf}$ of the complete length-$(M+N)$ Slepian sequences $\{u_d[m] \mid m \in \mathcal{I}_\text{AS}\}_{d=0}^{D-1}$ over the AS cycle interval $\mathcal{I}_\text{AS} = \{0, \ldots, M+N-1\}$. $\hat{\boldsymbol{c}}_{\hat{\imath}_{k_\text{r}}}[q] \triangleq [\hat{c}_{\hat{\imath}_{k_\text{r}},0}[q], \ldots, \hat{c}_{\hat{\imath}_{k_\text{r}},D-1}[q]]^T$ can be calculated from (5.13) (with $T_\text{tp}^{\hat{\imath}_{k_\text{r}}}$ replacing $T_\text{ps}^{k_\text{r}}$).

We note that to determine the subspace dimension D, the method of Sec. 3.3.3 in Chapter 3 is used, i.e., Eq. (3.32).

A summary of the above receive antenna subset selection algorithm for SIMO OFDM-based systems for time-varying frequency-selective channels is presented in Table 5.1.

Table 5.1: A K_{r}' out of K_{r} receive AS algorithm for SIMO OFDM-based systems for time-varying frequency-selective channels.

1)	The transmitter sends out $\lceil \frac{K_{\mathrm{r}}}{K_{\mathrm{r}}'} \rceil N_{\mathrm{ps}}$ OFDM training symbols in N_{ps} rounds of transmission at times $m \in \{T_{\mathrm{ps}}^1 \cup \ldots \cup T_{\mathrm{ps}}^{K_{\mathrm{r}}}\}$ using (5.5).
2)	The receiver calculates $\{\hat{g}_{k_{\mathrm{r}}}^{\mathrm{SP}}[m,q]\}$ for $k_{\mathrm{r}} = 1, 2, \ldots, K_{\mathrm{r}}$ and $q = 0, 1, \ldots, N_{\mathrm{sc}} - 1$ using (5.11).
3)	The receiver selects $\left\{\mathrm{AE}\ \hat{\iota}_1, \ldots, \mathrm{AE}\ \hat{\iota}_{K_{\mathrm{r}}'}\right\}$ corresponding to the first K_{r}' order statistics of $\left\{ \sum_{\substack{m=M \\ (m \neq T_{\mathrm{pf}})}}^{M+N-1} \sum_{q=0}^{N_{\mathrm{sc}}-1} \left| \hat{g}_{k_{\mathrm{r}}}^{\mathrm{SP}}[m,q] \right|^2 \right\}_{k_{\mathrm{r}}=1}^{K_{\mathrm{r}}}$.
4)	The transmitter sends out a length-N OFDM packet consisting of N_{pf} pilot symbols time multiplexed with N_{df} data symbols as (5.7).
5)	The receiver calculates $\{\hat{g}_{\hat{\iota}_{k_{\mathrm{r}}}}^{\mathrm{SE}}[m,q]\}$ for $k_{\mathrm{r}} = 1, 2, \ldots, K_{\mathrm{r}}'$ and $q = 0, 1, \ldots, N_{\mathrm{sc}} - 1$ using (5.14) for data decoding.

5.3.1 Extension to MIMO OFDM

In this section, we extend the above algorithm to accommodate MIMO OFDM-based spatial multiplexing systems for time-varying frequency-selective for per-packet switching. A description of the considered system model is first presented, and the algorithm is described next.

MIMO OFDM-based Spatial Multiplexing Model

Consider an N_{sc} subcarrier frequency MIMO OFDM-based spatial multiplexing system employing K_{t} transmit antennas and K_{r} receive antennas ($K_{\mathrm{r}} \geq K_{\mathrm{t}}$). The symbols for each AE are OFDM modulated using an N_{sc}-point inverse fast Fourier transform (IFFT) as illustrated in Fig. 5.3. The discrete time-domain channel responses have delayed multipath L taps as

$$\mathbf{H}[m,\ell'] \triangleq \sum_{\ell=0}^{L-1} \sqrt{P[\ell]}\mathbf{W}_{\ell}[m]\,\delta[\ell' - \ell] \tag{5.15}$$

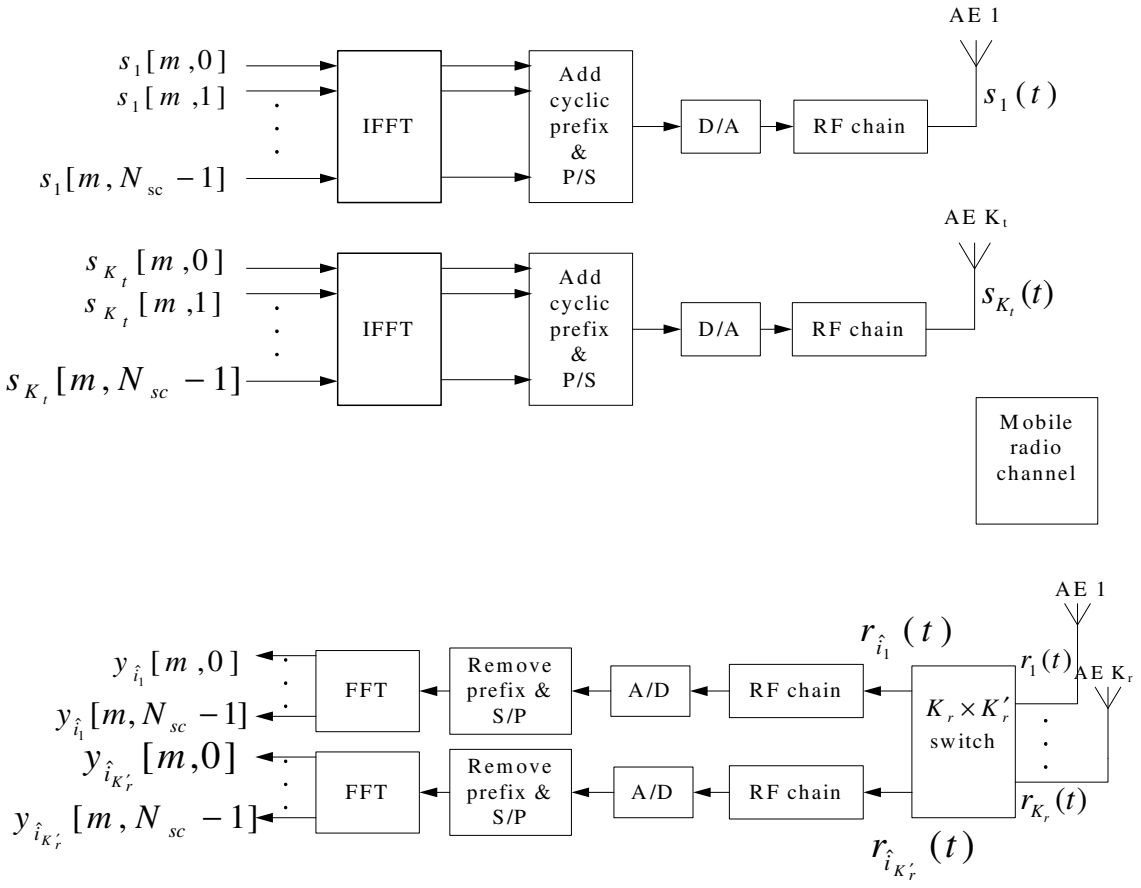

Figure 5.3: MIMO OFDM-based system model with receive antenna subset selection, for all the N_{sc} subcarriers, in time-varying frequency-selective fading.

where $P[\ell]$ for $\ell = 0, \ldots, L-1$ represents the channel power delay profile and $\mathbf{W}_\ell[m]$ denote the $K_{\mathrm{r}} \times K_{\mathrm{t}}$ discrete-time channel matrix for the ℓth tap. It is given by

$$\mathbf{W}_\ell[m] = \begin{bmatrix} w_{1,1}^{(\ell)}[m] & \ldots & w_{1,K_{\mathrm{t}}}^{(\ell)}[m] \\ \vdots & \ddots & \vdots \\ w_{K_{\mathrm{r}},1}^{(\ell)}[m] & \ldots & w_{K_{\mathrm{r}},K_{\mathrm{t}}}^{(\ell)}[m] \end{bmatrix} \tag{5.16}$$

where $w_{k_\mathrm{r},k_\mathrm{t}}^{(\ell)}[m]$ represents the ℓth tap channel associated with the k_r receive antenna and the k_t transmit antenna at time m. The cyclic prefix in each OFDM symbol is sufficiently long to suppress any possible ISI caused by the multipath propagation. At the receiver, OFDM demodulation is performed at each receive antenna using an N_sc-point fast Fourier transform (FFT), the frequency-domain input-output model for OFDM-based spatial multiplexing can thus be expressed as

$$\mathbf{y}[m,q] = \mathbf{G}[m,q]\,\mathbf{s}[m,q] + \mathbf{z}[m,q] \tag{5.17}$$

where $\mathbf{y}[m,q] \triangleq [y_1[m,q],\ldots,y_{K_\mathrm{r}}[m,q]]^T$ is the $K_\mathrm{r}\times 1$ received signal vector at the qth OFDM tone in the mth OFDM symbol, with $y_{k_\mathrm{r}}[m,q]$ the received symbol on the qth tone during the mth OFDM symbol at receive AE k_r for $k_\mathrm{r}=1,2,\ldots,K_\mathrm{r}$. In (5.17), $\mathbf{s}[m,q] \triangleq [s_1[m,q],\ldots,s_{K_\mathrm{t}}[m,q]]^T$ is the $K_\mathrm{t}\times 1$ transmitted signal vector at the qth OFDM tone in the mth OFDM symbol, with $s_{k_\mathrm{t}}[m,q]$ the transmitted symbol on the qth tone during the mth OFDM symbol from transmit AE k_t for $k_\mathrm{t}=1,2,\ldots,K_\mathrm{t}$. All modulated signals have unit average power, i.e., $\mathbb{E}\left[\mathbf{s}^\dagger[m,q]\,\mathbf{s}[m,q]\right]=1\ \forall\ m,q$. In (5.17), $\mathbf{z}[m,q] \triangleq [z_1[m,q],\ldots,z_{K_\mathrm{r}}[m,q]]^T$ is the $K_\mathrm{r}\times 1$ additive noise vector with zero-mean and covariance $N_\mathrm{o}\mathbf{I}_{K_\mathrm{r}}$, where $\mathbf{I}_{K_\mathrm{r}}$ the identity matrix of size K_r. The $K_\mathrm{r}\times K_\mathrm{t}$ frequency-domain time-varying channel matrix $\mathbf{G}[m,q]$ for subcarrier q is given by

$$\mathbf{G}[m,q] = \sum_{\ell=0}^{L-1}\mathbf{H}[m,\ell]\exp\left(-j\frac{2\pi q\ell}{N_\mathrm{sc}}\right) \tag{5.18}$$

for $q=0,\ldots,N_\mathrm{sc}-1$.

Receive Antenna Selection Algorithm for MIMO OFDM Systems

The above algorithm is converted to accommodate MIMO OFDM-based systems with $K_{\rm t}$ transmit and $K_{\rm r}$ receive antennas ($K_{\rm r} \geq K_{\rm t}$) out of which only $K'_{\rm r}$ ($K_{\rm t} \leq K'_{\rm r} < K_{\rm r}$) receive antennas are selected, as shown in Fig. 5.3, as follows: In the training phase, in total, $K_{\rm t}\left(\left\lceil \frac{K_{\rm r}}{K'_{\rm r}} \right\rceil N_{\rm ps}\right)$ OFDM training symbols are transmitted in $N_{\rm ps}$ rounds of transmission. In each round, $K_{\rm t}$ OFDM AS training symbols are transmitted disjointly in time from the $K_{\rm t}$ transmit AEs to each of the $\left\lceil \frac{K_{\rm r}}{K'_{\rm r}} \right\rceil$ subsets of antennas. This means that AEs $2, \ldots, K_{\rm t}$ do not transmit while AE 1 transmits its first OFDM pilot symbols to the first subset of antennas. Similarly, AEs $1, 3, \ldots, K_{\rm t}$ do not transmit while AE 2 transmits its first pilot symbols to the same first subset of antennas, and so on. In a manner similar to the SIMO case discussed previously, the duration between consecutive training symbols transmitted from AE $k_{\rm t}$ and AE $k_{\rm t}+1$ in each round to the same subset of antennas is $T_{\rm p} = \alpha T_{\rm os}$. Therefore, the duration between two consecutive training symbols transmitted from AE $k_{\rm t}$ in consecutive rounds of transmission to the same subset of antennas is $T_{\rm r} = K_{\rm t}\left\lceil \frac{K_{\rm r}}{K'_{\rm r}} \right\rceil T_{\rm p} = \alpha K_{\rm t}\left\lceil \frac{K_{\rm r}}{K'_{\rm r}} \right\rceil T_{\rm os}$. Thus AE $k_{\rm r}$ receives $N_{\rm ps}$ AS OFDM training pilots from transmit AE $k_{\rm t}$ at times $m \in T_{\rm ps}^{k_{\rm r},k_{\rm t}}$, where

$$\begin{aligned} T_{\rm ps}^{k_{\rm r},k_{\rm t}} &= \left\{ \left(\left(\left\lceil \frac{k_{\rm r}}{K'_{\rm r}} \right\rceil - 1 \right) K_{\rm t} T_{\rm p} + (k_{\rm t}-1)T_{\rm p} + (n_{\rm ps}-1)T_{\rm r} \right) \;\middle|\; n_{\rm ps} = 1, \ldots, N_{\rm ps} \right\} \\ &= \left\{ \alpha \left(\left(\left\lceil \frac{k_{\rm r}}{K'_{\rm r}} \right\rceil - 1 \right) K_{\rm t} + (k_{\rm t}-1) + (n_{\rm ps}-1) K_{\rm t} \left\lceil \frac{K_{\rm r}}{K'_{\rm r}} \right\rceil \right) T_{\rm os} \;\middle|\; 1 \leq n_{\rm ps} \leq N_{\rm ps} \right\} \\ &\triangleq \left\{ \alpha \left[\left(\left\lceil \frac{k_{\rm r}}{K'_{\rm r}} \right\rceil - 1 \right) K_{\rm t} + (k_{\rm t}-1) + (n_{\rm ps}-1) K_{\rm t} \left\lceil \frac{K_{\rm r}}{K'_{\rm r}} \right\rceil \right] \;\middle|\; n_{\rm ps} = 1, \ldots, N_{\rm ps} \right\} \end{aligned} \tag{5.19}$$

for $k_{\rm t} = 1, \ldots, K_{\rm t}$ and $k_{\rm r} = 1, \ldots, K_{\rm r}$, where in the last step, discrete-time notation is adopted. The AS training phase thus spans the discrete time $\mathcal{I}_{\rm ast} = \{0, 1, \ldots, M-1\}$, where $M = \alpha K_{\rm t} N_{\rm ps} \left\lceil \frac{K_{\rm r}}{K'_{\rm r}} \right\rceil$. In Step 2(a) of the previously described receive antenna subset selection algorithm, the receiver uses these AS pilot symbols to predict the frequency-domain channel gains $\{g_{k_{\rm r},k_{\rm t}}[m,q]\}$ for every subcarrier of transmit AE $k_{\rm t}$ and receive AE $k_{\rm r}$ via

$$\hat{g}^{\rm SP}_{k_{\rm r},k_{\rm t}}[m,q] = \boldsymbol{f}^T[m]\,\hat{\boldsymbol{c}}_{k_{\rm r},k_{\rm t}}[q] = \sum_{d=0}^{D-1} \hat{c}_d^{k_{\rm r},k_{\rm t}}[q]\,u_d[m], \quad m \in \mathcal{I}_{\rm padt} \backslash \left(T_{\rm pf}^{k_{\rm t}} \cup \mathcal{P}_{\rm nt}^{k_{\rm t}}\right) \tag{5.20}$$

where $\mathcal{P}_{\rm nt}^{k_{\rm t}}$ and $T_{\rm pf}^{k_{\rm t}}$ are given in (5.24) and (5.25), respectively. $\hat{\boldsymbol{c}}_{k_{\rm r},k_{\rm t}}[q] \triangleq \left[\hat{c}_0^{k_{\rm r},k_{\rm t}}[q], \ldots, \hat{c}_{D-1}^{k_{\rm r},k_{\rm t}}[q]\right]^T$ includes the basis expansion coefficients for subcarrier q. It is given by

$$\begin{aligned} \hat{\boldsymbol{c}}_{k_{\rm r},k_{\rm t}}[q] &= \Big(\sum_{m \in T_{\rm ps}^{k_{\rm r},k_{\rm t}}} \boldsymbol{f}[m]\,\boldsymbol{f}^{\dagger}[m]\,|p_{k_{\rm r},k_{\rm t}}[m,q]|^2 \Big)^{-1} \\ &\quad \times \sum_{m \in T_{\rm ps}^{k_{\rm r},k_{\rm t}}} y_{k_{\rm r},k_{\rm t}}[m,q]\,p^*_{k_{\rm r},k_{\rm t}}[m,q]\,\boldsymbol{f}^*[m] \end{aligned} \tag{5.21}$$

where $p_{k_{\rm r},k_{\rm t}}[m,q]$ is the unit average energy pilot modulating the qth tone during the mth OFDM symbol transmitted from AE $k_{\rm t}$ to receive AE $k_{\rm r}$. In (5.21), $y_{k_{\rm r},k_{\rm t}}[m,q]$ is the received training symbol on the qth pilot subcarrier given by

$$y_{k_{\rm r},k_{\rm t}}[m,q] = g_{k_{\rm r},k_{\rm t}}[m,q]\,p_{k_{\rm r},k_{\rm t}}[m,q] + z_{k_{\rm r},k_{\rm t}}[m,q], \quad m \in T_{\rm ps}^{k_{\rm r},k_{\rm t}}. \tag{5.22}$$

In Step 2(b) of the previously described algorithm, the receiver selects its receive subset of antennas $\{\text{AE } \hat{\imath}_1, \ldots, \text{AE } \hat{\imath}_{K'_{\rm r}}\}$ which contains the first $K'_{\rm r}$ order statistics

of $\left\{ \sum_{k_\mathrm{t}=1}^{K_\mathrm{t}} \left(\sum_{\substack{m=M \\ (m \neq T_\mathrm{pf}^{k_\mathrm{t}} \cup \mathcal{P}_\mathrm{nt}^{k_\mathrm{t}})}}^{M+N-1} \sum_{q=0}^{N_\mathrm{sc}-1} \left| \hat{g}_{k_\mathrm{r},k_\mathrm{t}}^{\mathrm{SP}} [m,q] \right|^2 \right) \right\}_{k_\mathrm{r}=1}^{K_\mathrm{r}}$. In Step 3, in the data transmission each transmit AE sends out a length-$N = N_\mathrm{df} + N_\mathrm{pf} + N_\mathrm{nt}$ OFDM packet containing N_df OFDM data symbols and N_pf OFDM pilot symbols with $N_\mathrm{nt} \triangleq (K_\mathrm{t} - 1) N_\mathrm{pf}$ no-transmission taking place. This is because the OFDM pilot symbols are transmitted disjointly in time from the transmit AEs to the selected subset of antennas. The symbol locations in the packet that carry the OFDM post-selection pilots are given by

$$\mathcal{P}_\mathrm{pf}^{k_\mathrm{t}} \triangleq \left\{ \left\lfloor \frac{(2n_\mathrm{pf} - 1) N}{2N_\mathrm{pf}} \right\rfloor + (k_\mathrm{t} - 1) \;\middle|\; n_\mathrm{pf} = 1, \ldots, N_\mathrm{pf} \right\} \tag{5.23}$$

for $1 \leq k_\mathrm{t} \leq K_\mathrm{t}$. The no-transmission positions in the packet for transmit AE k_t are given by

$$\mathcal{P}_\mathrm{nt}^{k_\mathrm{t}} \triangleq \left(\mathcal{P}_\mathrm{pf}^{1} \cup \ldots \cup \mathcal{P}_\mathrm{pf}^{K_\mathrm{t}} \right) \backslash \mathcal{P}_\mathrm{pf}^{k_\mathrm{t}}. \tag{5.24}$$

Since the AS training phase spans the discrete time $\mathcal{I}_\mathrm{ast} = \{0, 1, \ldots, M-1\}$ with $M = \alpha K_\mathrm{t} N_\mathrm{ps} \left\lceil \frac{K_\mathrm{r}}{K_\mathrm{r}'} \right\rceil$, the N_pf OFDM post-selection pilot symbols are thus received by the selected AEs at times $m \in T_\mathrm{pf}^{k_\mathrm{t}}$ for $k_\mathrm{t} = 1, \ldots, K_\mathrm{t}$, where

$$T_\mathrm{pf}^{k_\mathrm{t}} \triangleq \left\{ M - 1 + \left\lfloor \frac{(2n_\mathrm{pf} - 1) N}{2N_\mathrm{pf}} \right\rfloor + (k_\mathrm{t} - 1) \;\middle|\; n_\mathrm{pf} = 1, \ldots, N_\mathrm{pf} \right\}. \tag{5.25}$$

Thus, in total, $N_\mathrm{tp} = N_\mathrm{ps} + N_\mathrm{pf}$ OFDM training symbols are received by the selected AEs at times

$$T_\mathrm{tp}^{\hat{\iota}_{k_\mathrm{r}},k_\mathrm{t}} = T_\mathrm{ps}^{\hat{\iota}_{k_\mathrm{r}},k_\mathrm{t}} \cup T_\mathrm{pf}^{k_\mathrm{t}}, \qquad k_\mathrm{r} = 1, \ldots, K_\mathrm{r}' \tag{5.26}$$

where $T_{\rm ps}^{\hat{\iota}_{k_{\rm r}},k_{\rm t}}$ and $T_{\rm pf}^{k_{\rm t}}$ are given in (5.19) and (5.25), respectively. From these $N_{\rm tp}$ OFDM training symbols refined frequency-domain channel gain estimates $\{\hat{g}_{\hat{\iota}_{k_{\rm r}},k_{\rm t}}^{\rm SE}[m,q] \mid m \in \mathcal{I}_{\rm padt}\backslash(T_{\rm pf}^{k_{\rm t}} \cup \mathcal{P}_{\rm nt}^{k_{\rm t}})\}_{q=0}^{N_{\rm sc}-1}$ are obtained to decode data as

$$\hat{g}_{\hat{\iota}_{k_{\rm r}},k_{\rm t}}^{\rm SE}[m,q] = \boldsymbol{f}^T[m]\,\hat{\boldsymbol{c}}_{\hat{\iota}_{k_{\rm r}},k_{\rm t}}[q] = \sum_{d=0}^{D-1} \hat{c}_d^{\hat{\iota}_{k_{\rm r}},k_{\rm t}}[q]\,u_d[m]\,,\ m \in \mathcal{I}_{\rm padt}\backslash\left(T_{\rm pf}^{k_{\rm t}} \cup \mathcal{P}_{\rm nt}^{k_{\rm t}}\right) \quad (5.27)$$

where $\hat{\boldsymbol{c}}_{\hat{\iota}_{k_{\rm r}},k_{\rm t}}[q] \triangleq \left[\hat{c}_0^{\hat{\iota}_{k_{\rm r}},k_{\rm t}}[q],\ldots,\hat{c}_{D-1}^{\hat{\iota}_{k_{\rm r}},k_{\rm t}}[q]\right]^T$ in (5.27) can be calculated from (5.21) (with $T_{\rm tp}^{\hat{\iota}_{k_{\rm r}},k_{\rm t}}$ replacing $T_{\rm ps}^{k_{\rm r},k_{\rm t}}$). The pilot-assisted data transmission phase thus spans the discrete time $\mathcal{I}_{\rm padt} = \{M, M+1,\ldots,M+N-1\}$, where $M = \alpha K_{\rm t} N_{\rm ps}\left\lceil \frac{K_{\rm r}}{K_{\rm r}'}\right\rceil$ and $N = N_{\rm df} + N_{\rm pf} + N_{\rm nt}$.

We note that the method of Sec. 3.3.3 in Chapter 3 is used, i.e., Eq. (3.32) to determine the subspace dimension D. A summary is given in Table 5.2.

Table 5.2: A $K_{\rm r}'$ out of $K_{\rm r}$ receive antenna subset selection algorithm for MIMO OFDM systems for time-varying frequency-selective channels.

1)	The transmitter, equipped with $K_{\rm t}$ antennas, sends out $K_{\rm t}(\lceil \frac{K_{\rm r}}{K_{\rm r}'}\rceil N_{\rm ps})$ OFDM training symbols in $N_{\rm ps}$ rounds of transmission at times $m \in T_{\rm ps}^{k_{\rm r},k_{\rm t}}$ for $k_{\rm r} = 1,\ldots,K_{\rm r}$ and $k_{\rm t} = 1,\ldots,K_{\rm t}$ using (5.19).
2)	The receiver calculates $\{\hat{g}_{k_{\rm r},k_{\rm t}}^{\rm SP}[m,q]\}$ for $k_{\rm r} = 1,\ldots,K_{\rm r}$, $k_{\rm t} = 1,\ldots,K_{\rm t}$, and $q = 0,1,\ldots,N_{\rm sc}-1$ using (5.20).
3)	The receiver selects $\left\{\text{AE } \hat{\iota}_1,\ldots,\text{AE } \hat{\iota}_{K_{\rm r}'}\right\}$ corresponding to the first $K_{\rm r}'$ order statistics of $\left\{\sum_{k_{\rm t}=1}^{K_{\rm t}}\left(\sum_{\substack{m=M\\(m\neq T_{\rm pf}^{k_{\rm t}}\cup\mathcal{P}_{\rm nt}^{k_{\rm t}})}}^{M+N-1}\sum_{q=0}^{N_{\rm sc}-1}\left|\hat{g}_{k_{\rm r},k_{\rm t}}^{\rm SP}[m,q]\right|^2\right)\right\}_{k_{\rm r}=1}^{K_{\rm r}}$.
4)	Each transmit AE sends out a length-$N = N_{\rm df} + N_{\rm pf} + N_{\rm nt}$ OFDM packet consisting of $N_{\rm df}$ and $N_{\rm pf}$ OFDM data and pilot symbols, respectively, in which for $N_{\rm nt} = (K_{\rm t}-1)N_{\rm pf}$ symbols, no transmission of information is taking place.
5)	The receiver calculates $\{\hat{g}_{\hat{\iota}_{k_{\rm r}},k_{\rm t}}^{\rm SE}[m,q]\}$ for $k_{\rm r} = 1,2,\ldots,K_{\rm r}'$, $k_{\rm t} = 1,\ldots,K_{\rm t}$, and $q = 0,1,\ldots,N_{\rm sc}-1$ using (5.27) for data decoding.

5.4 Simulations

We now present numerical results to gain insight into the performance of the presented AS methods for time-varying frequency-selective channels. In the sequel, a system with K_{t} transmit and K_{r} receive antennas is denoted as $K_{\mathrm{t}} \times K_{\mathrm{r}}$, while a system with K_{t} transmit and K_{r} receive antennas out of which only K'_{r} are selected is denoted as $K_{\mathrm{t}} \times (K'_{\mathrm{r}}; K_{\mathrm{r}})$. Unless otherwise stated, the simulation parameters are as follows: $1 \times (1; K_{\mathrm{r}})$ SISO, $1 \times (K'_{\mathrm{r}}; K_{\mathrm{r}})$ SIMO, and $2 \times (K'_{\mathrm{r}}; K_{\mathrm{r}})$ MIMO OFDM-based systems are simulated. The basic unit of time for data transmission is one transmission time interval (TTI) which is 1 ms long and consists of 12 OFDM symbols [2]. The transmission bandwidth is 2.5 MHz, the sampling frequency $f_{\mathrm{s}} = 3.84$ MHz, and the sampling time $T_{\mathrm{s}} = \frac{1}{f_{\mathrm{s}}} = 0.2604$ μs. The number of subcarriers $N_{\mathrm{sc}} = 256$ (FFT size is 256), spaced 15 KHz apart. The cyclic prefix has $N_{\mathrm{g}} = 64$ samples (16.67 μs). This results in an OFDM symbol duration of $T_{\mathrm{os}} = (N_{\mathrm{sc}} + N_{\mathrm{g}})\, T_{\mathrm{s}} = 83.33$ μs. QPSK modulation is used [2]. At the receiver, the minimum mean-square error (MMSE) linear equalizer is used to recover the transmitted data. Before an AS cycle the $K_{\mathrm{t}} \times (K'_{\mathrm{r}}; K_{\mathrm{r}})$ simulated system can thus transmit data at $\frac{K_{\mathrm{t}} N_{\mathrm{sc}} \log_2(\mathtt{M})}{T_{\mathrm{os}}}$ bits/s. For example, the simulated $1 \times (1; K_{\mathrm{r}})$ system can transmit data at 6.144 Mb/s over a 2.5 MHz channel, i.e., the spectral efficiency is 2.4576 b/s/Hz. The packet duration is chosen to be 2 ms, i.e., 2 TTIs long. For SISO and SIMO systems, the packet consists of $N = N_{\mathrm{pf}} + N_{\mathrm{df}} = 24$ OFDM symbols, in which $N_{\mathrm{pf}} = 2$ OFDM pilot symbols are time-multiplexed with $N_{\mathrm{df}} = 22$ data OFDM symbols. As for MIMO systems, it consists of N_{df} and N_{pf} OFDM data and pilot symbols, respectively, in which for $N_{\mathrm{nt}} = (K_{\mathrm{t}} - 1)\, N_{\mathrm{pf}}$ symbols, no transmission of information is taking place, i.e., $N = N_{\mathrm{df}} + N_{\mathrm{pf}} + N_{\mathrm{nt}}$. During an AS cycle, the described systems can transmit data

at a rate of $\frac{K_{\mathrm{t}} N_{\mathrm{sc}} N_{\mathrm{df}} \log_2(\mathtt{M})}{(M+N)T_{\mathrm{os}}}$ bits/s. For example, for $K_{\mathrm{t}} = 1$, $K_{\mathrm{r}} = 2$, $K'_{\mathrm{r}} = 1$, $\alpha = 2$, and $N_{\mathrm{ps}} = 2$ the transmission efficiency is 1.899 b/s/Hz. The system operates at a carrier frequency $f_{\mathrm{c}} = 2$ GHz. A user moves with velocity $v_{\max} = 20$ km/h. This gives a Doppler frequency of $f_{\mathrm{D}} = 37.037$ Hz and maximum normalized Doppler frequency of $\nu_{\max} = 0.0031$. The multipath channel exhibits a 6-tap typical urban (TU) power delay profile [27], as defined in Table 5.3. It is among the most dispersive of typically simulated channel profiles. The channel delay is quantized to the nearest multiple of 0.2604 μs, as shown in Fig. 5.4, since the system sampling rate is 3.84 mega-samples per second. A Rayleigh fading channel with Clarke's Doppler spectrum for each tap

Table 5.3: The COST 207 6-tap typical urban (TU) channel model

Tap number	1	2	3	4	5	6
Delay (μs)	0	0.2	0.5	1.6	2.3	5.0
Fractional power	0.19	0.38	0.24	0.09	0.06	0.04

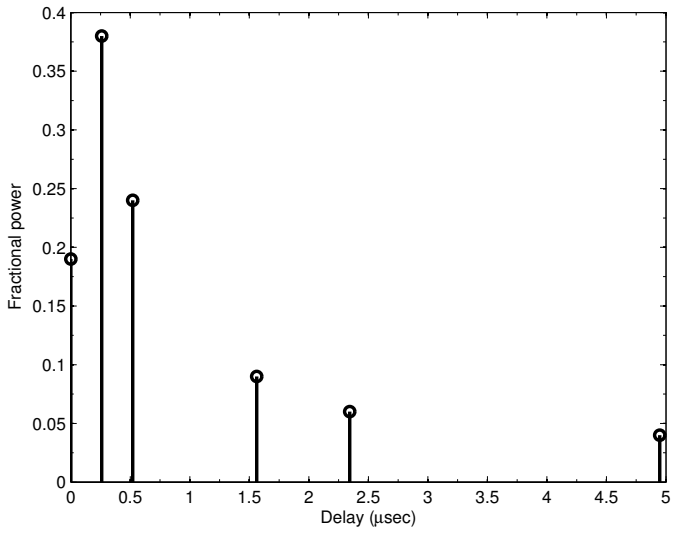

Figure 5.4: (Quantized) 6-tap typical urban (TU) power-delay profile (PDP).

is used [18]. The complex channel of the ℓth resolvable multipath component between the k_{r}th receive and k_{t}th transmit antennas is thus given by [18, 27]

$$w_{k_{\mathrm{r}},k_{\mathrm{t}}}^{(\ell)}[m] = \sum_{n_{\mathrm{path}}=0}^{N_{\mathrm{path}}} a_{k_{\mathrm{r}},k_{\mathrm{t}}}^{(\ell),n_{\mathrm{path}}} \exp\left(j2\pi\nu_{k_{\mathrm{r}},k_{\mathrm{t}}}^{(\ell),n_{\mathrm{path}}} m\right) \tag{5.28}$$

where the number of propagation paths composing each resolvable path is set to $N_{\mathrm{path}} = 20$. $a_{k_{\mathrm{r}},k_{\mathrm{t}}}^{(\ell),n_{\mathrm{path}}} = \frac{1}{\sqrt{N_{\mathrm{path}}}} \exp(j\psi_{k_{\mathrm{r}},k_{\mathrm{t}}}^{(\ell),n_{\mathrm{path}}})$ with phase angles $\psi_{k_{\mathrm{r}},k_{\mathrm{t}}}^{(\ell),n_{\mathrm{path}}}$ uniformly distributed over $[-\pi\ \pi)$. The Doppler shifts $\nu_{k_{\mathrm{r}},k_{\mathrm{t}}}^{(\ell),n_{\mathrm{path}}} = \nu_{\max}\cos(\alpha_{k_{\mathrm{r}},k_{\mathrm{t}}}^{(\ell),n_{\mathrm{path}}})$ with angles of incidence $\alpha_{k_{\mathrm{r}},k_{\mathrm{t}}}^{(\ell),n_{\mathrm{path}}}$ uniformly distributed in $[-\pi\ \pi)$. The path parameters $\{a_{k_{\mathrm{r}},k_{\mathrm{t}}}^{(\ell),n_{\mathrm{path}}}\}$ and $\{\nu_{k_{\mathrm{r}},k_{\mathrm{t}}}^{(\ell),n_{\mathrm{path}}}\}$ are modelled as independent and identically distributed [18]. They are assumed constant over an AS cycle but change independently from cycle to cycle.

The bit error rates (BER) of the proposed AS algorithms in Sec. 5.3 are presented next. For comparison, the BER performance of systems employing AS using linear interpolation/extrapolation [23, 31] and orthogonal Fourier based channel estimation/prediction methods [100] are also reported. Detailed descriptions of these techniques are given in Chapter 2. We now summarize the linear extrapolation/interpolation method for SIMO systems.

Using the frequency-domain channel gain estimates $\{\tilde{g}_{k_{\mathrm{r}}}[m,q] \mid m \in T_{\mathrm{ps}}^{k_{\mathrm{r}}}\}$ obtained from the observations over the AS training pilots at times $m \in T_{\mathrm{ps}}^{k_{\mathrm{r}}}$ in (5.6), linear extrapolation for each subcarrier is then carried out to obtain the frequency-domain channel gain estimates $\{\hat{g}_{k_{\mathrm{r}}}^{\mathrm{LE}}[m,q] \mid m \in \mathcal{I}_{\mathrm{padt}}\}$ over the data phase as

$$\hat{g}_{k_{\mathrm{r}}}^{\mathrm{LE}}[m,q] = \beta_{k_{\mathrm{r}},1}[q]\, m + \beta_{k_{\mathrm{r}},2}[q], \qquad m \in \mathcal{I}_{\mathrm{padt}} \tag{5.29}$$

where the 2×1 vector $\boldsymbol{\beta}_{k_{\mathrm{r}}}[q] \triangleq [\beta_{k_{\mathrm{r}},1}[q]\ \ \beta_{k_{\mathrm{r}},2}[q]]^T$ contains the coefficients of the

linear model. It is given by

$$\boldsymbol{\beta}_{k_\mathrm{r}}[q] = \left(\boldsymbol{V}_{k_\mathrm{r}}^T \boldsymbol{V}_{k_\mathrm{r}}\right)^{-1} \boldsymbol{V}_{k_\mathrm{r}}^T \tilde{\boldsymbol{g}}_{k_\mathrm{r}}[q] \tag{5.30}$$

where the $N_\mathrm{ps} \times 1$ vector $\tilde{\boldsymbol{g}}_{k_\mathrm{r}}[q]$ contains the frequency-domain channel gain estimates obtained from the observations over the training pilots at times $m \in T_\mathrm{ps}^{k_\mathrm{r}}$. Its N_ps entries $\{\tilde{g}_{k_\mathrm{r}}[m,q]\}$ for $q = 0, \ldots, N_\mathrm{sc}-1$ can be obtained from (5.6) as

$$\tilde{g}_{k_\mathrm{r}}[m,q] = y_{k_\mathrm{r}}[m,q]\, p_{k_\mathrm{r}}^*[m,q] \triangleq g_{k_\mathrm{r}}[m,q] + e_{k_\mathrm{r}}^\mathrm{n}[m,q], \quad m \in T_\mathrm{ps}^{k_\mathrm{r}} \tag{5.31}$$

where $e_{k_\mathrm{r}}^\mathrm{n}[m,q] \triangleq z_{k_\mathrm{r}}[m,q]\, p_{k_\mathrm{r}}^*[m,q]$ is the the frequency-domain channel estimation error resulting from the AWGN. In (5.30), the $N_\mathrm{ps} \times 2$ matrix $\boldsymbol{V}_{k_\mathrm{r}}$ is given by

$$\boldsymbol{V}_{k_\mathrm{r}} = \begin{bmatrix} T_\mathrm{ps}^{k_\mathrm{r}}[1] & 1 \\ \vdots & \vdots \\ T_\mathrm{ps}^{k_\mathrm{r}}[N_\mathrm{ps}] & 1 \end{bmatrix} \tag{5.32}$$

where $T_\mathrm{ps}^{k_\mathrm{r}}[n_\mathrm{ps}]$ for $n_\mathrm{ps} = 1, \ldots, N_\mathrm{ps}$ is the n_psth element of $T_\mathrm{ps}^{k_\mathrm{r}}$ in (5.5).

We note that the refined frequency-domain channel gain estimates $\{\hat{g}_{\hat{\iota}_{k_\mathrm{r}}}^\mathrm{LIE}[m,q] \mid m \in \mathcal{I}_\mathrm{padt}\}$ for the selected AEs $\{\hat{\iota}_{k_\mathrm{r}}\}_{k_\mathrm{r}=1}^{K_\mathrm{r}'}$, which are estimated using linear interpolation and extrapolation, can be obtained from (5.29)-(5.32) by replacing superscript $(\cdot)^\mathrm{LE}$ by $(\cdot)^\mathrm{LIE}$ and $T_\mathrm{ps}^{k_\mathrm{r}}$ by $T_\mathrm{tp}^{\hat{\iota}_{k_\mathrm{r}}}$. Note that $\boldsymbol{V}_{\hat{\iota}_{k_\mathrm{r}}}$ and $\tilde{\boldsymbol{g}}_{\hat{\iota}_{k_\mathrm{r}}}[q]$ are of sizes $N_\mathrm{tp} \times 2$ and $N_\mathrm{tp} \times 1$, respectively, since $N_\mathrm{tp} = N_\mathrm{pf} + N_\mathrm{ps}$ observations from pilots are used in this case.

5.4.1 SISO Systems

The BER of the proposed receive AS method in Sec. 5.3 for $1 \times (1;2)$ and $1 \times (1;4)$ systems are shown in Figs. 5.5 and 5.6, respectively. We note that the frequency-domain predicted channel gains $\left\{\hat{g}_{k_\mathrm{r}}^{\mathrm{SP}}[m,q]\right\}_{k_\mathrm{r}=1}^{K_\mathrm{r}}$ are used for AE selection, while the refined frequency-domain channel gain estimates $\left\{\hat{g}_{\hat{\imath}}^{\mathrm{SE}}[m,q]\right\}$ for the single selected AE $\hat{\imath}$ are used for data decoding. For comparison, we also show the BER performance of (i) $1 \times (1;2)$ and $1 \times (1;4)$ systems with perfect CSI and AS according to Step 2(b) in Sec. 5.3 $\big($with $g_{k_\mathrm{r}}[m,q]$ replacing $\hat{g}_{k_\mathrm{r}}^{\mathrm{SP}}[m,q]\big)$, (ii) a 1×1 system with perfect CSI, (iii) $1 \times (1;2)$ and $1 \times (1;4)$ systems employing AS based on Fourier channel prediction method according to Step 2(b) in Sec. 5.3, with the refined channel gain estimates obtained from Fourier based channel estimation used for data decoding, (iv) $1 \times (1;2)$ and $1 \times (1;4)$ systems employing AS based on linear channel extrapolation as Step 2(b) in Sec. 5.3, with the refined channel gain estimates obtained from linear channel interpolation used for data decoding, (v) $1 \times (1;2)$ and $1 \times (1;4)$ systems employing Slepian channel prediction and AS according to Step $2\,(b)$ in Sec. 5.3, with the frequency-domain predicted channel gains $\left\{\hat{g}_{k_\mathrm{r}}^{\mathrm{SP}}[m,q]\right\}$ used not only for selection but also for data decoding, and (vi) a 1×1 system employing Slepian channel prediction. It can be observed that the BER performance of the $1 \times (1;4)$ system employing the proposed AS algorithm achieves the same performance as a 1×1 system with perfect CSI. The proposed $1 \times (1;2)$ and $1 \times (1;4)$ systems also outperform the same $1 \times (1;2)$ and $1 \times (1;4)$ systems employing AS with linear interpolation/extrapolation method. For instance, the proposed $1\times(1;2)$ and $1\times(1;4)$ systems achieve SNR performance gains of about 1 dB and 0.5 dB over the $1 \times (1;2)$ and $1 \times (1;4)$ systems employing AS with linear interpolation/extrapolation at a

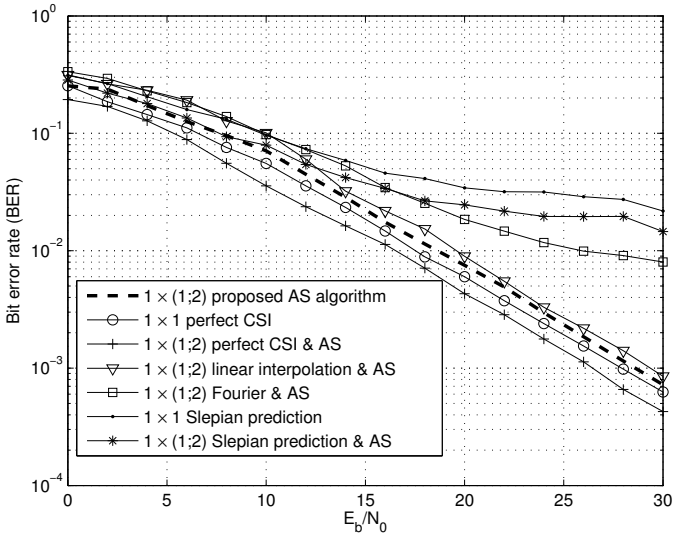

Figure 5.5: BER performance of the proposed AS algorithm for a $1 \times (1;2)$ OFDM-based system when the user velocity $v_{\max} = 20$ Km/h, corresponding to a maximum normalized Doppler frequency $\nu_{\max} = 0.0031$. (QPSK, packet length $N = 24$, $N_{\rm pf} = 2$ post-selection pilots, $N_{\rm df} = 22$ data symbols, and $N_{\rm ps} = 2$ AS training pilots, $T_{\rm p} = 2T_{\rm os}$).

BER $= 10^{-2}$, respectively. Also, error floors exist at moderate to high SNR for the $1 \times (1;2)$ and $1 \times (1;4)$ systems employing AS with the Fourier basis expansion method [100]. We note that the performance of the proposed $1 \times (1;2)$ and $1 \times (1;4)$ systems are about 2 dB and 2.5 dB worse than $1 \times (1;2)$ and $1 \times (1;4)$ systems employing AS with perfect CSI at BER of 10^{-3}, respectively.

Fig. 5.7 shows the effect of increasing the Doppler rate on the BER performance of the proposed AS algorithm for a $1 \times (1;4)$ system when the user velocity is increased to $v_{\max} = 80$ km/h corresponding to a Doppler frequency of $f_{\rm D} = 148.148$ Hz and a maximum normalized Doppler frequency of $\nu_{\max} = 0.0123$. Inspection of Figs. 5.6 and 5.7 reveals that a 0.0092 increase in Doppler frequency (i.e., a 296.78% increase) incurs a loss of approximately 2.5 dB in SNR at a BER of 10^{-3} for the $1 \times (1;4)$ system

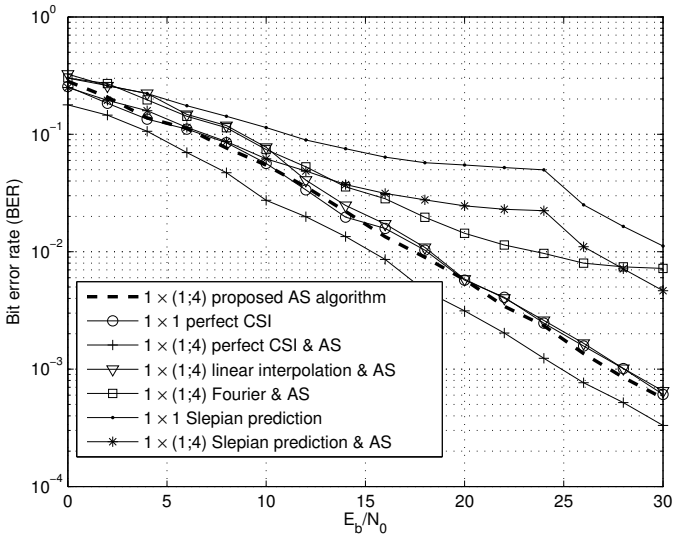

Figure 5.6: BER performance of the proposed AS algorithm for a $1 \times (1;4)$ OFDM-based system when the user velocity $v_{\max} = 20$ Km/h, corresponding to a maximum normalized Doppler frequency $\nu_{\max} = 0.0031$. (QPSK, packet length $N = 24$, $N_{\rm pf} = 2$ post-selection pilots, $N_{\rm df} = 22$ data symbols, and $N_{\rm ps} = 2$ AS training pilots, $T_{\rm p} = 2T_{\rm os}$).

employing the proposed AS algorithm. The same proposed system outperforms the $1 \times (1;4)$ system using AS method based on linear interpolation/extrapolation at high SNR levels (> 25 dB). It can also be observed that the performance of the proposed $1 \times (1;4)$ system is about 1 dB and 4 dB worse than the 1×1 and $1 \times (1;4)$ systems with perfect CSI at a BER of 10^{-2}, respectively.

Next, we consider the effect of the packet length on the BER performance of the proposed receive AS algorithm. Fig. 5.8 illustrates the BER performance of the proposed receive AS algorithm for a $1 \times (1;4)$ system when the packet duration is increased to 3 ms, i.e, it consists of 36 OFDM symbols. The maximum normalized Doppler frequency is kept $\nu_{\max} = 0.0123$ as in Fig. 5.7. It can be noticed that the $1 \times (1;4)$ systems using AS methods based on linear interpolation/extrapolation and

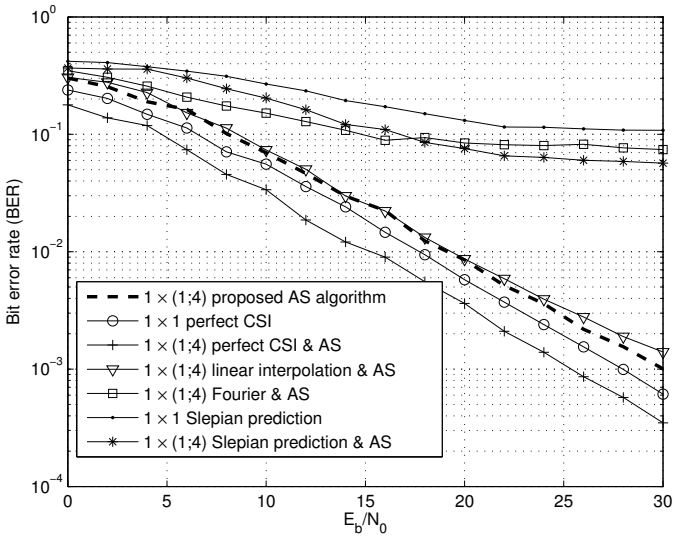

Figure 5.7: BER performance of the proposed AS algorithm for a $1 \times (1;4)$ OFDM-based system when the user velocity $v_{\max} = 80$ Km/h, corresponding to a maximum normalized Doppler frequency $\nu_{\max} = 0.0123$. (QPSK, packet length $N = 24$, $N_{\rm pf} = 2$ post-selection pilots, $N_{\rm df} = 22$ data symbols, and $N_{\rm ps} = 2$ AS training pilots, $T_{\rm p} = 2T_{\rm os}$).

orthogonal Fourier based prediction/estimation suffer from an irreducible error floor at high SNR levels. In contrast, the same $1 \times (1;4)$ proposed system does not exhibit a BER floor. It can be noticed that the performance of the proposed $1 \times (1;4)$ system is about 5 dB worse than that of $1 \times (1;4)$ system employing AS with perfect CSI at a BER of 10^{-2}.

Finally, note from Figs. 5.5-5.7 that the BER of $1 \times (1;4)$ systems employing the proposed AS algorithm is more than one order of magnitude lower than that of 1×1 systems with no AS, which also use one antenna for reception, at SNR = 30 dB.

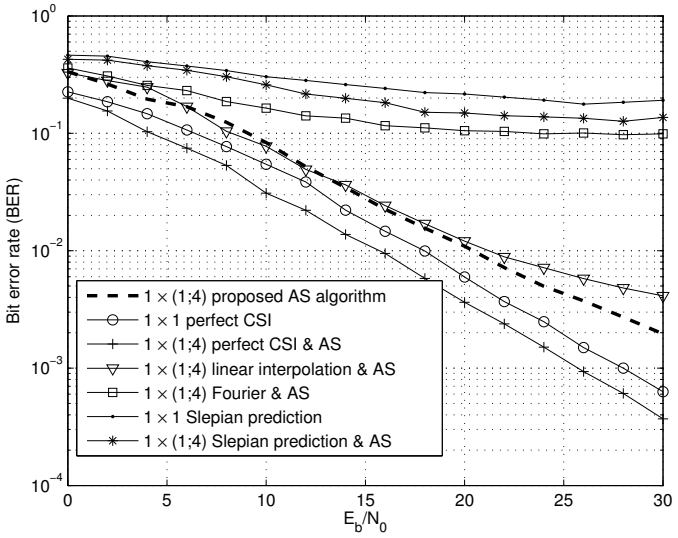

Figure 5.8: BER performance of the proposed AS algorithm for a $1 \times (1;4)$ OFDM-based system when the user velocity $v_{\max} = 80$ Km/h, corresponding to a maximum normalized Doppler frequency $\nu_{\max} = 0.0123$. (QPSK, packet length $N = 36$, $N_{\rm pf} = 2$ post-selection pilots, $N_{\rm df} = 34$ data symbols, and $N_{\rm ps} = 2$ AS training pilots, $T_{\rm p} = 2T_{\rm os}$).

5.4.2 SIMO Systems

The BER of the proposed receive AS algorithm for a $1 \times (2;6)$ system is shown in Fig. 5.9. We note that the frequency-domain predicted channel gains $\left\{\hat{g}_{k_{\rm r}}^{\rm SP}[m,q]\right\}_{k_{\rm r}=1}^{K_{\rm r}}$ are used for AEs selection, while the refined frequency-domain channel gain estimates $\left\{\hat{g}_{\hat{\iota}_1}^{\rm SE}[m,q], \hat{g}_{\hat{\iota}_2}^{\rm SE}[m,q]\right\}$ for the selected subset of antennas $\mathcal{S} = \{\text{AE } \hat{\iota}_1, \text{AE } \hat{\iota}_2\}$ are used for decoding. For comparison, we also show the BER performance of (i) a $1 \times (2;6)$ system with perfect CSI and AS according to Step 2(b) in Sec. 5.3 $\big($with $g_{k_{\rm r}}[m,q]$ replacing $\hat{g}_{k_{\rm r}}^{\rm SP}[m,q]\big)$, (ii) a 1×2 system with perfect CSI and maximum-ratio combining (MRC), (iii) a $1 \times (2;6)$ system employing Fourier basis expansion channel prediction and AS as Step 2(b) in Sec. 5.3, with the refined channel gain

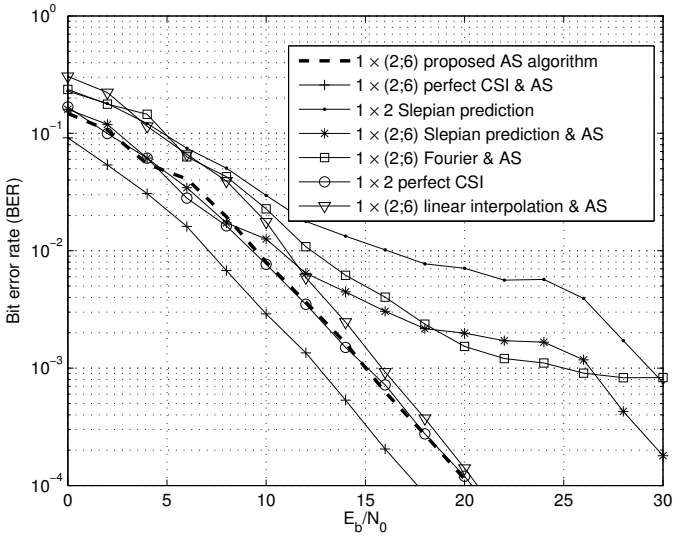

Figure 5.9: BER performance of the proposed AS algorithm for a $1 \times (2;6)$ OFDM-based system when the user velocity $v_{\max} = 20$ Km/h, corresponding to a maximum normalized Doppler frequency $\nu_{\max} = 0.0031$. (QPSK, packet length $N = 24$, $N_{\rm pf} = 2$ post-selection pilots, $N_{\rm df} = 22$ data symbols, and $N_{\rm ps} = 2$ AS training pilots, $T_{\rm p} = 2T_{\rm os}$).

estimates obtained using Fourier channel estimation used for data decoding, (iv) a $1 \times (2;6)$ system employing linear extrapolation for prediction and AS as Step 2(b) in Sec. 5.3, with the refined frequency-domain channel gain estimates obtained using linear interpolation are used to decode data, (v) a $1 \times (2;6)$ system employing Slepian channel prediction and AS according to Step 2(b) in Sec. 5.3, with the frequency-domain predicted channel gains $\left\{\hat{g}_{k_{\rm r}}^{\rm SP}[m,q]\right\}$ used not only for selection but also for data decoding, and (vi) a 1×2 system employing Slepian basis expansion channel prediction with MRC. Inspection of Fig. 5.9 reveals that the $1 \times (2;6)$ system employing the receive AS algorithm in Sec. 5.3 achieves the same BER performance as that of the 1×2 system with perfect CSI and MRC. The same proposed $1 \times (2;6)$ system outperforms the $1 \times (2;6)$ system employing AS with linear interpolation/extrapolation

method. For instance, the $1 \times (2;6)$ system employing the proposed AS method achieves SNR performance gains of about 2 dB and 1 dB over the same $1 \times (2;6)$ system employing AS with linear interpolation/extrapolation method at BER $= 10^{-2}$ and BER $= 10^{-3}$, respectively. It can also be noticed that an error floor occurs at moderate to high SNR for the $1 \times (2;6)$ system employing AS with Fourier techniques. Also, the proposed $1 \times (2;6)$ system is about 2 dB worse than the $1 \times (2;6)$ system employing AS with perfect CSI.

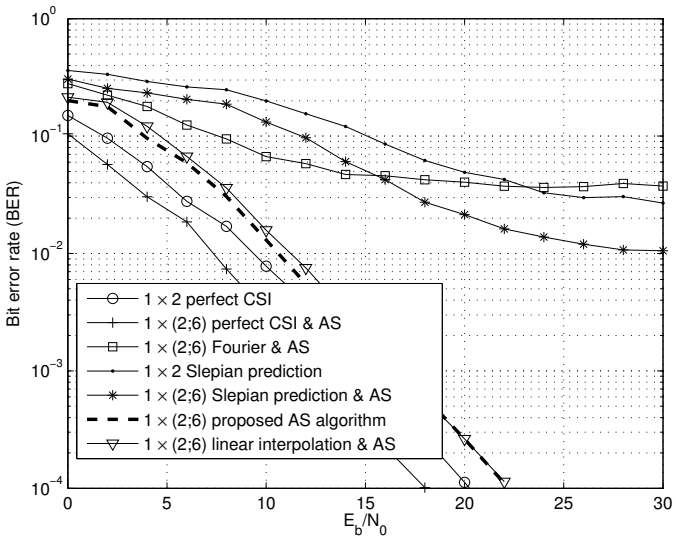

Figure 5.10: BER performance of the proposed AS algorithm for a $1 \times (2;6)$ OFDM-based system when the user velocity $v_{\max} = 80$ Km/h, corresponding to a maximum normalized Doppler frequency $\nu_{\max} = 0.0123$. (QPSK, packet length $N = 24$, $N_{\rm pf} = 2$ post-selection pilots, $N_{\rm df} = 22$ data symbols, and $N_{\rm ps} = 2$ AS training pilots, $T_{\rm p} = 2T_{\rm os}$).

Fig. 5.10 shows the effect of the Doppler frequency on the BER performance of the proposed AS algorithm for a $1 \times (2;6)$ system. The user velocity is increased to $v_{\max} = 80$ km/h. This gives a maximum normalized Doppler frequency of $\nu_{\max} = 0.0123$. From Figs. 5.9 and 5.10, it can be noticed that a 0.0092 increase in Doppler

frequency (i.e., a 296.78% increase) incurs a loss of approximately 2.5 dB in SNR at a BER of 10^{-4} for the $1 \times (2; 6)$ system employing the proposed AS algorithm. Note that the performance of the $1 \times (2; 6)$ system is about 2 dB and 5 dB worse than the 1×2 system with perfect CSI and $1 \times (2; 6)$ system employing AS with perfect CSI at a BER of 10^{-2}, respectively.

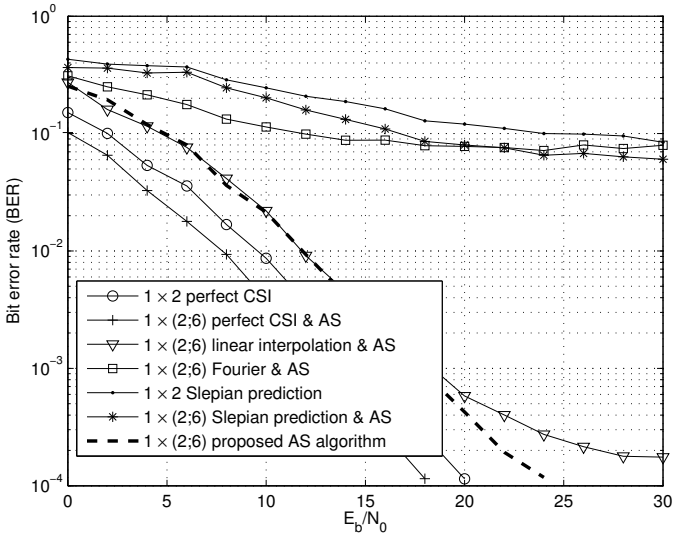

Figure 5.11: BER performance of the proposed AS algorithm for a $1 \times (2; 6)$ OFDM-based system when the user velocity $v_{\max} = 80$ Km/h, corresponding to a maximum normalized Doppler frequency $\nu_{\max} = 0.0123$. (QPSK, packet length $N = 36$, $N_{\rm pf} = 2$ post-selection pilots, $N_{\rm df} = 34$ data symbols, and $N_{\rm ps} = 2$ AS training pilots, $T_{\rm p} = 2T_{\rm os}$).

The effect of the packet length on the performance of the proposed receive AS algorithm for the same $1 \times (2; 6)$ system is depicted in Fig. 5.11. The packet duration is increased to 3 ms, i.e, it consists of 36 OFDM symbols. The maximum normalized Doppler frequency is kept $\nu_{\max} = 0.0123$ as in Fig. 5.10. From Figs. 5.10 and 5.11, it can be observed that increasing the number of symbols in a packet by 12 (i.e., a 50% increase) incurs a loss of approximately 2.5 dB in SNR at a BER of 10^{-4} for

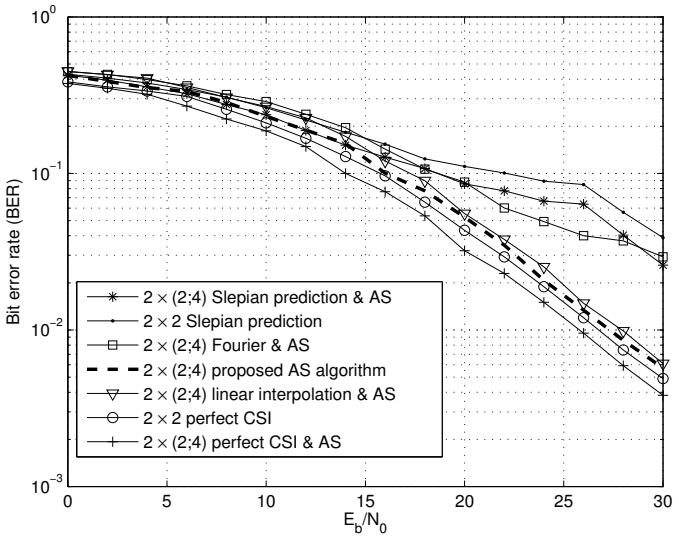

Figure 5.12: BER performance of the proposed AS algorithm for a $2 \times (2;4)$ OFDM-based system when the user velocity $v_{\max} = 20$ Km/h, corresponding to a maximum normalized Doppler frequency $\nu_{\max} = 0.0031$. (QPSK, packet length $N = 24$, $N_{\rm pf} = 2$ post-selection pilots, $N_{\rm df} = 20$ data symbols with $N_{\rm nt} = 2$ no transmission, and $N_{\rm ps} = 2$ AS training pilots, $T_{\rm p} = 2T_{\rm os}$).

the $1 \times (2;6)$ system employing the proposed AS algorithm. Also, an error floor occurs at moderate to high SNR for the $1 \times (2;6)$ system employing AS with linear interpolation/extrapolation technique. Finally, it can be noticed that the performance of the $1 \times (2;6)$ system is about 5 dB worse than the $1 \times (2;6)$ system employing AS with perfect CSI at a BER of 10^{-2}.

Finally, note from Figs. 5.9-5.11 that the BER of the $1 \times (2;6)$ system employing the proposed AS algorithm is about two orders of magnitude lower than that of the 1×2 system with no AS at SNR = 20 dB.

5.4.3 MIMO Systems

The BER of the proposed receive AS algorithm for a $2 \times (2;4)$ system is shown in Fig. 5.12. For comparison, we also show the BER performance of (i) a $2 \times (2;4)$ system with perfect CSI and AS according to Sec. 5.3.1 (with $g_{k_\mathrm{r},k_\mathrm{t}}[m,q]$ replacing $\hat{g}^{\mathrm{SP}}_{k_\mathrm{r},k_\mathrm{t}}[m,q]$), (ii) a 2×2 system with perfect CSI, (iii) a $2 \times (2;4)$ system employing Fourier channel prediction and AS as in Sec. 5.3.1. The refined channel gain estimates obtained using Fourier channel estimation are used for data decoding, (iv) a $2 \times (2;4)$ system employing linear extrapolation for channel prediction and AS as in Sec. 5.3.1. The refined channel gain estimates obtained using linear interpolation and extrapolation are used for data decoding, (v) a $2 \times (2;4)$ system employing Slepian channel prediction and AS according to Sec. 5.3.1, with the predicted channel gains $\left\{\hat{g}^{\mathrm{SP}}_{k_\mathrm{r},k_\mathrm{t}}[m,q]\right\}$ used not only for selection but also for data decoding, (vi) a 2×2 system employing Slepian channel prediction. Inspection of Fig. 5.12 reveals that the BER performance of the $2 \times (2;4)$ system employing the receive AS algorithm proposed in Sec. 5.3.1 approaches that of the 2×2 system with perfect CSI. The same proposed $2 \times (2;4)$ system is about 1 dB worse than the $2 \times (2;4)$ system employing AS with perfect CSI at BER $= 10^{-2}$. Also, an error floor occurs at moderate to high SNR for the $2 \times (2;4)$ system employing AS with Fourier techniques.

The effects of the Doppler frequency and packet length on the BER performance of the proposed AS algorithm for a $2 \times (2;4)$ system are shown in Figs. 5.13 and 5.14, respectively. The user moves with velocity $v_{\max} = 80$ km/h and the packet length is set to 36 OFDM symbols in Fig. 5.14. Inspection of Figs. 5.12 and 5.13, reveals that a 0.0092 increase in Doppler frequency (i.e., a 296.78% increase) incurs a loss of approximately 1.5 dB in SNR at a BER of 10^{-2} for the $2 \times (2;4)$ system employing the

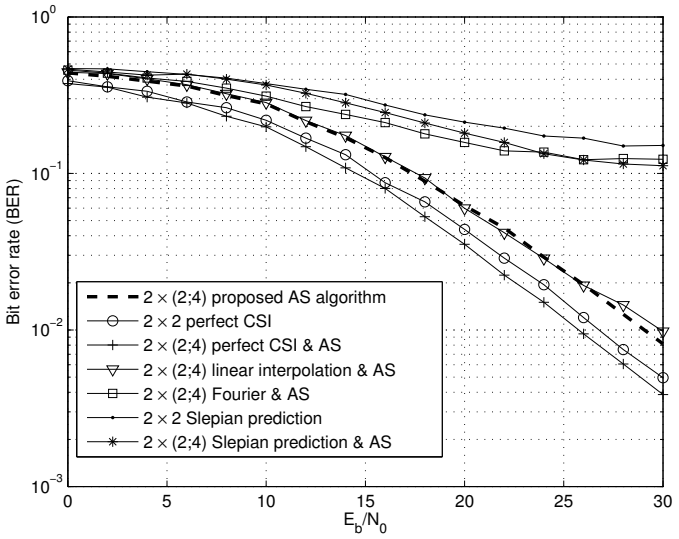

Figure 5.13: BER performance of the proposed AS algorithm for a $2 \times (2;4)$ OFDM-based system when the user velocity $v_{\max} = 80$ Km/h, corresponding to a maximum normalized Doppler frequency $\nu_{\max} = 0.0123$. (QPSK, packet length $N = 24$, $N_{\rm pf} = 2$ post-selection pilots, $N_{\rm df} = 20$ data symbols with $N_{\rm nt} = 2$ no transmission, and $N_{\rm ps} = 2$ AS training pilots, $T_{\rm p} = 2T_{\rm os}$).

proposed AS algorithm. From Figs. 5.13 and 5.14, it can be observed that increasing the number of symbols in a packet by 12 (i.e., a 50% increase) incurs a loss of 1 dB in SNR at a BER of 10^{-2} for the proposed $2 \times (2;4)$ system. An error floor exists at high SNR for the $2 \times (2;4)$ system employing AS with linear interpolation/extrapolation method. From Fig. 5.13 it can be observed that the performance of the proposed $2 \times (2;4)$ system is about 2 dB and 3 dB worse than the 2×2 system with perfect CSI and $2 \times (2;4)$ system employing AS with perfect CSI at BER of 10^{-2}, respectively. The same proposed $2 \times (2;4)$ system is about 4 dB worse than the $2 \times (2;4)$ system employing AS with perfect CSI at BER of 10^{-2}, as illustrated in Fig. 5.14.

Finally, note from Figs. 5.12-5.14 that the BER of the $2 \times (2;4)$ system employing

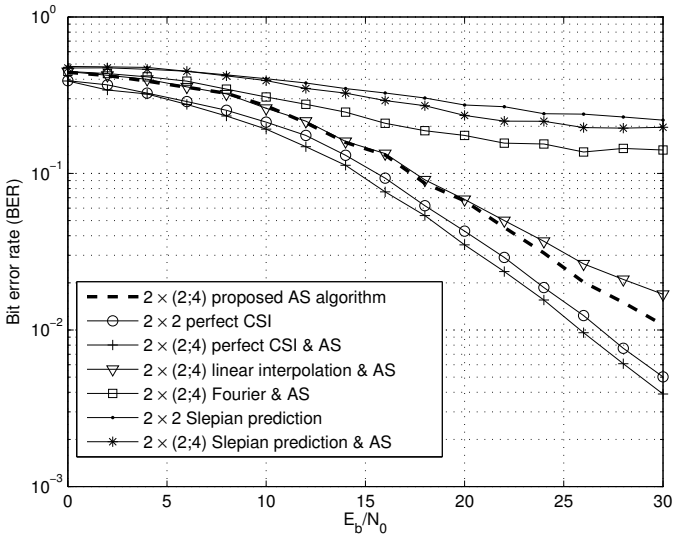

Figure 5.14: BER performance of the proposed AS algorithm for a $2 \times (2;4)$ OFDM-based system when the user velocity $v_{\max} = 80$ Km/h, corresponding to a maximum normalized Doppler frequency $\nu_{\max} = 0.0123$. (QPSK, packet length $N = 36$, $N_{\rm pf} = 2$ post-selection pilots, $N_{\rm df} = 32$ data symbols with $N_{\rm nt} = 2$ no transmission, and $N_{\rm ps} = 2$ AS training pilots, $T_{\rm p} = 2T_{\rm os}$).

the proposed AS algorithm is about one order of magnitude lower than that of the 2×2 system with no AS, which uses the same number of antennas for reception, at SNR $= 30$ dB.

5.5 Conclusions

Motivated by the observations that (i) the majority of the existing studies on antenna selection (AS) assume idealized quasi-static fading scenarios and/or perfect channel knowledge, and (ii) to date only few studies exist that deal with training for AS, in this chapter it is demonstrated that in realistic doubly-selective channels (time and frequency selective) OFDM can be combined with AS and, a gain can be observed

over OFDM systems with no AS using same number of antennas for reception. For example, the QPSK bit error rate of a MIMO system with $K_{\mathrm{t}} = 2$ transmit antennas selecting $K'_{\mathrm{r}} = 2$ out of $K_{\mathrm{r}} = 4$ receive antennas using the proposed AS method is about one order of magnitude lower than that of an OFDM system with no AS but using also $K_{\mathrm{r}} = 2$ receive antennas in channels with a normalized Doppler rate of 0.0031 at SNR = 30 dB. Specifically, training methods for receive antenna selection for SIMO and MIMO OFDM systems are proposed and evaluated for Doppler and delay spread fading channels using packet-rate antenna switching. The methods exploit the low training overhead and accuracy possible from the use of Slepian basis expansion channel prediction and estimation techniques. It is also shown that the presented methods provide performance gains for low and high Doppler rates over OFDM systems employing AS based on linear interpolation/extrapolation and orthogonal Fourier-based channel estimation/prediction techniques. For example, a gain in excess of 5 dB in SNR is found for QPSK bit error rate of the proposed SIMO system selecting $K'_{\mathrm{r}} = 2$ out of $K_{\mathrm{r}} = 6$ receive antennas in channels with a normalized Doppler rate of 0.0123. It is also noticed that the proposed AS schemes achieve the same performance as ideal systems with perfect CSI and no AS at the receiver.

Chapter 6

Conclusions

In this chapter, conclusions are drawn based on the principal results of the previous chapters. Some issues and recommendations for further research in this area are also discussed.

6.1 Summary and Conclusions

Chapter 3 studies training methods for single carrier single input–multiple output (SIMO) systems selecting one of a plurality of antennas for reception. Pilot-based algorithms for time-varying Doppler fading channels using packet and symbol-rate antenna switching are developed in Secs. 3.3.1 and 3.3.2, respectively. An approach to determine the subspace dimension that reduces the mean square error (MSE) of the Slepian basis expansion channel estimator/predictor is presented in Sec. 3.3.3. Analytical expressions for the symbol error probability (SEP) of MPSK for the proposed schemes are provided, along with corresponding simulations. The SEP expressions provide insight into the MPSK SEP of subcarriers for OFDM systems selecting the same antenna for all subcarriers. Simulation results are presented to compare the performance of the proposed AS schemes to that of orthogonal Fourier-based AS

methods as well as single antenna systems with perfect channel knowledge. It is found that the performance of the proposed AS scheme is superior to that of SISO systems with perfect CSI. For example, for a $1 \times (1;4)$ 4PSK system when the maximum normalized Doppler frequency $\nu_{\max} = 0.0038$, $N_{\rm ps} = 2$ training pilot symbols, and the packet consists of $N_{\rm df} = 40$ data and $N_{\rm pf} = 2$ post-selection pilot symbols, respectively, an SNR performance gain in excess of 10 dB is achieved at a PER $= 10^{-2}$. For the same settings, the performance of the same proposed $1 \times (1;4)$ 4PSK system is about 6 dB worse than a $1 \times (1;4)$ system employing AS with perfect channel knowledge at a 10^{-2} PER. It is observed that systems employing AS either with orthogonal Fourier-based prediction/estimation or without channel prediction exhibit error floors at moderate to high SNR. For any packet size, the SEP of an MPSK symbol received at time m in a time-varying channel for a SIMO system employing the proposed per-packet AS algorithm in Sec. 3.3.1 is lower bounded by that for a SIMO system employing symbol-by-symbol single receive AS as in Sec. 3.3.2. The reason for this is that selection is on per-packet basis rather than on per-symbol basis, i.e., selection is based on all predicted channel gains for all symbols in a packet. For example, for a $1 \times (1;4)$ 4PSK system when $\nu_{\max} = 0.0038$, $N_{\rm ps} = 2$ training pilot symbols, and the packet consists of $N_{\rm df} = 40$ data symbols and $N_{\rm pf} = 2$ pilot symbols, the SEP for the first 4PSK symbol for a $1 \times (1,4)$ system employing symbol-by-symbol instantaneous receive AS is about one order of magnitude less than that for a $1 \times (1,4)$ system employing per-packet AS at an SNR = 16 dB.

In Chapter 4, generalization to selecting a subset of a plurality of receive antennas under the same time-varying and frequency-flat channel conditions as in Chapter 3

is studied. A new training-based receive antenna subset selection algorithm for time-varying channels using packet and symbol-rate antenna switching is presented in Sec. 4.3. Simulation results in Section 4.5 show that the presented antenna subset selection scheme have the potential to offer superior performance over ideal SIMO systems with perfect channel knowledge. For example, when the maximum normalized Doppler frequency $\nu_{\max} = 0.0038$ with $N_{\rm ps} = 2$ AS training pilot symbols, $N_{\rm df} = 40$ data symbols and $N_{\rm pf} = 2$ post-selection pilot symbols, the proposed $1 \times (2; 6)$ 4PSK system achieves about 4 dB gain in SNR over the 1×2 system with perfect CSI and no AS at a PER $= 10^{-3}$. Performance analysis to evaluate the SEP of MPSK and MQAM in time-varying and frequency-flat fading with receive AS is provided in Sec. 4.4.2. By approximating the (complicated) first order conditional moments $\mu_{r_{\mathcal{S}_m}}[m]$ in (4.24) and second order conditional moments $\sigma^2_{r_{\mathcal{S}_m}}[m]$ in (4.25) of the MRC decision variable in (4.23), respectively, by estimates $\mu_{r'_{\mathcal{S}_m}}[m]$ in (4.35) and $\sigma^2_{r'_{\mathcal{S}_m}}[m]$ in (4.36), numerical integration is avoided and analytical MPSK and MQAM SEP expressions are, respectively, obtained in (4.30) and (4.43) using the virtual branch combining method. It is shown that the gap between simulated and analytical SEP approximation for MQAM is about 0.2 to 0.5 dB, while for MPSK for $\mathtt{M} > 4$ is about 0.2 dB and 1 dB for 4PSK.

In Chapter 5, antenna selection is applied to multiple antennas OFDM systems. Training AS schemes for SIMO and MIMO OFDM systems for doubly selective channels using packet-rate antenna switching are presented. Through simulation, the performance of the proposed scheme is compared to that of AS methods based on orthogonal Fourier and linear interpolation/extrapolation prediction/estimation methods. It is shown that SIMO systems employing the presented AS techniques achieve

the same performance as ideal SISO and SIMO systems with perfect CSI. The proposed systems also outperform the same SISO and SIMO OFDM systems employing linear prediction-based training with AS. For example with QPSK modulation, for a maximum normalized Doppler frequency $\nu_{\max} = 0.0031$, $N_{\text{ps}} = 2$ OFDM training pilots, and a packet consisting of $N_{\text{df}} = 24$ OFDM data symbols and $N_{\text{pf}} = 2$ OFDM post-selection pilots, both the proposed $1 \times (1; 4)$ and the ideal 1×1 SISO OFDM systems achieve a BER of 10^{-3} at an SNR = 27.5 dB. Similarly, the proposed $1 \times (2, 6)$ and ideal 1×2 SIMO OFDM systems achieve a BER of 10^{-3} at an SNR = 15 dB. The proposed $1 \times (1; 4)$ and $1 \times (2, 6)$ OFDM systems achieve SNR performance gains of about 0.5 dB and 2 dB over the same $1 \times (1; 4)$ and $1 \times (2, 6)$ systems employing AS with linear interpolation/extrapolation method at a BER = 10^{-2}. The BER performance of a MIMO OFDM system employing the proposed receive AS algorithm approaches that of the same MIMO OFDM based system with perfect CSI. For the same aforementioned settings, the BER performance of a $2 \times (2; 4)$ proposed AS system is about 0.2 dB worse than that of 2×2 MIMO system with perfect CSI. It is observed that error floors exist at moderate to high SNR for systems employing AS with orthogonal Fourier-based training for low and high Doppler values. Also, error floors occur at moderate to high SNR for systems employing AS with linear interpolation/extrapolation technique for a Doppler frequency value of $\nu_{\max} = 0.0123$. In contrast, no error floors arise with systems employing the presented AS training schemes.

6.2 Suggestions for Further Research

Presented here is a list of issues which merit further consideration.

- In this thesis, we have analyzed the SEP performance of SISO and SIMO systems employing the proposed AS training schemes. A more generalized analysis to evaluate the SEP of MPSK and MQAM for the proposed MIMO systems in Chapter 5 that comprise K_{t} transmit antennas and K_{r} receive antennas wherein $K_{\mathrm{t}} \leq K'_{\mathrm{r}} < K_{\mathrm{r}}$ are selected for reception over time-varying channels is of considerable interest.

- Although in Chapter 5 the COST 207 6-tap typical urban channel model is used, which is among the most dispersive of typically simulated channel profiles, it would also be beneficial to quantify the performance of the proposed AS training schemes using real-world channel measurement data [6, 50], i.e., in a measurement campaign in an outdoor urban scenario. This will evaluate the viability of the proposed methods in time-varying real world channels. Comparison with other existing schemes including orthogonal Fourier-based and linear interpolation/extrapolation channel estimation/prediction techniques using real channel measurement data is important as well.

- Further analysis might also be performed to include outage probability, which is defined as the probability that the instantaneous capacity is below a target value. Closed-form outage probability expressions for the presented schemes will allow to quantify the diversity order of the presented schemes.

- In Chapter 5, in the pilot-assisted data transmission phase OFDM pilot symbols with comprise pilot tones over all subcarriers are considered. The frequency domain channel coefficients at subcarriers are correlated. One may therefore consider using OFDM symbols in which some of the subcarriers carry pilot

tones and others carry data tones. This might reduce overhead and complexity. The same reasoning can be applied for the AS training phase. Simulation results that quantify the performance complexity tradeoff resulting from this overhead/complexity reduction is of interest.

Bibliography

[1] "Draft amendment to wireless LAN media access control (MAC) and physical layer (PHY) specifications: enhancements for higher throughput," Tech. Rep. P802.11n/D0.04, IEEE, Mar. 2006.

[2] "Technical specification group radio access network; evolved universal terrestrial radio access (E-UTRA); physical layer procedures (release 8)," Tech. Rep. 36.211 (v8.3.0), 3rd Generation Partnership Project (3GPP), 2008.

[3] "Universal mobile telecommunications system (UMTS); spreading and modulation (TDD) (3GPP TS 25.223 version 11.0.0 release 11)," Tech. Rep. ETSI TS 125 223 V11.0.0 (2012-09), 2012.

[4] S. M. Alamouti, "A simple transmit diversity technique for wireless communications," *IEEE J. Sel. Areas Commun.*, vol. 16, pp. 1451–1458, Oct. 1998.

[5] M.-S. Alouini and A. Goldsmith, "A unified approach for calculating error rates of linearly modulated signals over generalized fading channels," *IEEE Trans. Commun.*, vol. 47, pp. 1324–1334, Sep. 1999.

[6] J. B. Andersen, T. S. Rappaport, and S. Yoshida, "Propagation measurements and models for wireless communications channels," *IEEE Commun. Mag.*, vol. 33, pp. 42–49, Jan. 1995.

[7] R. Annavajjala and L. B. Milstein, "Performance analysis of optimum and suboptimum selection diversity schemes on Rayleigh fading channels with imperfect channel estimates," *IEEE Trans. Veh. Technol.*, vol. 56, pp. 1119–1130, May 2007.

[8] K. E. Baddour and N. C. Beaulieu, "Robust Doppler spread estimation in nonisotropic fading channels," *IEEE Trans. Wireless Commun.*, vol. 4, pp. 2677–2682, Nov. 2005.

[9] I. Bahceci, T. M. Duman, and Y. Altunbasak, "Antenna selection for multiple-antenna transmission systems: Performance analysis and code construction," *IEEE Trans. Inf. Theory*, vol. 49, pp. 2669–2681, Oct. 2003.

[10] ——, "Performance of MIMO antenna selection for space–time coded OFDM systems," in *Proc. IEEE WCNC*, Atlanta Georgia, USA, Mar. 2004, pp. 987–992.

[11] I. Berenguer and X. Wang, "MIMO antenna selection with lattice-reduction-aided linear receivers," *IEEE Trans. Veh. Technol.*, vol. 53, pp. 1289–1302, Sep. 2004.

[12] R. S. Blum and J. H. Winters, "On optimum MIMO with antenna selection," *IEEE Commun. Lett.*, vol. 6, pp. 322–324, Aug. 2002.

[13] J. K. Cavers, "An analysis of pilot symbol assisted modulation for Rayleigh fading channels," *IEEE Trans. Veh. Technol.*, vol. 40, pp. 686–693, Nov. 1991.

[14] B. Champagne, A. El-Keyi, and C.-C. Tu, "A subspace method for the blind identification of multiple time-varying FIR channels," in *Proc. IEEE Globecom*, Honolulu, Hawaii, USA, Nov. 2009.

[15] C.-E. Chen, "A computationally efficient near-optimal algorithm for capacity-maximization based joint transmit and receive antenna selection," *IEEE Commun. Lett.*, vol. 14, pp. 402–404, May 2010.

[16] Z. Chen, J. Yuan, and B. Vucetic, "Analysis of transmit antenna selection/maximal-ratio combining in Rayleigh fading channels," *IEEE Trans. Veh. Technol.*, vol. 54, pp. 1312–1321, Jul. 2005.

[17] L. J. Cimini, "Analysis and simulation of a digital mobile channel using orthogonal frequency division multiplexing," *IEEE Trans. Commun.*, vol. 33, pp. 665–675, Jul. 1985.

[18] R. H. Clarke, "A statistical theory of mobile-radio reception," *Bell Syst. Tech. J.*, vol. 47, pp. 957–1000, Jul.-Aug. 1968.

[19] S. Coleri, M. Ergen, A. Puri, and A. Bahai, "Channel estimation techniques based on pilot arrangement in OFDM systems," *IEEE Trans. Broadcast.*, vol. 48, pp. 223–229, Sep. 2002.

[20] M. Collados and A. Gorokhov, "Antenna selection for MIMO-OFDM WLAN systems," in *Proc. IEEE PIMRC*, vol. 3, Barcelona, Spain, Sep. 2004, pp. 1802–1806.

[21] J. Coon and M. Sandell, "Combined bulk and per-tone transmit antenna selection in OFDM systems," *IEEE Commun. Lett.*, vol. 15, pp. 426–428, 2010.

[22] L. Dai, S. Sfar, and K. B. Letaief, "Optimal antenna selection based on capacity maximization for MIMO systems in correlated channels," *IEEE Trans. Commun.*, vol. 54, pp. 563–573, Mar. 2006.

[23] C. de Boor, *A Practical Guide to Splines*. Springer-Verlag, 1978.

[24] M. Di Renzo and H. Haas, "Space shift keying (SSK-) MIMO over correlated Rician fading channels: Performance analysis and a new method for transmit-diversity," *IEEE Trans. Commun.*, vol. 59, pp. 116–129, Jan. 2011.

[25] F. A. Dietrich and W. Utschick, "Pilot-assisted channel estimation based on second-order statistics," *IEEE Trans. Signal Process.*, vol. 53, pp. 1178–1193, Mar. 2005.

[26] A. Duel-Hallen, S. Hu, and H. Hallen, "Long-range prediction of fading signals," *IEEE Signal Process. Mag.*, vol. 17, pp. 62–75, May 2000.

[27] M. Faili, *Digital Land Mobile Radio Communications-COST 207*. Brussels, Belgium: EC, 1989.

[28] G. S. Fishman, *Monte Carlo: Concepts, Algorithms, and Applications.*, 1st ed. Springer, 1996.

[29] G. J. Foschini, "Layered space–time architecture for wireless communication in a fading environment when using multi-element antennas," *Bell Labs Syst. Tech. J.*, vol. 1, pp. 41–59, Oct. 1996.

[30] G. J. Foschini and M. J. Gans, "On limits of wireless communications in a fading environment when using multiple antennas," *Wireless Personal Communications*, vol. 6, pp. 311–335, Jan. 1998.

[31] J. E. Freund, *Mathematical Statistics*, 5th ed. Prentice Hall, Inc., 1992.

[32] M. Gharavi-Alkhansari and A. B. Gershman, "Fast antenna subset selection in MIMO systems," *IEEE Trans. Signal Process.*, vol. 52, pp. 339–347, Feb. 2004.

[33] A. Ghrayeb and T. M. Duman, "Performance analysis of MIMO systems with antenna selection over quasi-static fading channels," *IEEE Trans. Veh. Technol.*, vol. 52, pp. 281–288, Mar. 2003.

[34] G. B. Giannakis and C. Tepedelenlioglu, "Basis expansion models and diversity techniques for blind identification and equalization of time-varying channels," *Proc. IEEE*, vol. 86, pp. 1969–1986, Oct. 1998.

[35] W. M. Gifford, M. Z. Win, and M. Chiani, "Antenna subset diversity with non-ideal channel estimation," *IEEE Trans. Wireless Commun.*, vol. 7, pp. 1527–1539, May 2008.

[36] A. Goldsmith, *Wireless Communications*. New York, NY, USA: Cambridge University Press, 2005.

[37] G. H. Golub and C. F. Van Loan, *Matrix Computations*. Baltimore, USA: The Johns Hopkins University Press, 1996.

[38] D. Gore, R. W. Heath, and A. Paulraj, "Transmit selection in spatial multiplexing systems," *IEEE Commun. Lett.*, vol. 6, pp. 491–493, Nov. 2002.

[39] D. Gore, R. Nabar, and A. Paulraj, "Selecting an optimal set of transmit antennas for a low rank matrix channel," in *Proc. IEEE ICASSP*, vol. 5, Jun. 2000, pp. 2785–2788.

[40] A. Gorokhov, D. Gore, and A. Paulraj, "Receive antenna selection for MIMO flat-fading channels: Theory and algorithms," *IEEE Trans. Inf. Theory*, vol. 49, pp. 2687–2696, Oct. 2003.

[41] A. Gorokhov, D. A. Gore, and A. J. Paulraj, "Receive antenna selection for MIMO spatial multiplexing: Theory and algorithms," *IEEE Trans. Signal Process.*, vol. 51, pp. 2796–2807, Nov. 2003.

[42] T. Gucluoglu and T. Duman, "Performance analysis of transmit and receive antenna selection over flat fading channels," *IEEE Trans. Wireless Commun.*, vol. 7, pp. 3056–3065, Aug. 2008.

[43] T. Gucluoglu and E. Panayirci, "Performance of transmit and receive antenna selection in the presence of channel estimation errors," *IEEE Commun. Lett.*, vol. 12, pp. 371–373, May 2008.

[44] S. Han and C. Yang, "Performance analysis of MRT and transmit antenna selection with feedback delay and channel estimation error," in *Proc. IEEE WCNC*, 2007, pp. 1135–1139.

[45] B. Hassibi and B. M. Hochwald, "How much training is needed in multiple-antenna wireless links?" *IEEE Trans. Inf. Theory*, vol. 49, pp. 951–963, Apr. 2003.

[46] R. W. Heath, S. Sandhu, and A. Paulraj, "Antenna selection for spatial multiplexing with linear receivers," *IEEE Commun. Lett.*, vol. 5, pp. 142–144, Apr. 2001.

[47] R. W. Heath and D. J. Love, "Multimode antenna selection for spatial multiplexing systems with linear receivers," *IEEE Trans. Signal Process.*, vol. 53, pp. 3042–3056, Aug. 2005.

[48] J. Holtzman and A. Sampath, "Adaptive averaging methodology for handoffs in cellular systems," *IEEE Trans. Veh. Technol.*, vol. 44, pp. 59–66, Feb. 1995.

[49] G. T. Irvine and P. J. McLane, "Symbol-aided plus decision-directed reception for PSK/TCM modulation on shadowed mobile satellite fading channels," *IEEE J. Sel. Areas Commun.*, vol. 10, pp. 1289–1299, Oct. 1992.

[50] M. A. Jensen and J. W. Wallace, "A review of antennas and propagation for MIMO wireless communications," *IEEE Trans. Antennas Propag.*, vol. 52, pp. 2810–2824, Nov. 2004.

[51] Y. Jiang and M. K. Varanasi, "The RF-chain limited MIMO system–part I: Optimum diversity-multiplexing tradeoff," *IEEE Trans. Wireless Commun.*, vol. 8, pp. 5238–5247, Oct. 2009.

[52] S. M. Kay, *Fundamentals of Statistical Signal Processing: Estimation Theory.* Upper Saddle River (NJ), USA: Prentice Hall, 1993.

[53] V. Kristem, N. B. Mehta, and A. F. Molisch, "A novel, balanced, and energy-efficient training method for receive antenna selection," *IEEE Trans. Wireless Commun.*, vol. 9, pp. 2742–2753, Sep. 2010.

[54] ——, "Optimal receive antenna selection in time-varying fading channels with practical training constraints," *IEEE Trans. Commun.*, vol. 58, pp. 2023–2034, Jul. 2010.

[55] ——, "Training and voids in receive antenna subset selection in time-varying channels," *IEEE Trans. Wireless Commun.*, vol. 10, pp. 1992–2003, Jun. 2011.

[56] G. Leus, S. Zhou, and G. B. Giannakis, "Orthogonal multiple access over time- and frequency-selective channels," *IEEE Trans. Inf. Theory*, vol. 49, pp. 1942–1950, Aug. 2003.

[57] Y. G. Li and L. J. Cimini, "Bounds on the interchannel interference of OFDM in time-varying impairments," *IEEE Trans. Commun.*, vol. 49, no. 3, pp. 401–404, Mar. 2001.

[58] Y. G. Li, N. Seshadri, and S. Ariyavisitakul, "Channel estimation for OFDM systems with transmitter diversity in mobile wireless channels," *IEEE J. Sel. Areas Commun.*, vol. 17, pp. 461–471, Mar. 1999.

[59] Y. G. Li, J. H. Winters, and N. R. Sollenberger, "MIMO-OFDM for wireless communications: Signal detection with enhanced channel estimation," *IEEE Trans. Commun.*, vol. 50, pp. 1471–1477, Sep. 2002.

[60] Y. Liu and S. D. Blostein, "Identification of frequency non-selective fading channels using decision feedback and adaptive linear prediction," *IEEE Trans. Commun.*, vol. 43, pp. 1484–1492, Feb/Mar/Apr/ 1995.

[61] Y. Liu, Y. Zhang, C. Ji, W. Q. Malik, and D. J. Edwards, "A low-complexity receive-antenna-selection algorithm for MIMO–OFDM wireless systems," *IEEE Trans. Veh. Technol.*, vol. 58, pp. 2793–2802, Jul. 2009.

[62] X. Ma, G. B. Giannakis, and S. Ohno, "Optimal training for block transmissions over doubly selective wireless fading channels," *IEEE Trans. Signal Process.*, vol. 51, pp. 1351–1366, May 2003.

[63] R. K. Mallik, "On multivariate Rayleigh and exponential distributions," *IEEE Trans. Inf. Theory*, vol. 49, pp. 1499–1515, Jun. 2003.

[64] H. Mehrpouyan, S. D. Blostein, and E. C. Y. Tam, "Random antenna selection & antenna swapping combined with OSTBCs," in *Proc. IEEE ISSSE*, 2007.

[65] A. F. Molisch and M. Z. Win, "MIMO systems with antenna selection," *IEEE Microw. Mag.*, vol. 5, pp. 46–56, Mar. 2004.

[66] A. F. Molisch, M. Z. Win, Y.-S. Choi, and J. H. Winters, "Capacity of MIMO systems with antenna selection," *IEEE Trans. Wireless Commun.*, vol. 4, pp. 1759–1772, Jul. 2005.

[67] A. B. Narasimhamurthy and C. Tepedelenlioglu, "Antenna selection for MIMO-OFDM systems with channel estimation error," *IEEE Trans. Veh. Technol.*, vol. 58, pp. 2269–2278, Jun. 2009.

[68] R. Narasimhan, "Spatial multiplexing with transmit antenna and constellation selection for correlated MIMO fading channels," *IEEE Trans. Signal Process.*, vol. 51, pp. 2829–2838, Nov. 2003.

[69] R. Narasimhan and D. Cox, "Speed estimation in wireless systems using wavelets," *IEEE Trans. Commun.*, vol. 47, pp. 1357–1364, Sep. 1999.

[70] K. Pahlavan and A. Levesque, *Wireless Information Networks*. New York, NY: Wiley, 1995.

[71] S. Prakash and I. McLoughlin, "Effects of channel prediction for transmit antenna selection with maximal-ratio combining in Rayleigh fading," *IEEE Trans. Veh. Technol.*, vol. 60, pp. 2555–2568, Jul. 2011.

[72] J. Proakis and M. Salehi, *Digital Communications*, 5th ed. McGraw-Hill Science, 2007.

[73] T. R. Ramya and S. Bhashyam, "Using delayed feedback for antenna selection in MIMO systems," *IEEE Trans. Wireless Commun.*, pp. 6059–6067, Dec. 2009.

[74] T. S. Rappaport, *Wireless Communications: Principles and Practice*, 2nd ed. Prentice Hall, Inc., 2002.

[75] G. M. Rebeiz, "RF MEMS switches: status of the technology," in *Proc. TRANSDUCERS*, vol. 2, Boston, Jun. 2003, pp. 1726–1729.

[76] H. A. Saleh and S. D. Blostein, "Single-cell vs. multicell MIMO downlink signalling strategies with imperfect CSI," in *Proc. IEEE Globecom*, Miami, Florida, USA, Dec. 2010.

[77] ——, "Receive antenna subset selection for time-varying channels using Slepian subspace projections," in *Proc. IEEE Globecom*, Anaheim, USA, Dec. 2012.

[78] H. A. Saleh, A. F. Molisch, T. Zemen, S. D. Blostein, and N. B. Mehta, "Antenna selection for time-varying channels based on Slepian subspace projections," in *Proc. IEEE ICC*, Ottawa, Canada, Jun. 2012.

[79] ——, "Receive antenna selection for time-varying channels using discrete prolate spheroidal sequences," *IEEE Trans. Wireless Commun.*, vol. 11, pp. 2616–2627, Jul. 2012.

[80] S. Sanayei and A. Nosratinia, "Antenna selection in MIMO systems," *IEEE Commun. Mag.*, vol. 42, pp. 68–73, Oct. 2004.

[81] M. Sandell and J. Coon, "Performance of combined bulk and per-tone antenna selection precoding in coded OFDM systems," *IEEE Trans. Commun.*, vol. 60, pp. 655–660, Mar. 2012.

[82] A. M. Sayeed, A. Sendonaris, and B. Aazhang, "Multiuser detection in fast-fading multipath environment," *IEEE J. Sel. Areas Commun.*, vol. 16, pp. 1691–1701, Dec. 1998.

[83] X. Shao, J. Yuan, and P. Rapajic, "Antenna selection for MIMO-OFDM spatial multiplexing system," in *Proc. IEEE ISIT*, Yokohama, Japan, Jun. 2003.

[84] W. Sheng and S. D. Blostein, "SNR-independent velocity estimation in a Rayleigh fading channel," in *Proc. IEEE ICASSP*, Orlando, Florida, USA, May 2002, pp. 2469–2472.

[85] H. Shi, M. Katayama, T. Yamazato, H. Okada, and A. Ogawa, "An adaptive antenna selection scheme for transmit diversity in OFDM systems," in *Proc. IEEE VTC*, vol. 4, Atlantic City, New Jersey, USA, 2001, pp. 2168–2172.

[86] D. Slepian, "Prolate spheroidal wave functions, Fourier analysis, and uncertainty–v: The discrete case," *Bell Syst. Tech. J.*, vol. 57, pp. 1371–1430, May-Jun. 1978.

[87] R. Steele, *Mobile Radio Communications*. New York: IEEE Press, 1992.

[88] G. L. Stüber, J. R. Barry, S. W. McLaughlin, Y. G. Li, M. A. Ingram, and T. G. Pratt, "Broadband MIMO-OFDM wireless communications," *Proc. IEEE*, vol. 92, pp. 271–294, Feb. 2004.

[89] Q. Sun, D. C. Cox, H. C. Huang, and A. Lozano, "Estimation of continuous flat fading MIMO channels," *IEEE Trans. Wireless Commun.*, vol. 1, pp. 549–553, Oct. 2002.

[90] Z. Tang, H. Suzuki, and I. B. Collings, "Performance of antenna selection for MIMO-OFDM systems based on measured indoor correlated frequency selective channels," in *Proc. ATNAC*, Melbourne, Australia, Dec. 2006, pp. 435–439.

[91] D. J. Thomson, "Spectrum estimation and harmonic analysis," *Proc. IEEE*, vol. 70, pp. 1055–1096, 1982.

[92] J.-J. Van de Beek, O. S. Edfors, S. K. Wilson, and O. P. Börjesson, "On channel estimation in OFDM systems," in *45th IEEE Vehicular Technology Conference*, vol. 2, Chicago, IL, USA, July 1195, pp. 815–819.

[93] R. Vaze and H. Ganapathy, "Sub-modularity and antenna selection in MIMO systems," *IEEE Commun. Lett.*, vol. 16, pp. 1446–1449, Sep. 2012.

[94] M. Z. Win and J. H. Winters, "Analysis of hybrid selection/maximal-ratio combining of diversity branches with unequal SNR in rayleigh fading," in *Proc. IEEE VTC*, 1999.

[95] ——, "Virtual branch analysis of symbol error probability for hybrid selection/maximal-ratio combining in Rayleigh fading," *IEEE Trans. Commun.*, vol. 49, pp. 1926–1934, Nov. 2001.

[96] J. H. Winters, J. Salz, and R. D. Gitlin, "The impact of antenna diversity on the capacity of wireless communication systems," *IEEE Trans. Commun.*, vol. 42, pp. 1740–1751, Feb/Mar/Apr 1994.

[97] W. Xie, S. Liu, D. Yoon, and J.-W. Chong, "Impacts of Gaussian error and Doppler spread on the performance of MIMO systems with antenna selection," in *Proc. WiCOM*, 2006.

[98] Z. Xu, S. Sfar, and R. S. Blum, "Analysis of MIMO systems with receive antenna selection in spatially correlated Rayleigh fading channels," *IEEE Trans. Veh. Technol.*, vol. 58, pp. 251–262, Jan. 2009.

[99] S. Zarrin and S. Gazor, "Analysis of partial phase combining, hybrid and transmit antenna selection schemes under channel estimation errors and feedback delay," in *Proc. CWIT*, Jun. 2007.

[100] T. Zemen and C. F. Mecklenbräuker, "Time-variant channel estimation using discrete prolate spheroidal sequences," *IEEE Trans. Signal Process.*, vol. 53, pp. 3597–3607, Sep. 2005.

[101] T. Zemen, C. F. Mecklenbräuker, F. Kaltenberger, and B. H. Fleury, "Minimum-energy band-limited predictor with dynamic subspace selection for time-variant flat-fading channels," *IEEE Trans. Signal Process.*, vol. 55, pp. 4534–4548, Sep. 2007.

[102] H. Zhang, H. Dai, Q. Zhou, and B. L. Hughes, "On the diversity order of spatial multiplexing systems with transmit antenna selection: A geometrical approach," *IEEE Trans. Inf. Theory*, vol. 52, pp. 5297–5311, Dec. 2006.

[103] H. Zhang, A. F. Molisch, and J. Zhang, "Applying antenna selection in WLANs for achieving broadband multimedia communications," *IEEE Trans. Broadcast.*, vol. 52, pp. 475–482, Dec. 2006.

[104] H. Zhang and R. Nabar, "Transmit antenna selection in MIMO OFDM systems: bulk versus per-tone selection," in *Proc. IEEE ICC*, Beijing, China, May 2008, pp. 4371–4375.

[105] K. Zhang and Z. Niu, "Adaptive receive antenna selection for orthogonal space-time block codes with channel estimation errors with antenna selection," in *Proc. IEEE Globecom*, 2005.

[106] X. N. Zheng and A. Ghrayeb, "Performance bounds for space-time block codes with receive antenna selection," *IEEE Trans. Inf. Theory*, vol. 50, pp. 2130–2137, Aug. 2004.

Appendix A

Derivation of the Conditional Mean and Variance for $r_{\hat{\imath}}[m]$ in (3.36) and (3.37)

If A and B are zero-mean jointly complex Gaussian, then [54, 55, 79]

$$\mathbb{E}\left\{A \,\middle|\, B\right\} = \mathbb{E}\left\{A\,B^*\right\}\left(\mathbb{E}\left\{B\,B^*\right\}\right)^{-1} B \tag{A.1}$$

$$\operatorname{var}\left\{A \,\middle|\, B\right\} = \operatorname{var}\left\{A\right\} - \mathbb{E}\left\{AB^*\right\}\left(\mathbb{E}\left\{BB^*\right\}\right)^{-1}\mathbb{E}\left\{BA^*\right\}. \tag{A.2}$$

From (A.1), it follows that $\mathbb{E}\{e_{\hat{\imath}}^{\mathrm{SE}}[m] \,|\, \hat{h}_{\hat{\imath}}^{\mathrm{SE}}[m]\} = \frac{\sigma^2_{e_{\hat{\imath}}^{\mathrm{SE}}}[m]}{1+\sigma^2_{e_{\hat{\imath}}^{\mathrm{SE}}}[m]}\,\hat{h}_{\hat{\imath}}^{\mathrm{SE}}[m]$ and $\mathbb{E}\{n_{\hat{\imath}}[m] \,|\, \hat{h}_{\hat{\imath}}^{\mathrm{SE}}[m]\} = 0$. Substituting and simplifying yields the desired conditional mean result in (3.36). Similarly, from (A.2) we get that $\operatorname{var}\{e_{\hat{\imath}}^{\mathrm{SE}}[m] \,|\, \hat{h}_{\hat{\imath}}^{\mathrm{SE}}[m]\} = \frac{\sigma^2_{e_{\hat{\imath}}^{\mathrm{SE}}}[m]}{1+\sigma^2_{e_{\hat{\imath}}^{\mathrm{SE}}}[m]}$ and $\operatorname{var}\{n_{\hat{\imath}}[m] \,|\, \hat{h}_{\hat{\imath}}^{\mathrm{SE}}[m]\} = N_{\mathrm{o}}$. Substituting and simplifying yields the conditional variance result in (3.37).

Appendix B

Derivation of the Conditional Mean and Variance for $r_{\mathcal{S}_m}[m]$ in (4.24) and (4.25)

From (4.14), we have that

$$\begin{aligned}
\mu_{y_{\hat{\imath}^m_{k_\mathrm{r}}}}[m] &\triangleq \mathbb{E}\{y_{\hat{\imath}^m_{k_\mathrm{r}}}[m]\big|\hat{h}^{\mathrm{SP}}_{\hat{\imath}^m_{k_\mathrm{r}}}[m], \hat{h}^{\mathrm{SE}}_{\hat{\imath}^m_{k_\mathrm{r}}}[m], d[m]\} + \mathbb{E}\{n_{\hat{\imath}^m_{k_\mathrm{r}}}[m]\big|\hat{h}^{\mathrm{SP}}_{\hat{\imath}^m_{k_\mathrm{r}}}[m], \hat{h}^{\mathrm{SE}}_{\hat{\imath}^m_{k_\mathrm{r}}}[m], d[m]\} \\
&= d[m]\,\mathbb{E}\{h_{\hat{\imath}^m_{k_\mathrm{r}}}[m]\big|\hat{h}^{\mathrm{SP}}_{\hat{\imath}^m_{k_\mathrm{r}}}[m], \hat{h}^{\mathrm{SE}}_{\hat{\imath}^m_{k_\mathrm{r}}}[m]\} \qquad \text{(B.1)} \\
\sigma^2_{y_{\hat{\imath}^m_{k_\mathrm{r}}}}[m] &\triangleq \mathrm{var}\{y_{\hat{\imath}^m_{k_\mathrm{r}}}[m]\big|\hat{h}^{\mathrm{SP}}_{\hat{\imath}^m_{k_\mathrm{r}}}[m], \hat{h}^{\mathrm{SE}}_{\hat{\imath}^m_{k_\mathrm{r}}}[m], d[m]\} + \mathrm{var}\{n_{\hat{\imath}^m_{k_\mathrm{r}}}[m]\big|\hat{h}^{\mathrm{SP}}_{\hat{\imath}^m_{k_\mathrm{r}}}[m], \hat{h}^{\mathrm{SE}}_{\hat{\imath}^m_{k_\mathrm{r}}}[m], d[m]\} \\
&= |d[m]|^2\mathrm{var}\{h_{\hat{\imath}^m_{k_\mathrm{r}}}[m]\big|\hat{h}^{\mathrm{SP}}_{\hat{\imath}^m_{k_\mathrm{r}}}[m], \hat{h}^{\mathrm{SE}}_{\hat{\imath}^m_{k_\mathrm{r}}}[m]\} + N_\mathrm{o} \qquad \text{(B.2)}
\end{aligned}$$

where $\mathbb{E}\{n_{\hat{\imath}^m_{k_\mathrm{r}}}[m]\big|\hat{h}^{\mathrm{SP}}_{\hat{\imath}^m_{k_\mathrm{r}}}[m], \hat{h}^{\mathrm{SE}}_{\hat{\imath}^m_{k_\mathrm{r}}}[m], d[m]\} = 0$ and $\mathrm{var}\{n_{\hat{\imath}^m_{k_\mathrm{r}}}[m]\big|\hat{h}^{\mathrm{SP}}_{\hat{\imath}^m_{k_\mathrm{r}}}[m], \hat{h}^{\mathrm{SE}}_{\hat{\imath}^m_{k_\mathrm{r}}}[m], d[m]\} = N_\mathrm{o}$.

If a and $\boldsymbol{b}$ are, respectively, zero-mean jointly complex Gaussian RV and random vector, then [53, 79]

$$\mathbb{E}\{a|\boldsymbol{b}\} = \mathbb{E}\{a\,\boldsymbol{b}^\dagger\}[\mathbb{E}\{\boldsymbol{b}\,\boldsymbol{b}^\dagger\}]^{-1}\,\boldsymbol{b} \qquad \text{(B.3)}$$

$$\mathrm{var}\{a|\boldsymbol{b}\} = \mathbb{E}\{a\,a^*\} - \mathbb{E}\{a\,\boldsymbol{b}^\dagger\}[\mathbb{E}\{\boldsymbol{b}\,\boldsymbol{b}^\dagger\}]^{-1}\,\mathbb{E}\{\boldsymbol{b}\,a^*\}. \qquad \text{(B.4)}$$

Denoting by $\hat{\boldsymbol{h}}_{\hat{\imath}^m_{k_\mathrm{r}}}[m] \triangleq [\hat{h}^{\mathrm{SP}}_{\hat{\imath}^m_{k_\mathrm{r}}}[m]\,,\ \hat{h}^{\mathrm{SE}}_{\hat{\imath}^m_{k_\mathrm{r}}}[m]]^T$, from (B.3) and (B.4) it follows that

$$\mathbb{E}\{h_{\hat{\imath}^m_{k_\mathrm{r}}}[m] \mid \hat{\boldsymbol{h}}_{\hat{\imath}^m_{k_\mathrm{r}}}[m]\} = \mathbb{E}\{h_{\hat{\imath}^m_{k_\mathrm{r}}}[m](\hat{\boldsymbol{h}}_{\hat{\imath}^m_{k_\mathrm{r}}}[m])^\dagger\}[\mathbb{E}\{\hat{\boldsymbol{h}}_{\hat{\imath}^m_{k_\mathrm{r}}}[m](\hat{\boldsymbol{h}}_{\hat{\imath}^m_{k_\mathrm{r}}}[m])^\dagger\}]^{-1}\hat{\boldsymbol{h}}_{\hat{\imath}^m_{k_\mathrm{r}}}[m] \tag{B.5}$$

$$\begin{aligned}\mathrm{var}\{h_{\hat{\imath}^m_{k_\mathrm{r}}}[m] \mid \hat{\boldsymbol{h}}_{\hat{\imath}^m_{k_\mathrm{r}}}[m]\} &= \mathrm{var}\{h_{\hat{\imath}^m_{k_\mathrm{r}}}[m]\} - \mathbb{E}\{h_{\hat{\imath}^m_{k_\mathrm{r}}}[m](\hat{\boldsymbol{h}}_{\hat{\imath}^m_{k_\mathrm{r}}}[m])^\dagger\} \\ &\quad [\mathbb{E}\{\hat{\boldsymbol{h}}_{\hat{\imath}^m_{k_\mathrm{r}}}[m](\hat{\boldsymbol{h}}_{\hat{\imath}^m_{k_\mathrm{r}}}[m])^\dagger\}]^{-1}[\mathbb{E}\{h_{\hat{\imath}^m_{k_\mathrm{r}}}[m](\hat{\boldsymbol{h}}_{\hat{\imath}^m_{k_\mathrm{r}}}[m])^\dagger\}]^\dagger. \end{aligned} \tag{B.6}$$

In (B.5), we have that

$$\begin{aligned}\mathbb{E}\{h_{\hat{\imath}^m_{k_\mathrm{r}}}[m](\hat{\boldsymbol{h}}_{\hat{\imath}^m_{k_\mathrm{r}}}[m])^\dagger\} &= [\mathbb{E}\{h_{\hat{\imath}^m_{k_\mathrm{r}}}[m](\hat{h}^{\mathrm{SP}}_{\hat{\imath}^m_{k_\mathrm{r}}}[m])^*\},\ \mathbb{E}\{h_{\hat{\imath}^m_{k_\mathrm{r}}}[m](\hat{h}^{\mathrm{SE}}_{\hat{\imath}^m_{k_\mathrm{r}}}[m])^*\}] \\ &= [1,\ 1] \end{aligned} \tag{B.7}$$

where the last equality follows from substituting the estimated channel gain $\hat{h}^{\mathrm{SE}}_{\hat{\imath}^m_{k_\mathrm{r}}}[m] \triangleq h_{\hat{\imath}^m_{k_\mathrm{r}}}[m] + e^{\mathrm{SE}}_{\hat{\imath}^m_{k_\mathrm{r}}}[m]$ with $h_{\hat{\imath}^m_{k_\mathrm{r}}}[m]$ the true channel gain, $e^{\mathrm{SE}}_{\hat{\imath}^m_{k_\mathrm{r}}}[m]$ the estimation error, and the predicted channel gain $\hat{h}^{\mathrm{SP}}_{\hat{\imath}^m_{k_\mathrm{r}}}[m] \triangleq h_{\hat{\imath}^m_{k_\mathrm{r}}}[m] + e^{\mathrm{SP}}_{\hat{\imath}^m_{k_\mathrm{r}}}[m]$ with $e^{\mathrm{SP}}_{\hat{\imath}^m_{k_\mathrm{r}}}[m]$ the prediction error. The variables $h_{\hat{\imath}^m_{k_\mathrm{r}}}[m]$ and $e^{\mathrm{SE}}_{\hat{\imath}^m_{k_\mathrm{r}}}[m]$ are uncorrelated. Also, $e^{\mathrm{SP}}_{\hat{\imath}^m_{k_\mathrm{r}}}[m]$ and $h_{\hat{\imath}^m_{k_\mathrm{r}}}[m]$ are uncorrelated. We have thus used $\mathbb{E}\{h_{\hat{\imath}^m_{k_\mathrm{r}}}[m](e^{\mathrm{SE}}_{\hat{\imath}^m_{k_\mathrm{r}}}[m])^*\} = 0$, $\mathbb{E}\{h_{\hat{\imath}^m_{k_\mathrm{r}}}[m](e^{\mathrm{SP}}_{\hat{\imath}^m_{k_\mathrm{r}}}[m])^*\} = 0$, and $\mathbb{E}\{|h_{\hat{\imath}^m_{k_\mathrm{r}}}[m]|^2\} = 1$.

Denoting by $\rho_{\hat{h}^{\mathrm{SP}}_{\hat{\imath}^m_{k_\mathrm{r}}}[m],\hat{h}^{\mathrm{SE}}_{\hat{\imath}^m_{k_\mathrm{r}}}[m]} \triangleq \frac{\mathbb{E}\{\hat{h}^{\mathrm{SP}}_{\hat{\imath}^m_{k_\mathrm{r}}}[m](\hat{h}^{\mathrm{SE}}_{\hat{\imath}^m_{k_\mathrm{r}}}[m]^*)\}}{\sigma_{\hat{h}^{\mathrm{SP}}_{\hat{\imath}^m_{k_\mathrm{r}}}[m]}\sigma_{\hat{h}^{\mathrm{SE}}_{\hat{\imath}^m_{k_\mathrm{r}}}[m]}}$ the correlation coefficient of $\hat{h}^{\mathrm{SP}}_{\hat{\imath}^m_{k_\mathrm{r}}}[m]$ and $\hat{h}^{\mathrm{SE}}_{\hat{\imath}^m_{k_\mathrm{r}}}[m]$, where $\sigma^2_{\hat{h}^{\mathrm{SP}}_{\hat{\imath}^m_{k_\mathrm{r}}}}[m]$ and $\sigma^2_{\hat{h}^{\mathrm{SE}}_{\hat{\imath}^m_{k_\mathrm{r}}}}[m]$ are, respectively, the variances of $\hat{h}^{\mathrm{SP}}_{\hat{\imath}^m_{k_\mathrm{r}}}[m]$ and

$\hat{h}^{\mathrm{SE}}_{i^m_{k_\mathrm{r}}}[m]$. In (B.5), $\mathbb{E}\{\hat{\boldsymbol{h}}_{i^m_{k_\mathrm{r}}}[m](\hat{\boldsymbol{h}}_{i^m_{k_\mathrm{r}}}[m])^\dagger\}$ can thus be expressed as

$$\begin{aligned}\mathbb{E}\{\hat{\boldsymbol{h}}_{i^m_{k_\mathrm{r}}}[m](\hat{\boldsymbol{h}}_{i^m_{k_\mathrm{r}}}[m])^\dagger\} &= \begin{bmatrix} \mathbb{E}\{|\hat{h}^{\mathrm{SP}}_{i^m_{k_\mathrm{r}}}[m]|^2\} & \mathbb{E}\{\hat{h}^{\mathrm{SP}}_{i^m_{k_\mathrm{r}}}[m](\hat{h}^{\mathrm{SE}}_{i^m_{k_\mathrm{r}}}[m])^*\} \\ \mathbb{E}\{\hat{h}^{\mathrm{SE}}_{i^m_{k_\mathrm{r}}}[m](\hat{h}^{\mathrm{SP}}_{i^m_{k_\mathrm{r}}}[m])^*\} & \mathbb{E}\{|\hat{h}^{\mathrm{SE}}_{i^m_{k_\mathrm{r}}}[m]|^2\} \end{bmatrix} \\ &= \begin{bmatrix} \sigma^2_{\hat{h}^{\mathrm{SP}}_{i^m_{k_\mathrm{r}}}}[m] & \frac{\rho_{\hat{h}^{\mathrm{SP}}_{i^m_{k_\mathrm{r}}}[m],\hat{h}^{\mathrm{SE}}_{i^m_{k_\mathrm{r}}}[m]}}{(\frac{1}{\sigma_{\hat{h}^{\mathrm{SP}}_{i^m_{k_\mathrm{r}}}}[m]\sigma_{\hat{h}^{\mathrm{SE}}_{i^m_{k_\mathrm{r}}}}[m]})} \\ \frac{\rho_{\hat{h}^{\mathrm{SE}}_{i^m_{k_\mathrm{r}}}[m],\hat{h}^{\mathrm{SP}}_{i^m_{k_\mathrm{r}}}[m]}}{(\frac{1}{\sigma_{\hat{h}^{\mathrm{SE}}_{i^m_{k_\mathrm{r}}}}[m]\sigma_{\hat{h}^{\mathrm{SP}}_{i^m_{k_\mathrm{r}}}}[m]})} & \sigma^2_{\hat{h}^{\mathrm{SE}}_{i^m_{k_\mathrm{r}}}}[m] \end{bmatrix}. \end{aligned} \tag{B.8}$$

Substituting (B.8) and (B.7) in (B.5) and (B.6), simplifying yields

$$\begin{aligned}\mathbb{E}\{h_{i^m_{k_\mathrm{r}}}[m] \mid \hat{h}^{\mathrm{SP}}_{i^m_{k_\mathrm{r}}}[m], \hat{h}^{\mathrm{SE}}_{i^m_{k_\mathrm{r}}}[m]\} &= \left(\frac{\sigma^2_{\hat{h}^{\mathrm{SE}}_{i^m_{k_\mathrm{r}}}}[m] - \sigma_{\hat{h}^{\mathrm{SE}}_{i^m_{k_\mathrm{r}}}}[m]\sigma_{\hat{h}^{\mathrm{SP}}_{i^m_{k_\mathrm{r}}}}[m]\rho_{\hat{h}^{\mathrm{SE}}_{i^m_{k_\mathrm{r}}}[m],\hat{h}^{\mathrm{SP}}_{i^m_{k_\mathrm{r}}}[m]}}{\sigma^2_{\hat{h}^{\mathrm{SP}}_{i^m_{k_\mathrm{r}}}}[m]\sigma^2_{\hat{h}^{\mathrm{SE}}_{i^m_{k_\mathrm{r}}}}[m](1-|\rho_{\hat{h}^{\mathrm{SP}}_{i^m_{k_\mathrm{r}}}[m],\hat{h}^{\mathrm{SE}}_{i^m_{k_\mathrm{r}}}[m]}|^2)}\right)\hat{h}^{\mathrm{SP}}_{i^m_{k_\mathrm{r}}}[m] \\ &\quad + \left(\frac{\sigma^2_{\hat{h}^{\mathrm{SP}}_{i^m_{k_\mathrm{r}}}}[m] - \sigma_{\hat{h}^{\mathrm{SP}}_{i^m_{k_\mathrm{r}}}}[m]\sigma_{\hat{h}^{\mathrm{SE}}_{i^m_{k_\mathrm{r}}}}[m]\rho_{\hat{h}^{\mathrm{SP}}_{i^m_{k_\mathrm{r}}}[m],\hat{h}^{\mathrm{SE}}_{i^m_{k_\mathrm{r}}}[m]}}{\sigma^2_{\hat{h}^{\mathrm{SP}}_{i^m_{k_\mathrm{r}}}}[m]\sigma^2_{\hat{h}^{\mathrm{SE}}_{i^m_{k_\mathrm{r}}}}[m](1-|\rho_{\hat{h}^{\mathrm{SP}}_{i^m_{k_\mathrm{r}}}[m],\hat{h}^{\mathrm{SE}}_{i^m_{k_\mathrm{r}}}[m]}|^2)}\right)\hat{h}^{\mathrm{SE}}_{i^m_{k_\mathrm{r}}}[m] \end{aligned} \tag{B.9}$$

$$\begin{aligned}\mathrm{var}\{h_{i^m_{k_\mathrm{r}}}[m] \mid \hat{h}^{\mathrm{SP}}_{i^m_{k_\mathrm{r}}}[m], \hat{h}^{\mathrm{SE}}_{i^m_{k_\mathrm{r}}}[m]\} &= 1 - \frac{\sigma^2_{\hat{h}^{\mathrm{SP}}_{i^m_{k_\mathrm{r}}}}[m] + \sigma^2_{\hat{h}^{\mathrm{SE}}_{i^m_{k_\mathrm{r}}}}[m]}{\sigma^2_{\hat{h}^{\mathrm{SP}}_{i^m_{k_\mathrm{r}}}}[m]\sigma^2_{\hat{h}^{\mathrm{SE}}_{i^m_{k_\mathrm{r}}}}[m](1-|\rho_{\hat{h}^{\mathrm{SP}}_{i^m_{k_\mathrm{r}}}[m],\hat{h}^{\mathrm{SE}}_{i^m_{k_\mathrm{r}}}[m]}|^2)} \\ &\quad + \frac{2\Re\{\rho_{\hat{h}^{\mathrm{SP}}_{i^m_{k_\mathrm{r}}}[m],\hat{h}^{\mathrm{SE}}_{i^m_{k_\mathrm{r}}}[m]}\}}{\sigma_{\hat{h}^{\mathrm{SP}}_{i^m_{k_\mathrm{r}}}}[m]\sigma_{\hat{h}^{\mathrm{SE}}_{i^m_{k_\mathrm{r}}}}[m](1-|\rho_{\hat{h}^{\mathrm{SP}}_{i^m_{k_\mathrm{r}}}[m],\hat{h}^{\mathrm{SE}}_{i^m_{k_\mathrm{r}}}[m]}|^2)} \end{aligned} \tag{B.10}$$

where $\Re\{\rho_{\hat{h}^{\mathrm{SP}}_{i^m_{k_\mathrm{r}}}[m],\hat{h}^{\mathrm{SE}}_{i^m_{k_\mathrm{r}}}[m]}\}$ denotes the real part of $\rho_{\hat{h}^{\mathrm{SP}}_{i^m_{k_\mathrm{r}}}[m],\hat{h}^{\mathrm{SE}}_{i^m_{k_\mathrm{r}}}[m]}$.

Substituting (B.9) and (B.10) in (B.1) and (B.2) and simplifying yields the conditional mean and variance results in (4.24) and (4.25), respectively.

Appendix C

Derivation of the Conditional Mean and Variance for $y_{\hat{\imath}_{k_r}^m}[m]$ in (4.32) and (4.33)

If a and b are zero-mean jointly complex Gaussian, then [54, 79]

$$\mathbb{E}\{a \mid b\} = \frac{\mathbb{E}\{a\, b^*\}}{\mathbb{E}\{b\, b^*\}}\, b \tag{C.1}$$

$$\mathrm{var}\{a \mid b\} = \mathbb{E}\{a\, a^*\} - \frac{\mathbb{E}\{a\, b^*\}\, \mathbb{E}\{b\, a^*\}}{\mathbb{E}\{b\, b^*\}}. \tag{C.2}$$

From (C.1), it follows that $\mathbb{E}\{e^{\mathrm{SE}}_{\hat{\imath}^m_{k_\mathrm{r}}}[m] \mid \hat{h}^{\mathrm{SE}}_{\hat{\imath}^m_{k_\mathrm{r}}}[m]\} = \frac{\sigma^2_{e^{\mathrm{SE}}_{\hat{\imath}^m_{k_\mathrm{r}}}}[m]}{1+\sigma^2_{e^{\mathrm{SE}}_{\hat{\imath}^m_{k_\mathrm{r}}}}[m]} \hat{h}^{\mathrm{SE}}_{\hat{\imath}^m_{k_\mathrm{r}}}[m]$ and $\mathbb{E}\{n_{\hat{\imath}^m_{k_\mathrm{r}}}[m] \mid \hat{h}^{\mathrm{SE}}_{\hat{\imath}^m_{k_\mathrm{r}}}[m]\} = 0$. Substituting in $\mathbb{E}\{y_{\hat{\imath}^m_{k_\mathrm{r}}}[m] \mid \hat{h}^{\mathrm{SE}}_{\hat{\imath}^m_{k_\mathrm{r}}}[m], d[m]\} = \hat{h}^{\mathrm{SE}}_{\hat{\imath}^m_{k_\mathrm{r}}}[m]d[m] - \mathbb{E}\{e^{\mathrm{SE}}_{\hat{\imath}^m_{k_\mathrm{r}}}[m] \mid \hat{h}^{\mathrm{SE}}_{\hat{\imath}^m_{k_\mathrm{r}}}[m]\}d[m] + \mathbb{E}\{n_{\hat{\imath}^m_{k_\mathrm{r}}}[m] \mid \hat{h}^{\mathrm{SE}}_{\hat{\imath}^m_{k_\mathrm{r}}}[m]\}$ and simplifying yields the desired conditional mean result in (4.32). Similarly, from (C.2) we get that $\mathrm{var}\{e^{\mathrm{SE}}_{\hat{\imath}^m_{k_\mathrm{r}}}[m] \mid \hat{h}^{\mathrm{SE}}_{\hat{\imath}^m_{k_\mathrm{r}}}[m]\} = \frac{\sigma^2_{e^{\mathrm{SE}}_{\hat{\imath}^m_{k_\mathrm{r}}}}[m]}{1+\sigma^2_{e^{\mathrm{SE}}_{\hat{\imath}^m_{k_\mathrm{r}}}}[m]}$ and $\mathrm{var}\{n_{\hat{\imath}^m_{k_\mathrm{r}}}[m] \mid \hat{h}^{\mathrm{SE}}_{\hat{\imath}^m_{k_\mathrm{r}}}[m]\} = N_0$. Substituting in $\mathrm{var}\{y_{\hat{\imath}^m_{k_\mathrm{r}}}[m] \mid \hat{h}^{\mathrm{SE}}_{\hat{\imath}^m_{k_\mathrm{r}}}[m], d[m]\} = |d[m]|^2 \mathrm{var}\{e^{\mathrm{SE}}_{\hat{\imath}^m_{k_\mathrm{r}}}[m] \mid \hat{h}^{\mathrm{SE}}_{\hat{\imath}^m_{k_\mathrm{r}}}[m]\} + \mathrm{var}\{n_{\hat{\imath}^m_{k_\mathrm{r}}}[m] \mid \hat{h}^{\mathrm{SE}}_{\hat{\imath}^m_{k_\mathrm{r}}}[m]\}$ and simplifying yields the conditional variance result in (4.33).

Appendix D

Derivation of the Conditional Mean and Variance for $X^{\mathbf{SE}}_{\hat{\imath}^m_{k_r}}[m]$ in (4.39) and (4.40)

From (C.1) and the fact that the complex coefficient of the zero-mean complex RVs a and b is $\rho_{a,b} \triangleq \frac{\mathbb{E}\{a\,b^*\}}{\sqrt{\text{var}\{a\}\,\text{var}\{b\}}}$, it follows that $\mathbb{E}\{\hat{h}^{\text{SE}}_{\hat{\imath}^m_{k_r}}[m]|\hat{h}^{\text{SP}}_{\hat{\imath}^m_{k_r}}[m]\} = \frac{\mathbb{E}\{\hat{h}^{\text{SE}}_{\hat{\imath}^m_{k_r}}[m](\hat{h}^{\text{SP}}_{\hat{\imath}^m_{k_r}}[m])^*\}}{\text{var}\{\hat{h}^{\text{SP}}_{\hat{\imath}^m_{k_r}}[m]\}}\,\hat{h}^{\text{SP}}_{\hat{\imath}^m_{k_r}}[m]$ $= \frac{\rho_{\hat{h}^{\text{SE}}_{\hat{\imath}^m_{k_r}}[m],\hat{h}^{\text{SP}}_{\hat{\imath}^m_{k_r}}[m]}\sqrt{\text{var}(\hat{h}^{\text{SE}}_{\hat{\imath}^m_{k_r}}[m])}}{\sqrt{\text{var}(\hat{h}^{\text{SP}}_{\hat{\imath}^m_{k_r}}[m])}}\hat{h}^{\text{SP}}_{\hat{\imath}^m_{k_r}}[m] = \frac{\rho_{\hat{h}^{\text{SE}}_{\hat{\imath}^m_{k_r}}[m],\hat{h}^{\text{SP}}_{\hat{\imath}^m_{k_r}}[m]}\sqrt{\zeta^{\text{SP}}_{\hat{\imath}^m_{k_r}}}}{\sqrt{\zeta^{\text{SE}}_{\hat{\imath}^m_{k_r}}}}\hat{h}^{\text{SP}}_{\hat{\imath}^m_{k_r}}[m]$, where $\zeta^{\text{SE}}_{\hat{\imath}^m_{k_r}}[m] \triangleq \frac{1}{1+\sigma^2_{e^{\text{SE}}_{\hat{\imath}^m_{k_r}}}[m]}$ $= \frac{1}{\text{var}(\hat{h}^{\text{SE}}_{\hat{\imath}^m_{k_r}}[m])}$ and $\zeta^{\text{SP}}_{\hat{\imath}^m_{k_r}}[m] \triangleq \frac{1}{1+\sigma^2_{e^{\text{SP}}_{\hat{\imath}^m_{k_r}}}[m]} = \frac{1}{\text{var}(\hat{h}^{\text{SP}}_{\hat{\imath}^m_{k_r}}[m])}$. Substituting and simplifying in $\mathbb{E}\{X^{\text{SE}}_{\hat{\imath}^m_{k_r}}[m]|\hat{h}^{\text{SP}}_{\hat{\imath}^m_{k_r}}[m]\} = \sqrt{b^{\text{SE}}_{\hat{\imath}^m_{k_r}}[m]}\,\mathbb{E}\{\hat{h}^{\text{SE}}_{\hat{\imath}^m_{k_r}}[m]|\hat{h}^{\text{SP}}_{\hat{\imath}^m_{k_r}}[m]\}$ yields the conditional mean result in (4.39). From (C.2) we get $\text{var}\{\hat{h}^{\text{SE}}_{\hat{\imath}^m_{k_r}}[m]|\hat{h}^{\text{SP}}_{\hat{\imath}^m_{k_r}}[m]\} = (1-|\rho_{\hat{h}^{\text{SE}}_{\hat{\imath}^m_{k_r}}[m],\hat{h}^{\text{SP}}_{\hat{\imath}^m_{k_r}}[m]}|^2)\text{var}\{\hat{h}^{\text{SE}}_{\hat{\imath}^m_{k_r}}[m]\}$. Substituting and simplifying in $\text{var}\{X^{\text{SE}}_{\hat{\imath}^m_{k_r}}[m]|\hat{h}^{\text{SP}}_{\hat{\imath}^m_{k_r}}[m]\} = b^{\text{SE}}_{\hat{\imath}^m_{k_r}}[m]\text{var}\{\hat{h}^{\text{SE}}_{\hat{\imath}^m_{k_r}}[m]|\hat{h}^{\text{SP}}_{\hat{\imath}^m_{k_r}}[m]\}$ yields the conditional variance result in (4.40).